THE EFFECT OF HYDROGEN ON THE PASSIVATION PROCESS OF IRON

By

A H JAFARI BSc MSc

A thesis submitted in partial fulfilment of the requirements for the degree of Doctor of Philosophy of the Council for National Academic Awards.

Department of Metallurgy and Materials Engineering

Sir John Cass Faculty of Physical Science and Technology

City of London Polytechnic

April 1990

To my patient wife Laleh

and my lovely daughters

Mikhak and Yaas

ABSTRACT

A thorough survey of the literature relating to the state of hydrogen in metals, factors influencing solubility and diffusion parameters has been reported. The experimental techniques available for studying these properties have been reviewed and the related theories of passivity compared as a foundation for proceeding with the experimental programme.

A new technique for studying the passivation phenomenon has been introduced. Application of the "hydrogen effusion technique" has allowed the investigation of incipient passivation of iron in 0.1 mol/l NaOH. Complementary experiments have been carried out with AC impedance measurements.The mechanism put forward shows a simultaneous Fe_2O_3 and $Fe(OH)_2$ formation followed by formation of γ-FeOOH. A final change converts $Fe(OH)_2$ to γ-FeOOH.The entry of hydrogen into iron substrate was found to be strongly influenced by the effect hydrogen has on the passivation mechanism, a feature that may be relevant in other metal systems, as well as in the phenomenon of stress corrosion cracking and hydrogen embrittlement.

A new technique for monitoring hydrogen movements in a thick metal sample has been developed. A mathematical model to explain the behaviour of hydrogen in such experiments has been developed. This gives a value of 2.04×10^{-5} cm^2 s^{-1} for the diffusion coefficient of iron which is in good agreement with the diffusion coefficient calculated for the thin iron membranes of 2.67×10^{-5} cm^2 s^{-1}

A relationship between the surface potential of an iron electrode and its thickness has been observed and a mathematical expression for it has been derived.The potential drift on iron and other metals has also been explained using this relationship.

Detailed analysis of data has provided other novel insights into the energetics of the diffusion of hydrogen and its state of charge in metals undergoing passivation.

ACKNOWLEDGEMENTS

The list of acknowledgements due to those who have in any way helped me to bring this work to a successful conclusion is a very long one indeed. Omission of any one name is a shortcoming of my memory and not a sign of ingratitude.

I start by expressing my deepest respect to the memory of the late Dr S P Wach who as the original director of study of this project helped me to initiate the research.His untimely departure was deeply felt and not only by the author of these lines.

Dr C J L Booker who took over this project midway, receives my utmost gratitude. The fact that the supervision of a project unrelated to his main line of research would bring extra pressure, never stopped him from stepping in to help. His reassuring support throughout this work and also in dealing with matters not directly related to this research, but essential for the continuation of the work will never be forgotten.

I also must thank Dr D Nuttall and his colleagues in British Gas who by providing me with AC impedance facilities helped to tackle this problem from a new angle. His through and uncompromising proof reading of this thesis is greatly appreciated.

Thanks are also due to Dr M Smith from the mathematics department of City of London Polytechnic who generously offered his mathematical expertise in solving the 3-D permeation problem.

The technical support for this project was varied and came from many quarters,but I must mention Messrs Alan and George Curtis, technicians of the City of London Polytechnic. The former made many complicated pieces from not more than basic drawings and the latter manufactured many intricate and non-standard glassware pieces essential to this research.

Also I must thank Dr D E Maggs for her continuous interest in the state of this project.

My deepest gratitude goes to my parents Ali Asghar and Afsar whose financial and moral support made the higher education a possible goal for me.

Above all it is my wife Laleh, a symbol of patience, dedication and self sacrifice who deserves to be thanked. She managed our affairs under very difficult circumstances and allowed me to work towards my goal.

.....I thank you all.

LIST OF CONTENTS PAGE

1.....INTRODUCTION

Hydrogen as real or suspected cause of so many problems associated with metals is effectively branded as most detrimental when it comes to failure analysis. However, considering the abundance of hydrogen on our planet in the form of water, it is hardly surprising that we come across its ill-effects so frequently. Furthermore, hydrogen as the first element of the Periodic Table and the smallest element is able to penetrate metals and have an omnipresence in them unrivalled by any other element.

With the exception of a few elements , hydrogen has a diffusion coefficient in metals, many orders of magnitude higher than their own self diffusion or the diffusion coefficient of any impurity element in them. Chemically, hydrogen is very potent and can combine with other elements, sometimes explosively to form compounds. As a general rule contact of hydrogen with metals is regarded as undesirable but again even in the production of iron there are trends towards direct reduction using hydrogen.

Hydrogen is also seriously considered as the possible source of energy for the Twenty First Century[1,2]. This could either be in the form of a clean burning gaseous fuel or possibly as the ultimate in energy production, the raw material in a fusion

factory in which hydrogen atoms are combined to form helium and in the process release unlimited amounts of energy. Either way the importance of such developments can hardly escape a generation increasingly faced with the challenges of a polluted atmosphere and the intrigues of a nuclear age.

Even now, hydrogen is an important raw material which is extracted at an annual rate of several billion cubic meters,world-wide, to feed the chemical industry. The storage and transfer of such a huge quantity demands a comprehensive knowledge about the elements involved. Hydrogen is also a by-product of certain electrochemical reactions where its presence is dramatically felt.

Many corrosion processes involve the hydrogen evolution reaction (HER) as the cathodic half cell which will give rise to the presence of hydrogen inside metals. It is practically impossible to engage in welding activities in the open air without introducing traces of hydrogen as a result of the breakdown of water (present as moisture in the atmosphere) in the high temperatures generated,and many technologists have a story or two about weld degradation in this way. Both pickling of scaled steel and cathodic protection may cause hydrogen occlusion in the metals. The melting process of iron and steel, by the virtue of their high temperatures, can cause water molecules to dissociate with the same eventual effect.

All this goes to show that the influence of hydrogen needs to be controlled rather than eliminated. The price of carelessness when dealing with hydrogen is paid through reduced ductility leading to catastrophic failures as the early aviation industry showed,or delayed fracture in the case of stress corrosion cracking (SCC) and corrosion fatigue (CF),by initiating and propagating microscopical cracks and blisters which in turn initiate and propagate these problems. Even small quantities of hydrogen (less than 1 ppm) can cause severe embrittlement and this makes the prevention of such ill-effects even more difficult.

In the case of iron, knowledge about the presence of hydrogen as an impurity is quite old, first referred to in 1863 by Claire-Deville and Troost[3] who showed that hot iron is easily permeated by hydrogen. It was Sieverts [4] who showed that hydrogen uptake by iron increases linearly with temperature, while the effect of the change of solubility for hydrogen in iron, due to phase transformation was noted in a publication by Luckemeyer and Schenk [5] some fifty years ago.

From the outset, the main concern of the investigators has been to elucidate the mechanism by which the tensile strength of metals, especially iron and steel is impaired by occluded hydrogen. This was first scientifically investigated in 1926 by Pfiel[6] who concluded that it is caused by atomic hydrogen

residing mainly around grain boundaries. It is not due to want of effort that the above mentioned statement as to the exact location of hydrogen in metals is still a point of contention. However, the picture now is much clearer than, say 20 years ago when in a study Wach[7] cited references to no less than eight proposed forms of hydrogen in metals, from molecular (H_2) to atomic (H^0), protonic (H^+), screened proton (H^{+-}) to negative ion (H^-), ion molecule (H_2^+) and methane (CH_4).

Recent work[8] lends credence to the hypotheses that hydrogen atoms entering iron give up their 1s electron to the conduction band of the host metal, which is the same as the protonic model. However, studies concentrating on the other transitional metals point to the possibilities such as screened proton and a hydrogen/metal bonding state[9].

Diffusion and solubility characteristics of hydrogen in iron and steel have been the subject of numerous investigations [10-15]. This has led to an effusion of data which for the uninitiated can be bewildering. For instance, a recent overview [117] covering the literature between 1961-81 reports a four order of magnitude variation (10^{-8} - 10^{-12} $m^2 s^{-1}$) in the room temperature values of diffusion coefficient of hydrogen in iron. This not only shows some real difficulties faced on the experimental side, but also a need for more basic research as to the state of

hydrogen in metals as well as its interaction with the metal matrix and internal/external surfaces.

The technique used in this work is the well-established [16-23] and mathematically sound [24-27] electrochemical permeation technique. The above method however, is not a surface-independent technique and this has been utilized to delve into another very important intrinsic property of iron, namely passivity. The phenomenon of passivity of iron has long been recognised, the first observation of it is ascribed to Kier[27] who in 1709 noted the passivity of iron in concentrated nitric acid. Iron, immersed in alkali becomes passive[19], however the nature of the film and the process of film formation is far from clear.

Although the passivity in iron has been widely researched [29-39], the overwhelming proportion of these studies is carried out during the anodic polarization of the metal. This being the case, the free passivation of iron, which exhibits its natural propensity in the course of passivation, has been neglected.

To the best of the author's knowledge, an attempt at elucidating the incipient passivation of iron under thermodynamically favourable conditions and the effect of hydrogen on this phenomenon has not been reported elsewhere.The aim of the present work has been to throw light on the mechanism by which iron

passivates in alkaline media without reference to the quasi-stable state of anodically polarized iron. The relationship between the hydrogen content of an iron membrane and its surface condition has been studied using E.M.F measurements as indicators of the activity of hydrogen in the metal.

During this research, an attempt has been made to clarify some basic ambiguities regarding the state of hydrogen inside iron, the relationship between the hydrogen content of iron/steel and its surface properties and some mathematical modelling to support this is provided. In pursuing these aims, we have found the need to correlate many of the above mentioned properties in the iron-hydrogen system and have attempted to do so. The present work is the result of this attempt.

2.....LITERATURE REVIEW

2.1.....INTRODUCTION

There are subjects which can be difficult when attempting to write about, mainly due to lack of sources of information, suitable experimental data or equally as important since the topic in question seems exhausted from new aspects. Hydrogen does not fall within any of the above groups and yet it is hard to write about it for reasons diametrically opposite tO those mentioned above. Sources of information seem unlimited and any author has a lot of reviewing to do before reaching a considered conclusion. When it comes to new ideas about hydrogen/metal systems, every year a number of original ideas are published, as controversy over the previous ones continues. With this background the following section has been produced.

2.2.....HYDROGEN ENTRY INTO IRON

2.2.1...INTRODUCTION

The source of hydrogen entry into metals can be broadly classified as either gaseous or electrolytic Although hydrogen gas on its own is present in the atmosphere at very low concentrations, i.e. less than 1 ppm [40], in certain processes this could prove sufficient [41] for introducing it into metals.The biggest source of hydrogen however is associated with

aqueous solutions.as many pre-treatments and/or uses of metals bring them into contact with such media. Aqueous solutions are not the only source of electrolytic hydrogen since molten salts can be even more potent sources due to their higher temperatures. Many organic products such as crude oil can also be an effective source. Any attempt at controlling hydrogen damage should therefore concentrate on the prevention of entry.

2.2.2...HYDROGEN ENTRY FROM THE GASEOUS PHASE

The instances where this route of entry is important are mainly the manufacturing or fabrication processes which need high temperatures such as casting or welding. Heat generated in these methods of production lead to molten pools of metal in which hydrogen can easily penetrate [3] and become established.

The hydrogen-iron phase diagram first proposed by Sieverts[4] and still valid, be it with minor modifications, shows the limits of solubility of hydrogen in molten iron. Figure 1 shows this diagram and demonstrates the propensity of iron for accommodating large amounts of hydrogen at moderate temperatures and also the dramatic increase in solution as the temperature nears the melting point.

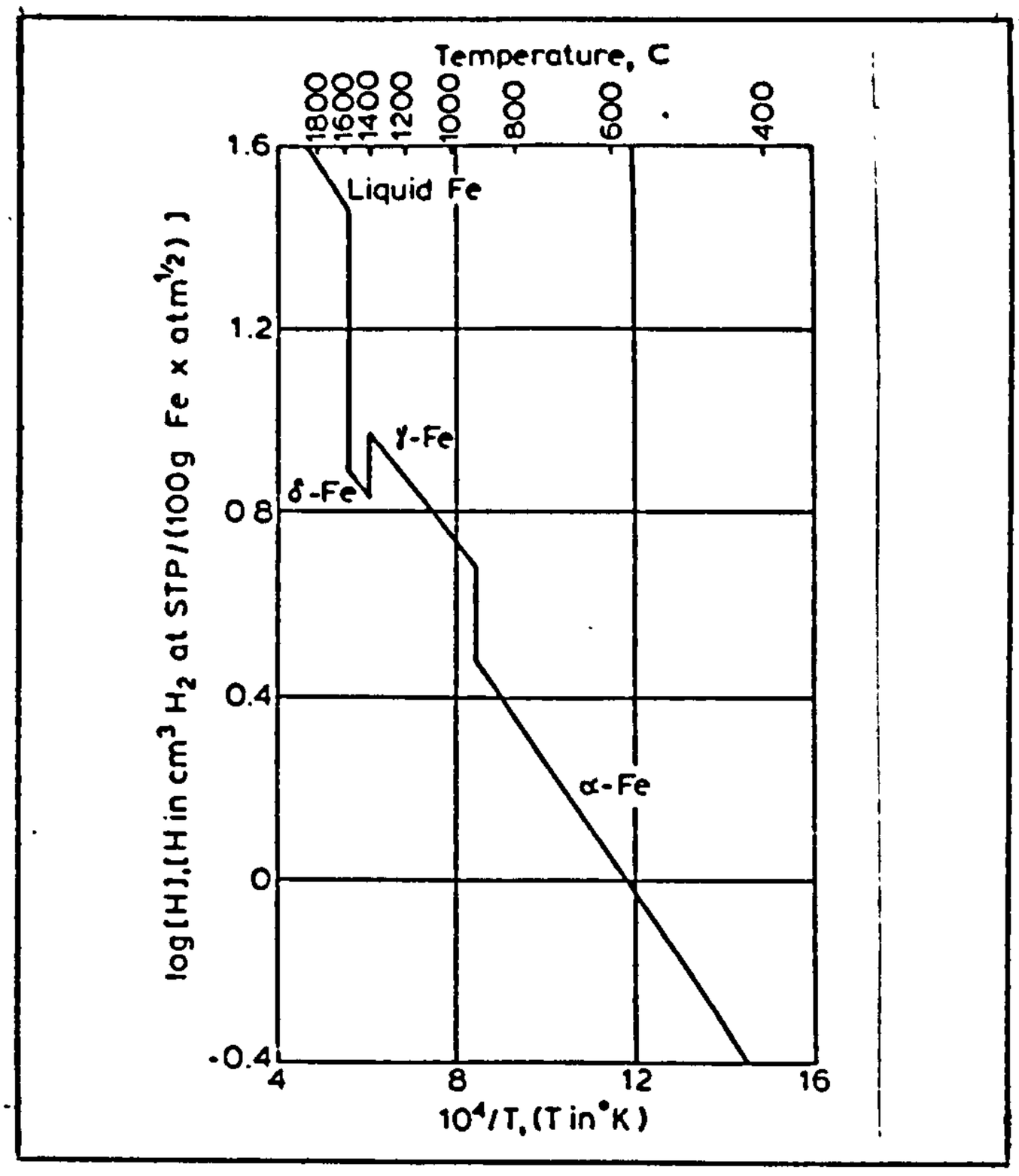

Fig.1 The Fe/H diagram for pure iron.After "Introduction to the Physical Metallurgy of welding" [41].

The presence of hydrogen can also arise from dissociation of water molecules present in the atmosphere through interaction with iron (1) or carbon (2) at high temperatures;

$$H_2O + Fe \rightleftharpoons FeO + H_2 \qquad (1)$$

$$H_2O + C \rightleftharpoons CO + H_2 \qquad (2)$$

More hydrogen can enter metals at high enough temperatures, as a result of the decomposition of any hydrocarbon present on the metal surface, such as oil and grease. The following two equations represent such an entry route.

$$CH_4 + 3Fe = Fe_3C + 2H_2 \qquad (3)$$

$$C_2H_6 + O_2 = 2CO + 3H_2 \qquad (4)$$

The hydrogen thus formed is then absorbed by iron. This is thought to happen in at least two stages[42]. Hydrogen molecules are adsorbed as cations (positive adatom) prior to formation of a hydrogen anion (H^-) on the surface.

$$H_2(g) \rightleftharpoons H_2^+(ads) + e^- \quad (5)$$

$$H_2^+(ads) + 3e^- \rightleftharpoons 2H^-(ads) \quad (6)$$

The adsorption of hydrogen on iron at low temperatures up to ambient , follows the Langmuirian isotherm [43] and then changes to Temkin coverage in the temperature range up to 240 C [44].

The kinetics of these reactions are shown to be controlled by migration of the initially adsorbed adatoms to those surface sites where potential energy is lower and could give rise to formation of H (ads) species. The above model is made more complicated by a middle step (8) in which H_2^+ (ads) is converted to H^+(ads) on iron, leading eventually to the (H^-) adion [45,46].

$$H_2(g) + Fe \rightleftharpoons H_2^+(ads) + Fe + e^- \quad (7)$$

$$H_2^+(ads) + Fe \rightleftharpoons 2H^+(ads) + Fe + e^- \quad (8)$$

$$2H^+(ads) + 2Fe + 4e^- \rightleftharpoons 2H^-(ads) + 2Fe \quad (9)$$

This sequence of events is thought to be energetically easier to achieve[45].

2.2.3...HYDROGEN ENTRY FROM AQUEOUS SOLUTIONS

Although hydrogen entry from the gaseous phase plays an important role in contamination of metals, by

far the biggest source of its introduction comes from aqueous solutions. This happens during two periods in the life of a metallic object, namely during the surface treatments such as pickling, electroplating, paint stripping as well as phosphating and cathodic protection or during corrosion processes encountered by metal while exposed to the atmosphere and/or aqueous environments.The mechanisms according to which hydrogen is evolved are fully dealt with in later sections. However,here the basic difference between the metal/gas interface and that of metal/electrolyte system is discussed.

The presence of a dense network of water dipoles in the electrolyte and also the competitive nature of absorption phenomenon results in complications compared with the two or three step adsorption mechanism in a gas/metal system.The cases where the metal/electrolyte interface undergo compositional change add to the complexity of the problem, as do situations where localized corrosion accompanies the adsorption .

Hydrogen can be introduced in at least two other ways. First, direct entry from lubricants and oils and also entry from molten salt baths. The first case, although not well researched [47], can be of importance when evaluating the relative integrity of internal combustion engines. Since no moving part of a working engine can work without lubrication and because lubricants contain hydrogen, such a route could be

significant. Swets[47] using deuterium as trace element for following the movement of hydrogen in bearings undergoing fatigue testing observed that the hydrogen concentrations were consistently twenty times greater than before the fatigue test. This, he argued indicates the decomposition of lubricant and the permeation of hydrogen into iron.

In the same way, hydrogen seems to penetrate pipelines and other installations in the oil industry. Sour crude oil containing H_2S as well as a variety of organic hydrocarbons come into contact with iron and steel and by natural dissociation, or due to the processing steps, generate hydrogen which penetrates the structure.

2.2.4...HYDROGEN ENTRY FROM MOLTEN ELECTROLYTES

Molten salt baths composed of neutral or acid sulphates of potassium and sodium ($KHSO_4$ and $NaHSO_4$) are commonly used and because of their high melting point, can give rise to concentrations of hydrogen 15-40 times that of aqueous solutions [48]. Figure 2 illustrates this by comparing hydrogen uptake for iron specimens charged from an aqueous solution (a), molten bath at 250° C (b) and 300° C (c).

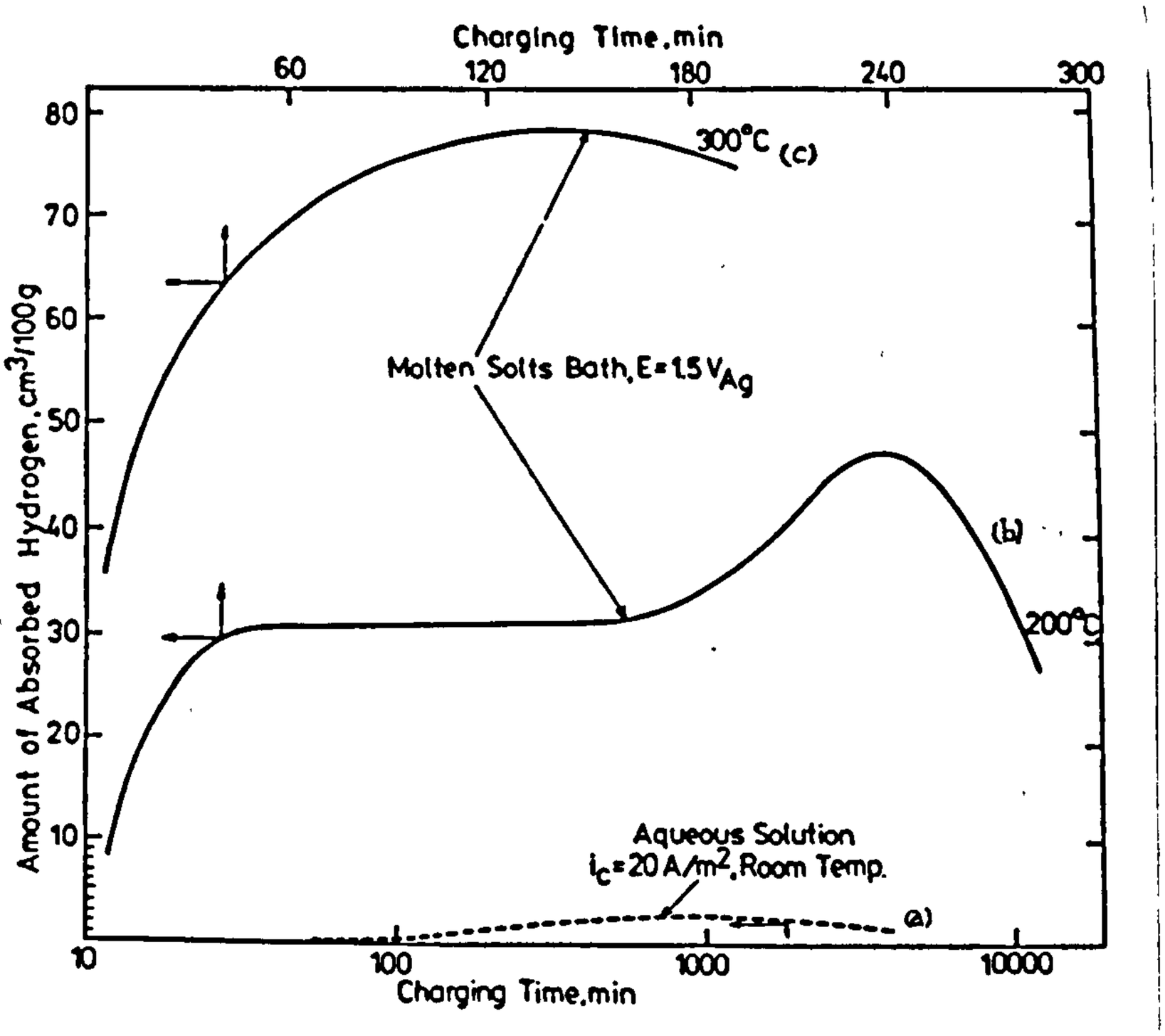

Fig.2 The effectof high temperature employed in molten baths on the hydrogen permeation compared to the charging from aqueous solutions at room temperature.After El-kholy et al [48].

2.3.....THE STATE OF HYDROGEN IN METALS WITH PARTICULAR REFERENCE TO IRON

2.3.1...INTRODUCTION

The state of hydrogen within the sub-lattice of metals is of fundamental importance for elucidating its interactions with the host metal. It is also important in clarifying some of the experimental anomalies encountered. Hence the topic has been the subject of numerous theories and hypotheses since thorough mathematical or experimental evidence has not always been available to support the arguments. However the overall conclusion however is that an atomic/protonic state fits well with many available data on iron.

2.3.2...ATOMIC HYDROGEN (H)

It is generally taken assumed that hydrogen resides in iron in the atomic form. Historically, the evidence for this is based on a variety of observations which show that hydrogen obeyed Sievert's law. This predicts a square root relationship between the atomic hydrogen uptake by the iron and the pressure of hydrogen over it. The thermodynamic argument supporting this conclusion predicts a dissociation step during which a hydrogen molecule is converted to two atoms which are then absorbed into the iron.

$$H_2 \rightleftharpoons 2H \qquad (10)$$

where the equilibrium constant is defined by:

$$K \rightleftharpoons a_H / p_{H_2} \qquad (11)$$

where "a" denotes the activity of hydrogen and "p" its partial pressure. If P is taken to be constant, then from equation (10) and (11) we obtain:

$$a_H = K \sqrt{P_{H_2}} = \text{constant} \qquad (12)$$

However, this can effectively be shown for relatively high temperatures, in excess of 300 C up to the molten state ie excluding ambient temperatures at which most anomalies occur. Another observation supporting this hypothesis as reported by Bodenstein [49] is that hydrogen effusing from a metal can react with oxygen and nitrogen. This argument neglects the possibility of the hydrogen molecule dissociating on the exit surface before combining with an energetically more favourable element like oxygen.

2.3.3....EVIDENCE FOR MOLECULAR HYDROGEN(H_2)

The existence of molecular hydrogen is also considered and several investigators [50-52] including de kazinczy[53] postulate that atomic hydrogen combines on lattice discontinuities to form molecular hydrogen. Some of the theories of hydrogen embrittlement [16,54-59] such as the "hydrogen pump theory" by Tiller and Schiffer[58] or the "pressure theory" by Zapffe and Siems [59] are based on this assumption.

Despite such evidence, there is virtual certainty that hydrogen does not start its passage through metals in the molecular form. The evidence for this comes not only from work on the kinetics of hydrogen evolution reaction on iron, but also from parallel investigations such as experiments concluded on nitrogen induced embrittlement

Sieradzki and Ficalora[60] have conclusively shown that pre-dissociating nitrogen molecules, which normally do not go through such a step on a metallic surface (unlike hydrogen), before introduction into a steel substrate, results in embrittlement of the metal. This is in contrast to the usual introduction of nitrogen with steel,in which it dissolves in the molecular state and does not give rise to any emmbrittlement. Keirchheim et al [61] have shown the presence of hydrogen in the atomic form on purely thermodynamic considerations such as changes of free

enthalpy of its solution in metals. Existence of the hydrogen molecule (H_2) side by side with atomic hydrogen has also been reported. Kuk et al [62] using a high performance,time-of-flight atom probe has detected these two states in grain boundaries and has not found any evidence for protonic hydrogen.

2.3.4...NEGATIVE (H^-) POSITIVE (H^+) HYDROGEN IONS

There is also theoretical as well as experimental evidence for the negative hydrogen ion(H^-) immediately under the surface of the transitional metals,however the work function difference measurements on Pd and Fe have shown negative changes for this property which indicates a positively charged hydrogen ion [63].This shows the importance of studies on the location of hydrogen in metals since in the context of hydrogen/metal interaction the properties concerned are affected.Hydrogen sites can change both sign as well as the work function value.Barker and Rideal [64] report the migration of hydrogen towards the anodic side of an aluminium alloy membrane and have interpreted it as the evidence for negative hydrogen ion (H^-) inside metals.This entails the acceptance of an extra electron by hydrogen in its"s"shell from the electronic cloud of the host metal.Another expansion for this observation (ignored by the authors) could be the presence of "screened" protons as suggested by other workers which does not necessitate any electron donation or acceptance but relies on the "shielding" of a proton by

a number of electrons. Other investigations [65-70] have produced evidence for negative as well as positive hydrogen ions. An interesting proposal on the presence of the hydrogen ion molecule (H_2^+) has been made by Suhrmann et al [71]. Kirst and McQuistan [72] report evidence of such a case entails donation of one electron from two paired atoms to the Fermi level of the host metal.

2.3.5...HYDROGEN PRESENT AS COMPOUNDS

Different compounds are also postulated and in some cases identified. Methane. gas has been positively identified [73-77] but this is thought to be the result of the presence of impurities, in this case carbon, which on combination with hydrogen give rise to methane [78-79] or other compounds in mild steel. However they have not established a clear mechanism for this phenomenon.

2.3.6...HYDRIDES OF IRON

Hydride formation in iron is another subject of controversy in the Fe-H system. While hydrides of other metals such as Ni, V, Nb ,Ti, Ta and U have been positively identified, the case for iron is far from clear. There are three main types of hydrides which can satisfy the different hydrogen/substrate atom ratios. Most bcc metals seem to have the lowest hydrogen/metal (H/M) ratio of one. For these, a monohydride model MH with a NaCl type lattice has been suggested. Many hydrides of

these configurations are identified such as VH, NbH and TaH. Pd and Ni among the fcc metals seem to have this structure as well. It is important to realise that hydride formation can be localized and therefore even H/M ratio of 0.05 can lead to formation of nickel hydride [80]. This could be explained when it is realized that hydride formation in this system is restricted to a 20-30 μm thick layer immediately under the charging side[80] leading to a much higher H/M ratio there. This hydrogen first establishes a random solid solution in nickel and then wherever there are regions of higher hydrogen concentration e.g. due to trapping,the hydride formation proceeds X-ray studies confirm that there are always two phases in the surface layer- the nickel hydride (β-phase) and the solid solution of hydrogen in nickel (α-phase) [81]. Other forms of hydride such as dihydrides MH_2 and trihydrides MH_3 have been postulated and observed [82].

The common objection to an iron hydride hypothesis stems mainly from the fact that the solubility of hydrogen in α-iron at room temperature is in the order 0.02 ppm [83], clearly too low to sustain a bulk hydride of even the simplest type. The other proof seems to be the lack of success in detection of such compounds in iron . However, as in the case of nickel, hydride formation in iron can be highly localised, leading to pockets of hydride wherever the hydrogen concentration, due to inhomogenieties and lattice imperfections,could reach the necessary critical level.

The lack of experimental evidence for such structures could well be the result of the less sensitive methods employed.

Kuk et al[82] using field emission techniques claims to have detected both FeH and FeH compounds at a propagating crack in an iron alloy. Other authors [84,85] in quite recent works refer to iron hydride and have also established the electronic structure of such hydrides. Frey and Kruger [85] having identified the hydride as FeH, determined that its electronic structure closely resembles that of adsorbed hydrogen ion on the iron surface. Conclusive proof for iron hydride formation needs more work since until the hydride can be separately produced from the elements and its properties tested, the differentiation between hydrogen sitting in an energetically favourable site and hydrogen forming a bond with its neighbouring atoms, is rather difficult solely on the basis of atom ratios.

2.3.7...PROTONIC HYDROGEN

Protonic hydrogen in metals is one form which is widely reported[68,86-91] and is based on the simple band theory of metals. Hydrogen atoms dissolved in transition metals are thought to give up their 1s electron fully to the conduction band of the host metal. If the Fermi level lies within the d-band, holes in it are filled as the hydrogen concentration

increases[91].This hypothesis, which in effect combines the atomic and the protonic models, gets its credence from thermodynamic data as well as considerations from the physical properties of transition metals containing hydrogen [92].

For instance, the magnetic property dependence of such alloys on the electron to atom ratio, ie the ratio of the number of outer electrons of all atoms in the alloy,including the substrate atoms, alloying elements as well as hydrogen atoms, to the total number of atoms closely follows the dependence of enthalpy of solution for hydrogen in these alloys on the same electron/atom ratios. This means as the electron/atom ratio increases, the hydrogen dissolution tends to become endothermic and therefore more difficult[92]. Figure 3 depicts this dependence.

The explanation for such a relationship is based on an electron theory which assumes that hydrogen atoms use their sole electron to stabilize the half empty d-band in those metals and alloys which have less than five electrons in these shells. As this figure shows, metals like Mo(4d5, 5s1) or Cr(3d5, 4s1) which exhibit strong metallic bonds,exhibit endothermic enthalpies of solution accounting for a lower tendency for absorbing hydrogen [93].

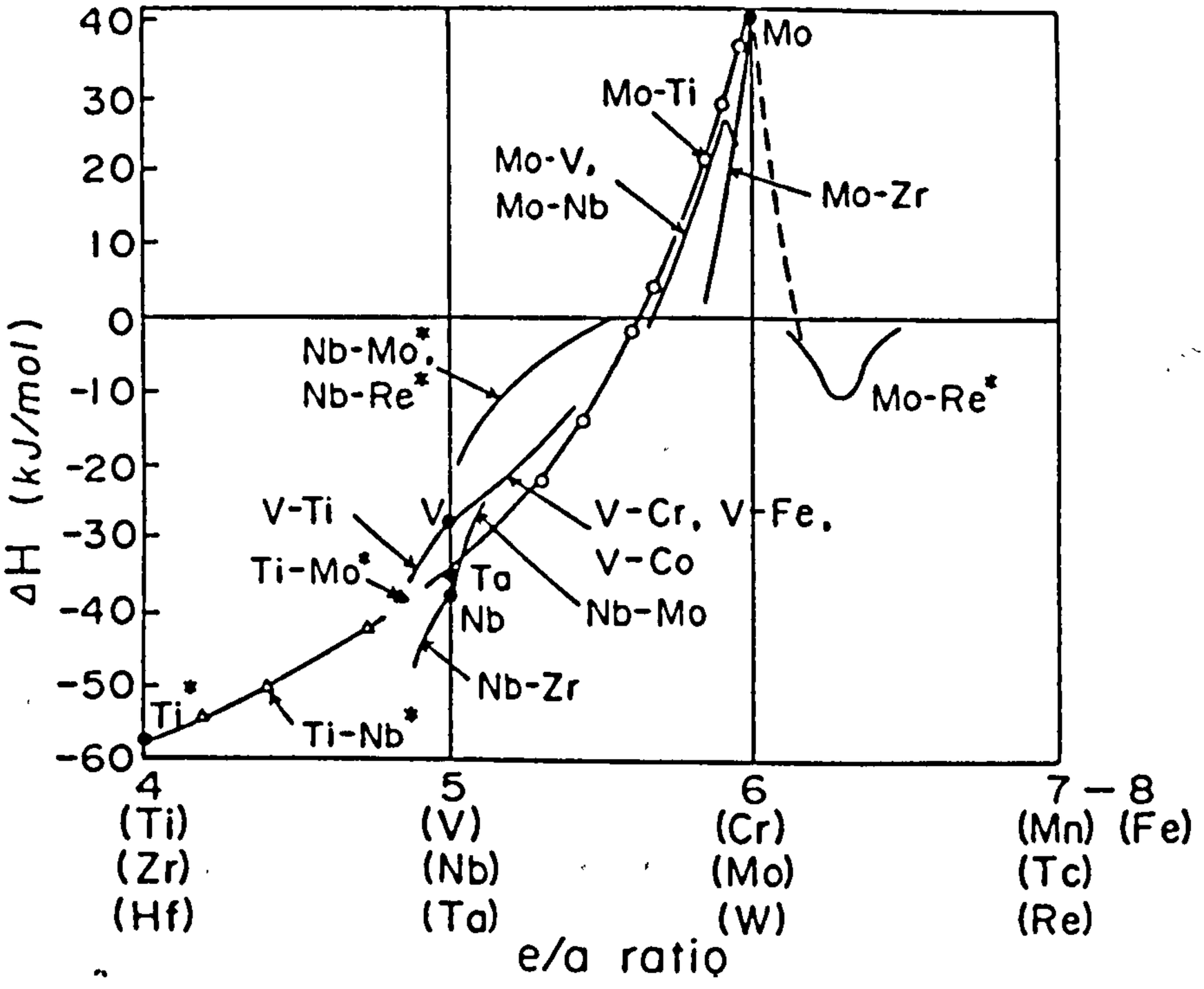

Fig.3 the relationship between the heat of solution of hydrogen in some metals and their alloys with their electron to atom ratio. After Euguchi and Morozumi[92].

Elements like Ti or Nb with less than 5 electrons in their d-band use the 1s electron to fill in their last band and in the process stabilize the hydrogen as well. This accounts for the ease with which hydrogen dissolves in elements of group IVb of the Periodic Table as well as their very exothermic heats of solution for hydrogen. However, the same explanation cannot interpret cases of high electron/atom ratio such as Fe(3d ,4s).

2.3.8...THE SCREENED PROTON FORM

The shortcomings of a wholly protonic model adds to the relevance of the screened proton $(H^+)^-$ model as it can explain some of the anomalies, by accepting the concept of a variable hydrogen ion size [91,92]. This could arise from different levels of coverage of proton by the conduction band electrons of the solvent atoms which in turn could result from modulation of the hydrogen nuclei energy level.

Overall, the accepted forms of hydrogen in the transition metals seems to be reducing to one or combination of the following models, ie molecular, atomic or screened protonic while the presence of other forms especially hydrides even in iron cannot be ruled out.

2.4.....LOCATION OF HYDROGEN IN METALS

2.4.1...INTRODUCTION

The microscopic location of hydrogen is important since it has a bearing on the solubility and migration of hydrogen. It is also important for understanding such effects as damage trapping, impurity interactions, bubble nucleation inside the matrix, blistering and embrittlement phenomena .It often forms

the basis for the interpretation of other experimental and theoretical studies involving hydrogen.

The problem of identifying the location of hydrogen in metals is best studied from the viewpoint of the sublattice structure of the host metal since this is the controlling factor when it comes to accommodating hydrogen. However,some generalities could be made such as, in small quantities, hydrogen dissolved in metals forms solid solutions and hydrogen dissolution in all cases is interstitial, not substitutional. This is evident from the diminutive size of the hydrogen atom.

It is also tenable to say that the occupancy of interstices is dependent on the hydrogen concentrations which in turn is controlled by both the partial pressure of hydrogen over the metal as well as the temperature.For many years,the limited understanding of the mechanisms involved in interactions of metal/metal as well as metal/hydrogen atoms had restricted the ways of tackling this problem.Cosequently, a model in which hydrogen as positive/negative ions sitting randomly in the host lattice was generally accepted.

The preoccupation with the embrittling properties of hydrogen seemed to be satisfied by the assumption that the very fast diffusion of hydrogen, rather than its instantaneous location is the paramount factor which alone could satisfy the practical as well as

theoretical considerations. However, the existence of widespread anomalies inexplicable in terms of such a simple theory led to more rigourous analysis of the problem using the quantum mechanical theory[94].

The use of more sensitive and accurate experimental techniques namely a variety of neutron diffraction methods such as incoherent neutron scattering[95,96], channelling[97], diffuse[94] and quasi-elastic neutron scattering as well as high performance time-of-flight atom probe[82] have revolutionised our perception of this topic and its priority in elucidating the .exact nature of the interactions of hydrogen within metals.

2.4.2...EFFECT OF TRAPPING

One major difficulty when studying the location of hydrogen in metals is the interpretation of hydrogen with the discontinuities in the lattice i.e. point defects or other dislocations as well as inhomogeneities such as impurities or grain boundaries within the lattice, which collectively are known as traps.

The concept of hydrogen trapping which is discussed in detail in section 2.5 is basically concerned with the interactions of hydrogen and the sub-lattice of the host metal; based on the energetics of abnormalities in the structure of the metal. This means that hydrogen in its diffusion through any

metallic substrate is either stopped or delayed in certain energetically favourable sites where, if it was a perfect lattice it would not have resided.

This entails differentiating between the "normal" sites where hydrogen travels in its diffusion path solely on the basis of compatibility of its jump frequency with the height of the energy well of that particular site -and"abnormal" sites- chosen by the hydrogen as a result of a directional push given to it by their possibly deeper energy wells.

The very low solubility of hydrogen in iron makes the study of preferential locations in the H/Fe system even more difficult. Wert[98] argues that hydrogen at low concentrations in a defect-free single crystal of iron will form a random solid solution. By implication,in a polycrystaline structure (by definition full of imperfections) ,the location where hydrogen sites are much more likely to be dictated by "traps" present. This argument could prove difficult to refute not least because of the very low solubility of hydrogen in iron making error-free results rather difficult to obtain. However, this model is not a reliable substitute for accurate site occupancy studies in iron and steel.

2.4.3...OCTAHEDRAL AND TETRAHEDRAL OCCUPANCY REGIMES

Work to establish the possible location for hydrogen , trapping aside, has not concentrated on either tetrahedral or octahedral interstitial locations in fcc, bcc or cph metals. Figure 4 illustrates these two positions in bcc and fcc lattices.It has been shown that there are three octahedral and six tetrahedral interstitial sites per Fe atom, in a bcc lattice (Fig.4a). Figure 4b illustrates these positions in a fcc lattice. Again there are one octahedral and two tetrahedral sites per atom corresponding to four octahedral and eight tetrahedral positions in a fcc cell having four atoms.

X-ray measurements have established the position of hydrogen in alloys. Bastien et al [99] concluded that at ambient temperatures, hydrogen atoms reside preferentially in tetrahedral sites along the (112) planes.This was based on the broadening of (112) spots in Laue patterns of hydrogen-charged steel specimens.

Work on the partial molar value of hydrogen in iron seems to support such conclusions. It is clear that hydrogen, although small, dilates the lattice and also by interaction with the metal atoms, leads to alteration of the force constants within the substrate. Oriani[100] found the molar volume of hydrogen in a bcc substrate to be around 2×10^{-6} m^3 mol which requires a radius of 0.092 nm for hydrogen in a "hard sphere"

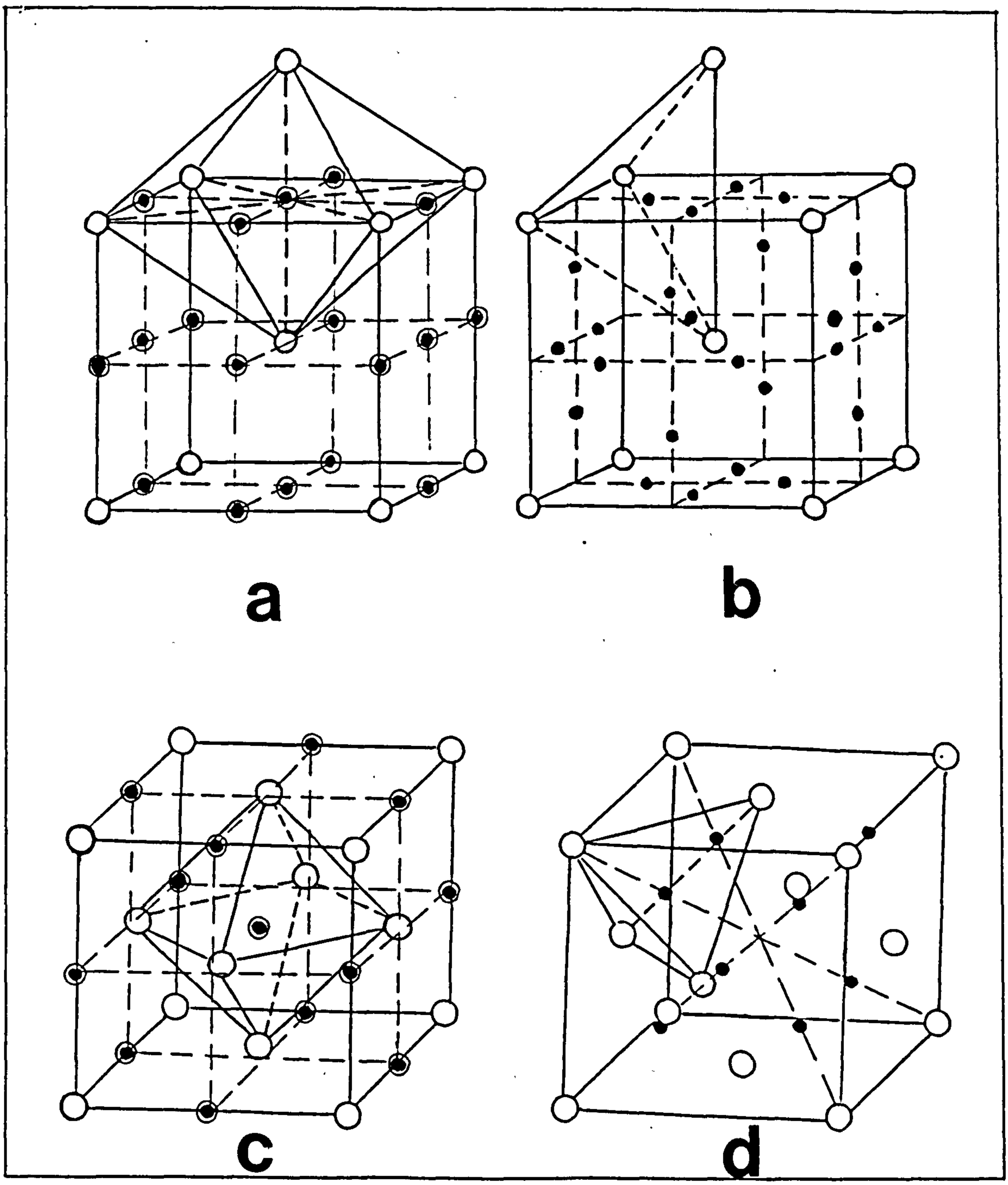

Fig.4 The octahedral and tetrahedral positions in b.c.c. and f.c.c. lattices
(a) octahedral b.c.c. (c) octahedral f.c.c.
(b) tetrahedral b.c.c. (d) tetrahedral f.c.c.

model. This compares closely with other findings [16,101,102] as well as empirically deduced size for hydrogen atom in different metals which is reported as being $3x10^{-30}$ m^3/atom ie a ball of radius 0.089 nm in a "hard sphere" model [103].

In a bcc iron lattice, the octahedral site can only accommodate an atom with a radius of 0.019 nm and the more widely spaced tetrahedral sites can accept an atom of 0.036 nm radius, without physically distorting the lattice which leads to some degree of shift and blurring of the diffraction patterns. However, X-ray measurements are vulnerable to spurious results in site location studies and the same degree of broadening of diffraction spots attributed to hydrogen,could be produced by cold working specimens by as little as 5%. Our understanding of the electronic structure of metals and alloys also indicates the simple hard sphere model of hydrogen/ metal atoms could not explain many of the experimental anomalies.

Gonzalez [104]and Oriani[105] assumes octahedral occupancy by hydrogen in his investigation of thermal and chemical forces on hydrogen.In another publication, Oriani [106] uses the concentration of octahedral sites (site/m^3 Fe) of iron as the basis of calculations for applying his "trapping theory" to data published by other workers, and gives a figure of $2.6x10^{29}$ sites/m^3 of occupiable positions.Ferro[107] theorized that hydrogen diffusing in iron will adopt a path which is defined by

the octahedral interstices in the lattice. This model predicts a low elastic strain associated with such movement and according to Bryam et al[108], it has been observed in high temperature diffusion work.

Other workers have postulated the same occupancy regime. They have used the number of octahedral sites in their calculations [109], assuming the exclusivity of such sites for hydrogen location. However, evidence for tetrahedral occupancy of hydrogen in iron is as notable and it seems that more recent work[110,111] lendssupport to this view. The evidence derives mainly from the studies on hydrogen .in other bcc metals especially niobium.Sprinter[112] andStump[113] working independently show tetrahedral occupancy in niobium. Advanced studies by Seegar on muons, which at 1/7 of mass of hydrogen,are thought of as a lighter version of it, indicate the same tetrahedral occupancy in iron. There are also theoretical considerations supporting this argument [114].

2.4.4...DUAL OCCUPANCY REGIME

Thermodynamic analysis of hydrogen solubility in iron seemsto suggest a "dual occupancy" model in which at lower temperatures hydrogen resides in tetrahedral sites but as the temperature rises, the octahedral sites are progressively occupied[115]. The increase in entropy associated with elevated temperatures observed for hydrogen can therefore be

accounted for by the increase in disorder due to the occupancy of octahedral sites. The case of bcc iron/carbon system is an example of interstitial solid solution for which the measured data show, contrary to the case of hydrogen a constant enthalpy and entropy of solution over a wide temperature range. This entails a single occupancy (octahedral) regime [116].

The dual occupancy model for iron/hydrogen at the moment seems to be the most appropriate since it satisfies many of the requirements dictated by experimental anomalies[117]. However further work using more sensitive analytical techniques could change the accepted views on this subject altogether. An example of this is the recent work by Kuk et al [82] who by using atom probe were able to detect hydrogen directly. In their study the only hydrogen found in any form was at the grain boundaries, while locations elsewhere in the bulk of the metal were devoid of hydrogen.

2.5.....HYDROGEN SOLUBILITY IN IRON

2.5.1...INTRODUCTION

The solubility of hydrogen in metals is of great interest both from the technological view point and in regard to its applicability to the thermodynamic

and kinetic arguments based on the classical Arrhenius type equations of solubility. It is therefore relevant to review the major techniques used for the determination of hydrogen solubility before discussing explanations of the data.Subsection 2.5.5 is devoted to certain anomalous results and also the possible explanations proposed in the literature. The topic of trapping which has a strong bearing on this property, will be discussed in detail in a subsequent section.

2.5.2..SOLUBILITY MEASUREMENT TECHNIQUES

These may be classified as high and low temperature methods.

(a) High Temperature Techniques

The general procedures employed involve the equilibrium, quench, analysis techniques [115,118]. Variation of the extraction methods revolve on the temperature range used and the way the gas is collected.For instance, the vacuum extraction technique uses a sample of iron or steel up to 10 g mass. The cleaned and degreased sample is introduced into a furnace at 20^{o} -650^{o}C. The gas thus evolved is collected and measured manometrically [119,120]. The limit of detection for this technique is as low as 0.01 ppm of hydrogen.

A somewhat similar method is developed in which the sample is heated at 650^{o}C but the gas evolved is collected in a stream of an inert gas such as argon at

atmospheric pressure and then analysed[121]. This is usually referred to as the carrier-gas technique. The vacuum fusion method involves vacuum melting a hydrogen bearing membrane in a graphite crucible at 1550-1650 C. The evolved gases (CO, N_2, H_2) are continuously removed and chromatographically analysed. The high temperature techniques are generally less prone to surface effects and therefore the reproducibility of the results is quite good.

(b) Low Temperature Techniques

This category is mainly conducted in electrolytic media[16-18,122] and utilizes the oxidation of hydrogen atoms,diffusing out of an electrolytically or otherwise charged metal membrane. Since the atoms of hydrogen are encouraged to readily oxidize, both catalytically, using Pd plated beds and also thermodynamically, through the manipulation of the free energy of the system by maintaining an appropriate electrode potential. In theory, detection of changes due to as little as 10^{12} atoms of hydrogen is possible. However, these techniques are adversely affected by surface phenomena and require special surface treatments[117].

2.5.3...INFLUENCE OF TEMPERATURE ON SOLUBILITY

At high temperatures up to the melting point of iron, the variation of hydrogen solubility with temperature obeys the Arrhenius type exponential relationship:

$$S = \beta \exp(\Delta \bar{H}^{\circ}_{H} / RT) \cdot \exp(\Delta \bar{S}^{xs}_{H} / R) \quad (13)$$

Where $\Delta \bar{H}^{\circ}_{H}$ and $\Delta \bar{S}^{xs}_{H}$ are the partial molar enthalpy and excess entropy of solution for hydrogen respectively, and β is a factor determined by the gas pressure and the number of available interstitial sites per atom in the lattice. When $\Delta \bar{H}^{\circ}_{H}$ is positive the solution of H is endothermic and when $\Delta \bar{H}^{\circ}_{H}$ is negative it is exothermic. In the case of iron various works[104,123,124] have shown $\Delta \bar{H}^{\circ}_{H}$ to be positive which means the solution should increase as the temperature rises.

Attempts to find a specific set of values for the variables in equation (13), in order that it can represent the entire temperature range for solubility measurements are quite old [123,125,126]. However there are serious problems with such methods since none have been able to satisfy and explain the observed solubilities of hydrogen in iron. In later sections the effects of trapping and alloying on solubility are discussed but here the temperature effect alone will be considered.Figure 1, showing the solubility of hydrogen at different temperatures shows the influence of three distinct phase transformations in the iron substrate on the hydrogen solubility.

The temperature independent term $\beta \exp \Delta \bar{S}^{xs}_{H} / R$ is responsible for quantifying these, in solubility calculations. This is attributed to higher value of the constant which in turn has resulted from the change of occupancy regime during phase transformations. The

term $\Delta\bar{H}^{\circ}_{H}$ also contributes to the overall change, since the enthalpy of solution is different for each of the phases. Kubachewski [124] proposes the following formula for the hydrogen solubility at 1 atm pressure in the α and δ phases:

$$(\text{at\% H})^{-1} = \exp(3169 / T) + 4.622 \qquad (14)$$

He also proposes another formula for γ-iron at 1 atm:

$$\text{at\% H} = [\exp(3249.5/T) + 2.935] \qquad (15)$$

Kuchi and McLellan[117] present another expression for α-iron that covers the entire temperature range 0° -150°C :

$$\frac{\Theta_H^{mix}}{\Theta_H^{Tet}} = 1 + \frac{\beta_{oct}}{\beta_{Tet}} \exp\left(\frac{\Delta\bar{H}^{\circ}_{H}}{kT}\right) \exp\left(\frac{-\Delta\bar{S}^{xs}_{H}}{k}\right) \qquad (16)$$

$\Theta_H^{mix.}$ =hydrogen solubility in dual occupancy regime at higher temperatures

$\Theta_H^{Tet.}$ =hydrogen solubility at low temperature (tetrahedral sites only)

β_{oct}, β_{Tet} =the number of octahedral or tetrahedral sites per lattice atom (3 and 6 respectively)

$\Delta\bar{H}^{\circ}_{H} = \bar{H}^{Tet}_{H} - \bar{H}^{oct}_{H}$ ($\bar{H}_H$ denotes enthalpy of solution for hydrogen)

$\Delta\bar{S}^{xs}_{H} = \bar{S}^{Tet}_{H} - \bar{S}^{oct.}_{H}$ ($\bar{S}_H$ denotes entropy of solution for hydrogen)

the variables $\Delta\bar{H}^{\circ}_{H}$ and $\Delta\bar{S}^{\circ}_{H}$ are evaluated as -22.56 kJ mol^{-1} and -6.000 kJ mol^{-1} respectively from the analysis of other worker's data. Fujita [127] simplifies this equation and expresses it as follows,

$$\text{at\%H} = \exp(-3109/T) + 24.53 - 4.03T \qquad (17)$$

This formulation of the relationships fits the selective data well, within the -400° to 1500°C excluding the γ-phase measurements.

2.5.4...INFLUENCE OF PRESSURE ON SOLUBILITY

The role of pressure on the concentration of hydrogen in iron is expressed effectively by Sievert's law. This is especially valid for the molten phase of iron but has been shown to be operative at the solid phase as well[124]. As expected, for a ferrous material subjected to a constant external pressure P, the following equilibrium holds.

$$H_2 \rightleftharpoons 2H \qquad (18)$$

the equilibrium is defined as

$$K = a^2_{\langle H \rangle} / P_{H_2} \qquad (19)$$

where $a_{\langle H \rangle}$ is the activity of dissolved hydrogen. At constant pressure:

$$a_{\langle H \rangle} = K\sqrt{P} \qquad (20)$$

since

$$a_{\langle H \rangle} = \gamma_{\langle H \rangle} \cdot X_{\langle H \rangle} \qquad (21)$$

where $\gamma_{\langle H \rangle}$ is the activity coefficient and $X_{\langle H \rangle}$ the atom fraction of dissolved hydrogen. Hence,

$$X_{\langle H \rangle} = K / (\gamma_{\langle H \rangle} \cdot \sqrt{P}) \qquad (22)$$

On rearrangement $X_{\langle H \rangle} = K \cdot \sqrt{P}$. which is the Sievert's square root law. The pressure enhances the solubility of hydrogen to the extent that at 250C and 6 MPa pressure, the hydride FeHx has been synthesized[128]. Antonov has produced a pressure-temperature diagram (FIg.5) which exhibits three phases resulting from the change of solubility hydrogen with pressure[128].

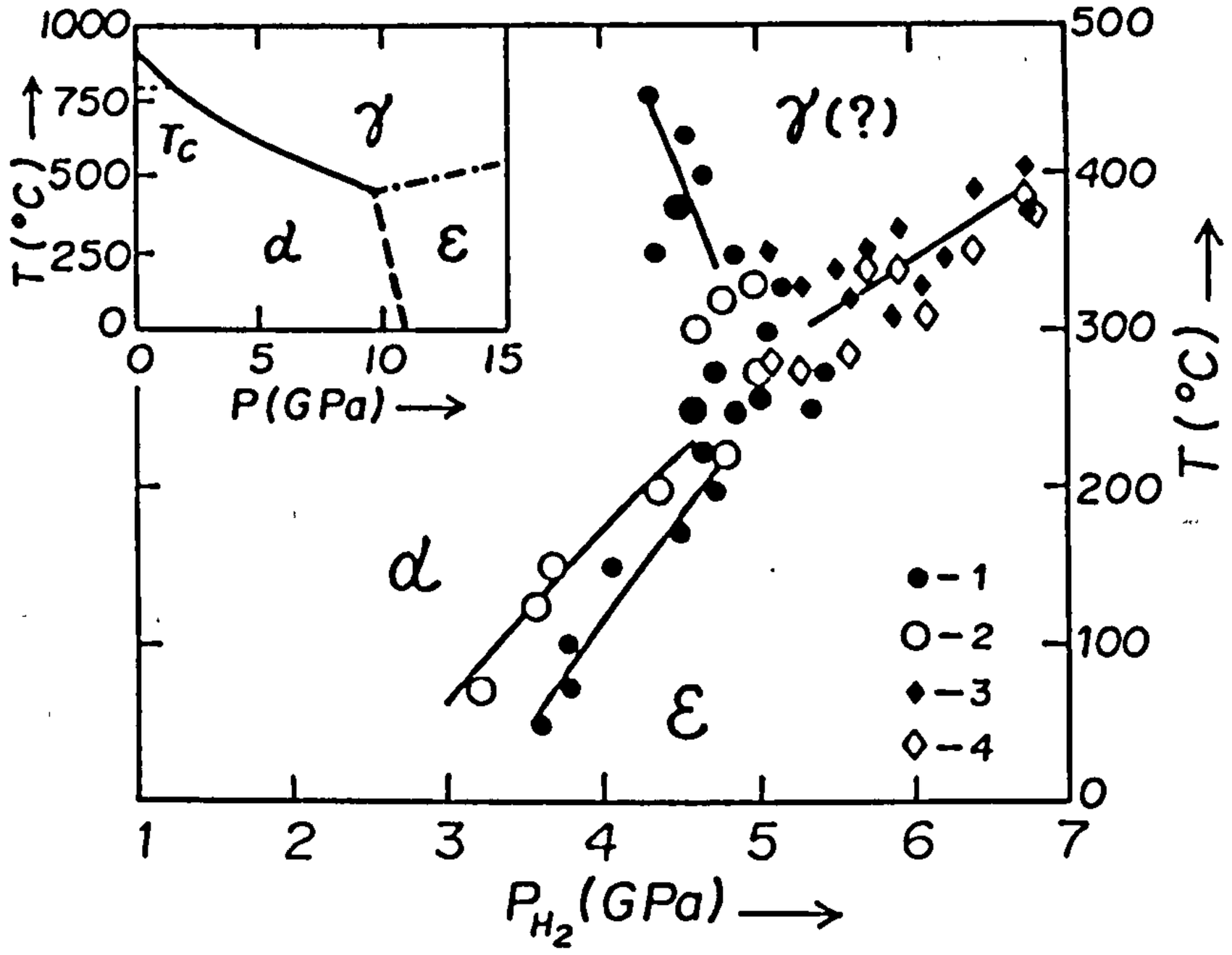

Fig.5 The domain of solubility of different hydrogen/iron compounds under high pressure [128].

2.5.5...ANOMALOUS SOLUBILITY DATA

Figure 1 which shows the limits of solubility for hydrogen in iron cannot be used at temperatures below 400C [50,129] where most anomalies occur and hydrogen shows its greatest embrittling characteristic. The solubility of hydrogen in iron, just like its location is very much affected by the thermomechanical history of the substrate. This means hydrogen can be trapped by the "damaged" parts of the substrate and be present in the metal in quantities which ideally it should not have exhibited .

Figure.6 shows a plot for the solubility of hydrogen in iron from several sources

[5,10,13,115,118,125,130-134].Evidently,asthe temperature decreases towards the 400°C threshold, more anomalies creep in, to the extent that a significant positive departure from linearity is observed. At lower temperature ranges, the divergence of the points is quite large, bordering on two orders of magnitude difference at room temperature. These experimental discrepancies have been analysed from different angles and there seems to be major contributory factors for such behaviour. These could be classified as:

(i) trapping effects

(ii) effect of alloying elements

(iii) the intrinsic nature of such behaviour

In the subsequent sections the evidence and the thinking behind each of the above will be elaborated.

(i) Influence of Trapping on the Solubility

Trapping effects are the result of interactions between hydrogen atoms and the unusually deep sites where the potential well encourages a higher concentration of hydrogen. Traps can be caused in several ways. Most commonly, cold work or other mechanical processes introduce dislocations as well as vacancies and voids into the structure. Therefore understanding of these defects relies on the knowledge of the thermal as well as mechanical history of the specimen. Traps can also be associated with such metallurgical factors as grain boundaries, impurities and alloying elements. Trapping at the surface sites

arising from the pretreatment or experimental procedures is also important.

At higher temperatures i.e. above 300°C the role of trapping from the internal traps is much less predominant. This is obvious since as Fig.6 shows (dotted line), vacancies are present at too low a concentration to be the effective mechanism within this temperature range [117]. Moreover Mclellan [14] calculates that the explanation of such deviations from Arrhenius behaviour in terms of internal defects alone, requires high concentrations and/or very deep trapping sites[14,135] of high binding energy, at least in the order of 30 kJ mol^{-1}. This entails the specimens being heavily cold-worked and inadequatly annealed which, on account of the reported information on the condition of the sample used, [13,16-20,22,136] is not the case. This raises the question of what sort of traps can escape the prolonged annealing pretreatments, or more likely could form as a result of faulty pretreatments. The presence of micro-voids and micro-cracks on the surface of heavily deformed metals is widely reported[106,139]. It has been shown that such defects could not be removed by vacuum annealing[137,138]. Work by Samuels [140] clearly shows that mechanical abrasion produces "Beilby" layers on the surface of metals. Such layers contain large concentrations of voids and dislocations, again not removed by the annealing. Therefore, a pretreatment in which the annealing precedes the mechanical polishing could prove a good

source of uncompensated damage, enough to cause most of these anomalies.

Kuchi and McLellan[117] are of the opinion that only those data which are obtained with electrochemically polished samples prior to hydrogenation could guarantee error free results. This argument is supported by the low temperature solubility measurements which show the the lowest solubility when the membranes were electropolished as part of their pretreatment and the results closely follow the calculations based on the Arrhenius formulae for solubility [10].

The corollary so far is that the change of hydrogen solubility in iron with degree of cold work depends on the concentration of lattice defects thus introduced and their interaction with hydrogen[117]. Non-equilibrium or unsaturable traps such as screw dislocations are usually removed upon annealing, accompanied by the formation of secondary defects or, at high temperatures, recovery [98]. These complex phenomena are a function of annealing temperature and time. However, at sufficiently low temperatures it is possible to consider the system Fe/H/Defect as representing a quasi-static equilibrium and treat the defect thermodynamically. The traps discussed here, therefore, are the stable type associated with dislocations, voids or grain boundaries [21], the only proviso being that the data should have been obtained

from electrochemically polished samples to remove the defect-rich surface layers[13,139].

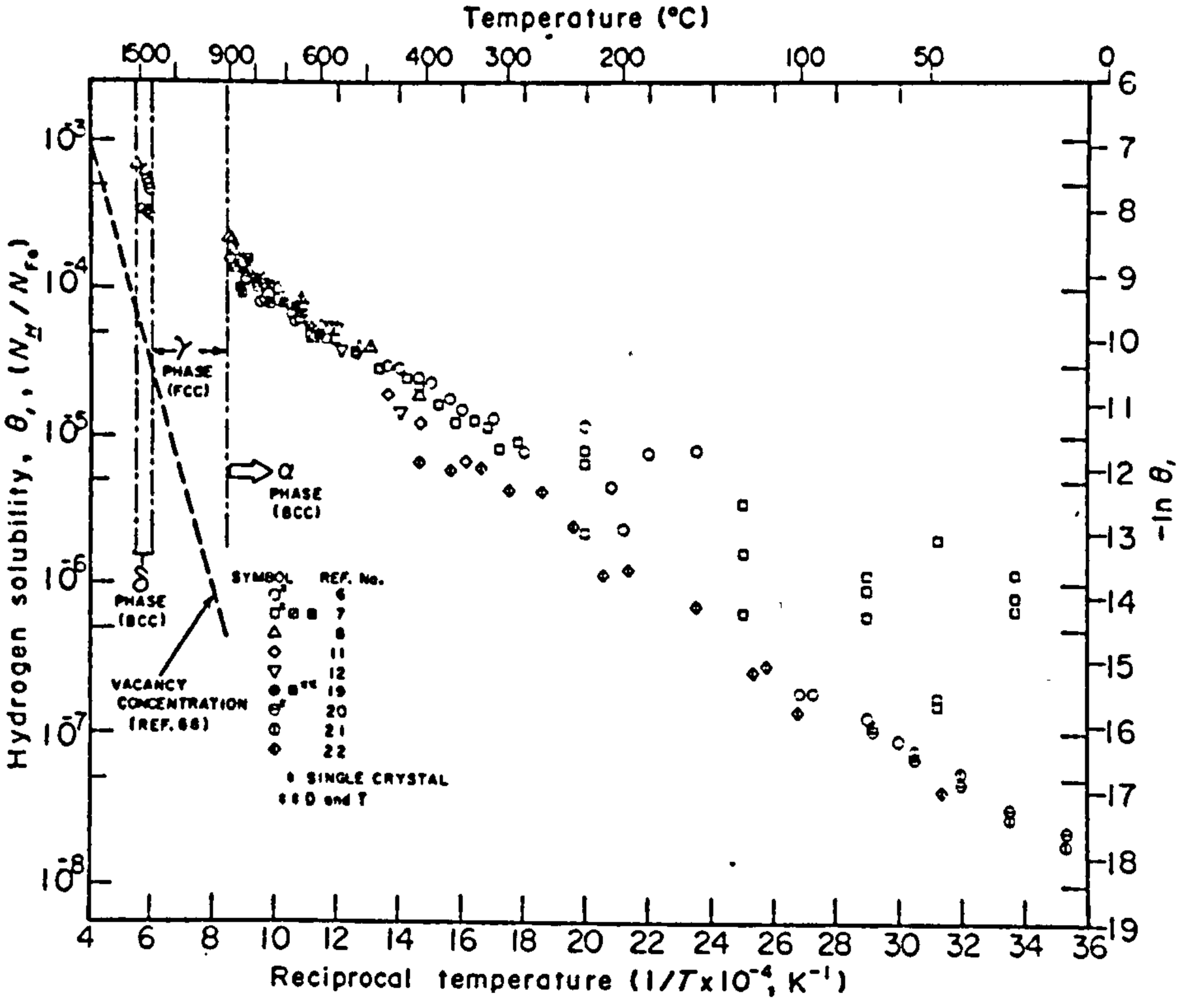

Fig.6 Solubility data for hydrogen in iron illustrating the scatter of data specially at lower temperatures[117].

An iron sample containing "N" atoms will have "N Φ" internal trapping sites if "Φ" represents the density of the trapping sites in relation to the total number of iron atoms. Of the "N " hydrogen atoms, "N_T" are located in defect sites and "N_L" are in the normal lattice sites(i.e. tetrahedral sites at low temperatures). The distribution function for "N_T" and "N_L" dependence on temperature is a Fermi-Dirac type, given as [14]:

$$X = \frac{(N\Phi - N_T) \cdot N_L}{[N(1-\Phi) - N_L] \cdot N_T} \qquad (23)$$

and $X = \exp(\Delta G / kT)$ (24)

where ΔG is depth of the trapping site's energy well with respect to the normal tetrahedral site. If "$N\cdot\Phi$", and also $\Phi \ll 1$ i.e. the specimen is not heavily cold-worked to have an unusually high ratio of trapping sites, then equation(23) can be simplified to:

$$X = \Phi \cdot N_L / N_T \qquad (25)$$

ΔG in terms of enthalpy ($\Delta \bar{H}$) and the entropy of the solution ΔS is

$$\Delta G = \Delta H - T\Delta S \qquad (26)$$

Now assuming that ΔS is temperature independent within the chosen range, then the total hydrogen concentration in the cold-worked material $\Theta_H^{C.W.}$ is:

$$\Theta = \Theta \ [1+\alpha\Phi(\Delta \bar{H}/kT) \qquad (27)$$

where

$$\Theta = (N_T+N_L)/N \qquad (28)$$

$$\alpha = \exp(-\Delta S/k) \qquad (29)$$

$$\Theta = N_L/N \qquad (30)$$

Using this mathematical modelling for solubility in the defect bearing substrate, the binding energy of the trapping sites is calculated as 33.9 kJ mol^{-1}. Yamakawa et al using direct transmission electron microscopy and correlated X-ray diffraction techniques [13], measured the true dislocation density " Φ'" within a cold-worked mild steel sample. Using their data, the value "$\alpha\Phi$" is calculated as $2.04\times10^{-16}\Phi'$. Assuming that each line of dislocation yields one trapping site per unit cell length along the dislocation line, then the number of such sites per metal atom is:

$$\Phi = \Phi' \, d.N_A / a.M \qquad (31)$$

where d = density of iron g/cm^3

N_A = Avogadro's number, 6.02×10^{23} mol^{-1}

a = lattice parameter of iron

M_{Fe} = atomic weight of iron

This calculation yields the result $\Phi = 4.31 \times 10^{-16} \Phi'$, which is in good agreement with the calculated value above[117]. The value ΔH calculated from these data also compares well with the reported estimates for this property, by Kumnick and Johnson [141] ,59.9 kJ mol^{-1}, Gibala[109], 26.79 $kJmol^{-1}$ and that given by Oriani [106], 27.2 $kJmol^{-1}$.

(ii) The Influence of Alloying Elements on Trapping

The endothermic characteristic of hydrogen dissolution in iron and steel, presents difficulties in the study of the influence of alloying constituents on its solubility. An impurity element with exothermic heat of solution will therefore influence this positively[129].Since the γ-phase is more accommodating for hydrogen, those elements which have a stabilizing effect on the austenitic phase tend to enhance the solubility as well[142]. Any secondary phase precipitation i.e. carbide, oxide, nitride etc can also lead to a larger increase in solubility [143-145]. Alloying elements can exist inside the metal in different forms. Such an atom can be a solute, segregated atom at grain boundaries, a precipitated compound with iron itself, or other impurity, etc. Each of the above has different characteristics when it

comes to enhancing or retarding hydrogen solubility. Figure 7 illustrates the effect of different alloying elements on hydrogen solubility in molten iron.

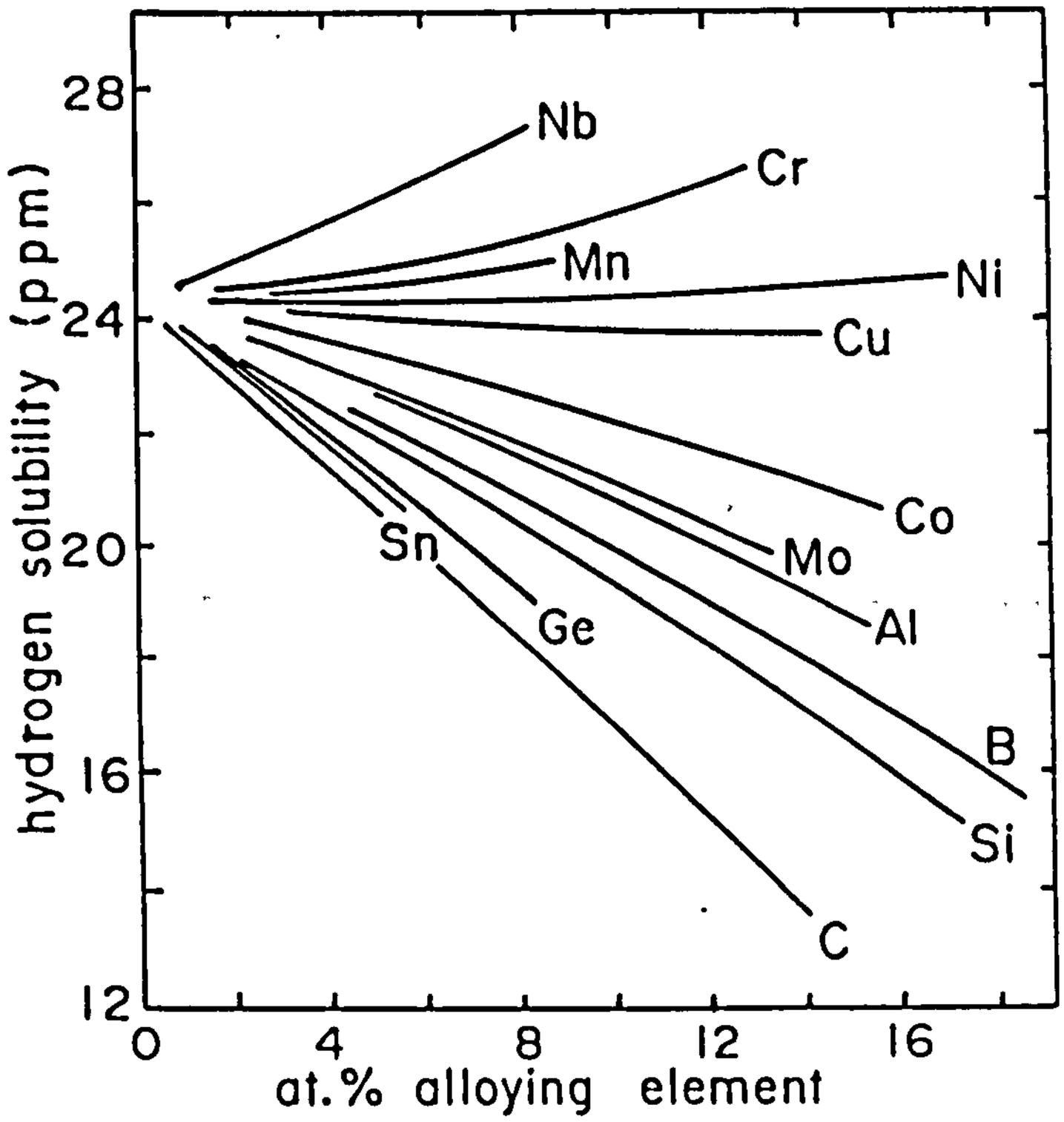

Fig.7 The solubility of hydrogen in various binary alloys of iron in molten phase after [146].

Here, as the state of these alloying elements is doubtlessly the solute form,drawing conclusions becomes much easier.The data depicted in Fig.7 can be explained in terms of electronic forces between hydrogen and iron atoms. As it is generally assumed, hydrogen, upon dissolving in iron and steel, gives up its excess electron to the electronic cloud of its host, any element that could cause an electron vacancy in this collective electron gas is bound to stabilize hydrogen. It does this by helping the hydrogen atom to achieve local neutrality. The impurities to the left of iron in the Periodic Table, act as such and their

effectiveness depends on the relative position in the Periodic Table with respect to iron.

So, Nb or Cr have much more enhancing power than say Cu. The same applies to the elements to the right of iron. Sulphur, phosphorus and carbon are all repellants of hydrogen in molten iron. The formulation of these attractive or repulsive characteristics is based on the concept of interaction energy ϵ_i^H, the interaction energy between hydrogen and a foreign atom (i).

The sign and magnitude of ϵ_i^H ,interaction coefficient dictates the relationship between H and the atom (i) in an iron substrate.

$$\ln \gamma_H = \text{LN } \gamma_H^{\bullet} + \sum \epsilon_i^H \cdot X_i \qquad (32)$$

where γ_H= activity coefficient for H in presence of (i)

$\gamma_H^{\bullet}$= activity coefficient for H without (i)

X_i= atom fraction of the element (i)

When $\epsilon_i^H < 0$ an attractive force exists between H and (i), where an $\epsilon_i^H = 0$ indicates no interaction between them . A positive ϵ_i^H , predicts a repulsive force between the hydrogen and the alloying element.The picture is not so clear as far as solid iron is concerned. Here many mechanisms act together and therefore a simple electronic model is inadequate. For instance C, Si, Mn, Cr are reported to enhance the solubility of H in solid iron, in that order[147], which is in contrast to the above mentioned model. A comprehensive model should

therefore take into account the chemical affinity of H for the particular alloying element, the electron/atom ratio and density of states at the Fermi level (see section 1 also), in order to be able to explain many seemingly contradictory results.

The other very important factor in explaining the role of impurities is the role of oxygen. The penetration of oxygen cannot be inhibited. *E*ven under ultra-high vacuum annealing conditions , absorption is observed at 10^{-8} Pa. In the case of normal vacuum (10^{-3} - 10^{-4} Pa), the surface coverage by active oxygen reaches unity.

It is notable that Fe, Co, Ni which show anomalously high hydrogen solubilities at low temperatures all exhibit an increasing solubility for oxygen in the order Fe(0.01 at%O_2) , Co(0.03 at%O_2) , Ni(0.05 at%O_2) which exactly replicates their degree of exhibited anomaly for hydrogen solubility. The proposed mechanism is that absorbed oxygen acts as an inhibitor toward grain boundary diffusion by hydrogen, leading to enhanced retention of hydrogen there. However, since the role of grain boundaries in hydrogen diffusion is still unclear [111], this explanation may be only partially true.

(iii) Anomalous Intrinsic Hydrogen Solubility Due to Interactions of Hydrogen and Iron

The assumption that the behaviour of hydrogen could and should be explicable by some Arrhenius type equation has been around for some time. Many unfruitful attempts to find a consistent single relationship to establish the desired linearity have been made. The consideration given to the literature in this review so far has been concerned with bringing down the range of scatter to a manageable level, by discarding those data which were obtained by questionable specimen preparation methods.

However, even the most reliable and self-consistent of data seem to suffer from a non-linearity at around 200C [117,51] which leads to a definite departure from Arrhenius-type behaviour. Figure 8 shows the data chosen for their conformity to the selection rules which should minimize the spurious surface effects.

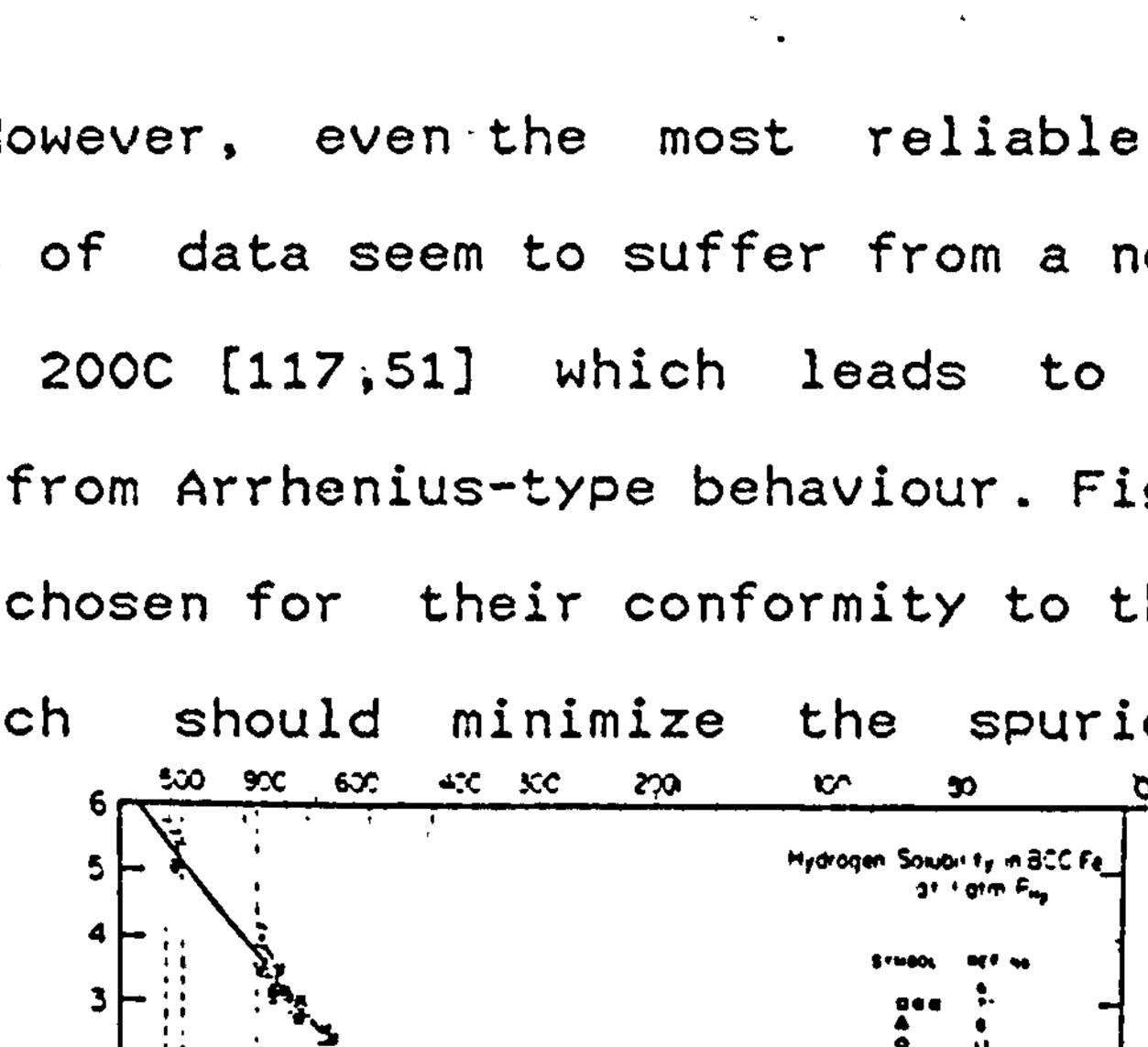

Fig.8 Selected solubility data conforming to the criteria for surface independent results [117]

Mclellan and Sutter[148] using the same criteria were able to detect similar curvature for hydrogen solubility in nickel. In this case, they have argued that the dissolved hydrogen atoms act as harmonic oscillators, jumping between different energy states due to temperature variations. Therefore, the intrinsic interactions between isolated hydrogen atoms (and thus concentration independent) and the nickel lattice seems to be the only valid explanation for such non-linearity.

The other explanations such as interaction between hydrogen atoms and the trapping sites require trapping locations of such depth and/or concentration which would be unreasonably high.The notion of H-H pairs or higher order clusters of them are also rejected on the basis of the lack of corresponding anomalies for the diffusion measurements.

deSilva and McLellan [115] propose a cloud occupancy mechanism for hydrogen in iron which hydrogen atoms in the form of bond oscillators interact with the interstitial sites. At low temperatures, the tetrahedral sites are exclusively occupied;but as the temperature increases, more octahedral sites are engaged and this could account for the increase in entropy at elevated temperatures. They have also formulated the chemical potential (partial molar free energy) for dissolved hydrogen in the substrate as:

$$\mu_H = \frac{\Theta_H^{mix.}}{\left\{\beta_{oct.}/\beta_{Tet.}\ \exp(\Delta\bar{H}/kT)\ \exp(-\Delta\bar{S}/k+1)\,\beta T\right\}} + \bar{H}_H^{Tet.} - T\bar{S}_H^{Tet} \quad (33)$$

is given before and the parameters are as described in equation(16). Here the change in $T, \Delta\bar{S}$, β and $\Delta\bar{H}$, $\Theta_H^{mix.}$ is such to minimize μ_H. They conclude that the deviation observed in the H-Fe system is a natural phenomenon rather a discrepancy.

2.6.....TRAPPING

2.6.1...INTRODUCTION

In the preceding sections reviewing both the solubility data and the preferred location of hydrogen, it has been shown that these properties exhibit such a degree of inconsistency that explanations and terms of the conventional Arrhenius models are rendered untenable. Such difficulties necessitate the introduction of more complex approaches by incorporating the concept of trapping.

Although it is Darken and Smith [149] who are credited to have coined the term"trapping"through their observations on hydrogen uptake by cold-worked iron in 1949, there seems to be an earlier explanation of such phenomenon by Smith[150] in his "rift theory". Smith

assumes the hydrogen to be accommodated in lattice discontinuities or fissures, called rifts. Moreover, contrary to Darken and Smith, this theory also gave an account of such "rifts" which were supposed to be permanent structural damage in the sublattice, extending over many interatomic distances.

Later on, density measurements studies by Keeler and Davis [151] led to the hypothesis that the traps in question could be voids filled with hydrogen gas. However, they rejected this idea on the grounds that such cavities will have hydrogen pressures of 500 atm or more which they thought unattainable for the trapped hydrogen in equilibrium with an atmosphere of hydrogen gas at 1 atm pressure. The idea of voids, either macro or micro size, to be the cause of abnormal behaviour of hydrogen in iron and steel at low temperatures was revived by the work of Bockris et al[16] who showed its effectiveness in explaining the initiation and propagation of cracks. Concentrating on the diffusion problem in steel below 400°C McNabb and Foster[152] modified Fick's laws of diffusion to present a mathematical model for the behaviour of hydrogen. This model was subsequently modified by Oriani [106], and many other workers to take into account different aspects of the hydrogen-trap interactions. The most important contribution to this topic has been made by the introduction of detailed analysis of different trap types as well as their retention energies.This has developed a predominantly thermodynamic argument into

one with clear kinetic features which can, not only complement the former but also has opened exciting routes to alloy design for reduced susceptibility to hydrogen embrittlement.

2.6.2...TRAPS AND ANTI-TRAPS

The common notion that hydrogen is simply immobilized in its journey through a metal matrix as it approaches a trap is misleading. The best analogy to explain hydrogen-trap interaction is a vehicle travelling on a hilly road. The probability of an atom of hydrogen jumping into a new.site is represented by the vehicle's speed which decreases as it tackles an upward slope, remains constant during cruising on an even course and markedly increases on a downhill slope. In such a model the even part of the road represents the undamaged lattice sites (ie tetrahedral or octahedral sites) while the downward slope a trap and the upward slope an anti-trap.

2.6.2.1.Traps

When a hydrogen atom jumps from a normal lattice site into a trap, the probability of an eventual return to its former site is reduced. The degree of this reduction depends on the temperature and binding energy of the trap as well as its type.The reasons for a jump probability modification leading to trapping of hydrogen are two fold [153]. Either there exists a force that pushes the hydrogen in a preferred

direction and by implication makes the backward movement less likely, or the lattice matrix in which the hydrogen moves is distorted so that the energy barriers are modified. The former case is labelled an "attractive trap" and the latter a "physical trap".Like most phenomenon these represent the two extremes of a spectrum within which the majority of normal traps are located somewhere in between the extremes and as such are called "mixed traps".

(i) Attractive Traps

Figure 9 represents the potential energy diagram for an attractive trap.The height of the successive energy barriers(E) is constant while clearly there is an energetic incentive (ΔE) for any hydrogen atom moving from A to B or C.

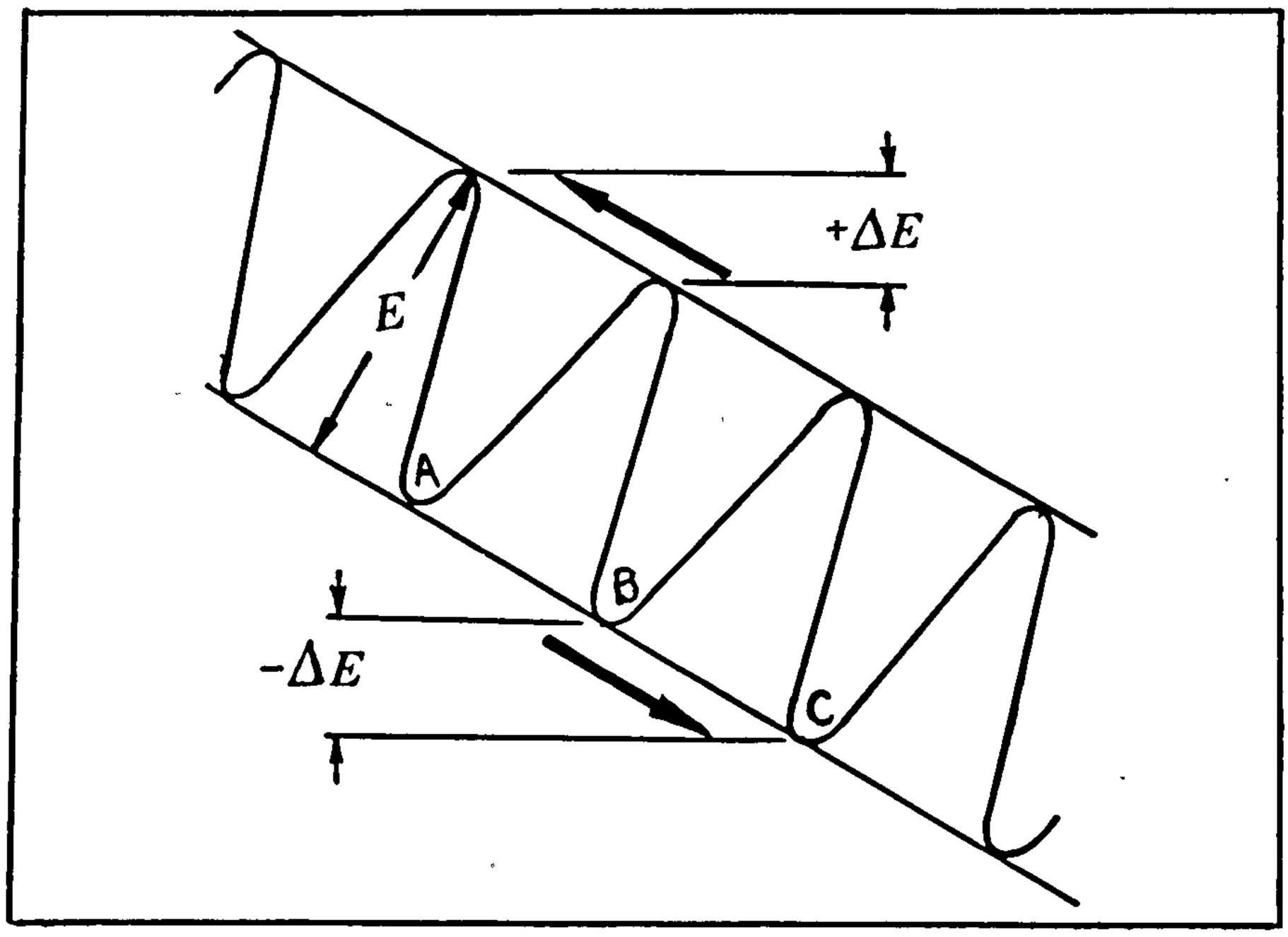

Fig.9 Schematic of energy steps characterizing the role of attractive forces on hydrogen diffusion[153].

The four forces acting on a diffusing atom through a crystal lattice are:

(a) electric fields

(b) stress fields

(c) temperature gradient

(d) chemical potential

Each of the above can be operative in an attractive trap.In the case of electric fields, dissolved hydrogen in transition metals gives up its excess electron to the collective electron gas of the metal to become a screened proton. Any defect that introduces an electron vacancy in the cloud will attract the wandering hydrogen as it provides the prospect of local electronic neutrality to the benefit of both component species. This is a broad definition of an electrical force [154] and has been detected in the case of impurities to the left of the host metal in the Periodic Table.

The stress induced forces are the result of tensile stress fields which are generated through the presence of dislocations, grain boundaries and inclusions or fissure like crack tips. Obviously these represent some distortion of the matrix of the metal and hence such traps also have a physical character. Fig 10 show how the potential energy barrier height has made the possibility of C ⟶ B ⟶ A direction for a diffusing hydrogen atom extremely unlikely.

Forces due to the thermal gradient act principally as a result of changes in solubility .The solubility of hydrogen in iron decreases dramatically

as the temperature falls and as any metal in which a heterogeneous temperature distribution exists, establishes temperature gradients, the flow of hydrogen to the hotter zones occurs. The potential energy for such a phenomenon is shown in the Fig.9, provided that no phase transformation is experienced in the cooling process. A purely attractive trap will use any of the above forces to attract diffusing hydrogen and keep it therein.

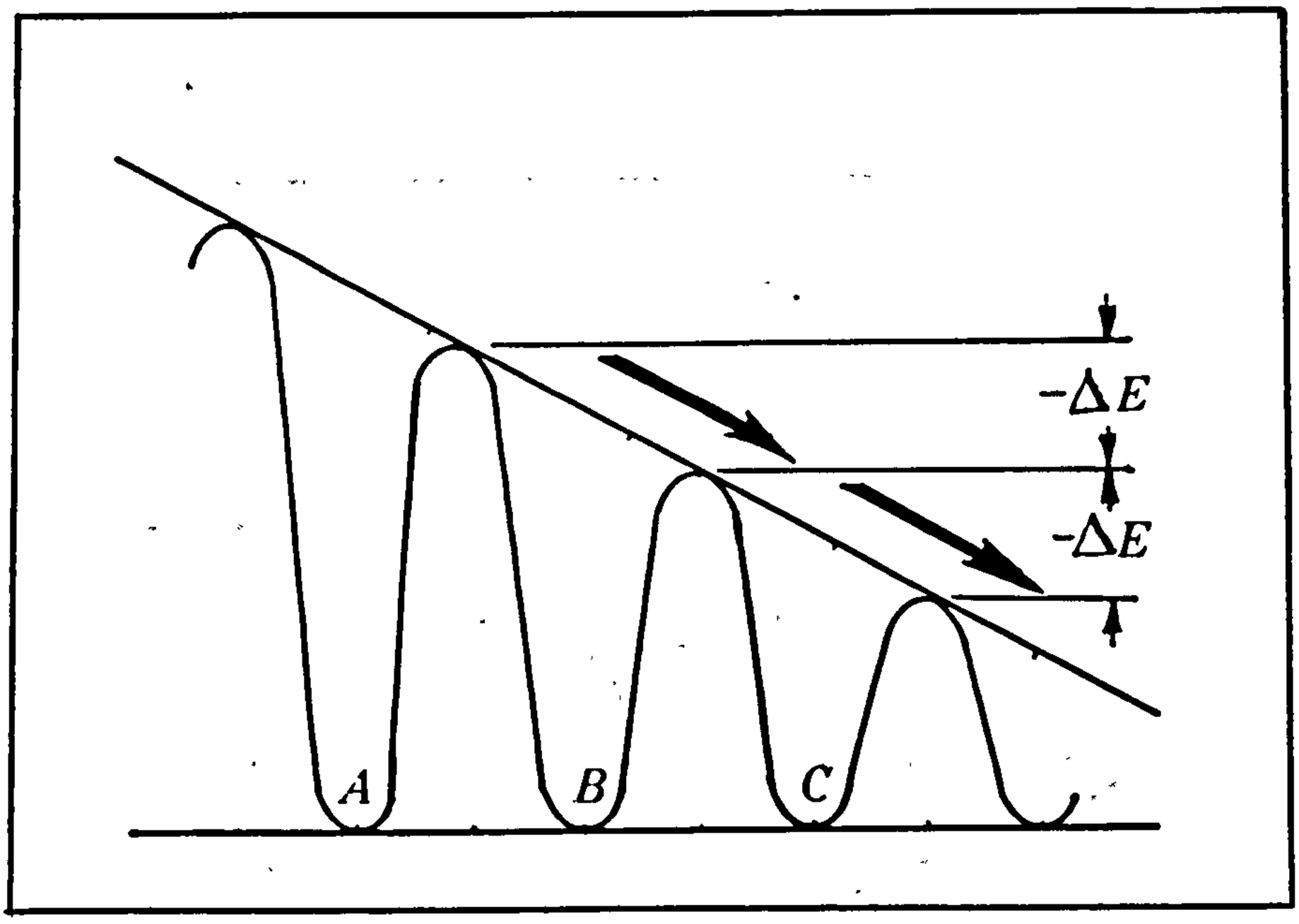

Fig 10 Illustrates the changes in the energy barrier of the metal matrix resulting from stress field[153].

The case of chemical potential difference is dealt with separately under the heading of "diffusion". It will be appreciated that this is the main driving force behind any natural diffusion process.

Fig.11 depicts an attractive trap in which,once the diffusing hydrogen reaches the trap's domain, it will be sucked into the centre of the inhomogeneity. A

convincing case for attractive traps is given by Pielaszek[155,156] who showed that in nickel substrates occluded with hydrogen, hydride nuclei are formed at places of preferential hydrogen occlusion, mostly dislocations. Due to the much larger lattice parameter of the hydride, a stress gradient is established across the hydride-nickel substrate interface. The stresses so induced,multiply and rearrange the dislocations as well as attracting the permeating hydrogen to that region. This ensures a sustained hydride growth although the overall H/Ni atom ratio is quite small.

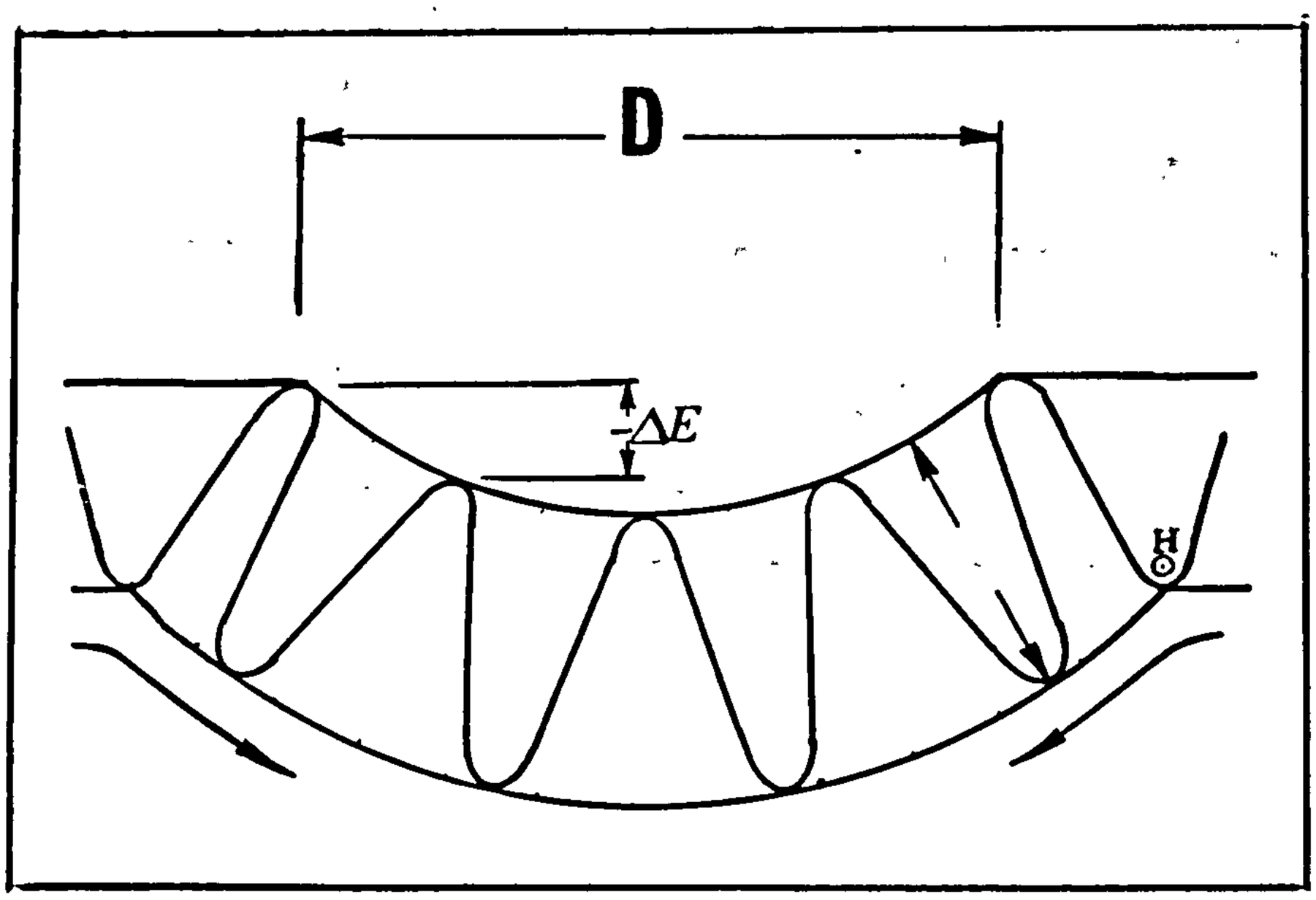

Fig 11 Schematic of energy barriers and the domain of an attractive trap.

(ii) Physical Traps

The nature of such traps are such that hydrogen is not sucked into, but rather falls randomly into one as a result of a single diffusion jump. Fig.12 shows such a trap where a hydrogen atom (A) has equal opportunity to jump to positions (B) or (C) but, once located in (C), energetically it is more favourable for

hydrogen to remain there. The kind of traps encountered in this category are: grain boundaries, particle-matrix interfaces, voids, and pile-ups of dislocations.

Generally speaking any modification of the ideal crystal lattice leading to structural damage creates this kind of energetically favourable site.

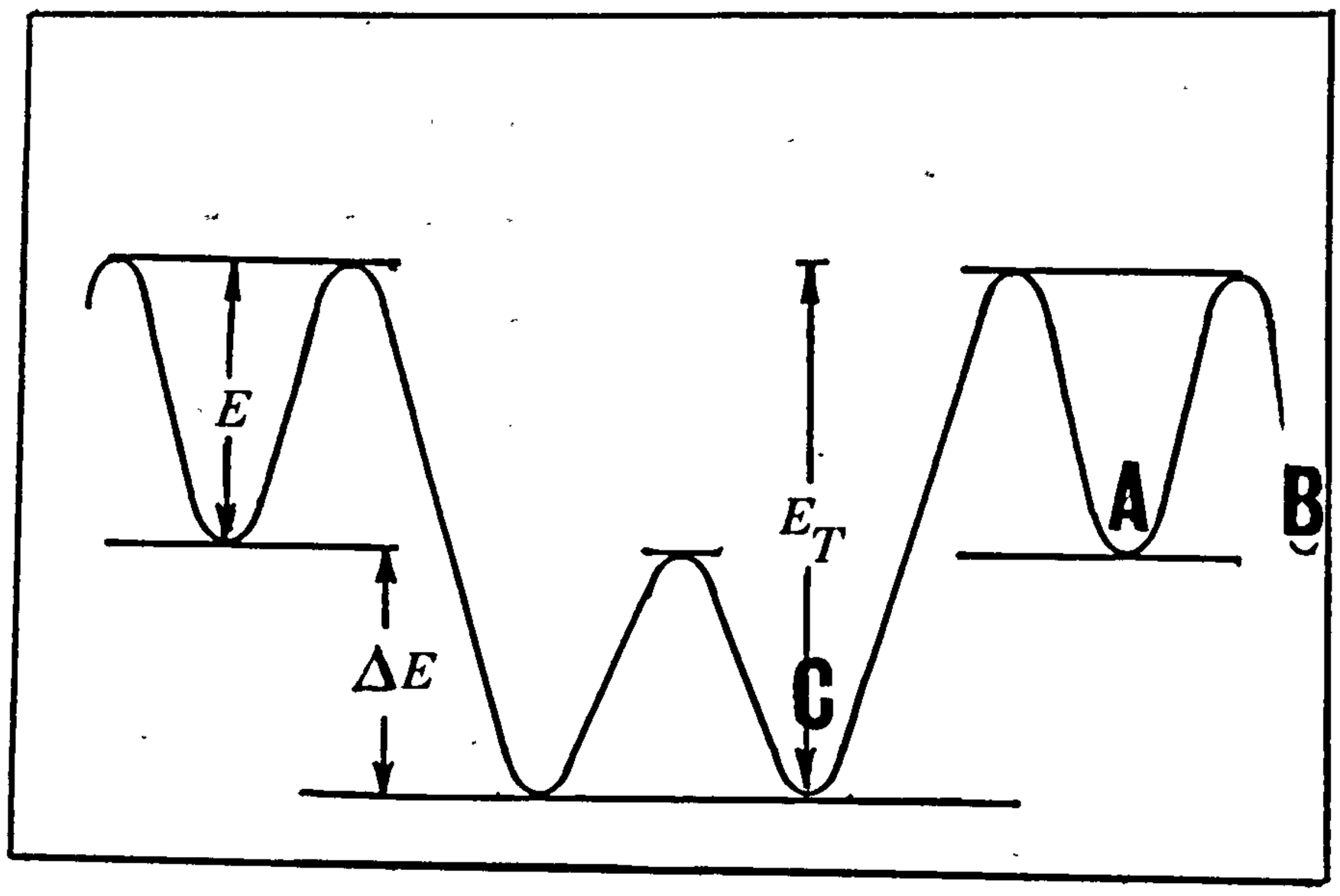

Fig.12 Schematic representation of a physical trap.

(iii) Mixed Traps

Needless to say, the presence of traps of an exclusively singular nature (physical or attractive) is extremely unlikely. The typical trap site shows a combination of these two characteristics as shown in Figure 13.The following examples illustrate this point. The electric field mentioned earlier as an attractive trap exists wherever there are physical defects present in the lattice. Another example of a mixed trap is an edge dislocation interacting with a hydrogen atom[153].

An attractive force could form as a result of a stress field accompaning a physical trap, due to the mechanical displacement of the neighbouring atoms . Fig.13 exhibits such a configuration and its effect on the energy wells of the adjacent sites.

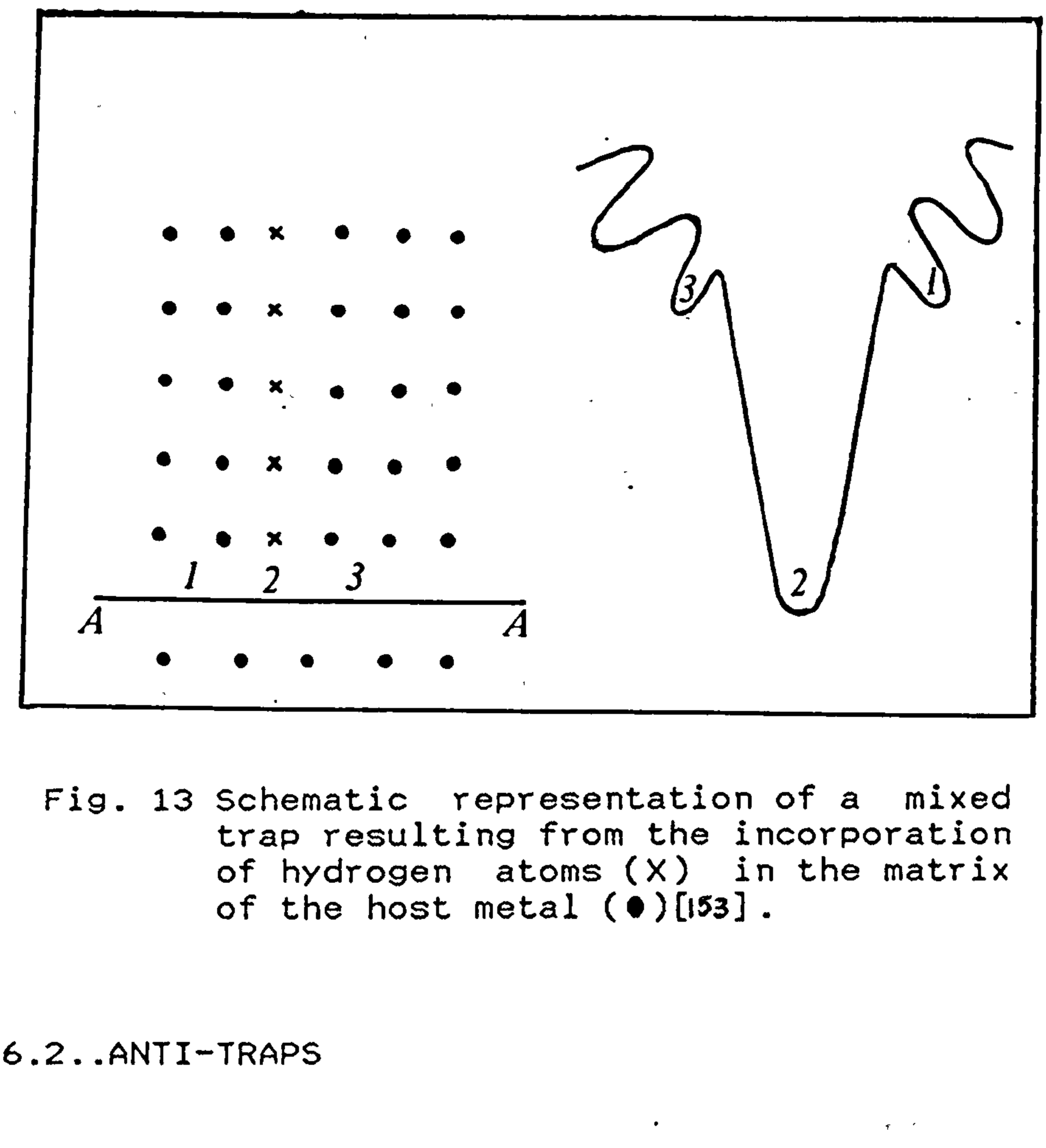

Fig. 13 Schematic representation of a mixed trap resulting from the incorporation of hydrogen atoms (X) in the matrix of the host metal (●)[153].

2.6.2..ANTI-TRAPS

In regions of the lattice where the potential energy of some sites is higher than that of normal sites, the anti-trap concept is operative. As in the case of traps, there can be either a gradual increase in the height of the energy barriers or an abrupt rise. The former is known as a "repeller" while the later is called an "obstacle". Fig.14 exhibits the potential energy wells of such anti-traps. Here again a purely

"repeller" or "obstacle" anti-trap is rare and mixed anti-traps are more prevalent. The physical examples of such anti-traps are interstitial or substantial elements to the right of the host metal in the Periodic Table which provides extra electrons to the conduction band of the host. This creates a repulsive electronic force against hydrogen atoms which need to shed their unpaired electron.

Elements like Cd, Ag, Zn, Cu, and metalloids such as S, P, As, Sb act in this way for an iron substrate. Any internal interface with adsorbed repellers (such as metalloids) can act as an effective repeller rather than a physical trap. On the other hand, any heterogeneity such as inclusion which do not dissolve hydrogen can be an obstacle while its interface with the host matrix will be a physical trap.

2.6.3...REVERSIBILITY OF TRAPS

A trap can hold on to its captured hydrogen providing that several factors act together. Such dependence constitutes the trap reversibility concept, the most important of which are the binding energy of the trap and its temperature dependence. A trap of binding energy, E, can keep a hydrogen atom as long as the chance of escape from it, "P", remains low. The temperature dependence of this can be expressed by a probability function:

$$P = k \exp(-E/kT) \qquad (34)$$

While T is low and E is high, the trapped atom will have little chance of escape. This constitutes an irreversible trap, examples of which are mostly physical such as voids, grain boundaries, cracks and particle interfaces in the metal matrix ie TiC, Fe_3C, MnS. Other factors effecting the reversibility of a trap are the mode of transport of hydrogen in the lattice (ie interstitial jumps,dislocation transport, short circuit paths etc) which indicates whether the hydrogen atom can attain sufficient mobility to surmount the relevant energy barriers and also reach the concentration levels which can change its nature from irreversible to reversible. This happens through a reduction in the retention strength of an irreversible trap, as the number of hydrogen atoms in it is increased.

The interaction of different traps with each other is another factor in establishing whether or not a trap is irreversible. Grain boundaries are nominally as effective as dislocations in binding the hydrogen while the interfaces of internal voids and/or nitrides and carbides with the matrix have bigger binding energies[157]. When dislocations make contact with such defects, chemical potential differences force hydrogen to leave the dislocation core and reside in the interface with a corresponding reduction in its free energy. Titanium is known to have a binding energy comparable with screw dislocations but not edge dislocations[157], so it can remove hydrogen from such dislocations. This clearly shows the importance of the

relative strength of the traps rather than their absolute values, when reversibility is considered. Reversible traps are extremely important for the understanding of hydrogen embrittlement phenomena and also its prevention since, if undetected, they could release hydrogen under favourable conditions to the propagating cracks.

Tables 1 and 2 are a comprehensive summary of different traps and anti-traps together with their bonding energies. The fact, emerging from the tables, that some elements could act as both traps and anti-traps, underlines the difficulties associated with both the trap identification and the possible use of these concepts in alloy design.

The corollary of this section is that the role of traps on the diffusion and solubility of the hydrogen in metals and alloys, as well as their influence on the susceptibility of iron and steel to hydrogen embrittlement and stress corrosion cracking makes the study of this phenomenon invaluable to both theoretical scientists as well as the practicing engineer. The concept of alloy design using traps, although very young, is a promising route which could provide a mechanism for counteracting some of the ill-effects of hydrogen.

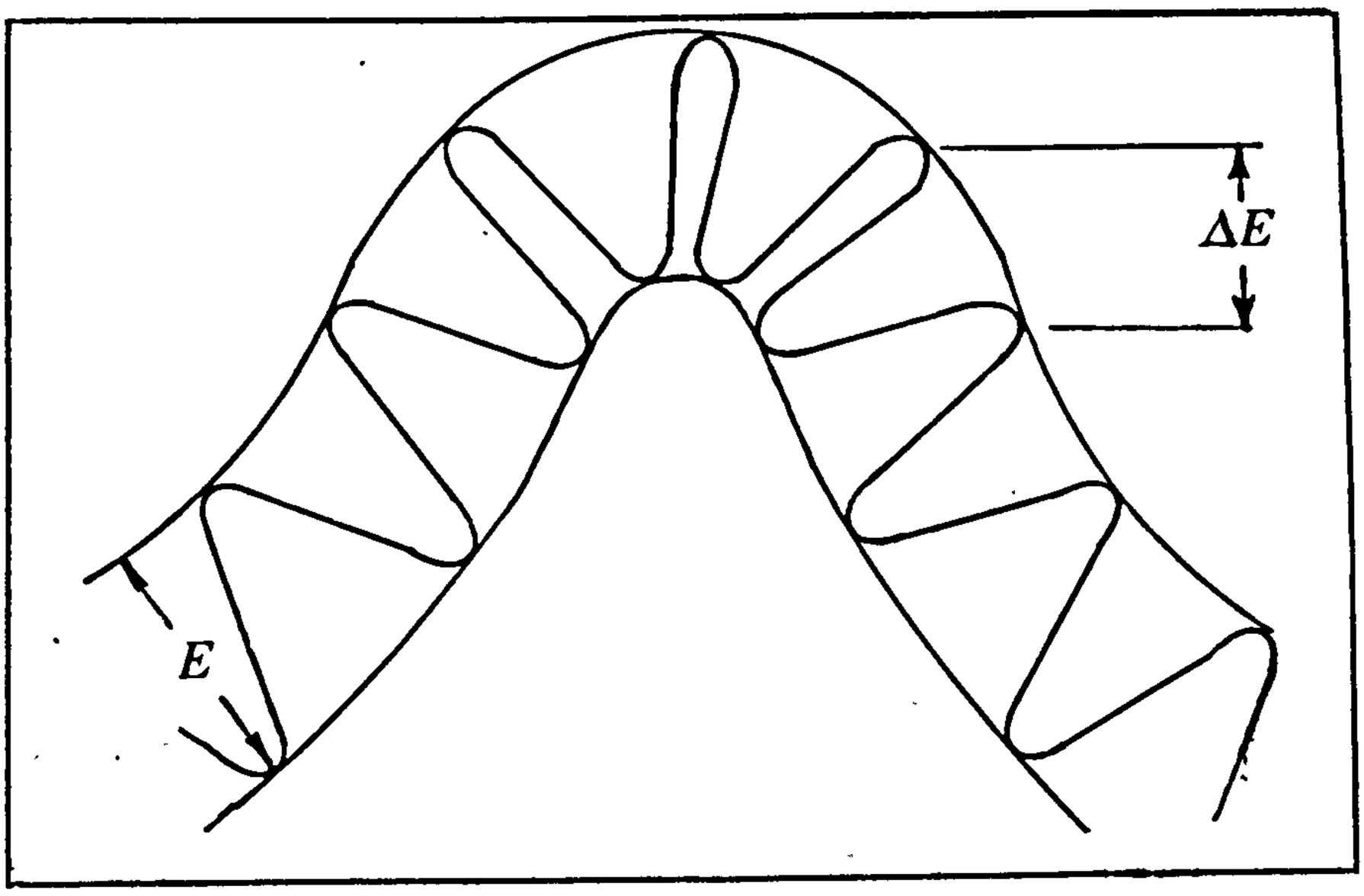

Fig.14 The energy diagram for a repellant anti-trap.

Table-1 Classification of anti-traps in iron

ANTI — TRAPS'		
TYPE	EXAMPLES	
punctual or atomic size	elements to the right of iron in the Periodic Table Co Ni Cu Zn Rh Ag Cd	elements with a positive interaction energy Cu Al Au Mo Rh Ga Co Ge O H B As W si Sb Sn C N S Ni Cd Pd Pt In P Ag
one dimensional (linear)	any row of atoms with a $\epsilon_H^i > 0$	
two dimensional (planar)	internal surfaces with layers of adsobed repellers such as metalloids.	
three dimensional (volume)	any foriegn particle which induces compressive stresses in the matrix and/or does not dissolve hydrogen.	

Table-2 Classification of hydrogen traps in iron. After Oriani[158] and Pressoyre[153].

TYPE	EXAMPLES of TRAPS	E_T/ev	TRAP CHARACTER	DOMAIN OF INFLUENCE	REF.	TYPE	EXAMPLES of TRAPS	E_T/ev	TRAP CHARACTER	DOMAIN OF INFLUENCE	No. of TRAPS N_T
punctual or atomic size	elements to the left of Fe in the periodic table			only a few inter-atomic spacing		one dimensional (linear)	dislocation core (screw)	0.310	reversible	30 Å	10^{13} -10^{19}
	Mn	0.090	reversible				dislocation core (mixed)	0.610	reversible		$4x10^{13}$-$4x10^{19}$
	Cr	0.100	"								
	V	0.160	"								
		0.220	"								
			"				particle/ matrix interface				
	Ti	0.270	getting more irreversible			two dimensional (planar)	TiC	0.980	irreversible	diameter of the particle	$5x10^{18}$
		0.270					Fe C	0.870	"		"
		0.500					MnS	0.800	"		"
	Sc	0.710	"				AlN	0.670	"		"
	□	0.800	"								
	Ca	0.980	"				grain boundaries	0.270 to 0.800	reversible irreversible		10^{13} 10^{17}
	K	0.980	irreversible								
	elements with negative interaction energy						twins		reversible	a few inter-atomic spacing	
	Ni	0.083	reversible				internal free surfaces	0.720 to 1.00			10^{15}
	Mn	0.090									
	Cr	0.100		only a few inter-atomic spacing		three dimensional (volume)	micro-voids	0.540		dimension of the defect	volume dependent
	V	0.160					voids	0.300			
	Ce	0.160									
	Nb	0.160					particles (inclusions)				
	Ti	0.270									
	O	0.710									
	Ta	0.980	irreversible								

2.7.....DIFFUSION OF HYDROGEN IN IRON

2.7.1...INTRODUCTION

The movement of a foreign atom inside the matrix of a host media constitutes a diffusion phenomenon. The diffusivity of hydrogen in metals is generally high. For example, in the case of vanadium at ambient temperatures, $2x10^{12}$ jumps/sec/atom of hydrogen are observed [197]. This mobility becomes even more striking when it is compared with some interstitial diffusants like N, C, O for which in this same media and temperature, diffusion coefficients 15-20 orders of magnitude lower are found [160]. Explanation of such phenomenon requires a fundamental understanding of the diffusion process, as well as the establishment of a frame of reference within which the theory could be evaluated.For hydrogen, the mechanism by which it moves within an iron lattice has not as yet been thoroughly elucidated.As a result, there is a large scatter in the result, as evident in Fig.15 for hydrogen diffusion coefficient measurements in bcc iron which could be attributed to both a poorly defined frame of reference as well as an inadequate theory. Owing to these factors a host of hypotheses have been suggested as the possible cause of this scatter as well as numerous Arrhenius type equations associated with each set of data.

2.7.2...THEORY OF HYDROGEN DIFFUSION

Table 3 lists some of the available Arrhenius type expressions in the literature based on the data collected for the Fe-H system.None of the proposed models covers the entire range of temperature from ambient to the molten state. In his overview of the subject Kehr[161] attempts a possible explanation of the extreme mobility of hydrogen and its anomalous behaviour through a multi-regime diffusion mechanism. This has been illustrated schematically in Fig. 16.

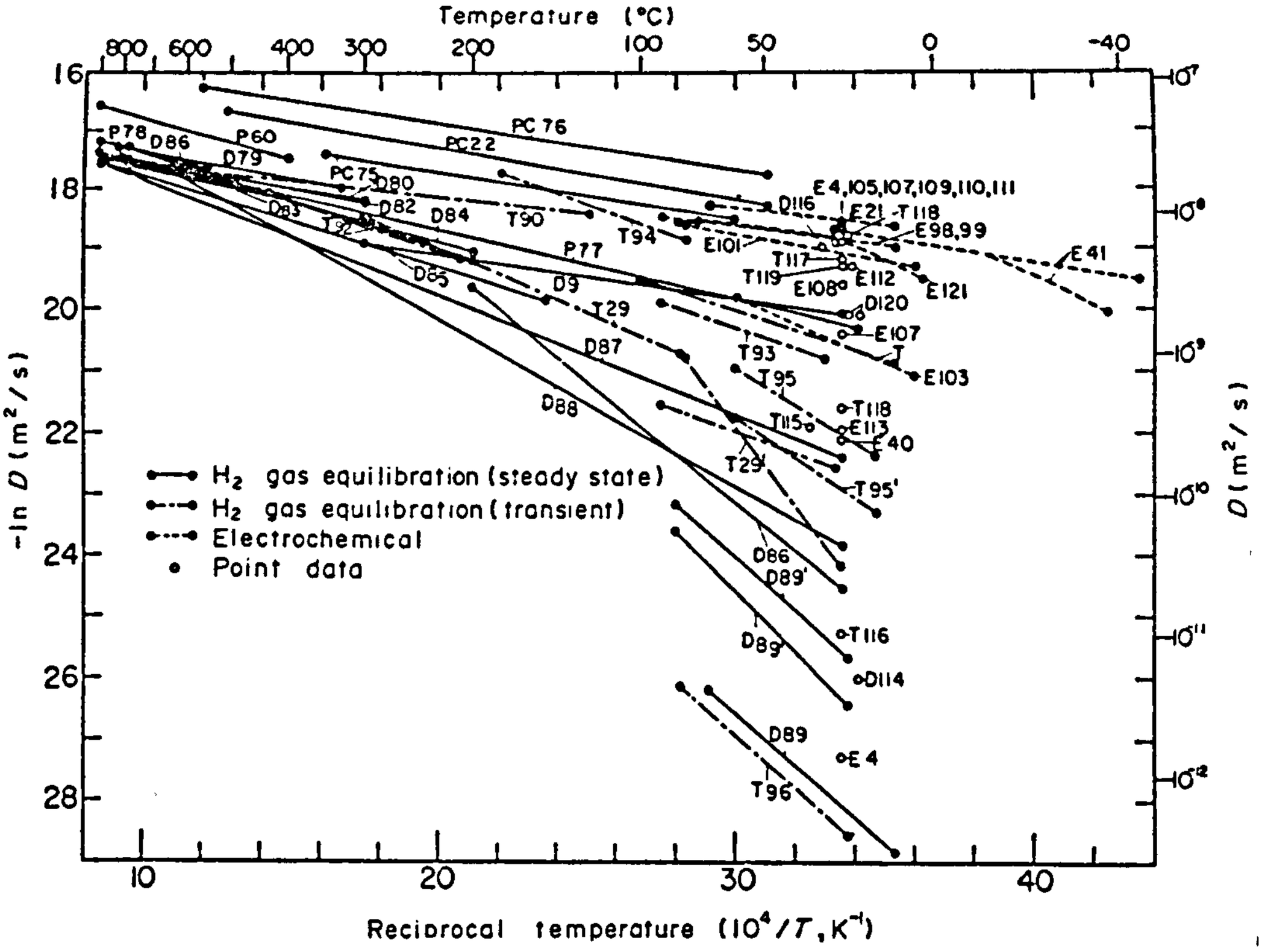

Fig.15 Graphic representation of the scatter encountered in the diffusivity measurements by different workers[117]

The hypothesis relies on the wave-like movement of hydrogen which resembles that of a muon or an electron, due to the minute size of the dissolved proton. This implies a lower bonding energy between normal lattice sites and the hydrogen atoms as well as the

Table-3 Diffusion coefficients for hydrogen in α-iron[117].

METHOD of ANALYSIS	D_{298}/m^2s^{-1}	ACTIVATION ENERGY kJ/mol	FREQUENCY FACTOR $D_o/m^2 s^{-1}$	TEMPERATURE RANGE K	FLUX MEASUREMENT TECHNIQUE	SPECIMEN PURITY	SURFACE PREPARATION	YEAR
H_2 gas equilibration technique	6.75E-9	6.70	1.01E-7	342-619	steady state permeation	99.9%	Pd coated	1975
	1.58E-8	6.70	2.30E-7	320-833		zone refined	"	1972
	9.27E-9	7.07	1.61E-7	322-779		"	"	1978
	1.61E-9	9.54	7.60E-8	293-1073		"	"	1947
	1.30E-9	10.80	1.02E-7	823-1173		pure Fe	-	1959
	1.64E-9	12.10	2.17E-7	623-1173		-	-	1950
	4.45E-9	5.86	4.74E-8	599-1089		-	-	1971
	1.87E-9	6.03	2,14E-8	298-573		pure Fe	-	1975
	3.54E-9	6.53	4.95E-8	298-878		-	-	1958
	-	7.70	-	473-973		99.98%	-	1969
	2.50E-9	8.04	6.42E-8	573-1173		-	-	1966
	1.05E-9	9.17	6.70E-8	703-1000		Armco iron	-	1969
	9.72E-10	11.30	9.30E-8	473-1047		99.96%	-	1958
	5.04E-10	12.80	8.85E-8	423-1173	desorption	99.9%	-	1956
	6.26E-10	13.40	1.40E-7	423-1083		-	-	1960
	1.80E-10	16.10	1.20E-7	298-1173		-	-	1958
	4.32E-11	22.40	3.65E-7	298-923		99.9%	-	1961
	2.22E-11	32.70	1.20E-5	298-437		99.996%	-	1960
	6.39E-13	35.60	1.10E-6	283-343		99.67%	-	1969
	7.67E-12	36.20	1.70E-5	296-357		98.6%	-	1969
	3.59E-12	40.80	5.10E-5	296-357		99.67%	-	1969
	6.24E-9	4.52	3,87E-7	299-357		98.6%	-	1963
	1.15E-9	13.00	2.20E-7	283-966		99.9%	-	1970
	5.33E-10	13.70	1.42E-7	282-373		-	-	1964
	2.38E-10	13.80	2.20E-7	303-363		99.8%	-	1961
	2.42E-9	15.10	1.10E-6	353-450		-	-	1966
	3.12E-10	17.60	3.80E-7	353-573	transient	99.8%	-	1977
	2.74E-10	24.80	6.10E-6	228-333		-	-	1970
	1.19E-10	27.20	6.50E-6	293-333		Armco Fe	-	1970
	4.39E-9	36,50	1.10E-6	296-353		iron B	-	1940
	1.31E-10	69.10	1.70E+1	298-353		-	-	1977
	1.55E-10	14.30	5.00E-8	298-363		-	-	1958

Table- 3 Continued

METHOD of ANALYSIS	D_{298}/m^2s^{-1}	ACTIVATION ENERGY kJ/mol	FREQUENCY FACTOR D_o/m^2s^{-1}	TEMPERATURE RANGE K	FLUX MEASUREMENT TECHNIQUE	SPECIMEN PURITY	SURFACE PREPARATION	YEAR
	8.72E-9	4.86	6.20E-8	283-343	adsorption	-	-	1981
	6.33E-9	5.57	6.00E-8	283-348		single crystal	Ni plated	
						99.9%		1966
	6.33E-9	5.57	6.00E-8	283-343		Armco iron	Pd coated	1965
	7.36E-9	6.70	1.10E-7	230-300		"	"	1978
electrochemical	-	7.03	-	283-333		single crystal	"	1978
					electrochemical			
	5.10E-9	7.49	1.05E-7	278-353		99.996%	"	1974
	6.07E-8	9.21	2.50E-6	283-343	adsorption/	-	-	1971
	1.15E-9	17.60	1.40E-6	278-333		99.8%	-	1974
	-	18.80	-	313-363	desorption	-	-	1973
technique	7.20E-7	5.60	7.60E-8	223-323		zone refined 99%	Ni coated	1980
					technique			
	4.43E-7	4.86	6.20E-8	283-343		single crystal 99.99%	Pd coated	1981
	7.36E-7	4.20	4.90E-8	223-323		99.99%	"	1981
	8.75E-7	1.76	4.3E-7	-		-	-	1982

possibility of quantum effects such as "tunnelling" between the adjacent energy wells leading to the direct occupation of a neighbouring site without acquiring the saddle point energy levels needed for a classical diffusion jump.

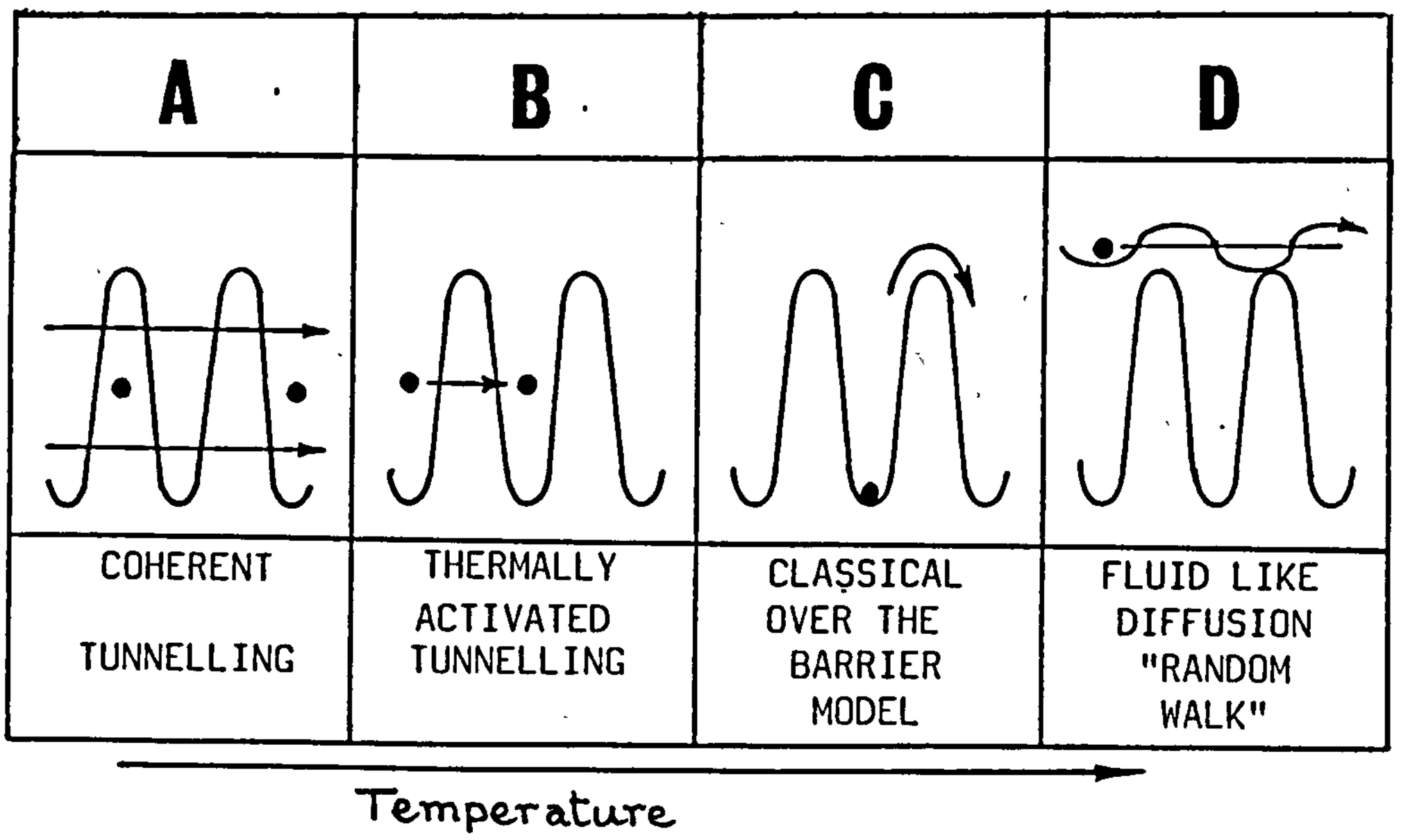

Fig.16 Diffusion processes of a light interstitial at different temperature levels.[161]

Figure 17 shows how a proton in a normal site could by-pass an intermediate energy barrier and settle in an adjacent site. The deep energy well (A) in Fig.17 could itself be the result of an important characteristic of hydrogen-lattice interaction, which is the relaxation of the matrix around the solute (H). The thermal fluctuations of the atoms of the host metal provide the activation energy required for the hydrogen to raise its energy level to that of its neighbouring site, but not to the saddle point energy point between the two

sites,and at this point the hydrogen atom simply tunnels its way through to the neighbouring site to occupy it, resulting in the relaxation of the lattice around it in the new position, this mechanism could operate only at relatively low temperatures [159,162], therefore,as the temperature is raised the classical "over the barrier" jump mechanism, should predominate.

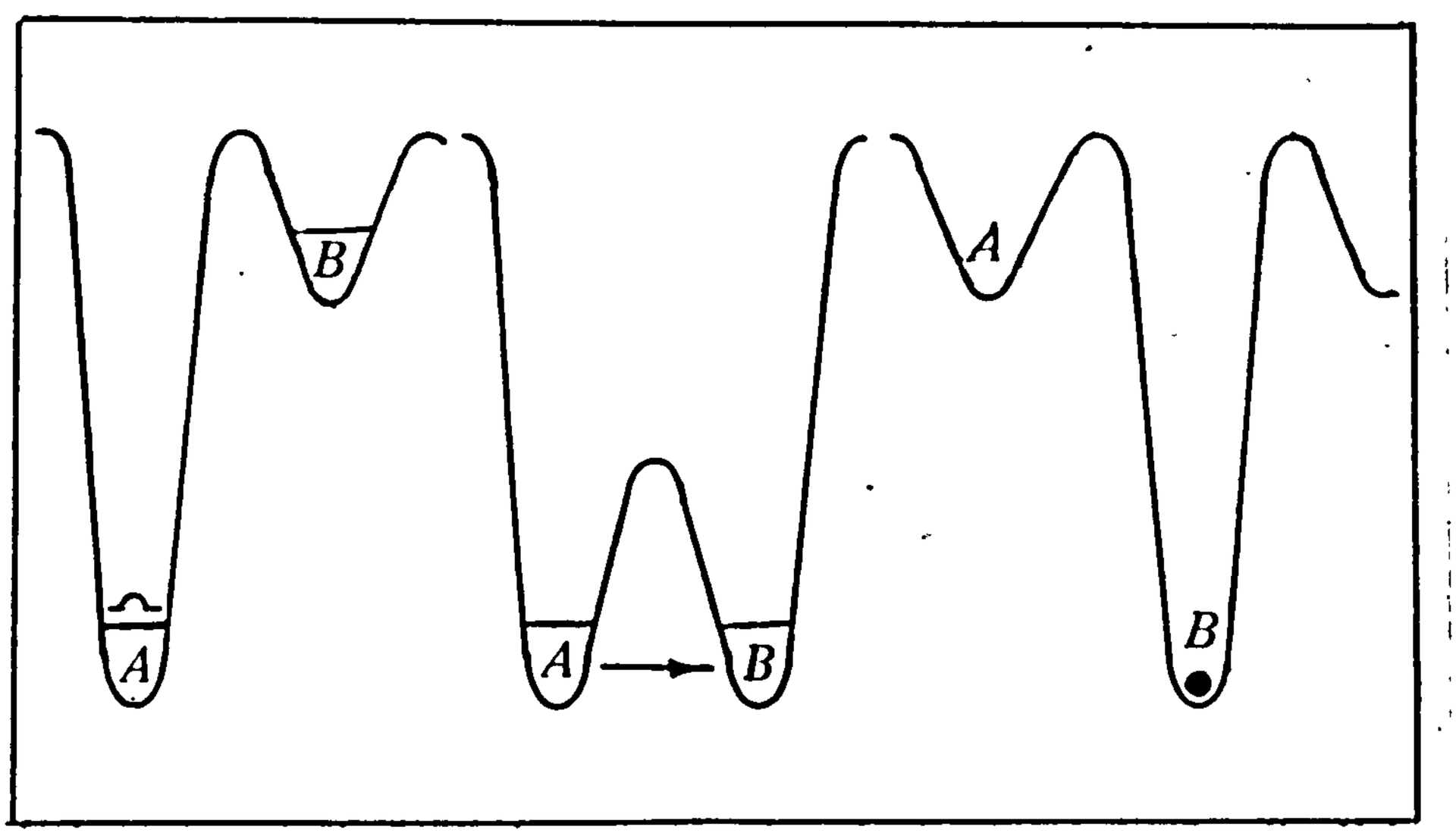

Fig 17 The tunnelling phenomenon for hydrogen in the site (A) leading to occupation of site (B)[161].

Since the relaxation time for the iron matrix is much longer than the duration of a single jump, the possibility of a single jump over several energy barriers should also be considered [163]. The dual occupancy model discussed in the earlier section provides yet another mechanism for explaining the kinetics of hydrogen mobility in iron. Fig.18 shows the tetrahedral and octahedral positions in an Fe crystal. de Silva et al [115] have shown that in the dual

occupancy model the proposed change from tetrahedral (T) to octahedral (O) occupancy with increased temperature, results in changes in the partial enthalpy and entropy of the system which in turn are reflected in the kinetics of the system. In a classical Arrhenius diffusion model, the T-T jumps are expected to be prevalent at low temperatures. As the temperature increases, O-sites become active and the hydrogen atom already in the T-sites has the option of T-T or T-O-T jumps; and if in an octahedral site, the O-T-O path is also possible.

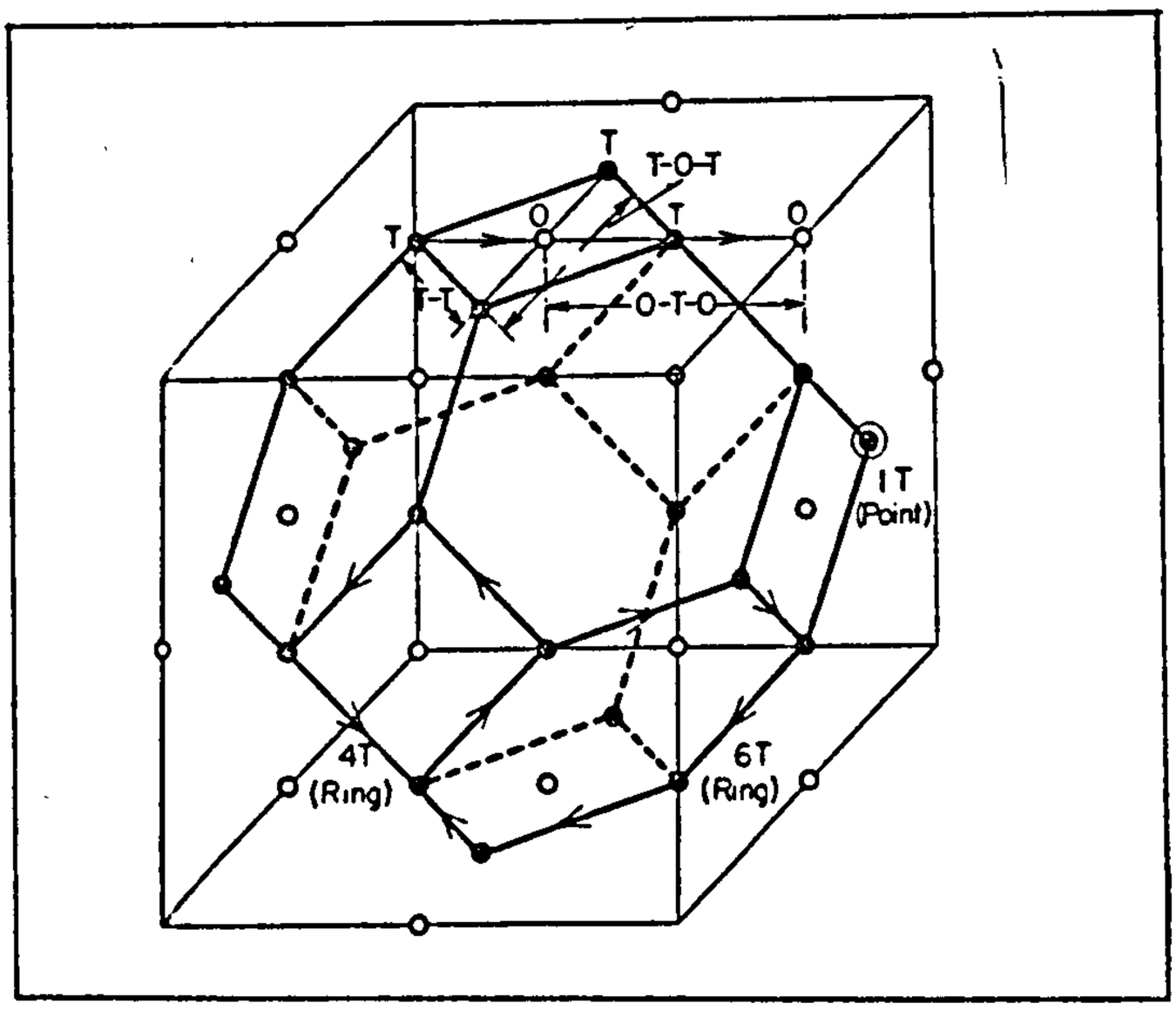

Fig 18 The octahedral and the tetrahedral positions in a bcc lattice. The T-T, T-O-T and the O-T-O jump paths as well as 4T and 6T ring jump paths[117].

The following equation (35) formulates the influence of such a dual occupancy mechanism on the lattice diffusion of hydrogen.

$$D_L = \Phi D^{T-T} + (1 - \Phi) D^{O-T-O} \qquad (35)$$

where

D_L =lattice diffusivity of hydrogen

Φ =fraction of hydrogen atoms using T-T path

Φ =fraction of hydrogen atoms using T-T path

D^{T-T}, D^{OT-O} =diffusivity of hydrogen atoms during the O-T-O T-T and O-T-O jumps.

Kuchi and McLellan[117], have shown it to be most consistent with the data sifted from spurious results. This model has also been complemented by an assortment of "chain occupancy" models [114,164] in which 4T or 6T rings are formed due to the long distance distribution of the hydrogen wave function. Richie et al [165] have discussed this phenomenon extensively.However the significance of the contribution made by such rings remains questionable since the energy difference between such configurations is very small i.e. 1-5 eV [114,164,167,168].

At still higher temperatures it may be too assumed that hydrogen behaves like a solute atom in a liquid or heavy gas since hydrogen moves as a band wave whose potential energy is well above that of the metal. This is known as fluid-like diffusion [161,169,170] and is mainly controlled by the number of collisions between the hydrogen and lattice atoms. Kedzierzawski [171] has compiled the following table for the possible mechanisms of the diffusion in metals. As discussed in section 6, the deviations in the solubility data arise

directly from spurious "surface effects". Kuchi and McLellan[117] are of the opinion that the diffusion data are also distorted due to such effects. Accordingly, they have been able to reduce the scatter in the accumulated data over the years by eliminating those sets of results for which sample preparations include heavy cold-work or mechanical polishing. However, this still leaves nearly two orders of magnitude difference between the lowest and the highest diffusion coefficient at room temperature to be explained. This requires more understanding of some fundamental interactions between H-H and H-lattice atoms.

2.7.3...FICK'S LAWS OF DIFFUSION

While the theories described earlier are more or less new, attempts in formulating the hydrogen mobility problem the best tool used by the majority of the workers in this field is still a direct form or modifications of Fick's laws of diffusion. The force behind any large volume diffusion process is the difference of chemical potentials of the diffusing species (μ) leading to establishment of the flux (J).

Table 4 The proposed mechanisms for hydrogen diffusion in iron.

MECHANISM	MODEL	D/T RELATIONSHIP
	Coherent tunneling	$D = B\,T^{-9}$
SMALL	Direct process (high temp. limit)	$D = CT^{-\frac{1}{2}}\exp(-E_a/RT)$
SMALL	(low temp. limit)	$D = A\,T^{-7}$
*POLARON	Local tunneling states	-
*POLARON	Tunneling through excited states	-
*POLARON	Lattice activated process	$D = D_o\exp(-E_a/RT)$
	Classical theory of over the barrier jump	$D = D_o\exp(-E_a/RT)$
	Quantum mechanical modifications of classical theory	$D = D_o'\exp(-E_a/RT)$
	Fluid like diffusion	-

* A hydrogen accompanied by local lattice distortion behaves analogous to a polaron, i.e. an electron accompanied by a lattice deformation field in dielectrics.

$$J = -D \text{ grad } C = -D\frac{\partial \mu}{\partial C} \text{ grad } C \qquad (36)$$

Fick's equations for diffusion processes are:

$$J(x,t) = -D \text{ grad } C = -D\frac{\partial C(x,t)}{\partial x} \qquad (37)$$

and $$\partial C/\partial t = D\ \nabla C \qquad (38)$$

Table 5 Forms of the Laplacian operator for different geometries

GEOMETRY OF THE MEMBRANE	VARIABLES	$\nabla^2 C$	EXAMPLES
Linear	X	$\frac{\partial^2 C}{\partial X^2}$	Planar disk
Rectangular	X,Y,Z	$\frac{\partial^2 C}{\partial X^2}+\frac{\partial^2 C}{\partial Y^2}+\frac{\partial^2 C}{\partial Z^2}$	cuboid electrode
Spherical	r	$\frac{\partial^2 C}{\partial r^2}+\frac{2}{r}\left(\frac{\partial C}{\partial r}\right)$	Hanging drop electrode
Cylinder	r	$\frac{\partial^2 C}{\partial r^2}+\frac{1}{r}\left(\frac{\partial C}{\partial r}\right)$	Wire electrode

2.7.3.1.Boundary Conditions in The Electrochemical Problems

To solve Fick's second diffusion law for any geometry, it is necessary to integrate $\nabla^2 C$. This can only be done if additional information in the form of boundary conditions are provided to express the surface conditions of the electrode as well as the initial hydrogen content. The diffusivity calculated with a wrong set of boundary conditions is bound to give an erroneous result. The solution for Fick's First and Second laws in the specific case of the electrochemical permeation technique is discussed in the following section.

2.7.4...THE THREE DIMENSIONAL DIFFUSION PROBLEM

While the use of thin electrodes in diffusion studies has a long standing tradition,the applicability and the accuracy of this"unidirectional mass transport" assumption is being questioned [172-174] Bauer et al

[175] have shown that the measured diffusion coefficient of hydrogen (D^*) in Nb,for two distinctive geometries ie a thin foil and a cylindrical wire, presented in Fig.19, exhibit a striking dependence on the geometry of the sample.

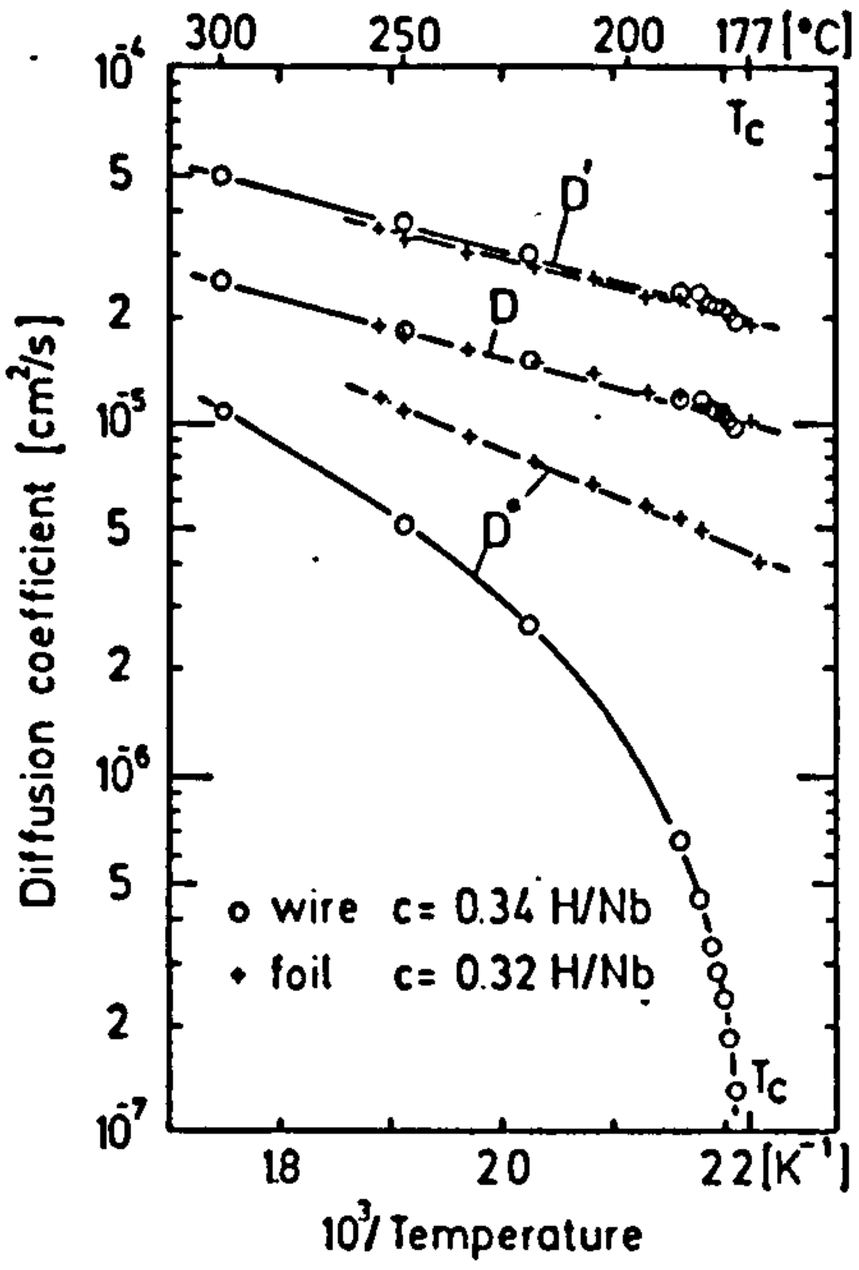

Fig.19 Comparison of the lattice diffusion coefficient for hydrogen in Nb, for wire and foil membranes[175]

This is thought to be due to the long-range elastic interaction between dissolved hydrogen atoms which affect ($\partial\mu$ / ∂ C), the driving force of the diffusion process and hence the diffusivity becomes dependent on the geometry of the sample[172-174]. It is argued that "tracer" diffusivity measurements are less prone to incorporate such a factor since they take into account a number of variables, which directly or indirectly relate to the H-H and H-M interactions[176]. The following mathematical analysis illustrates the three dimensional mass transport of hydrogen within the Fickian Diffusion Laws. The apparent diffusivity of hydrogen in a cube as shown here is of practical importance

since it has relevance to many industrial objects and utilities. Fick's second law to be solved for a three dimensional diffusion is:

$$(1/D)(\partial C/\partial t)=(\partial^2 C/\partial x^2 + \partial^2 C/\partial y^2 + \partial^2 C/\partial z^2) \quad (39)$$

In a rectangular cube a with 2a and 2b and 2c as sides,

$$-a<x<a \ , \ -b<y<b \ , \ -c<z<c \quad (40)$$

The boundary condition for such 'a' at (x=0,y=0,z=0) could be expressed as:

$$C(x,t)=0 \ @ \ t=0 \ @ \ -a<x<a \quad (41)$$

$$C(y,t)=0 \ @ \ t=0 \ @ \ -b<y<b \quad (42)$$

$$C(z,t)=0 \ @ \ t=0 \ @ \ -c<z<c \quad (43)$$

$$C(x,t)=Co \ @ \ t>0 \ @ \ x=-a \ \& \ x=a \quad (44)$$

$$C(y,t)=Co \ @ \ t>0 \ @ \ y=-b \ \& \ y=b \quad (45)$$

$$C(z,t)=Co \ @ \ t>0 \ @ \ z=-c \ \& \ z=c \quad (46)$$

The general solution to this problem as given by Crank[177] could be deduced by considering the solution to the one dimensional problem. If (C_1) is the solution to the one dimensional problem then

$$\partial C_1/\partial t = D(\partial^2 C/\partial X^2) \quad (47)$$

A general solution for the three dimensional problem could be written as:

$$C_1/Co = 1 - \sum f(x,y,z) \exp(-\nu t) \quad (48)$$

where f(x,y,z) and ν are different for each term in the series but are not functions of time(t), while (ν) is not a function of x, y, z. For a flux (J) of diffusant through the media,

$$J_\infty = C_0 \sum g. \exp(-\nu . t) \quad (49)$$

and the total amount of diffusant absorbed during time (t) is:

$$M_T = \int_o^t J\,dt = Co\sum g\left[\frac{-\exp(-t\,\nu) + \nu}{\nu}\right] \qquad (50)$$

where g is geometric factor but not a direct function of x, y, z or t. Hence the total amount of hydrogen reaching a point A(x,y,z) within the slab of metal of the initially zero concentration at the time (t) could be given as:

$$C1/C_o = 1 - \frac{64}{\pi^3}\sum_{l=0}^{\infty}\sum_{m=0}^{\infty}\sum_{n=0}^{\infty}\frac{(-1)^{l+m+n}}{(2l+1)(2m+1)(2n+1)} \times \cos\frac{(2l+1)\,X}{2a}\cos\frac{(2m+1)\,Y}{2b}\cos\frac{(2n+1)\,Z}{2c} * \exp(t.\alpha_{l,m,n}) \qquad (51)$$

$$\text{where } \alpha = \frac{\pi^2 D}{4}\sum\left[\left(\frac{2l+1}{a}\right)^2 + \left(\frac{2m+1}{b}\right)^2 + \left(\frac{2n+1}{c}\right)^2\right] \qquad (52)$$

Integration of C1, over the whole surface (dx.dy.dz), during the time t, gives (J_t) the rate of absorption of hydrogen into the metal cube.

$$J_t\Big|_{\substack{x=0\\y=0\\z=0}} = \frac{d}{dt}\int_{-a}^{a}\int_{-b}^{b}\int_{-c}^{c} C1\,dx\,dy\,dz \qquad (53)$$

for which the following solution applies

$$J_t = \left(\frac{64}{\pi^3}\right)^2 C\,abc\sum\sum\sum\frac{\alpha_{l,m,n}\cdot\exp(-t.\alpha_{l,m,n})}{(2l+1)^2(2m+1)^2(2n+1)^2} \qquad (54)$$

Integration of J_t with respect to time renders the total quantity of hydrogen absorbed into the matrix of the cuboid.

$$M(t)= \int_0^t J_t\,dt = \left(\frac{64}{\pi^3}\right)^2 \cdot C_o \cdot abc \sum_{l=0}^{\infty} \sum_{m=0}^{\infty} \sum_{n=0}^{\infty} \frac{-\alpha_{l,m,n}^2 \cdot \exp(-t\alpha_{l,m,n})}{(2l+1)^2 \cdot (2m+1)^2 \cdot (2n+1)^2} \quad (55)$$

The above solutions assume a constant concentration on all the faces of the cube. In the 3-D experiments the concentration of hydrogen on two of the **monitored** faces was maintained at zero and not C. To avoid anomalies, a new derivation based on the actual experimental boundaries is presented in Appendix 1 with the derived formula used in the interpretation of data. As will be discussed in the following section, a perfect matrix could only be theoretically assumed and hence modifications as a result of "trapping phenomenon" are required.

2.7.5...THE DIFFUSION PROCESS IN PRESENCE OF TRAPS

The "ideal matrix for which all the usual solutions of Fick's law are applicable, is a rarity. There are not only damaged parts of the structure as was described earlier in section 2.6, acting as "physical traps", but the very presence of hydrogen in the lattice can modify it in such a way that the simple "over the barrier" diffusion concept requires modification. Consequently hydrogen in a typical iron substrate either pauses in traversing the lattice or simply becomes immobilized for the whole duration of its presence in the matrix unless a suitable thermal fluctuation gets it moving again.

Prior to the work of Darken and Smith[149], the kinetics of hydrogen diffusion had not been studied in terms of sub-scale kinetics of the membranes and as such, no mechanism was proposed for explaining the anomalies encountered. The first analysis of this problem, based on the "local equilibrium" between hydrogen inside the traps and those in the "normal sites",put forward by McNabb and Foster[152] represents a rigourous mathematical analysis of the problem and therefore until recently, was very much the basis of other work concerned with trapping analysis [106,178-182]. Without going into the detailed mathematical derivations of the formulae (shown in detail in reference[152]), their equation for the concentration and diffusivity interdependence in a thin membrane containing traps will be reproduced here:

$$\partial C/\partial t + N_T(\partial n/\partial t) = D\,\partial^2 C/\partial X^2 \qquad (56)$$

$$\partial n/\partial t = K.C(1 - n) - P.n \qquad (57)$$

where n=fraction of the total traps occupied

K=rate constant for trapping of hydrogen

P=rate constant for the release of hydrogen from traps

N_T=number of traps per unit volume of the metal

C,D,t=have their usual significance namely concentration, diffusion coefficient and time.

A comparison of (1/K) and (1/P) values with the relaxation time of a lattice jump could determine

whether a trap is of reversible or irreversible nature. A substantially positive difference will indicate an irreversible trapping regime , while a small difference will indicate a reversible one. For reversible type traps the following equation was derived

$$D_{app}/Dl = 1/[1+(N_H K)/N] \quad (58)$$

where

N_H = the number of hydrogen atoms dissolved in the lattice

D_{app} = the apparent diffusivity of hydrogen

and for the full range of trapping the following expression has been proposed:

$$t = \frac{L^2}{6D_{app}}\left[1+\frac{3\alpha}{\beta}+\frac{6\alpha}{\beta^2}+\frac{6\alpha}{\beta^3}(1+\beta)\mathrm{Log}(1+\beta)\right] \quad (59)$$

where

t_1 =time lag, s

L = membrane thickness, m

Dapp= apparent diffusivity, $m^2\ s^{-1}$

α = N .K/P, dimensionless constant

N_T =number of traps per unit volume of the host metal

β =Co.K/P, dimensionless constant

Co=hydrogen concentration at the input side

The above equation could be simplified according to the degree of coverage of traps. When the traps are mostly occupied, i.e. after prolonged and systematic hydrogen charging, the ratio Co.K/P is greater than unity, while at the start of the process of charging the sample's traps are mostly unaffected and Co.K/P tends to have a

value much less than unity. The intermediate step therefore, can be detected by a value of (C_o.K/P)=1.

The following expressions are suggested for each of the above situations:

for C_o.K/P ⟩⟩1

$$D_{app}=D_L/[(1+3N)/C] \quad (60)$$

for C_o.K/P ⟨⟨1

$$Dapp=D_L/[(1+\alpha)] \quad (61)$$

for C_o.K/P = 1

$$Dapp=D_L/[1+\alpha(1-\frac{\alpha}{2})+\beta^2] \quad (62)$$

Oriani's review [106] on this topic was of importance since it made the new approach comprehensible by rearranging the McNabb and Foster's work. The following general relationship between Dapp and D_L was proposed by Oriani:

$$D_{app}=D_L\frac{\partial C_L}{\partial C_T}=D_L\left[1+\frac{N_T.N_L.K}{N_L+KC_L}\right]^{-1}$$

$$=D_L C_L/[C_L+C_L(1-\theta_T)] \quad (63)$$

where

N_T=number of trap sites per unit volume of the metal

N_L=number of normal sites per unit volume of the metal

K =$a_{H,in\ traps}/a_{H,in\ the\ lattice}$, the ratio ↓

between the activity of hydrogen in traps to that of normal sites.

$C_L = N_L.\theta$, the concentration of hydrogen atoms per unit volume of normal lattice sites.

θ_T=fraction of the total hydrogen atoms occupying the trapping sites

when $\theta_T << 1$, then the equation (61) reduces to:

$$D_{app} = D_L C_L / C_T \qquad (64)$$

All the formulae mentioned up to now could be used as diagnostic tools for evaluation of the prevalence or otherwise of the trapping sites as well as the degree of coverage of traps. The number of papers and reviews dealing with the trapping problem has grown dramatically over the past decade [178-188] and a comprehensive overview of all the different approaches employed is beyond this work. However, Table 6 is an attempt to provide the reader with a number of expressions derived by different workers in this field.

Table-4 The proposed equations for D_L and D_{app}. In this table: D_{app}=apparent diffusivity/m^2s^{-1} , T= Temperature/K°
D_L^{app}=lattice diffusivity/m^2s^{-1}

TRAP TYPE OR TRAPPING MECHANISM	D_L IN TERMS OF D_{app}	DEFINITION OF THE PARAMETERS
reversible or irreversible	$D_L = D_{app}/[(1+\frac{N_T K}{P})(\frac{3}{K'})(\frac{\sqrt{K'}}{\tanh\sqrt{K'}}-1)]$	N_T =number of traps per unit volume K=rate constant for trapping of hydrogen P =rate constant for release of hydrogen from traps K' =capture strength of the traps
slow trapping or rapid untrapping	$D_L = (\frac{1}{6}+\frac{N_T}{2m_o})(\frac{L^2}{t_L})$	N_T=number of atoms per unit of volume m =1/M; M=number of H atoms in each trap C_o =lattice concentration of hydrogen at the time t t_L=time-lag constant
reversible or irreversible	$D_L = (\frac{N_T \cdot T}{N_L \cdot L}+1)D_{app}$	θ_T =fraction of available traps occupied θ_L =fraction of available lattice sites occupied
MIXED TRAPPING	$D_L = 1/\theta_{app}\cdot[\frac{\gamma}{D_T\theta_T}+\frac{1-\gamma}{D_L\theta_L}]^{-1}$ $\theta_{app}=\gamma\theta_T+(1-\gamma)\theta_L$	γ = the ratio of the average thickness of defects to that of the bulk material
MIXED TRAPPING	$D_L = D_{app}\cdot[1+N_T K''\cdot\exp(\Delta E/kT)]^{-2}$	K"=pre-exponential factor N_T =number of traps per unit of volume k =Boltzman factor ΔE =binding energy of the trap site
traps and anti-traps	$D_{app}(N_T,N_B)=D_{app}/[1-N_B-N_T(1-\delta)]$ $\delta=\frac{X(1-N_B-N_T)N}{N_T\cdot(1-X)}$	N_T =number of traps per unit of volume N =number of blocked sites (anti-traps) per unit volume of the metal X =fraction of the interstitial atoms in the trapping site

2.7.6..EXPERIMENTAL METHODS OF DIFFUSIVITY MEASUREMENTS

Hydrogen diffusion is studied with a variety of techniques which broadly speaking fall within two categories "macroscopic" diffusion or "microscopic" effects related to diffusion, from which a diffusivity value could be determined.

The first category includes all those techniques which are based on the solution of Fick's first and second laws. A technique which uses the first is known as a steady-state method, while the ones which are concerned with the solution of the second law for calculation of diffusivity are classified as non-steady-state. Within each group, there are a number of techniques which will be discussed here. However, no attempt will be made to describe them in detail or derive their mathematical basis with the exception of the permeation technique used in this project.

2.7.6.1.The Indirect Methods Based on Non-Fickian Diffusion

These methods are the only direct equilibrium calculation of the diffusivity and hence could be regarded as the true measure of mobility of a single atom. The list of such methods has grown over the years and now include the following seven methods:

(i) Internal Friction Technique

Due to a stress induced redistribution of atoms in interstitial solution in a matrix, it is possible to measure the effect of small quantities of a diffusant on the long range order of the metal by measuring stresses induced or relaxed within it. The most common techniques in this category are the Gorskey effect, Snoek effect as well as the Zener effect.

(ii) Sintering Method

The sintering of a known quantity of powder at a suitable temperature results in the fusion of the particles and from the depth of penetration of particles in each other,the diffusivity could be measured.

(iii) Quasi-Elastic Neutron Scattering

In this method the sample is bombarded by low energy neutrons and the spectrum of the reflected or scattered neutrons from the dissolved protons is analysed for the calculation of diffusivity. A substantial "minimum concentration" of diffusant is necessary to obtain reliable data as there is a lot of background scatter due to the matrix atoms.

(iv) Mossbauer Spectroscopy

This method relies on the identification and the continuous monitoring of Mossbauer isotopes implanted in the lattice and their interaction with an interstitial atom. This leads to a change in spectrum as the Mossbauer atoms are disturbed and hence the degree of change is related to the diffusing atoms and their mobility.

(v) Nuclear Magnetic Resonance (N.M.R)

Direct measurement of (D) using N.M.R has been performed by double-pulse spin echo technique. This not only gives the (D) but also the time spent in each lattice site and therefore the jump frequency.

2.7.6.2.Concentration Gradient Based Methods

Various techniques used for charging a membrane with hydrogen and its detection can be used for the classification of these methods. These include:

(a) gas phase techniques

(b) electrochemical techniques

(c) mixed electrochemical/gas phase techniques

Up to the advent of the electrochemical techniques which have a great versatility with respect to variation in temperature and input pressure, gas phase methods were the most common techniques used. However, their mode of detection which needs U.H.V. for the purpose of hydrogen diffusion is cumbersome and has largely been replaced by the electrochemical techniques

Electrochemical methods on the other hand combine ease of operation with a high degree of accuracy [23-25,189,190].Hydrogen generated by the electrolysis of water on one side is detected at the other surface by applying an anodic potential sufficiently high to ensure the oxidation of hydrogen atoms arriving there. Mixed techniques which utilize both gas phase charging and electrochemical hydrogen

detection,are used in the high pressure and temperature studies of hydrogen-metal systems.

(I) Steady State Techniques

Any of the modes of charging and detection described above could be used to establish a chemical potential gradient across a membrane and the steady state flux resulting measured (Fig.20-a). One advantage of the steady state flux is its immunity towards trapping effects[106,152] on hydrogen diffusivity. Once the steady state flux is established, by maintaining constant concentrations C1 and C2 at the input and the exit sides respectively, the diffusion coefficient could be calculated from:

$$J = \frac{D(C_1 - C_2)}{L} \qquad (64)$$

where L is the membrane thickness.

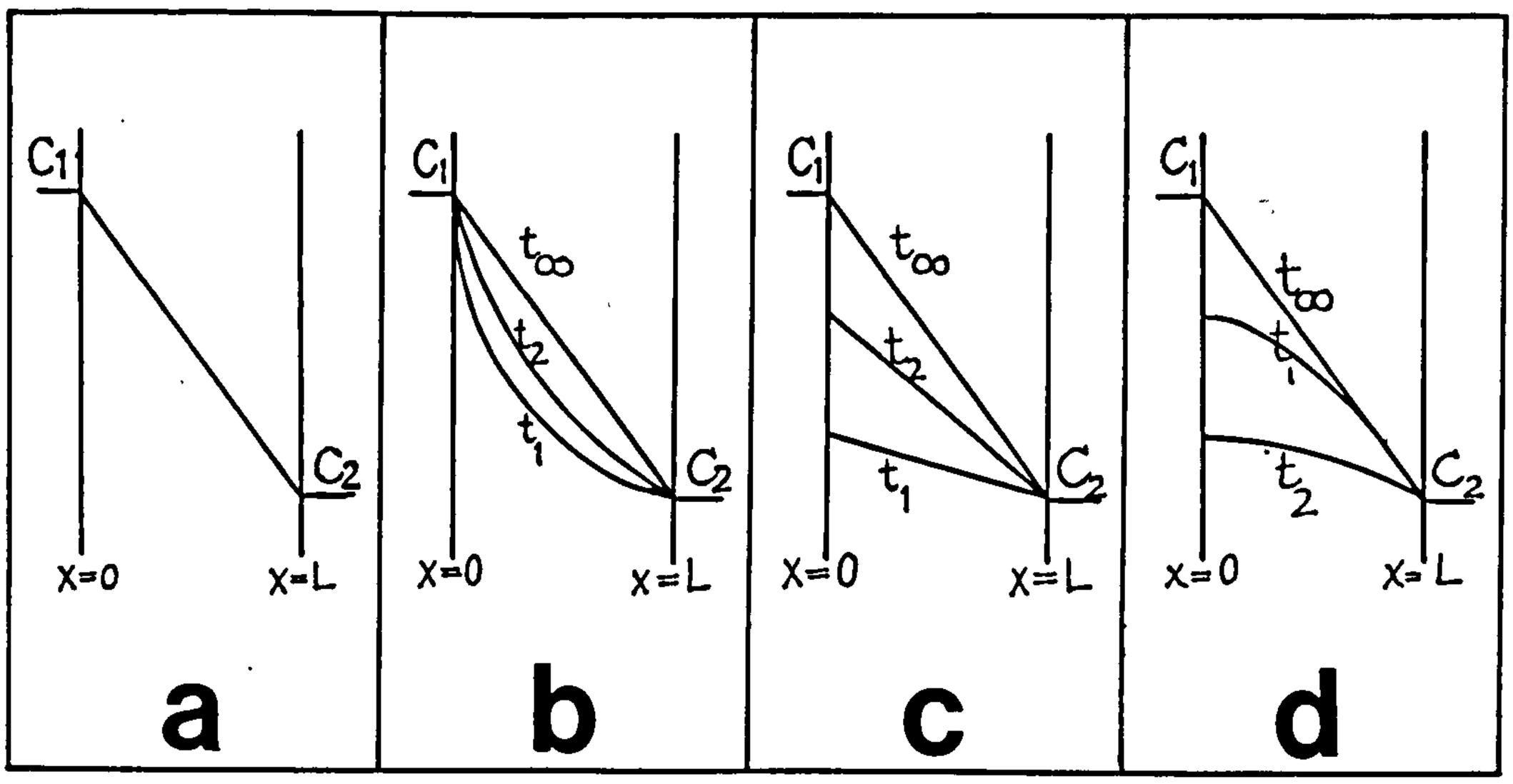

Fig.20 The schematic presentation of potentiostatic(a) and galvanostatic charging(b) with the steady state(c) as well as the decay transients(d). After Parly[191].

(II) Non-Steady State Techniques

These methods rely on the transient part of hydrogen charging or discharge from a membrane. This is a non-stationary condition for which Fick's second law needs to be solved[177]. Fig.20 b,c,d depict different variations of this method. The solution of the second law

$$\frac{\partial^2 C}{\partial X^2} = \frac{1}{D}\left(\frac{\partial C}{\partial t}\right), \text{ for } \quad 0<X<L \tag{65}$$

requires the integration of the above equation for which a set of boundary conditions is necessary. There are a variety of boundary conditions and once defined, the above equation could be solved using well-known mathematical techniques such as Laplacian Transforms, Fourier Series or the method of separation of variables.

Generally speaking, there are two types of experimental results which may be treated by the solution of equation (63). These are either the data related to the duration of the charging or results gathered during the "degassing" and "decay" phase which follows the abrupt termination of charging. Either set of data can be interpreted in a variety of ways, depending on boundary conditions, some of which are reported here.

(II-a) Laplace Transform Method for Constant Potential Charging

This situation applies to the case of a constant hydrogen gas pressure at the charging side i.e. a potentistatically controlled charging regime. The assumption here is that a membrane of thickness (L) is

initially totally hydrogen free. As the charging current is applied, the surface concentration C, jumps to a value of Cs, and is thus maintained(Fig.20 b). The other surface,X=L, maintains a continuous zero hydrogen concentration regardless. These conditions are formulated as [25,192]:

$$C = 0 \quad @ \quad 0 < X < L \quad @ \quad t = 0 \tag{66}$$

$$C = C \quad @ \quad X = 0 \quad @ \quad t > 0 \tag{67}$$

$$C = 0 \quad @ \quad X = L \quad @ \quad t > 0 \tag{68}$$

$$0 < C < C \quad @ \quad 0 < X < L \quad @ \quad t > 0 \tag{69}$$

for a permeation experiment during the charging

$$\frac{J_t}{J_\infty} = \frac{2L}{(\pi Dt)^{1/2}} \sum_{n=0}^{\infty} \exp[-(2n+1)\cdot L^2 / 4Dt] \tag{70}$$

where J_∞ and J_t are the steady state and flux after time(t),respectively.Using the dimensionless parameter $\tau = Dt/L^2$, and taking the first term approximation (n=0), the final result is:

$$\frac{J_t}{J_\infty} = \frac{2}{(\pi \cdot \tau)^{1/2}} \exp(-1/4\,\tau) \tag{71}$$

For a permeation experiment during the decay phase the initial conditions are different and as such the boundary conditions need to be modified [23,25,193] as follows:

$$C_x = C_s \quad @ \quad 0 < X < L \quad @ \quad t = 0 \tag{72}$$

$$C_x = 0 \quad @ \quad X = 0 \quad @ \quad t > 0 \tag{73}$$

$$C_x = 0 \quad @ \quad X = L \quad @ \quad t > 0 \tag{74}$$

$$C_x \neq 0 \quad @ \quad 0 < X < L \quad @ \quad t > 0 \tag{75}$$

The expression for the decay permeation is:

$$\frac{J_t}{J_\infty} = 1 - \frac{2L}{(\pi \cdot Dt)^{1/2}} \sum_{n=0}^{\infty} \exp[-(2n+1)\cdot L^2 / 4Dt] \tag{76}$$

or in dimensionless form and for n=0

$$\frac{J_t}{J_\infty} = 1 - \frac{2}{(\pi \ Dt)^{1/2}} \sum_{n=0} \exp(-1/4\,\tau) \qquad (77)$$

(II-b) Fourier Series Solution for the Potentiostatic Charging Method

The same initial and boundary conditions are applicable to the rise and decay transients here since the only variation is the mathematical solution to the equation(64). The change of concentration (C) with time and the depth of penetration (X) is formulated as:

$$C(X,t) = Cs - \frac{Cs\ X}{L} + \frac{2}{\pi} \sum_{n=1}^{\infty} - \frac{Cs}{n} \sin\left(\frac{n \cdot \pi \cdot X}{L}\right) \exp(-Dn \cdot \pi \cdot t / L^2) \qquad (78)$$

The flux or the permeation current is defined as:

$$J_t = - FD \left[\partial C(X,t) / \partial X \right]_{X=L} \qquad (79)$$

differentiating equation (78) with respect to X, gives J_t as:

$$J_t = \frac{zFDCs}{L} \left[1 + 2 \sum_{n=1}^{\infty} (-1)^n \exp(-n^2 \cdot \pi^2 \cdot Dt/L^2)\right] \qquad (80)$$

as $t \longrightarrow \infty$, the steady state flux is given as:

$$J_\infty = zFDCs / L \qquad (81)$$

hence

$$J_t / J_\infty = 1 + 2 \sum_{n=0}^{\infty} (-1)^n \exp(-n^2 \cdot \pi^2 \cdot Dt / L^2) \qquad (82)$$

finally the first term approximation of equation (82) with Dt/L is:

$$J_t / J_\infty = 1 - 2\exp(-\pi^2 \cdot \tau) \qquad (83)$$

The permeation decay transient using this mathematical solution is:

$$J_t/J_\infty = 1 - 2\exp(-\pi^2 \cdot \tau) \quad (84)$$

(II-c) Permeation Transient for a Precharged Sample

Since many problems associated with trapping could be eliminated if the reversible (saturable) traps are filled first, precharging of samples is of importance. However, this would change the initial condition and as such necessitate new solutions for the equation (64). For a potentiostatically charged sample these boundary conditions apply

$$C=Co \quad @ \quad 0<X<L \quad @ \quad t=0 \quad (85)$$

$$C=C_s \quad @ \quad X=0 \quad @ \quad t>0 \quad (86)$$

$$C=0 \quad @ \quad X=L \quad @ \quad t>0 \quad (87)$$

$$0<C<C_s \quad @ \quad 0<X<L \quad @ \quad t>0 \quad (88)$$

A trigonometrical series type of solution of the equation (64) can be derived [177] by the method of separation of variables and the final result is:

$$\frac{C-C_0}{Cs-C_0} = \frac{\Delta C_1}{\Delta C_2} = 1 - \frac{4}{\pi} \sum^{n} \frac{(-1)}{(2n+1)} \frac{\cos(2n+1)\cdot\pi\cdot X}{L} \times$$

$$\exp[-(2n+1)^2\cdot\pi^2\cdot D\, t/\, L^2] \quad (89)$$

since

$$J_{t,1} = -zFD[\partial \Delta C1/\partial X] \quad @ \ X=L \quad (90)$$

$$J_{t,2} = -zFD[\partial \Delta C2/\partial X] \quad @ \ X=L \quad (91)$$

it can be shown that

$$\frac{J_t}{J_\infty} = 1 - \sum_{n=0}^{\infty} \frac{(-1)^n}{2n+1} \exp\left[\frac{-(2n+1)^2 \pi^2 Dt}{L}\right] \quad (92)$$

The first term approximation of equation (92) using n=0 and $\tau = Dt/L^2$ will lead to:

$$\frac{J_t}{J_\infty} = 1 - \frac{4}{\pi} \exp(-\pi^2 \cdot \tau) \qquad (93)$$

The boundary conditions pertaining to decay transients of such a precharged sample are those of (72), (73), (74) and (75) above.

$$\frac{J_t}{J_\infty} = \frac{4}{\pi} \sum_{n=0}^{\infty} \frac{(-1)^n}{2n+1} \exp\left[\frac{-(2n+1)^2 \cdot \pi^2 \cdot Dt}{L}\right] \qquad (94)$$

The n=0 approximation and substituting for $j=Dt/L^2$ will result in:

$$\frac{J_t}{J_\infty} = \frac{4}{\pi} \exp(-\pi^2 \cdot \tau) \qquad (95)$$

(II-d) The Multiple Transient Technique

A useful variation of the electrochemical technique is the "multiple transient" method. This is best suited for diffusivity calculations.If the initial prevailing surface concentration,C_1, is established and is and then by increasing (rise) or decreasing (decay) of the charging current, I_c, a new concentration, C_2, is established and is maintained until a new steady-state (J_{t,C_2}) is reached, the boundary conditions in this case are described by:

$C=Co$ @ $0<X<L$ @ $t<0$ (96)

$C=C_1$ @ $X=0$ @ $t_1=0$ (97)

$C=0$ @ $X=L$ @ $t_1=0$ (98)

$\left.\begin{matrix} C_1<C<C_2 \\ C_2<C<C_1 \end{matrix}\right\}$ @ $0<X<L$ @ $t_2>0$ (99)

Using these boundary conditions gives:

$$\frac{J}{z\,F} = \frac{D \cdot C_0}{L} + 2(C1-C_0)\sum_{n=0}^{\infty}(-1)^n\left(\frac{D}{\pi t}\right)^{1/2}\exp\left[\frac{-(2n+1)L}{4Dt}\right] \quad (100)$$

The first term approximation together with substitution for $\tau = Dt/L^2$ results in:

$$\frac{J_t - J_1^{\infty}}{J_2^{\infty} - J_1^{\infty}} = \frac{2}{\sqrt{\pi\tau}}\exp(-\tau/4) \quad (101)$$

For the build up (rise transient), equation (102) below could be derived on the same principle as the decay phase.

$$\frac{J_t - J_2^{\infty}}{J_2^{\infty} - J_1^{\infty}} = \frac{2}{\sqrt{\pi\tau}}\exp(-\tau/4) \quad (102)$$

where

J_t = flux at any time t, s

J_1^{∞} = the first steady state flux

J_2^{∞} = the second steady state flux

τ = Dt/L^2 , dimensionless parameter

(II-e) Permeation Transient for the Constant Flux Charging

This case deals with a surface which is being galvanostatically controlled (Ic=constant) so as to maintain a constant rate of hydrogen charging. The boundary conditions pertaining to this case are:

$$C = 0 \quad @ \quad 0<X<L \quad @ \quad t=0 \quad (103)$$

$$J = -D[\partial C(X,t)/\partial X]$$

$$@ \quad X=0 \quad @ \quad t>0 \quad (104)$$

$$C = 0 \quad @ \quad X=L \quad @ \quad t>0 \quad (105)$$

the final expression in this case is[194-196],

$$\frac{J_\tau}{J^{\infty}} = 1 - \frac{4}{\pi}\sum_{n=0}^{\infty}\frac{(-1)^n}{2n+1}\exp\left[\frac{-(2n+1)^2\cdot\pi^2\cdot Dt}{4L^2}\right] \quad (106)$$

Using similar simplifications as before results in

$$\frac{J_t}{J^{\infty}} = 1 - \frac{4}{\pi} \exp(-\frac{\pi^2 \tau}{4}) \qquad (107)$$

During the decay for this case, the initial condition is[192],

$$J_t = DC_x/L = \text{constant}$$

$$@ \quad 0<X<L \quad @ \quad t=0 \qquad (108)$$

while the boundary conditions are:

$$\begin{cases} J = 0 \quad @ \quad X=0 \quad @ \quad t>0 \\ C = 0 \end{cases} \qquad (109)$$

$$C = 0 \quad @ \quad X=L \quad @ \quad t>0 \qquad (110)$$

$$0<C<C \quad @ \quad 0<X<L \quad @ \quad t>0 \qquad (111)$$

hence

$$\frac{J_t}{J_{\infty}} = \frac{4}{\pi} \sum_{n=0}^{\infty} \frac{(-1)^n}{2n+1} \exp[\frac{-(2n+1)^2 \cdot \pi^2 \cdot Dt}{4L^2}] \qquad (112)$$

and in dimensionless form, the (n=0) approximation of the above is given as:

$$\frac{J_t}{J_{\infty}} = \frac{4}{\pi} \exp(-\pi^2 . \tau / 4) \qquad (113)$$

There are many more variations in the electrochemical methods [194] which could not be included in this survey. The diffusion coefficient can be obtained from the above expression in a variety of ways. Both curve fitting[25,193] and numerical procedures [197] can be adopted. Other methods are based on the use of different time constants, t_b , t_l , t_i , $t_{1/2}$, t_d shown in Fig.21. The break-through time(t_b) is defined as the time taken for the first atoms of hydrogen to reach the surface (X=L), while t_i is the time taken for the permeation curve to reach its "inflection point" [194]. Time-lag (t_l), one of the more utilized time constants

which historically has been the first one to be used [198,199] in diffusion and permeability studies, refers to the time taken for the areas between the X-axis and the permeation curve (excluding the steady state plateau) equals that of the permeation curve (now including the plateau) and an asymptote to the curve at J_∞..

The graphical representation of the method (Fig.21) shows how a value of J_t/J_∞ =0.63, coincides with this constant. The half-time and the decay time are used during the decay phase and refer to the time taken for the decay curve to reach half its original value, normalised with respect to J ,i.e. J_t/J_∞=0.5 and the relaxation time after which (J_∞) starts to decrease, respectively. A summary of all the possible formulae derived for the diffusivity calculations from the experimental curves is presented in Table 6.

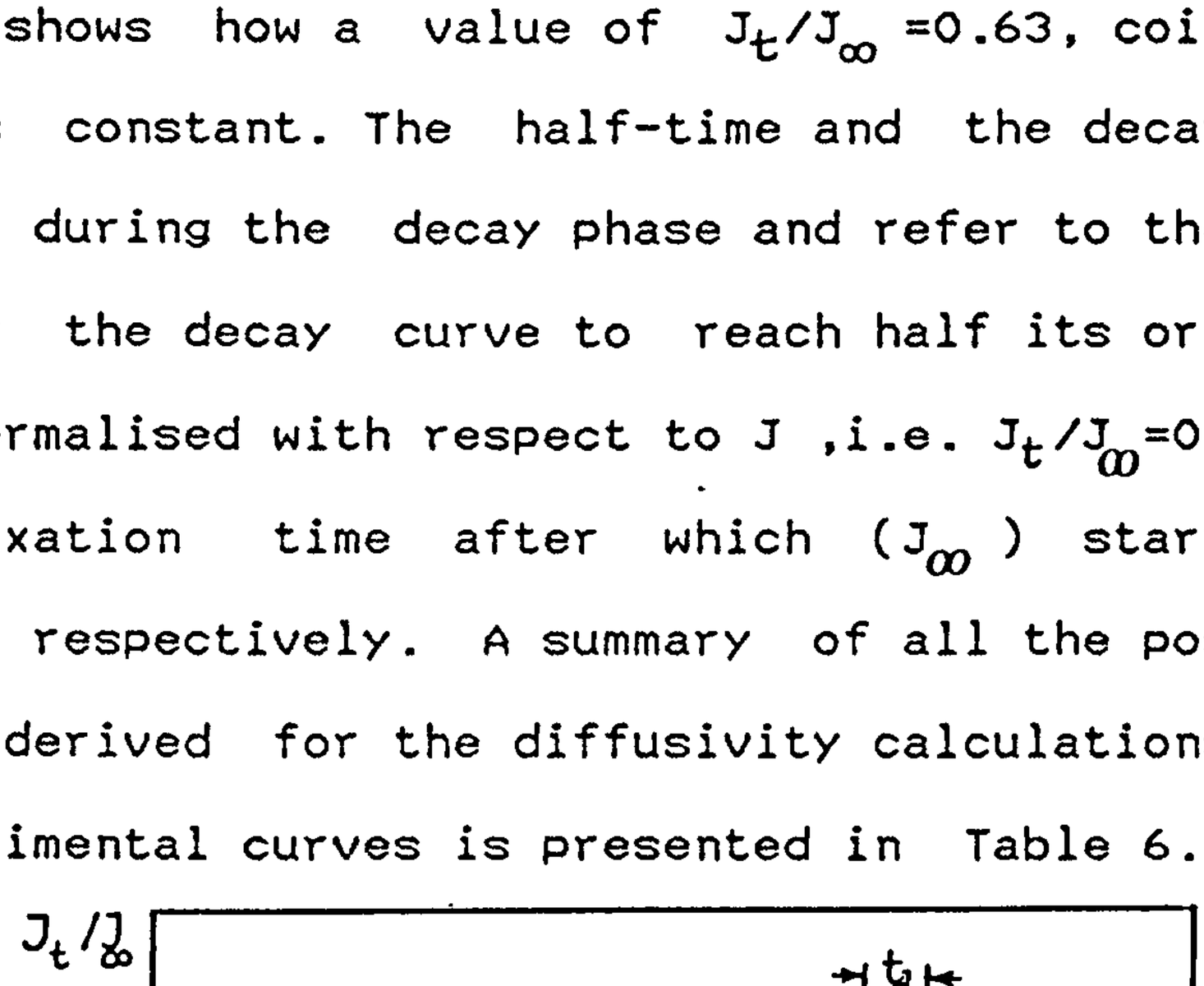

Fig.21 A typical permeation - time curve exhibiting both the rise and the decay transients as well as the steady-state plateau.t_b ,t_i ,t_l ,$t_{1/2}$,t_d are described in the text.

Table 6 The summary of expressions derived for diffusivity calculations from the permeation expressions

TIME CONSTANT	EXPRESSIONS FOR "D" CALCULATION			
	HYDROGEN CHARGING REGIME			
	CONSTANT CONCENTRATION		PRECHARGED SAMPLE	CONSTANT FLUX
t_b	$\frac{0.5L^2}{\pi^2 t_b}$	$\frac{0.5L^2}{\pi^2 t_b}$	$\frac{0.19L^2}{\pi^2 t_b}$	$\frac{0.76L^2}{\pi^2 t_b}$
t_i	$\frac{2LN(4L)^2}{3\pi^2 t_i}$	$\frac{0.09L^2}{t_i}$	$\frac{3L^2}{8} \frac{LN3}{t}$	$\frac{3L^2}{8} \frac{LN3}{t}$
t_l	$\frac{L^2}{6} \frac{}{t_l}$	$\frac{0.17L^2}{t_l}$	$\frac{L^2}{8} \frac{}{t_l}$	$\frac{L^2}{2} \frac{}{t_l}$
$t_{1/2}$	$\frac{0.138L^2}{t_{1/2}}$	$\frac{0.138L^2}{t_{1/2}}$	$\frac{0.095L^2}{t_{1/2}}$	$\frac{0.38L^2}{t_{1/2}}$
t_d	$\frac{L^2}{\pi^2 t_d}$	$\frac{L^2}{4\pi^2 t_d}$	$\frac{L^2}{\pi^2 t_d}$	$\frac{L^2}{\pi^2 t_d}$

The formulae in Table 6 do not reflect the "trapping phenomenon" and as such should be used carefully when applied to test-samples which have undergone a high degree of cold-work in their mechanical history; if so, the expressions in section 2.7.5 should be used. The other shortcoming of these formulae is the neglect of the surface characteristics of the charging side prior to charging and during decay.

It so happens that in the case of iron and steel, permeation studies in sodium hydroxide solutions are used most extensively and it will be shown later that the surface of any iron membrane, not protected by a layer of Pd,will passivate resulting in incorporation

of a measure of false time-lag due to the period taken for the surface to be reduced so that the hydrogen can permeate through. Hufine and Williams[200] report a one thousand fold reduction in hydrogen permeation rate when a continuous passive film is present on a stainless steel substrate. The same problem arises during the decay phase, when the surface film formed makes the entry side of specimen impermeable to hydrogen and as such,affects the relaxation time,t.Very few papers [193,201] consider these problems and therefore this is one source of possible error,not widely taken into account. There are solutions to the composite material diffusion problem[83], which should be employed if there are surface oxides or sub-surface layers which disturb the homogeneities of the membrane.

2.7.7...ANOMALOUS PERMEATION CURVES

The presence of abnormal transient curves was first observed by Devanathan and Stachurski[24] and has been the subject of many studies [178-180]. In a recent paper Wu [178] gives an extensive account of all abnormal permeation curves. The most common abnormal feature is a maximum in the hydrogen flux followed by a slow decline as depicted in Fig.22-a .The curves (a) to (e) show substrata which have undergone structural damage.Bockris et al[202] give the following expression for the changes of hydrogen concentration with time and distance in a damaged planar membrane.

$$C(X,t)=(1+K)C_0\left[\sum_{n=0}^{\infty}(-1)^n \operatorname{erfc}\left\{\left[\left((X+2nL)\sqrt{1+\tau K}\right)/2\sqrt{Dt}\right]\right.\right.-$$

$$\sum_{n=0}^{\infty}(-1)^{n}\,\mathrm{erfc}(-X+2L+2nL)\,\sqrt{1+\tau K}/2\,\sqrt{D\tau}) \qquad (114)$$

and the following, for the permeability in presence of traps

$$P = \frac{FDC_0}{\sqrt{\pi}} \cdot \frac{2}{L} \cdot \left(\frac{L^2}{Dt}\right)^{1/2} \exp\left[\frac{-L^2(1+\tau \cdot K)}{4D\tau}\right] \qquad (115)$$

where

K=equilibrium constant for $[H_L] \rightleftharpoons [H_T]$

X

X=distance from the charging side

$\tau = Dt/L^2$ dimensionless parameter

Co=the steady-state concentration of hydrogen

n=an integer (0,1,2,3..)

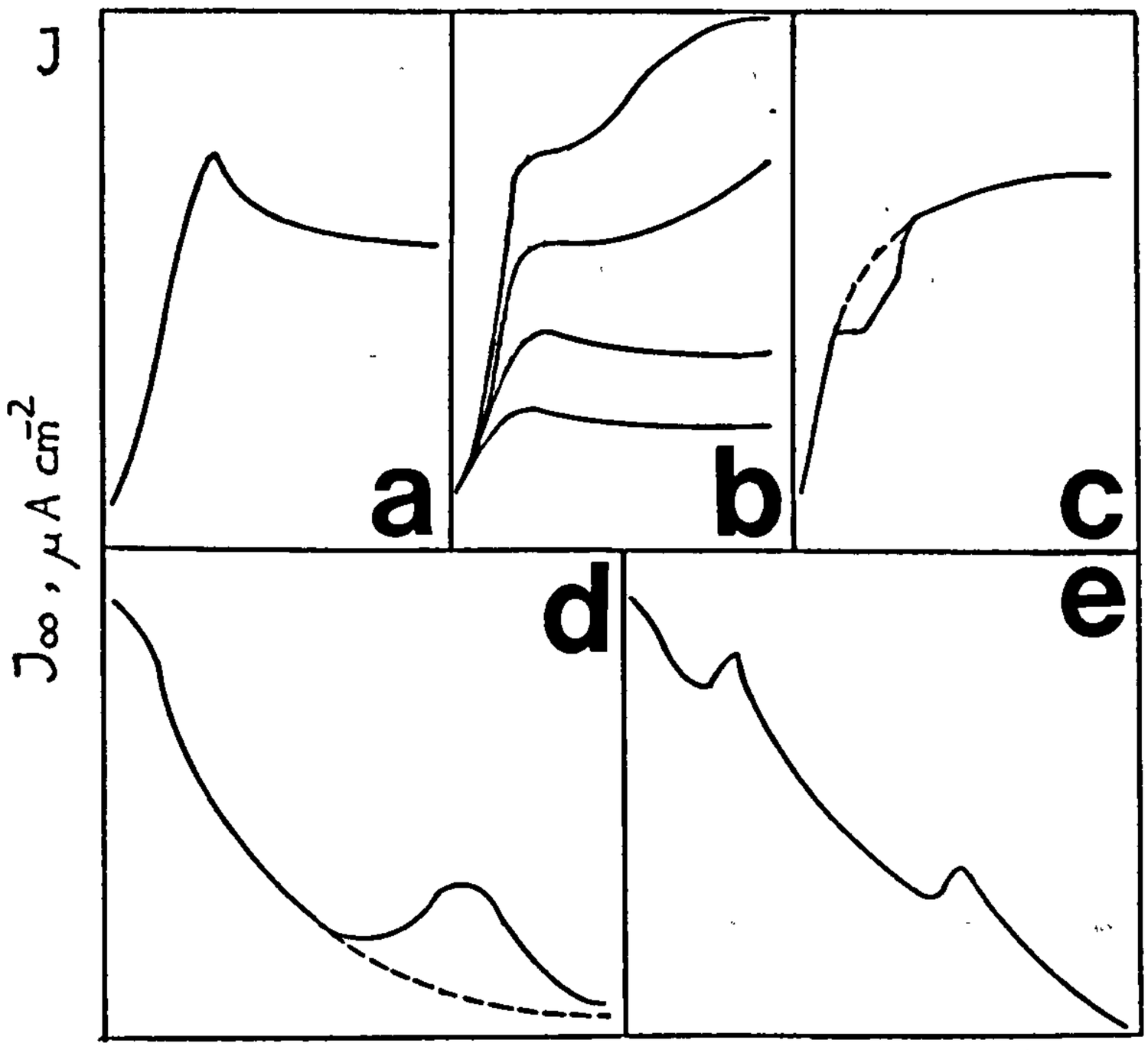

Fig.22 Schematic representation of the effect of trapping on the permeation curves during rise (curves a, b, c) and decay (curves d, e) phases.

The maximum value of current density which can be maintained on the charging side without causing damage in the lattice is given in the literature from as little as 430 μAcm^{-2} [203] to 800μA cm^{-2}[16] for Armco iron, and much higher for different grades of steels.

Apart from the damage caused by too high a charging current, the damage sustained during sample preparation is as important in setting this threshold since such deformities are not totally eliminated[137,204] even after long periods of annealing. The same is true of Beilby layers formed under the surface of the metal after mechanical polishing. Park and Waber[205] have shown through positron annihilation studies of such surface layers to be full of dislocations and also the depth of deformation to be a function of the polishing time and grit size. They also detected a maximum concentration of defects at about 4 μm below the surface.The total depth of deformation in their studies in an iron single crystal,mechanically polished using a 240 grit, wet SiC paper, was around 25 μm.Using similar mechanical polishing, Lee et al[206] could demonstrate that a 25 μm . removal of the surface layer of pure iron sample results in one order of magnitude increase in the diffusivity of hydrogen.

The above points,if overlooked,could result in even greater anomalies than that encountered normally in the study of hydrogen diffusion . As described in the previous sections, further work is needed on the nature of H-M and H-H and H-discontinuities before a comprehensive model for hydrogen could be formulated. In the meantime, use of the present approximations for the specific and well-defined conditions could be justified.

2.8.....THE HYDROGEN EVOLUTION REACTION (HER) ON IRON

2.8.1...INTRODUCTION

One aspect of hydrogen entry into iron as discussed in the first section is the variety of entry channels dependent on aqueous media for the provision of hydrogen. The formation of hydrogen on a metal surface is the result of the breakdown of the solvent, i.e. water, which is governed by both thermodynamic as well as kinetic considerations. The dissociation of water during electrolysis happens in a layer of solution only a few nanometers thick[207]. However the properties of this layer are influenced by those of the bulk solution and the metal. The problem of the HER from a purely thermodynamic viewpoint is to establish whether the potential energy in a natural cell or one with impressed current is low enough to cause the breakdown of hydrated protons or water molecules according to the general reactions below:

$$2H_3O^+(aq) + 2e^- \rightleftharpoons H_2(g) + 2H_2O \qquad (116)$$

@ pH=0 E=0.70 V

$$H_3O^+(aq) + H_2O + 2e^- \rightleftharpoons H_2(g) + (OH)^- \qquad (117)$$

@ pH=7 E=-0.41 V

$$2H_2O(l) + 2e^- \rightleftharpoons H_2(g) + 2(OH)^- \qquad (118)$$

@ pH=14 E=-0.828 V

In practice however, kinetic rather than thermodynamic considerations account for any experimentally observed rate of reaction. This, translated into the mechanism of a corrosion process, means that in a potential range

which favours metal dissolution, it is the rate of cathodic reaction that determines the speed with which the metal corrodes.

2.8.2...THE KINETICS OF DISCHARGE OF HYDROGEN IONS

Hydrogen generation on an iron surface is a multi-step process which makes the task of elucidating its kinetics more complex. The steps through which a hydrated proton $(H_3O^{\cdot})^+$ should proceed before it can be discharged as a molecular hydrogen are as follows:

$$(H_3O^{\cdot})^+_{bulk} \longrightarrow (H_3O^{\cdot})^+_{metal/electrolyte\ interface} \quad (119)$$

Reaction (119) represents the "transport step" in which the hydrated protons are brought to the phase boundary through diffusion, migration or even convection inside the electrolyte.

$$(H_3O^{\cdot})^+ + e^- \longrightarrow H_{ad} + H_2O \quad (120)$$

Reaction (120) constitutes a "discharge step", The hydrated proton after arriving at the interface receives an electron from the collective electron cloud of the metal to attain electrical neutrality as an adatom. Reaction (120) is also known as the "Volmer reaction" [190].

$$H_{ad} + H_{ad} \longrightarrow H_2 \quad (121\text{-a})$$

$$H_{ad} + H_3O^+ + e^- \longrightarrow H_2 + H_2O \quad (121\text{-b})$$

The above reactions (121-a) and (121-b) represent the "desorption step". Both reactions result in a molecule of hydrogen. However, as is evident from the reactions, this molecule is not capable of breaking its bonds with

the metal surface and as such, it will still be loosely attached to the surface. There are various terms used for this step as it is referred to as the "combination" or "recombination" step. The individual reactions during the second step are also referred to as [190] "Tafel reaction", "Tafel recombination" or "chemical desorption" in which (121-a) is considered; and "electrochemical desorption", "ion-atom desorption" or "Heyrovsky reaction" by which (121-b) is referred. The problematic hydrogen entry into the metal substrate can happen at this step and could be represented as:

$$H + M \rightleftharpoons M\text{-}H_{ad} \qquad (122)$$

A fifth step includes the coalescence of hydrogen ad-molecules by surface diffusion to form pockets of gas which could overcome both the surface bond energy as well as the static pressure of the solution and as such this could be identified as the "final desorption" step.

$$nH \rightleftharpoons nH_2(g) \qquad (123)$$

The above mechanism, using $(H_3O)^+$, is only applicable to acid solutions (pH<7), since in neutral or basic solution,the concentration of hydrated protons is too low to sustain those reactions and direct electro-chemical reduction of water molecules is needed [190] for such solutions.The sequence of reactions therefore is as follows:

$$H_2O + e^- \rightleftharpoons H_{ad} + OH^- \qquad (124)$$

The prevalence of water molecules in an aqueous solution eliminates the need for the transport step in such solutions and the "adsorption step" proceeds

immediately. This is then followed by either "chemical" (125-a) or "electrochemical" (125-b) reaction.

$$H_{ad} + H_{ad} \rightleftharpoons H_2 \qquad (125\text{-a})$$

$$H_{ad} + H_2O + e^- \rightleftharpoons H_2 + OH^- \qquad (125\text{-b})$$

Once in the adsorbed form, the following steps, i.e. "adsorption" or "final desorption" are identical for alkaline solution to that of acid solution. Apart from pure gold, most metal cathodes dissolve (absorb) hydrogen, be it only a small quantity of the discharged hydrogen. Palladium is a notable exception in that, at low current densities, it is capable of dissolving all the discharged hydrogen.

2.8.2.1.The Rate Determining Step in the HER

The concept of a rate determining step (rds) is purely kinetic as it compares the speed with which different steps in a multi-stage event proceed. The overall speed of an "event" is dictated by the slowest step in that process. For the general three stage mechanism described above, each single step could be the rate determining step while the other two reactions remain in equilibrium. There are four possible routes as follows:

1 -Discharge (D) followed by Chemical Desorption (CD)

1.1-Discharge (D) as rds

$$H_2O \xrightarrow{r.D.S} H_{ad} \longrightarrow H_2 \qquad (126)$$

1.2-Chemical Desorption (CD) as rds

$$H_2O \rightleftharpoons H_{ad} \xrightarrow{r.D.S} H \qquad (127)$$

2 -Discharge (D) followed by Electrochemical Desorption (ED)

2.1-Discharge as rds

$$H_2O \xrightarrow{r.D.S} H_{ad} \rightleftharpoons H_2 \quad (128)$$

2.2-Electrochemical Desorption (ED) as rds

$$H_2O \rightleftharpoons H_{ad} \xrightarrow{r.D.S} H_2 \quad (129)$$

3 -Coupled Discharge (D) and chemical Desorption (CD).

In this model the reverse steps for both reactions are negligible and therefore reactions proceed independently,although sequentially.

$$H_2O + e^- \longrightarrow H_{ad} + OH^- \quad (130)$$

$$H_{ad} + H_{ad} \longrightarrow H_2 \quad (131)$$

4 -Coupled Discharge (D) and Electrochemical Desorption (ED)

$$H_2O + e^- \longrightarrow H_{ad} + OH^- \quad (132)$$

$$H_{ad} + H_2O + e^- \longrightarrow H_2 + OH^- \quad (133)$$

The following table shows the suggested HER mechanisms for different metals.

Table 7 Mechanism of HER on different metals in different media. (*) more than one mechanism suggested, (+) acid media, (-) alkali media

MECHANISM	METAL
slow discharge,fast recombination	Pb,Sn,Tl,Hg,Mn,Ga Cd,Ni,Pd^+,Cu^*,W^*,Rh^+, Au^-, Pd^-
slow discharge,fast electrochemical desorption	Fe, Ag
fast discharge,slow recombination	Rh^*,Ir,Pt,Pd^*
fast discharge,slow electrochemical	Ti,Au^+,Mo^-,Mo
coupled discharge and recombination	Fe^*

2.8.3...HYDROGEN PERMEATION TECHNIQUE AS A TOOL FOR ESTABLISHING THE "HER" MECHANISM

Diagnostic criteria for the mechanisms proposed in Table 7 are derived from the slope of Tafel plots i.e. potential versus logarithm of current density and in some cases from capacitance measurements [208]. Potentiometric studies rely on the relationship between the charging current density (i_c) and the overpotential (η) associated with that current. Equation (134) gives the rate of forward cathodic reaction based on i_c and η

$$i_c = i_o . \exp[-(1-\beta)\nu\eta/RT] \qquad (134)$$

where

i_c =charging current, A m^{-2}

i_o =exchange current density, A m^{-2}

ν =stoichiometric number=number of unit charges transferred during one act of rate determining reaction.

β =symmetry factor $0 < \beta < 1$

F =Faraday's constant, 96 487 C mol^{-1}

η =overpotential, V

R =gas constant, 8.314 J mol^{-1}

T =absolute temperature, K

Rearranging the equation (134) gives an expression for η as

$$\eta = \frac{2.303RT}{\alpha} Log i_o + \frac{2.303RT}{\alpha} Log i_C \qquad (135)$$

This is the well known Tafel equation which has been used as early as 1922 by Bodenstein[50] to establish the mechanism of HER. The advent of the electrochemical permeation technique with its versatility towards change of variables, has enabled more accurate investigation of this phenomenon.

In the case of iron, since the entry step into the metal (122) competes with the desorption step, the evaluation of I_{∞} (permeation current measured on the anodic side) the surface potential and an accurate knowledge of the exchange current density, i_o, can enable the observer to identify intermediate steps by which the hydrogen has been generated and also the rate determining step involved. The flux of hydrogen at permeation through an iron membrane at steady state will be:

$$J_{\infty} = \frac{D(C_1 - C_2)}{L} \qquad (136)$$

since in the permeation technique, C_2 is kept at zero, the overall reaction will be,

$$J_{\infty} = DC_o / L \qquad (137)$$

where C_o is the concentration of hydrogen discharged immediately under the surface. For such a flux the following general mechanism applies[209]:

cathode side			anode side	
$H \rightleftharpoons H \longrightarrow$		Flux through the membrane	$\longrightarrow$	H^+ measured as I_{∞} (138)
ads	abs			

where K_{+1} and K_{-1} are the rates of forward and reverse reactions.If diffusion through the membrane is slow enough to be the rate determining step, the rates of absorption and desorption should be in equilibrium and as such:

$$K_{+1}\left(1 - \frac{N_o}{N_i}\right) = K_{-1}C_o(1 - \theta) \qquad (139)$$

where θ =surface coverage, the fraction of available sites for hydrogen on the cathode surface actually occupied by it.

N_o =number of interstitial sites per unit volume of metal occupied by hydrogen

N_i =total number of interstitial sites available for hydrogen occupation.

At low coverages $N_0 \ll N_i$ and hence $N_0 / N_i \longrightarrow 0$ and $(1-\theta) \longrightarrow 1$; therefore

$$K_{+1}\theta = K_{-1}C_o \quad \text{or} \quad C_o = (K_{+1}/K_{-1})\,\theta \tag{140}$$

substituting for C_o in equation (137) results in:

$$J_\infty = D(K_{+1}/K_{-1})\,\theta\,/L \tag{141}$$

J_∞ in terms of number of moles of hydrogen permeating will be:

$$J_\infty = I_\infty / zFA \tag{142}$$

where I_∞=permeation current, A

z =hydrogen charge

F =Faraday's number, 96487 $Cmol^{-1}$

A =surface area, m^2

equation (141) will now be :

$$I_\infty/zFA = D(K_{+1}/K_{-1})\ /L \tag{143}$$

$$\text{or} \quad I_\infty = zFDA(K_{+1}/K_{-1})\,\theta\,/L \tag{144}$$

this clearly shows that the permeation current is proportional to coverage with adsorbed hydrogen. Accurate determination of the coverage therefore, is of importance since this could establish the coverage regime operative under the experimental conditions.

This could either be a Langmurian (at low coverages) or a Temkin regime for high coverages[209]. There are other diagnostic calculations which have been used such as the check for linearity of I_∞ versus $I_C^{1/2}$ curves[210]. Mcbreen and Genshaw [210] using this and

other data have proposed the possible mechanisms for HER on a series of metals including iron which is reproduced in Table 8.

2.8.4...KINETICS OF THE HYDROGEN EVOLUTION REACTION ON IRON

There are several proposed mechanisms for HER on iron [190,208,210-214] in the literature. The diagnostic criteria for these come in part or wholly from the slopes of the Tafel plots together with other data as discussed in the previous section. Mcbreen and Genshaw[210] measured the different variables for Tafel as well as plots of overpotential vs logarithm of permeation current density and permeation vs charging current density. These are shown in Table 8.

Table 8 The diagnostic criteria used to determine HER mechanism.

MECHANISM	$-\eta$ / LN ic		$-\eta$ / LN i_∞		$i_\infty = k\ ic$	
	LANGM.	TEMKIN	LANGM.	TEMKIN	LANGM.	TEMKIN
DISCHARGE (rds), CHEM. DES.	2RT/F	2RT/F	0	0	-	-
DISCHARGE, CHEM. DES. (rds)	RT/F	RT/F	RT/F	RT/F	1	1
DISCHARGE (rds), ELECTROCH. DES.	2RT/F	RT/F	RT/F	RT/F	-2	-1
DISCHARGE, ELECTROCH. DES. (rds)	2RT/3F	RT/F	RT/F	RT/F	2/3	1
COUPLED DISCH-CHEM DESORPTION	2RT/F	3RT/F	4RT/F	3RT/F	1/2	1
COUPLED DISCHARGE ELECTROCHEM DESORPTION	2RT/F	2RT/F	0	0	-	-

Using the above diagnostic analysis, much work has been expended verifying the mechanisms of the HER on iron. The following models are the result of such attempts.

Model A put forward by Bockris et al[189,215] postulates a pH independent HER according to which hydrogen enters into iron from the adsorbed state and is therefore in competition with bubble formation. Furthermore , the adsorption is argued to be the result of a coupled discharged-chemical desorption sequence with discharge stage the rate determining step.

MODEL A

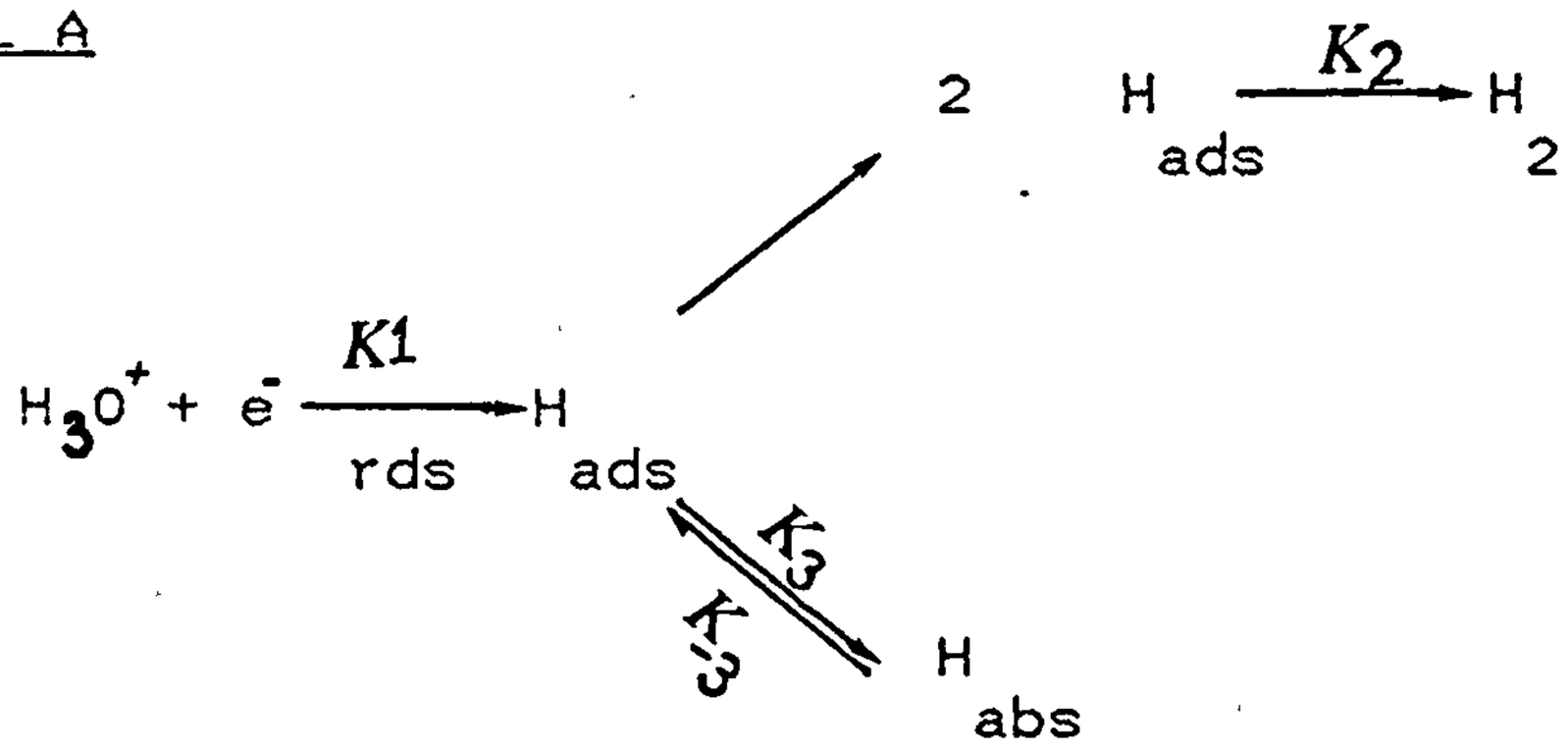

(145)

Model A has had the benefit of corroborative evidence from experiments in acid (H_2SO_4) and alkali (NaOH) in the temperature range of 18-80° C. The values of Tafel slope (=-0.120 V decade^{-1} = 2RT/F) and $\partial\eta$ / ∂LN I_{∞}=-0.240 V decade^{-1} = 4RT/F) together with the linearity of I_{∞} vs $i_c^{1/2}$ curves all correspond well with those suggested in Table 8 for such a regime.

There is another model (B) suggested by Bogotskaya [213]. The assumption here is that hydrogen absorption into iron depends on an elementary step which preceed the adsorption and therefore hydrogen

entry is in direct competition with the adsorbed step(146).

MODEL B

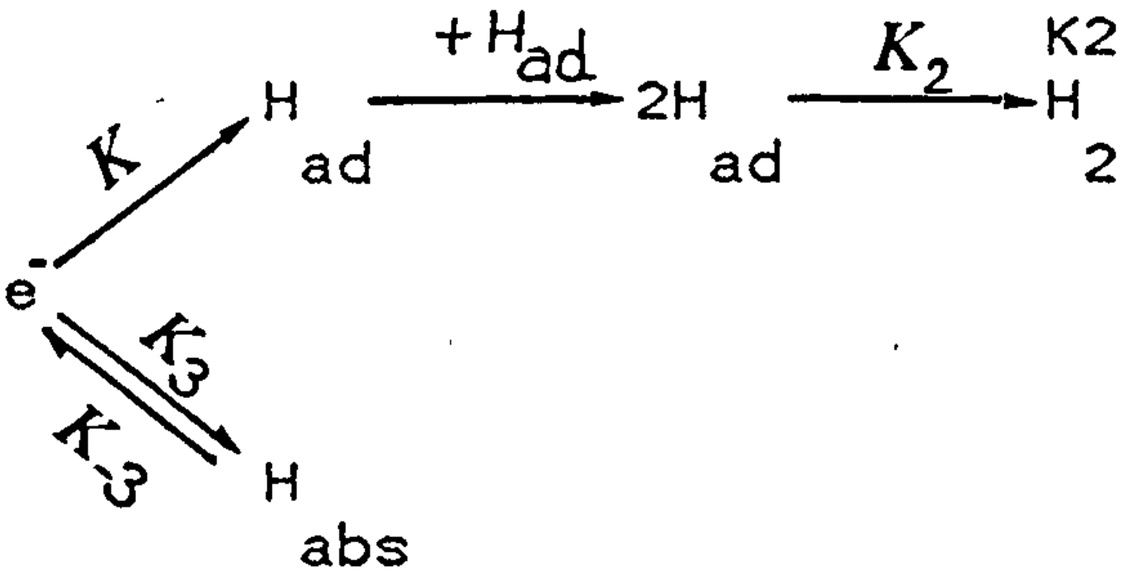

(146)

Although mathematical models proving the possibility of such mechanisms is available [216] and the existence of a precursor to the adsorbed state is theoretically possible [217], model B as far as the hydrogen entry into iron is concerned seems to be overtaken by the Bockris model.Many workers have confirmed [218,219] model A as the valid mechanism for HER on iron.

Devanathan and Stachurski [218] who suggested a slow discharge step found the same fast electrochemical desorption reaction during the high coverage regime (Temkin regime) as the Bockris model. Kim and Wilde's work [219] also confirms the conclusion of Bockris et al. Amongst even older work the value of - 0.122 and -0.118 V decade^{-1} for Tafel plot slopes in acid and alkali media respectively is reported by Pentland[208] which corresponds well to the mechanism proposed by model A.

Daft et al[190] calculating exchange current densities for different possible reactions for HER on iron conclude that the model A is operative in the

entire pH range, although he found evidence of simultaneous Tafel and Heyrovski reactions during the desorption step.

2.8.5...RELATIONSHIP BETWEEN THE EXCHANGE CURRENT DENSITY AND THE ATOMIC NUMBER OF METALS

The exchange current density for any electrochemical reaction represents the ease with which it can proceed and hence is an important kinetic factor. The following table shows the available data on the exchange current density of the HER on different metals in acid and alkali solutions. Some of the values have been averaged in the interest of space as well as ease of use in table. The comprehensive collection of these date may be found in Ref[220].

Table 9 i_o values for the HER on different metals

METAL	log i_o , Acm-2	
	pH<7	pH>7
Ag	- 5.91	-6.11
Au	- 4.99	-5.64
Bi	-10.05	-
Cd	-10.77	-
Cu	- 6.83	-6.09
Fe	- 5.72	-6.06
Ga	-10.00	-
Hg	-11.58	-
In	-11.28	-
Mo	- 6.89	-6.55
Nb	- 7.54	-6.82
Pb	-12.45	-
Pd	- 2.40	-5.01
Pt	- 3.37	-3.51
Re	- 5.04	-
Rh	- 2.96	-4.85
Te	- 6.85	-8.25
Ti	- 7.24	-
W	- 6.53	-7.06
Zn	-10.80	-

The values of i_o from the above table plotted, against atomic number of the elements[190] show precise periodicity.Hence in each long period of the Periodic Table, the activity increases first with atomic number,reaches a maximum at the metals of group (VIII),decreases quite sharply with a minimum at the metals of group (II-B) or (III-B) and again increases with further increase of the atomic number. Kita who observed this periodicity, presents a quantitative explanation based on the change of activity of metals in the Periodic Table. Fig. 23 illustrates this as yet qualitative relationship [190].

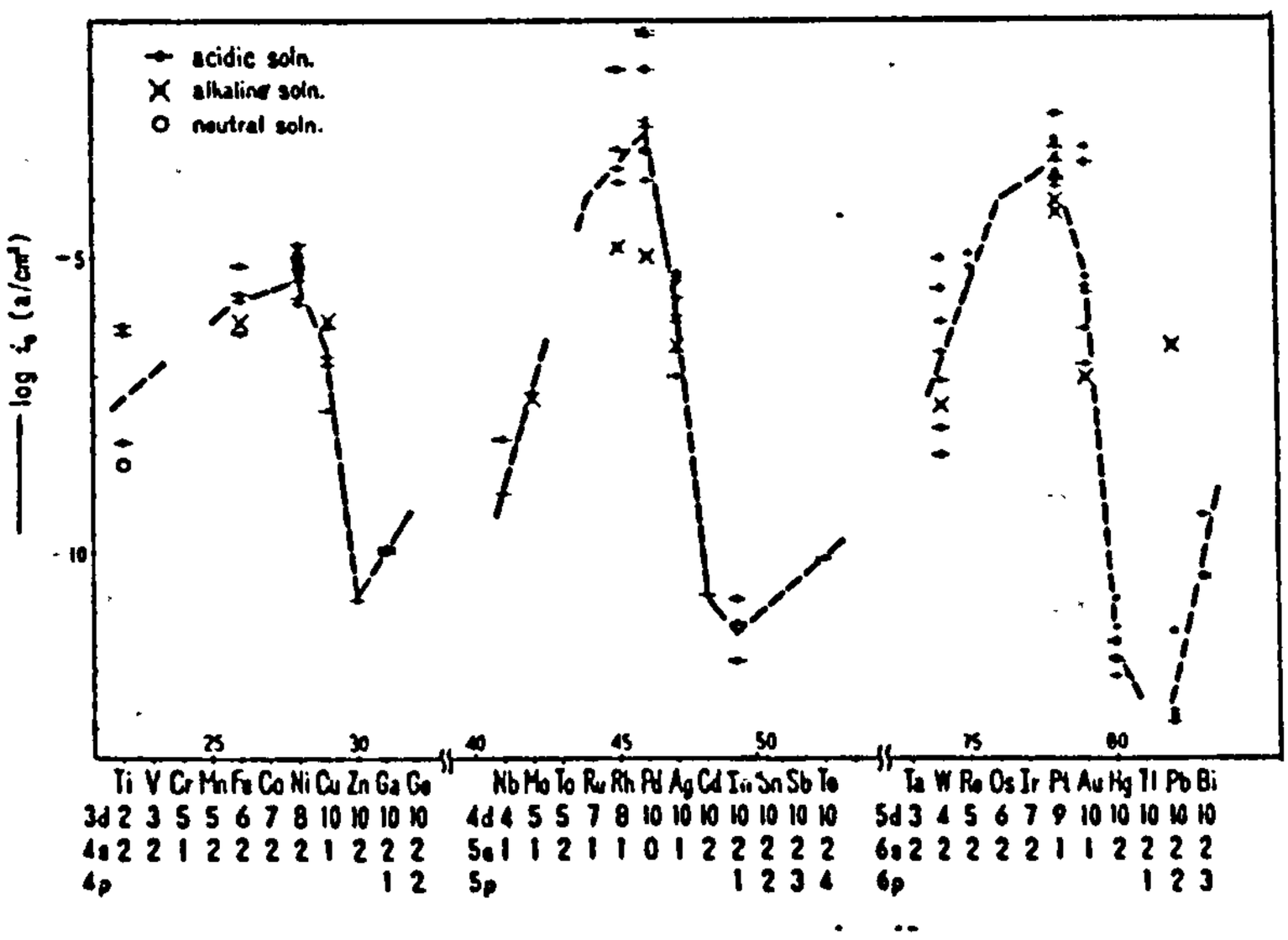

Fig.23 The periodicity encountered in the plots of i_o vs atomic number and the activity vs atomic number[220].

In the case of iron, the effect of its work-function on the hydrogen evolution reaction is studied by Daft[190].

2.8.6...Hydrogen Adsorption-Desorption on Iron

The topic of hydrogen adsorption on metallic surfaces has been mainly studied by measuring the heat of adsorption of hydrogen gas on ultra-clean, mainly

single crystal surfaces. The results however could be taken to be valid for hydrogen-iron bondings within a substrate or in the surface layers [221], albeit with modifications.

Any metallic surface which contains a low number of hydrogen atoms (low coverage), will give rise to very mobile hydrogen ad-atoms. As the coverage increases, the repulsive interactions between the ad-atoms reduces the mobility. This in turn could bring about a long range order to these atoms. The existence of such an ordered over-layer has been positively identified on Fe ⟨110⟩ while the Fe⟨111⟩ and Fe⟨100⟩ planes show no such ordered structure[45].

Indeed in chemisorption, new electronic configurations can be formed by sharing electrons between the adsorbed species and the substrate[222]. Nordlander et al[223] suggest a negative bonding energy of -2.70 eV for Fe-H chemisorbed bond. This agrees well with the experimental results reported elsewhere [45].

Fig.24, shows the relationship between the heat of adsorption of hydrogen on different metals in each row of the Periodic Table and shows the general trends for chemisorption on transition metals to be a decrease in the adsorption energy from the left hand side to the right.

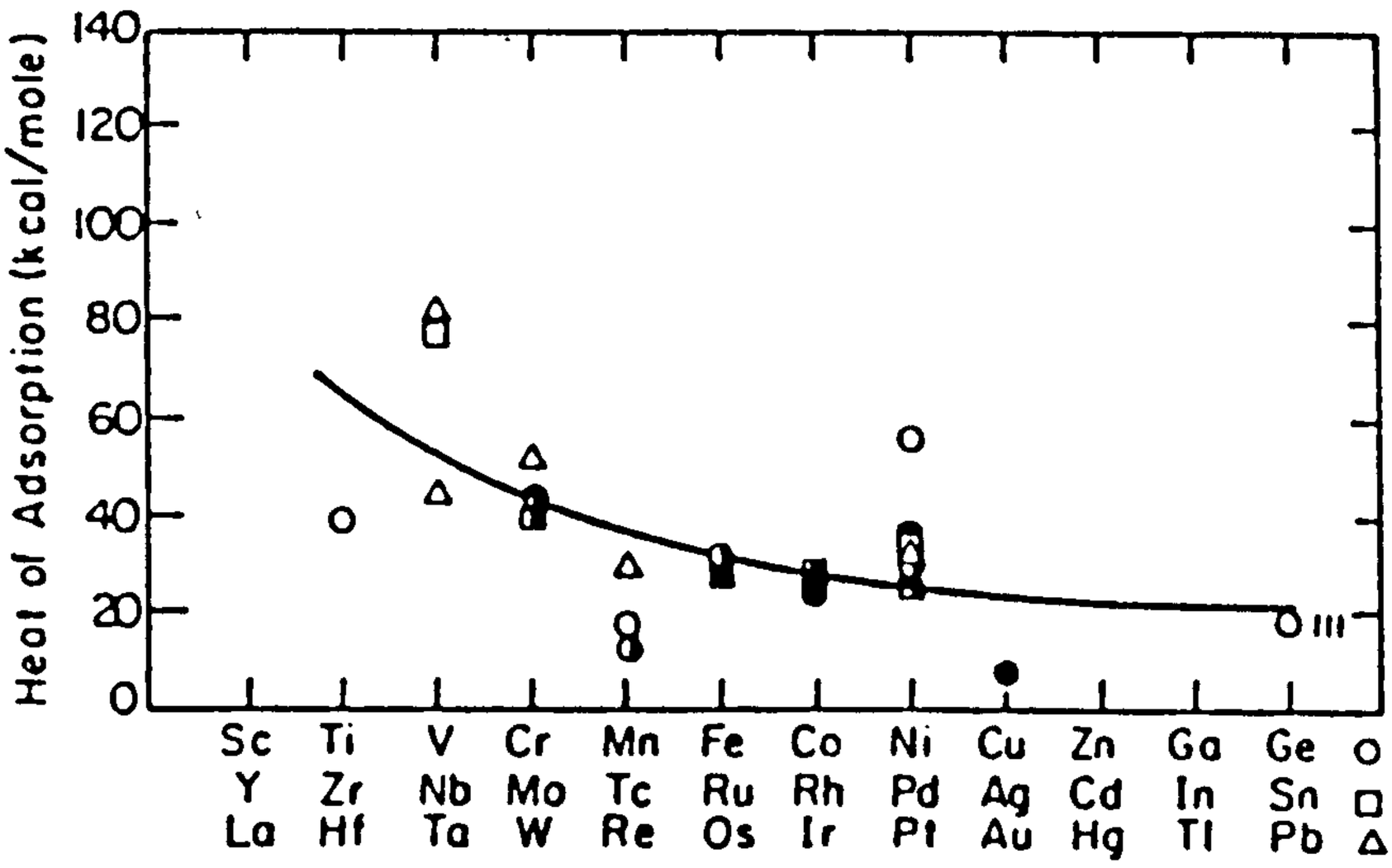

Fig.24 the relationship between the heat of adsorption and atomic number[224].

The reason for this could be in the electronic nature of chemisorption in which the 1s electron of hydrogen and metal Sp electrons contribute to the energy while the d. band electrons are responsible for the periodicity effects. When the metal surface interacts with the environments (liquid or gaseous) the problem is more complex since chemisorption or surface reactions, with the formation of three dimensional compounds can induce surface segregation.The three dimensional products such as oxides , are of practical interest since if the temperature is high enough, the hydrogen is capable of reducing them [225,226].This could be of importance when we remember that hydrogen permeation is drastically reduced on formation of even the thinnest oxide barriers. When considering the chemisorption of hydrogen on alloy surfaces, one must take into account, not only the "identity" of each element present, but also the "ensemble" effect [227] in the adsorption where a combination of surface sites

are required so that the process of adsorption could progress. An obvious example would be the case for the dissociation of the molecules of a gas and the adsorption of the atoms, which requires a "right" arrangement of sites.

An inert atom, unwilling to participate in the process of the dissociation, therefore will markedly affect the probability of this event. Hydrogen is strongly adsorbed on all transition metals; Fe, Cr, Ni, Mo[45]. The adsorption of H on these metals is dissociative. However, there is no activation energy necessary[45]. Sub-surface bonding of hydrogen has been shown both experimentally [228,229] and theoretically [230]. These indicate very deep potential wells below the surface in addition to the potential wells responsible for the adsorption of hydrogen above the surface. Results obtained for different metals; Ni, Pt, Pd, Fe, Cr and Cu show that hydrogen can be located in sites under the surface. This phenomenon is obviously very important when considering the entry of hydrogen into and its egress . . from the iron substrates. As will be discussed in a later chapter, this could well be the cause of a given surface reaction such as a passivation-depassivation process.

2.8.7...The Hydrogen-Iron Bond

The enthalpy change (heat of adsorption) can be related to the formation of a polarised, covalent bond between an adsorbed atom or molecule and a surface

atom. For the dissociative chemisorption of hydrogen on transition metals the heat of adsorption is related to the bond energies of M-H and H-H pairs[231]. Fig.25 shows the metal-hydrogen interaction in terms of their potential energy. The negative interaction indicates a non-activated chemisorption process.

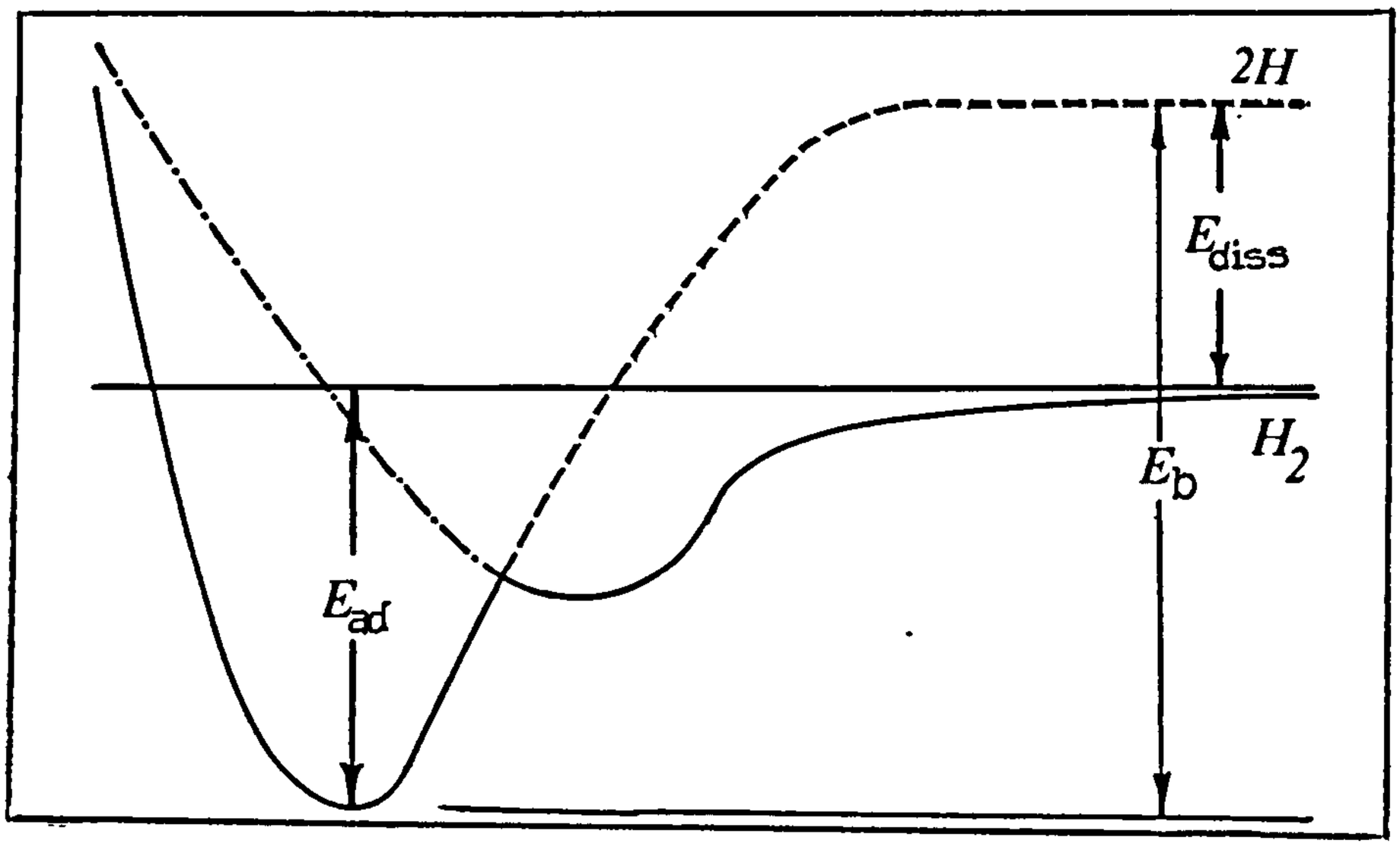

Fig.25 Schematic representation of energy changes during the chemisorption of hydrogen on a surface.

The energy balance is given;

$$E_{ad} + E_{dis} == 2E_b(M\text{-}H) \qquad (147)$$

where E_{ad} =adsorption energy

E_{dis} =the energy required for the dissociation of the H molecules

E_b =Fe-H bond energy

The energy of an Fe-Fe bond is taken as 1/6 of the heat of sublimation, so that such a bond will be around 70 kJ/mol. Since E_{ad} is assumed to be zero and E_{dis} for hydrogen is 432 kJ/mol, the strength of an Fe-H bond can be calculated as:

$$0 + 432 = 2E_b(Fe\text{-}H) \qquad (148)$$

and $E_b(Fe\text{-}H) = 216$ kJ/mol

This is in good agreement with the experimental results[231] which give,the E_b(Fe-H) as 282 kJ/mol.

The problem with such calculations is that they often presume participation of certain molecules while the actual process is usually far more complex. For instance in the case of iron-hydrogen, the process of dissociation may actually involve several ionic hydrogen states and a final dissociated form. While the value of 432 kJ/mol is correct for a molecule of hydrogen, the same value for H is only 255 kJ /mol.

The question of hydrogen induced change in the Fe-Fe bond is of prime importance in the case of hydrogen embrittlement. Although there is no definite evidence of such effects, a simple idea would be that these actually weaken the Fe-Fe bond. Messer et al [232] has investigated S/Ni,S/Fe and H/Fe systems and have not found any experimental evidence for weakening of Fe-Fe or Ni-Ni bond due to the solute (H).This is not to say, that hydrogen has no effect on the substrate, quite the contrary, the presence of hydrogen leads to bonding states between the solute and the matrix which are many times stronger than the matrix's bond energy.The value of Fe-Fe bond energy of 70 kJ/mol should be compared with 282 kJ/mol, the Fe-H bond strength.The importance of any such bond formation on the overall energetics of the system could not be ignored although a hydrogen bonding state may not necessarily reduce the bond strength of the host metal.

2.9.....PASSIVITY

2.9.1...INTRODUCTION

The passive state of a metal produced by previous exposure or treatment, causes it to behave as a more noble metal.The metal then becomes more resistant to dissolution and to corroding media than would be expected from its normal position in the electrochemical series.

The phenomenon of passivity has long been recognized. One of the first observation is ascribed to Kier[27] who in 1790 noted the passivity of iron in concentrated nitric acid. However, there are other scientists credited with this discovery and depending on the sources consulted names like Lomonosow[233] who is reported to have observed the phenomenon in 1738 and Wenzel[234] who has made such observation in 1782 are encountered. Anodic passivation is said to have been discovered by Heisinger and Berzelius (in 1807)[234] while Schonbein [235] has reported the discovery of this phenomenon in 1836.

Faraday's paper explaining the passivation of iron in the form of "skin development" theory has also won him the reputation of being the discoverer of this phenomenon[235]. Many solutions other than nitric acid are known to induce this state and a brief list of such solutions includes,silver, lead, and mercuric nitrates;

potassium permanganate, potassium dichromate, chloric acid, chromic acid, arseniOUS acid, sulphuric acid containing nitrous oxide as well as copper potassium nitrate and ammoniacal copper solutions. Iron is frequently being rendered passive by anodic treatment in which the metal is polarized to potentials more positive than its corrosion potential in a particular electrolyte. It also may be passivated by exposure to nitric oxide or the vapours of strong nitric acid and at least for pure iron, a degree of passivity results from the exposure to atmospheric oxygen[242].

Many theories attempting to explain this phenomenon have been put forward [237-240] of which the protective oxide formation formulated by Bennet [28] in 1917, seems to be most applicable to the available data. However, the case for amorphous films, especially in the case of atmospheric passivity,is as convincingly supported by the experimental data [241]. In this section, we attempt to expound the subject with special regard to passivity in alkaline solution.

2.9.2...POURBAIX DIAGRAMS

The concept of passivity could be elucidated if two parameters, potential and pH, influencing it are brought together in a mathematical model. Pourbaix [242] was first to use the available experimental data, and calculated data to produce diagrams in which the relationship between the surface potential and pH were

illustrated. The relationship between the potential and the concentration of chemical species involved is described by the Nernst equation,

$$E=E^{o} - RT/zF \ Ln \ K \qquad (148)$$

and

$$K= \frac{a \ (oxidized \ species)}{a \ (reduced \ species)} \qquad (149)$$

where E=surface potential, V

E^{o}=reversible electrode potential, V

R=gas constant=8.314 J/ mol/ K

T=absolute temperature, K

z=number of electrons exchanged during one act of charge transfer

F=Faraday's constant=96487 C/mol

a=activity

Using this formula and the mathematical expression for the pH as:

$$pH= - \log[H^{+}] \qquad (150)$$

where $[H^{+}]$=concentration of hydrogen ions.

A system of boundaries could be constructed which establish whether a certain reaction is thermodynamically possible.

In the case of pure iron in contact with distilled water, this approach leads to the diagram shown in Fig.26 . The model predicts that over the whole range of pH at potentials less than -1.20 V vs SHE, the metal, (represented by Fe) is protected from corrosion. As the pH is decreased, the potential necessary for maintaining this protection needs to be more anodic i.e. -0.70 V (SHE) in the 0-7 pH

range. As the pH is increased the potential needed to maintain immunity falls to -1.22 V due to the ease with which oxides/complex ions are formed. If the metal/ solution system in question is incapable of generating and holding such a noble potential, the degradation of the metal occurs and corrosion ensues.

This leads to the identification of two main domains in such diagrams -"immunity" and "corrosion". The third domain specified by "passivity" is,in effect, nothing but the extension of the "corrosion" zone. This is a result of the nature of interactions between the ions formed within this region (i.e. ferrous and/or ferric for iron) and water molecules and an extremely slow rate of progress is established. Pourbaix [242] has shown that this explains the experimental observations satisfactorily.

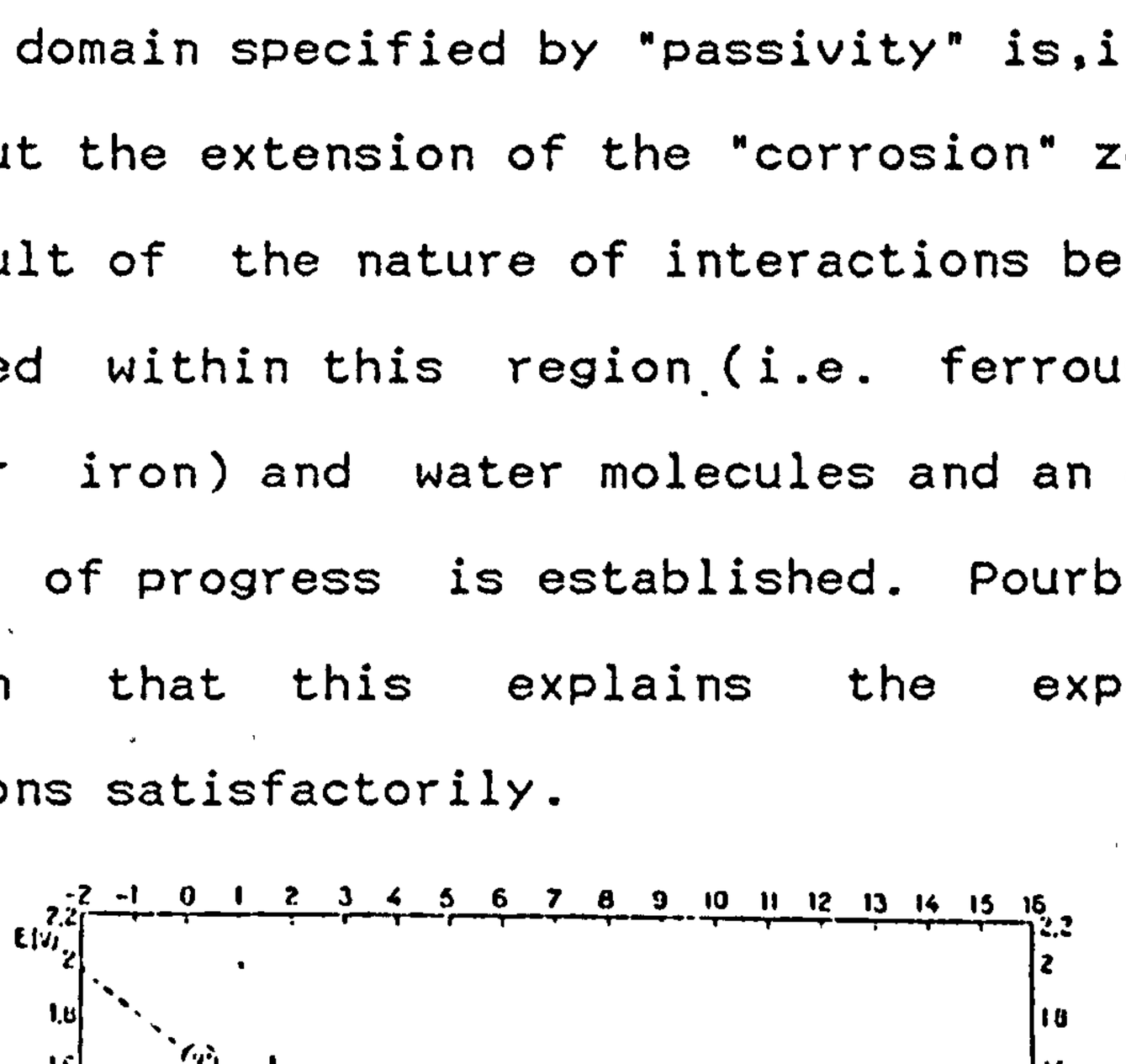

Fig.26 Potential-pH diagram for Fe-H_2O system at 25 C After Pourbaix[242].

The principal reactions in Fig.26 are shown in the Table 10.Some of the reactions which involve H^+ ions result in pH terms.Since protons critically affect the direction of the reaction,their generation and the diffusion of it is important for an understanding of the passivation phenomenon.In the literature search,the role of stored hydrogen in a metal substrate and its influence on the process of passivation in contrast to the hydrogen present in the electrolyte,

has not been previously investigated.

Table 10 The proposed reactions for Fe-H_2O interaction according to Pourbaix[242].

REACTION	E/pH/Concentration relationship
$Fe=Fe^{2+}+2e^-$	$E=-0.440+0.0295\ Log[Fe^{2+}]$
$Fe=Fe^{3+}+3e^-$	$E=-0.0370+0.0197\ Log[Fe^{3+}]$
$Fe^{2+}=Fe^{3+}+e^-$	$E=0.7710+0.0591\ Log[Fe^{2+}/Fe^{3+}]$
$2HFeO_2^-=Fe_2O_3+H_2O+2e^-$	$E=-1.1390-0.0591\ Log[HFeO^-]$
$HFeO_2^-+H_2O=Fe(OH)_3+2e^-$	
$Fe^{2+}+2H_2O=HFeO_2^-+3H^+$	
$Fe^{3+}+H_2O=FeOH^{2+}+H^+$	$E=-2.4300+pH$
$2HFeO^-=Fe(OH)_2+H_2O+2e^-$	$E=-0.8100-0.0591\ Log[HFeO^-]$
$Fe^{2+}+2H_2O=HFeO_2^-+3H^+$	$E=-31.580+3pH-\ Log[HFeO_2^-/Fe^{2+}]$
$Fe^{3+}+H_2O=FeOH^{2+}+H^+$	$E=-2.43+pH-Log[FeOH^{2+}/Fe^{3+}]$
$FeOH^{2+}+H_2O=Fe(OH)_2^++H^+$	$E=-4.69+pH-Log[Fe(OH)_2^+/Fe(OH)^{2+}]$
$Fe^{2+}+H_2O=FeOH+H+e^-$	$E=0.7710+0.0591\ Log[Fe/Fe^{2+}]$
$Fe^{2+}+2H_2O=Fe(OH)_2^++2H^++e^-$	$E=0.0914-0.0591pH+$ $0.0591Log[Fe(OH)_2^+/Fe^{2+}]$
$HFeO_2^-+H^+=Fe(OH)_2^++e^-$	$E=-0.675+0.0591pH+$ $0.0591Log[Fe(OH)_2^+]/[HFeO_2^-]$
$HFeO_2^-+2H^+=FeO_4^{2-}+5H^++4e^-$	$E=1.001-\ 0.0738pH+$ $0.0148Log[FeO_4^{2-}/HFeO_2^-]$
$Fe^{3+}+4H_2O=FeO_4^{2-}+8H^++3e^-$	$E=1.7-0.158pH+$ $0.0197Log[FeO_4^{2-}/Fe^{3+}]$
$3Fe+4H_2O=Fe_3O_4+8H^++8e^-$	$E=-0.085-0.0591pH$
$2Fe+3H_2O=Fe_3O_4+6H^++6e^-$	$E=-0.051-0.0591pH$
$Fe+2H_2O=Fe(OH)_2+2H^++2e^-$	$E=-0.047-0.0591pH$
$2FeO+H_2O=Fe_2O_3+2H^++2e^-$	$E=-0.057-0.0591pH$
$3FeO+H_2O=Fe_3O_4+2H^++2e^-$	$E=-0.197-0.0591pH$
$2Fe_3O_4+H_2O=3Fe_2O_3+2H^++2e^-$	$E=\ 0.221-0.0591pH$
$Fe_3O_4+5H_2O=3Fe(OH)_3+H+e$	$E=\ 1.288-0.0591pH$
$Fe^{2+}+H_2O=FeO+2H^+$	$E=-13.00-Log[Fe^{2+}]-2pH$
$FeO+H_2O=HFeO_2^-+H^+$	$E=-18.30-Log[HFeO_2^-]+pH$
$2Fe^{3+}+3H_2O=Fe_2O_3+6H^+$	$E=-0.720-Log[Fe^{3+}]-3pH$
$2Fe+4H_2O=2Fe(OH)_2+4H^++2e^-$	$E=\ 4.840-Log[Fe(OH)_2]-3pH$
$2FeOH^{2+}+H_2O=Fe_2O_3+4H^+$	$E=-2.150-Log[FeOH^{2+}]\ -2pH$

The Pourbaix diagrams do not involve the mechanism of the passivation process and so the steps involved in the reaction processes are summed up in one overall equation.However, this does not invalidate them as diagnostic models for the behaviour of the metals in electrolytes, but implies that some of the intermediate steps and even the end-products of the processes could be those either not considered in the above table as proposed by Pourbaix or that they exist in domains where they have not been considered. The proposed mechanism for iron passivation will be reviewed in the next section.

2.9.3...MECHANISTICS OF IRON PASSIVATION

The electrochemical processes are notoriously difficult to elucidate as was discussed in the very basic case of the HER. The passivation of iron, because of its multivalent states , which could result in numerous intermediate ionic or molecular products, proves even more complex.

This fact is well illustrated by the multitude of papers and reviews [243-252] which have been published in recent years expressing diverse views. The best phenomenological definition of the passivity comes from Vetter as "....drastic decrease of corrosion current density (i,corr) as a measure of metal dissolution which, in turn, is dependent on the

electronic and ionic conductivity of the passive film" [253]. This is shown schematically in Fig.27 .

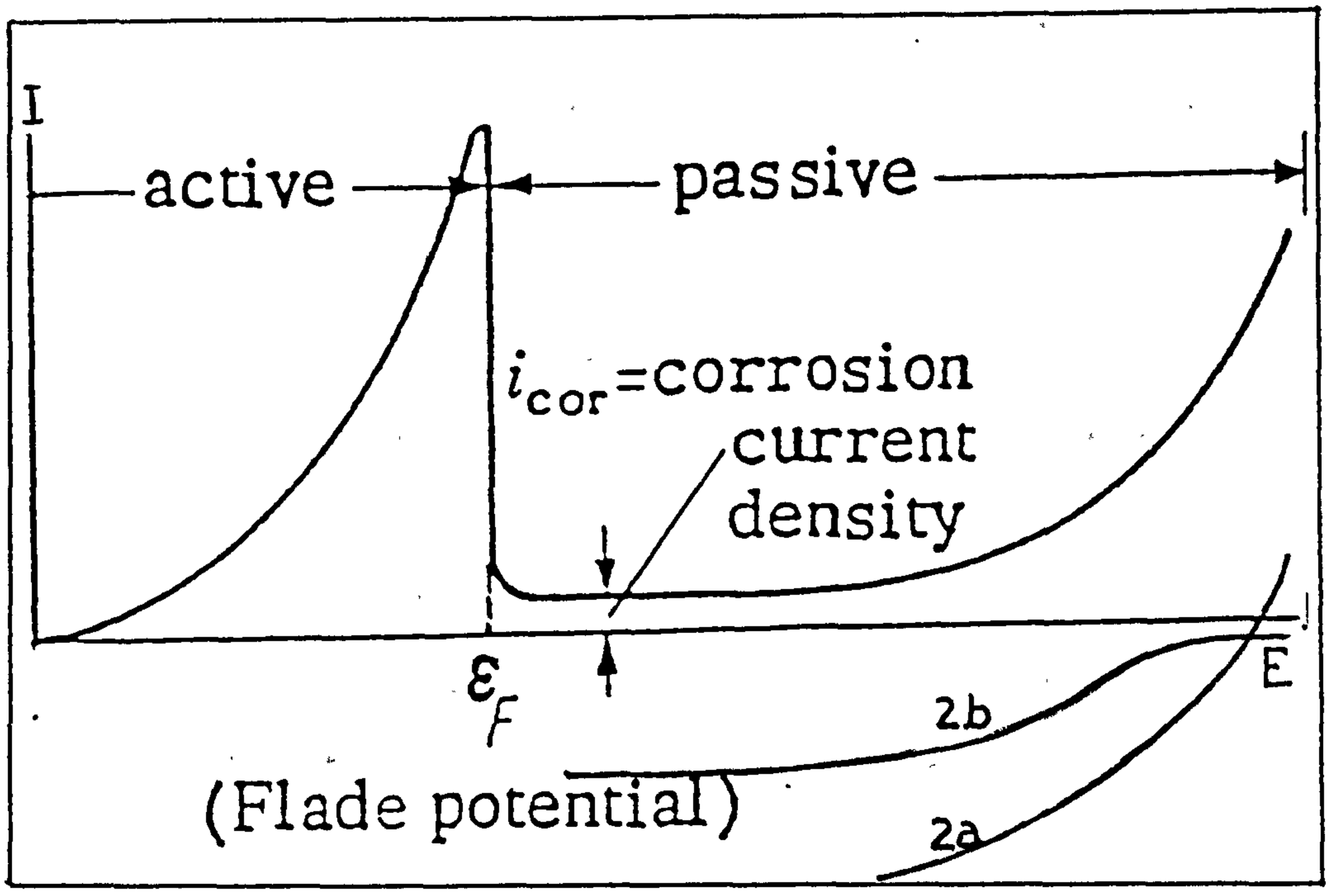

Fig.27 Schematic of a typical current-voltage plot showing transition from active to passive domains. After Vetter [255].

The potential above which passivity occurs is known as the "Flade" potential (E_F). This transition could be achieved through three different processes.

a) anodic polarisation

b) electrolytic passivation

c) atmospheric film formation

of these, the first case has been extensively researched [243-252,254] while the other two cases have been rather neglected. The reason for this is the ease with which the variables may be controled and data obtained in the anodic polarisation studies. The general principle of passivation applies to all the above; if there are no redox components present in

solution, a current density i, which is greater than ($i_{,corr}$) (c.f. Fig.27) is necessary to push the active /passive equilibrium around (E_{corr}, i_{corr})in the direction of passivation. Once this maximum in the current potential curve has been reached, the current may be reduced again [255].

This basic behaviour must be justified for passivation in oxidising electrolytes just the same. If the active/passive transformation constitutes the partial anodic curve, the partial cathodic current-potential (curve a,b) should be added to the anodic one so that the total anodic current available for the passivation process is calculated. The requisites of passivity in this case are:

$$\left| i_{red.} \ @ \ E_F \right| > i_{corr.} \ @ \ E_F \qquad (151)$$

and $$E_F < E_{ox,Red.} \qquad (152)$$

By adding curves (1), (2a) and (2b) in Fig.27 and checking if the basic requirements (151) and (152) are satisfied, the electrolyte is able to passivate the active metal without external current. Vetter[253] argues that this situation is realized in the case of iron in concentrated HNO_3. Heusler [256] suggests this explanation for alkali solutions that contain air because they provide the small anodic partial current densities (corrosion current) required in alkali solutions. Oxidants such as Ce^{4+}, Cr_2O_3, Fe^{3+} etc do not passivate iron in acid solutions since equation (151) is not fulfilled (curve 2b). However, redox systems of this type may sustain an existing state of passivation

with a mixed potential E_p and as such may be able to maintain a passive state, although not to initiate it (curve 2b). In the case of metals whose Flade potential E_F is more negative than the potential E of the HER in that solution, the reduction of H^+ ions to H_2O may be considered as a process of the type exhibited by curves 2a and 2b in Fig.27. For this reason, metals such as Al, Ti and Ta are passivated in aqueous electrolytes that may even be free of oxygen. These metals, to which one should add Cr/Ni-stainless steels become passive on contact with water.

2.9.4...PASSIVATION THEORIES

The broad view of passivation theories reveals the existence of two schools of thoughts -"Adsorption" and "Oxide Film" theories.The following Figure 28 below illustrates the main possible passivating mechanisms on a metal.

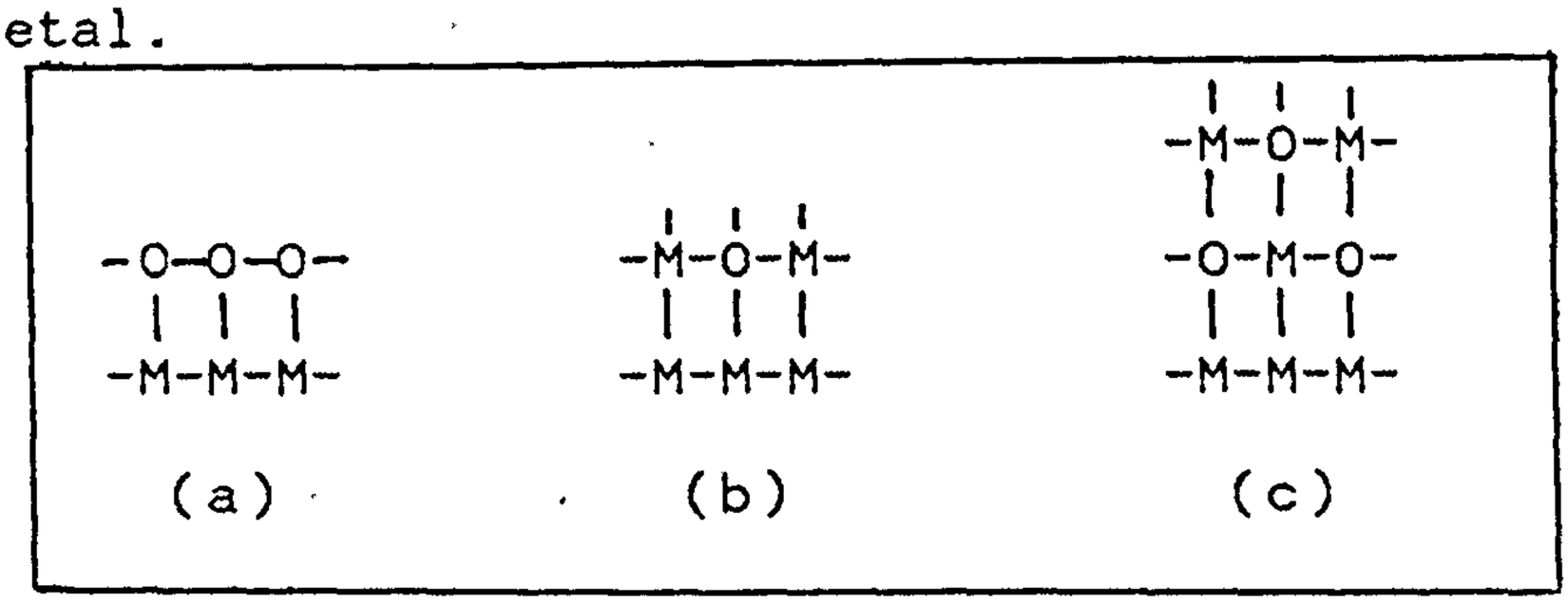

Fig. 28 Characterization of passivity films. (a) adsorbed layer, (b) mono-molecular oxide, (c) three dimensional oxide.

2.9.4.1.The Adsorption Theory

The adsorption theory has been developed by Uhlig, Frumkin, Kabanov and Kolotyrkin [315]. According

to the latter, passivation is described as "a specific case of the widespread phenomenon of the change in the kinetics of the electrode reaction due to adsorption of oxygen from water molecules", for which the following formula is suggested:

$$i = K\ C\ [\exp(\alpha_1 \cdot F/RT)].E \qquad (153)$$

where i =dissolution rate of the metal, A/cm^2

$\alpha_1 = \beta \cdot z$, transfer coefficient

β =0.5 symmetry factor

C =number of atoms/ cm^2 =C exp(-o F/Rt).E

E =applied potential,V

C =number of atoms per square centimetre before the process of passivation sets in.

K =constant

The anodic process in this model would be metal dissolution through the adsorbed film, coupled with the competitive adsorption of anions. Uhlig [238, 258] has developed a parallel chemisorption theory in which the magnitude of the work function of the metal and the enthalpy of sublimation determine the transport kinetics of ions and/or electrons through the film.

2.9.4.2.Oxide Film Theory

The assumption here is that a two or three dimensional oxide film, thick enough to be studied in situ is responsible for passivity.Muller[259] and Vetter[255] are amongst the first to have developed this theory. The model postulates a multi-layer structure in the form of metal/oxide/electrolyte in which the oxide is formed as a result of a potential

more positive than the equilibrium potential of the substrate. Sato[260,261] proposes a specific model for transition metals such as Fe, Ni, Co, based on the effect of the ratio of film thickness (L),and metal/electrolyte interface potential difference ($\varphi_{M/E}$) on the dissolution rate of metal.If the film thickness varies linearly with ($\varphi_{M/E}$),the dissolution rate is independent of potential.

The "sandwich" structure thus proposed implies consecutive steps in which metal ion first crosses from the lattice to the oxide phase, diffuses through the oxide and is finally transferred through the oxide/solution interface by the hydration process when the ion enters the solution side of the electrochemical interface. In the above model, the Helmholtz potential (φ) is governed by the relationship:

$$\varphi_H = \frac{\varphi_{M/E}}{1+(L\cdot\epsilon_H / \delta\epsilon_{ox})} \qquad (154)$$

where ϵ_H =dielectric constant of Helmholtz plane

ϵ_{ox}=dielectric constant of oxide layer

Accordingly, the adsorption of oxygen atoms reduces (φ_H) thus contributing to metal passivation, although the electro-dissolution can increase with ($\varphi_{M/E}$) keeping the kinetics within the adsorbed layer comparable to that in the oxide monolayer.

This model has been very successful in explaining passivity induced by adsorption as postulated by Uhlig [240] as well as other proposed models [262, 263].Generally,the modifications to the oxide film

theory could be summarised in six broad classifications. Fig.29 below illustrates these variations.

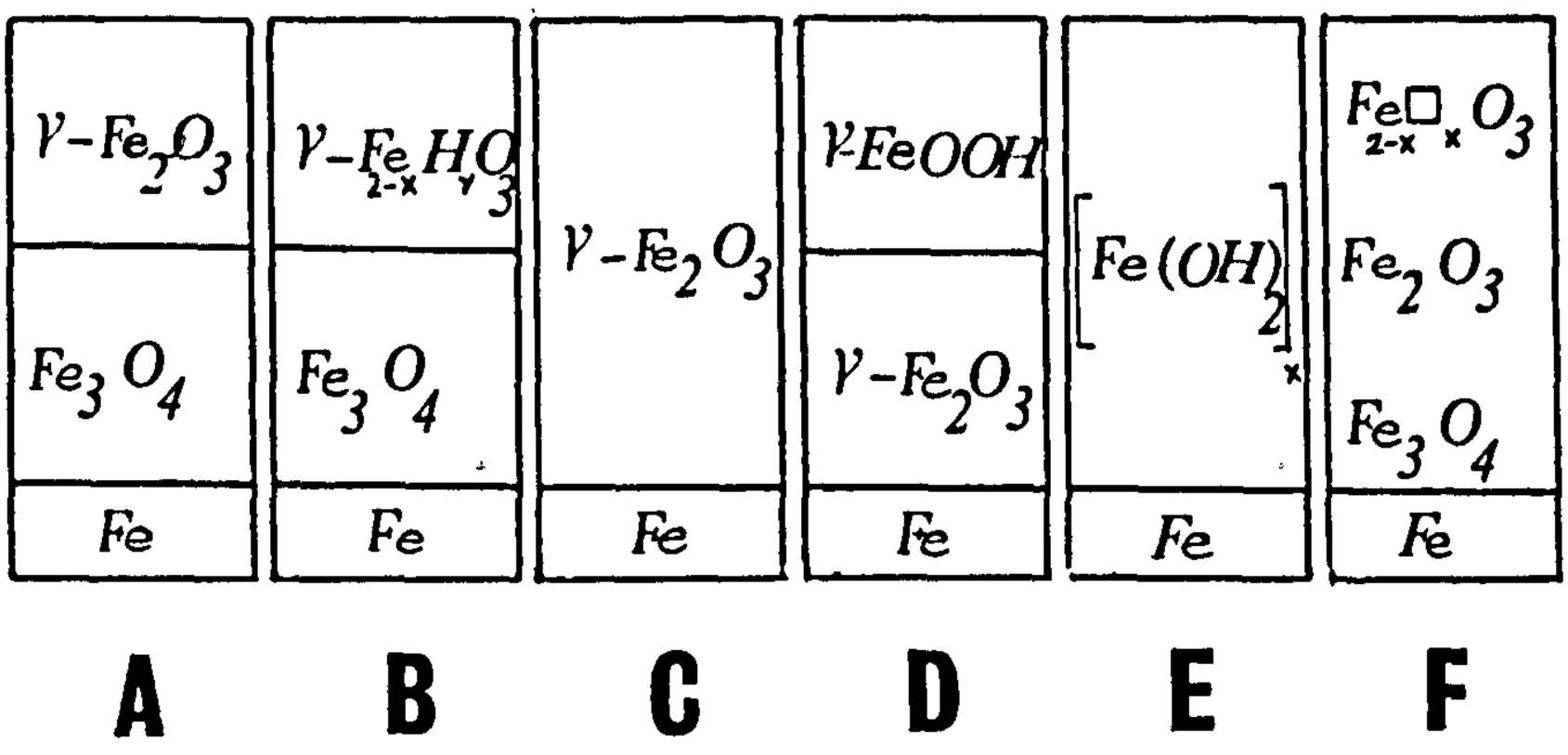

Fig.29 Illustration of different multi-layered structures proposed for Fe passivation

Sato et al [35,264] suggest the first configuration for acid induced passivity and model(D) for the alkali solutions.Bockris et al[265,266] using Auger spectroscopy to analyse the film,have found it to consist of $Fe(OH)_2$ in a polymeric layered structure and therefore conclude that anhydrous γ-Fe_2O_3 widely reported in electron diffraction studies, is the result of the dehydration due to electron bombardment. Cohen and co-workers [267,268] suggest another variation in which an outer layer of γ- FeOOH is formed from the dissolved iron in the solution. Vetter [269] proposes a cation deficient film , represented in Fig.29-f. The possibility of this film containing some hydrogen as a stabilizing agent for γ-Fe_2O_3 has also been explored[270]

2.9.5...SUMMARY OF THE PROPOSED ACTIVE-PASSIVE TRANSITION MODELS

A number of different mechanisms have been suggested for this process for which experimental data

exists. However, most of them do not give credence to one another and this is a sign of the inadequacy of mathematical modelling as well as in the experimental data gathering.

2.9.5.1.Bockris Model

Bockris et al [271] assume simultaneous film formation as well as metal dissolution on the surface. It has been confirmed through ellipsometric measurements, that under constant potential, a linear relationship exists between (L), the film thickness and time (t) which later on becomes logarithmic. The corresponding reaction sequence has been proposed:

$$Fe + OH^- \rightleftharpoons FeOH + e^- \quad (155)$$

ANODIC DISSOLUTION

$$FeOH \xrightarrow{rds} FeOH^+ + e^- \quad (156)$$

$$FeOH^+ \rightleftharpoons Fe^{2+} + OH^- \quad (157)$$

FILM FORMATION

$$Fe\ OH \rightleftharpoons HO\ Fe \quad (158)$$

$$HO\ Fe + OH^- \longrightarrow Fe(OH)_2 + e^- \quad (159)$$

The electro-dissolution and the passivation take place in parallel. Step (158) exhibits exchange between Fe and O atoms during the film growth, which is assisted by the presence of defects.

2.9.5.2.Bech-Nielsen Model

Bech-Neilsen [29,272-275] proposesa mechanism applied to iron in acid media which involves a two stage active dissolution.

$$Fe^{\circ} + 2X \rightleftharpoons Fe^{\circ}(X)_2 \quad (160\text{-a})$$

$$Fe(X_2)+H_2O \rightleftharpoons Fe^{I}(OH^-)(X_{ads})+H^+ +X+e^- \quad (160\text{-b})$$

$$Fe^{II}(OH^-)(X)_{ads}+H_2O \xrightarrow{rds} Fe^{II}(OH^-)_2(X) +H^+ +e^- \quad (160\text{-c})$$

$$Fe^{II}(OH^-)_2(X)_{ads} \longrightarrow Fe^{II}(OH^-)_2(X) \quad (160\text{-d})$$

The second stage involves:

$$Fe^{II}(OH^-)_3(X)_{ads}+3H_2O \rightleftharpoons Fe^{II}(OH^-)(X)_{ads}+3H^+ +X+2e^- \quad (161\text{-a})$$

$$Fe^{II}(OH^-)_3(X)_{ads}+ H^+ \longrightarrow Fe^{II}(OH^-)_2(X) +H_2O \quad (161\text{-b})$$

$$Fe^{II}(OH^-)_2(X)+ X \longrightarrow Fe^{II}(OH^-)_2(X)_2 \quad (161\text{-c})$$

$$Fe^{II}(OH^-)_2(X)_2+ H^+ \longrightarrow Fe^{II}(X)_2 +H_2O \quad (161\text{-d})$$

$$Fe^{II}(X)_2 \longrightarrow Fe^{II}(aq)+2X \quad (161\text{-f})$$

Finally a passivation process

$$Fe(OH)(X) +mH\ O \rightleftharpoons Fe(OH)+mH+X+e \quad (162)$$

where m=1 or 2, and X is any anion molecule X. The influence of anion adsorption and pH is qualitatively explained through this model.

2.9.5.3.Lorenz Model

This model[276-278] explains the behaviour of the active passive transition of iron in slightly acid solutions in the absence of oxygen and surface active species. The sequence of steps is as follows:

$$Fe + H_2O \rightleftharpoons (FeOH)_{ads} + H^+ + e^- \quad (163)$$

$$(FeOH)_{ads} \longrightarrow FeOH^+ + e^- \quad (164)$$

$$FeOH^+ + H^+ \rightleftharpoons Fe^{2+}_{aq} +H_2O \quad (165)$$

$$(FeOH)_{ads.} + H_2O \rightleftharpoons [Fe(OH)_2]_{ads} + H^+ + e^- \quad (166)$$

$$[Fe(OH)_2]+A^- \longrightarrow FeOH^+ + A^+ + OH^- \quad (167)$$

$$Fe_{(s)}[Fe(OH)_2]_{ads}+A^- \longrightarrow FeOH^+ + [FeOH]_{ads}+A^-+e^- \quad (168)$$

$$Fe_{(s)}[Fe(OH)_2]+H_2O \rightleftharpoons Fe_{(s)}[Fe(OH)_3]_{oxide}+H^+ +e^- \quad (169)$$

The active dissolution is basically the same as the Bockris model but in the transition region on inhibiting the membrane represented by $[Fe(OH)_2]_{ads}$ species are formed. This membrane develops a non-porous oxide layer in the subsequent steps.

2.9.5.4.Schwabe Model

Schwabe [280-282] postulates a kinetic model based on the following scheme;

$$Fe + H_2O \rightleftharpoons FeOH + H^+ + e^- \quad (170)$$

$$FeOH \longrightarrow FeOH^+ + e^- \quad (171)$$

$$Fe + H_2O \longrightarrow FeOH^+ + H^+ + 2e^- \quad (172)$$

$$FeOH^+ + H^+ \rightleftharpoons Fe^{2+} + H_2O \quad (173)$$

$$Fe + H_2O \rightleftharpoons FeOH + H^+ + e^- \quad (174)$$

$$FeOH + H_2O \longrightarrow Fe(OH)_2 + H^+ + e^- \quad (175)$$

$$Fe(OH)_2 \rightleftharpoons FeO + H_2O \quad (176)$$

$$FeO + 2H^+ \rightleftharpoons Fe^{2+} + H_2O \quad (177)$$

$$FeO + 2A^- + H_2O \longrightarrow FeA_2 + 2\,OH^- \quad (178)$$

If (i_1) denotes the rate of active dissolution and (i_2) is the rate of film formation reactions for a degree of coverage (θ), the total current for the above mechanism is:

$$i = i\,(1-\theta)(i_1 + i_2) \quad (179)$$

and the rate or change of surface coverage (θ) results:

$$d\theta/dt = C.i_2(1-\theta) - K\theta - B\theta \quad (180)$$

where C =proportionality constant

K and B =rate constants for oxide dissolution

The solution of the above equation under the initial conditions of t=0, θ=0, gives current/time and

potential/time relationships which are qualitatively in good agreement with experimental data.

2.9.5.5.Epelboin and Keddam Model

Using the concepts suggested by Franck and Fitzhugh [283], and developed by Epelboin and Keddam [249,284], this model is based mainly on the results of AC impedance experiments.

$$(Me) + S \xrightarrow{K1} (Me)\,S^{+m} + me \qquad (181)$$

$$(Me) + 2S \underset{K_{-2}}{\overset{K_{+2}}{\rightleftharpoons}} (Me)\,S^{+n} + ne \qquad (182)$$

Where (Me) is a metal and (S) is either a neutral or charged species in solution, participating in the anodic reaction.Reaction (181) yields a soluble species $(Me)\,S_2^{+m}$ and (182) gives $(Me)\,S_2^{+n}$ species which passivates a fraction (θ) of the electrode surface. On the assumption of a Langmuirian adsorption isotherm for MeS_2 the steady rate of metal electro-dissolution can be explained as:

$$V_m = K_{+1} \cdot K_{-2} \cdot C_s / (K_{+2} \cdot C_s^2 + K_{-2}) \qquad (183)$$

and in terms of diffusion flow of species S,

$$V_d = (D/\delta_N)(C_{s,o} - C_s) \qquad (184)$$

where C_s and $C_{s,o}$ stand for concentration of species S at interface and bulk of the solution respectively. D, is the diffusion coefficient of S, δ_N,is the diffusion layer thickness. By equating $V_m = V_d$ a third degree equation in "C" is obtained which for an appropriate set of parameters and sufficiently large $\delta_{N/D}$ has three roots, ranging from zero to C. Each root corresponds to

a dissolution rate at given potential. The computed E-i curve shows a diffusion-limiting current. Through the calculation of the Faradaic impedance, this model can be characterized more quantitatively. Six types of diagram can be predicted in the complex plane from the variation of the faradaic impedance with frequency. The model explains the potential-current curves and the impedance variations of the Fe/H_2SO_4 system. The experimental results were quantitatively interpreted by computer simulations[244] on the basis of the following reaction model

$$\begin{array}{ccccc} & & Fe^*(I) & & \\ & & \rightleftharpoons & & \\ Fe & \longrightarrow & Fe(II) & \longrightarrow & Fe(II)aq \\ & & & & Fe^*(II)ad \\ & & & \searrow & \\ & & & & Fe(II)ad \longrightarrow Passivity \end{array} \qquad (185)$$

2.9.5.6.Arvia's Model

The use of the triangularly modulated potential sweep and AC impedance measurements over a wider range of pH has enabled Arvia et al [284,285] to formulate a mechanism of passivation for Fe in oxygen free aqueous solutions.

$$Fe_b[Fe(H_2O)] \rightleftharpoons Fe_b[Fe(OH)] + H^+ + e^- \qquad (186\text{-a})$$

$$Fe_b[Fe(OH)] \rightleftharpoons Fe_b[Fe(OH)_2] + H^+ + e^- \qquad (186\text{-b})$$

$$Fe_b[Fe(OH_2] \longrightarrow Fe_b[Fe(OH)]^* \qquad (187)$$

$$Fe_b[Fe(OH)] \longrightarrow Fe_b[Fe(OH)]^* \qquad (188)$$

$$Fe_b[Fe(OH)] + H_2O \longrightarrow Fe_{b_{x-1}}[Fe(H_2O)] + FeOH^+ + e^- \qquad (189\text{-a})$$

$$Fe_{b_x}[Fe(OH)]^* + H_2O \longrightarrow Fe_{b_{x-1}}[Fe(OH)_2] + FeOH^+ + H^+ + 2e^- \qquad (189\text{-b})$$

$$Fe_{b_x}[Fe(OH)]^* + H_2O \longrightarrow Fe_{b_{x-1}}[Fe(H_2O) + FeOH^+ + H^+ + e^- \qquad (190\text{-a})$$

$$Fe_{b_x}[Fe(OH_2)]^* + H_2O \longrightarrow Fe_{b_{x-1}}[Fe(OH)_2] + FeOH^+ + H^+ + 2e^- \qquad (190\text{-b})$$

and finally oxide formation

$$Fe_{b_{X-n}}[Fe(OH_2)] + H_2O \rightarrow Fe_{X-1}[Fe^{II}\text{-hydrated oxide}] \underset{+H^+ + e^-}{} \quad (191)$$

$$Fe\ (II)\text{-hydrated oxide}] \longrightarrow [Fe(III)\text{-oxyhydroxide}] + H_2O + H^+ + e^- \quad (192)$$

$$H^+ + FeOH^+ \rightleftharpoons Fe^{2+} + H_2O \quad (193\text{-a})$$

$$FeOH^+ + H_2O \rightleftharpoons Fe(OH)_2 + H^+ \quad (193\text{-b})$$

where b denotes bulk and brackets indicate a product formed on the surface.

The above summary is by no means a complete list of all the proposed mechanisms in the literature or cover all the possible permutation of the species involved or the steps postulated however, it does contain the major contributors proposing the more widely accepted mechanisms up to date.

2.9.6...THEORY OF THE AC IMPEDANCE MEASUREMENTS

2.9.6.1.INTRODUCTION

Few techniques can be used in situ to study passivation.The main class of such experimental techniques is optical.In many respects, the use of ellipsometry and other optically oriented systems is very advantageous in the study of surfaces.However, for many applications alternating current methods could identify interfacial properties without needing the special surface treatments so essential to optical methods.They can also break new ground in identifying processes and products, with reference to the massive accumulation of data available to the researcher from the past hundred

years of electrochemical studies.However,the same could not be said about the optical techniques which still need to isolate and then identify the properties of films whether on iron or other substrates. One shortcoming of the AC impedance theoreticians has been their preoccupation with mathematical analysis, leading to a surfeit of literature filled with mathematical arguments that perplexes all but the most persistent of readers.

2.9.6.2.The Principles of AC Techniques

The AC impedance technique used in this project is based on the superimposition of small perturbations of (+10 mV) over the potential of the surface under examination.This results in a transient in the E-I behaviour of the system which is then measured and recorded allowing detailed analysis of different phenomena. Using these high accuracy measurements of the response to the imposed perturbations, repeated if necessary over a long period a system could be thoroughly investigated. Since the perturbations are so small,treating them as linearized potential/current (E-I) characteristic is possible [287]. In such experiments, a three electrode cell with working(W), counter (C) and a non-polarisable reference electrode (R) connected to a rapid response potentiostat which can slowly polarize the membrane and in doing so superimpose a sinusoidal component E of perhaps ±5 to ±10 mV magnitude on the surface at each step. Fig.28

below shows such a typical experimental arrangement. Since a sinusoidal voltage can be expressed as:

$$E = E^* \sin \omega t \qquad (161)$$

where E =the imposed potential, V

E^* =the amplitude of the wave used, V

$\omega = 2\pi f$ =angular frequency, rad/s

f =conventional frequency, Hz

t =time, s

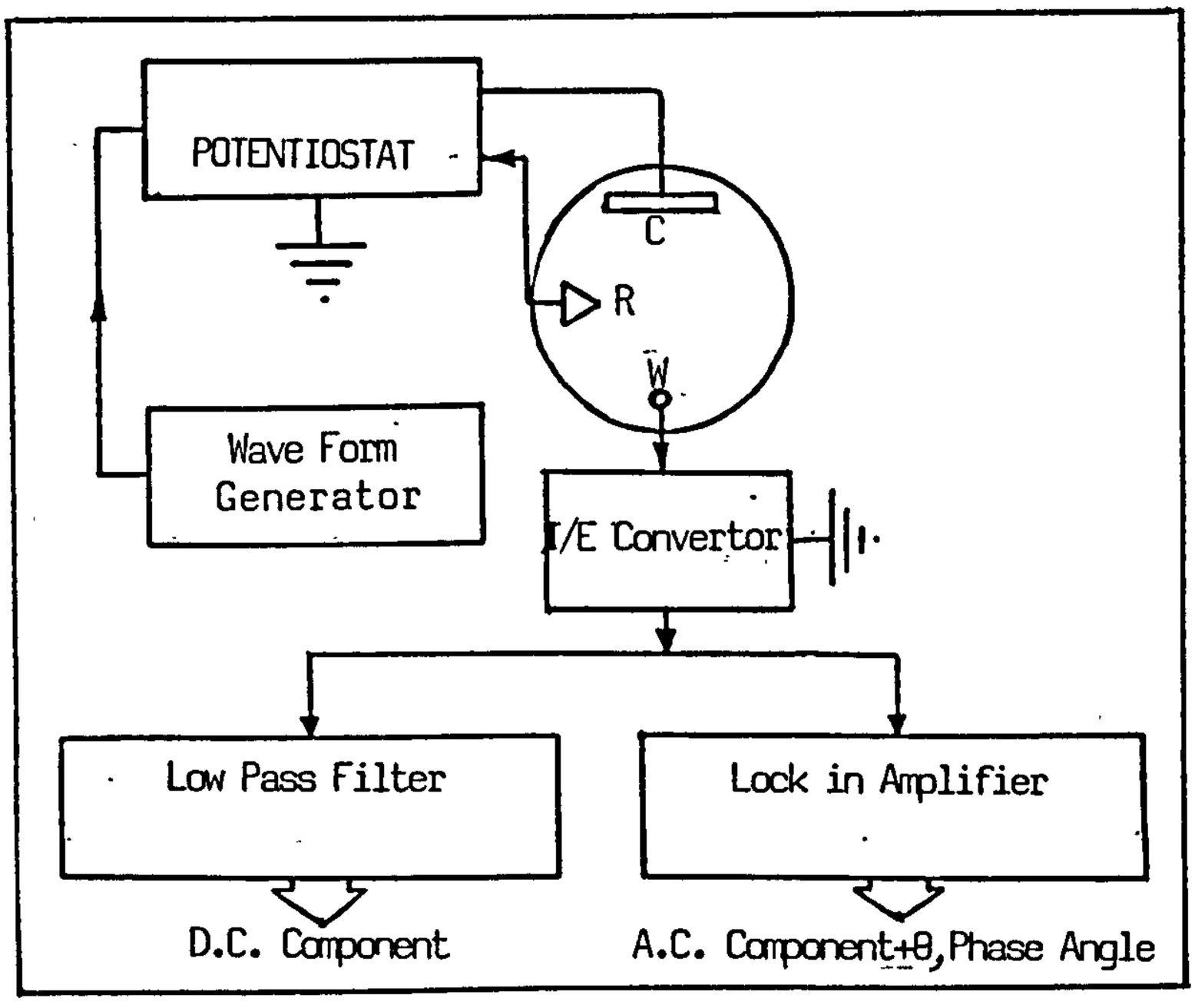

Fig.30 Schematic diagram of an AC impedance experiment

The observed voltage E is the component of the vector describing the voltage. The current resulting from such perturbation has the following expression:

$$I = I^* \sin(\omega t + \theta) \qquad (195)$$

where I =the observed current, A

I^* =the amplitude of the current wave, A

$\omega = 2\pi f$ =angular frequency, rad/s

θ =phase angle between the current and potential

"θ" could be positive or negative, depending on whether the voltage and current are in or out of phase. The

relationship between E and I, can therefore be explained in terms of a constant phase difference (θ), between the vectors of E and I as this remains constant throughout.For the following circuit, these representations could be made;

a) The Case of a Simple Resistance (R)

Here a resistance across which a sinusoidal voltage $E=E^{*}$ sin ωt is applied is considered. The phase angle is zero as the vector diagram of Fig.31 demonstrates.

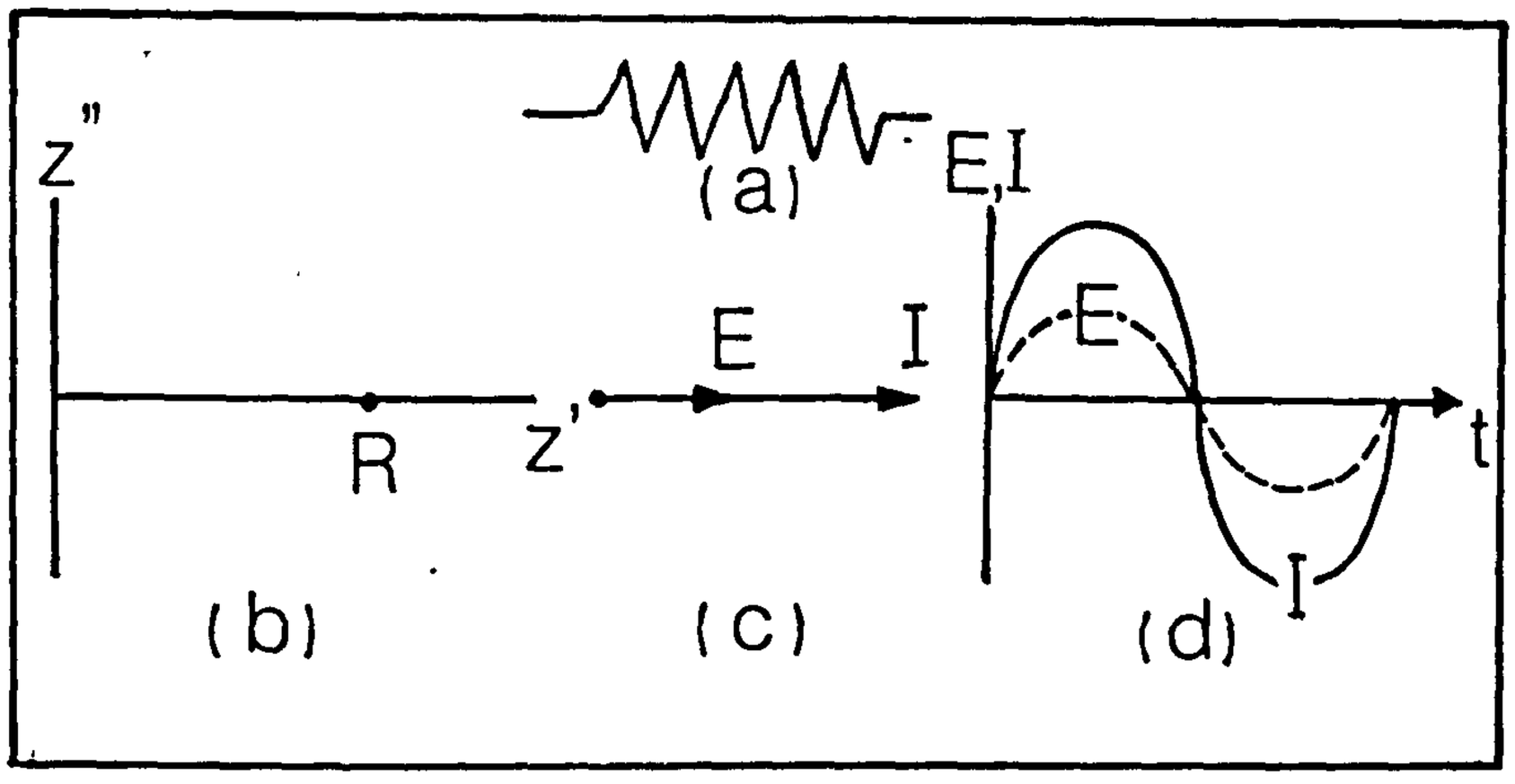

Fig.31 Schematic representation of (a) a simple resistance and the real - imaginary impedance (Nyquist) plot of its impedance (b), together with vector (c) and E vs t and I vs t diagrams (d) for it.

b) Case of a Pure Capacitance

For a pure capacitor "C" the following relationships holds.

$$Q = E.C \qquad (196)$$

and $$I = C(\partial E/\partial t) \qquad (197)$$

where Q =the quantity of electricity stored in a capacitance

Then $I = \omega.C.E \cos \omega t$ (198)

or $I = E/X \sin(\omega t + \pi/2)$ (199)

where I =observed current

X =reactance of the capacitor

The phase angle in this case evidently is $+\pi/2$ and therefore current leads the voltage. Fig.32-c represents the vector diagram for such a configuration. Notation (j) used represents the imaginary part of a complex number. Taking this into account, one could represent the impedance of such a capacitor (Fig.32-b) on two axes.The X- axis representing the real and the Y-axis the imaginary part so that the out of phase position of the two is demonstrated.

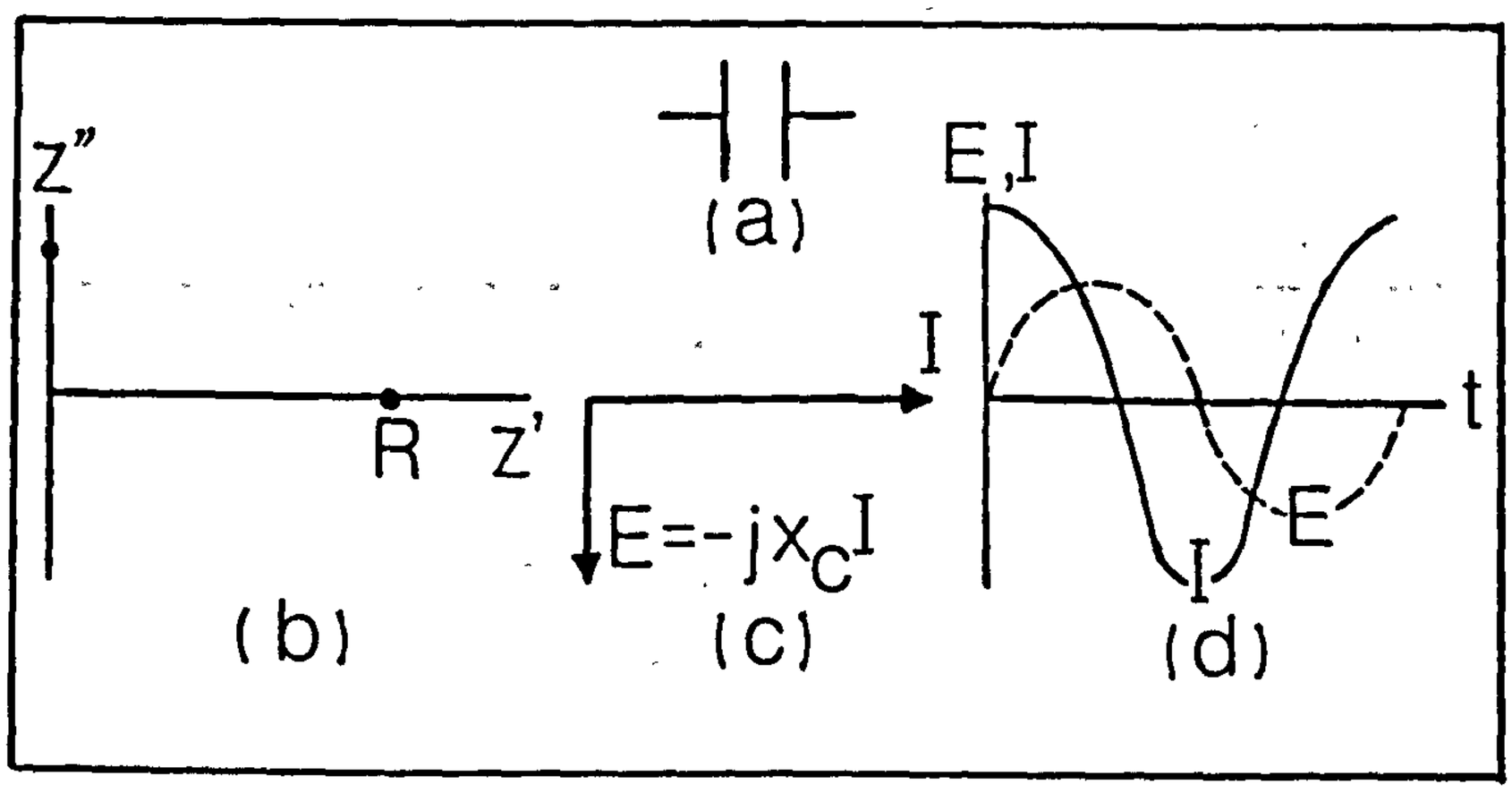

Fig.32 Vector diagram for an alternating voltage across a single capacitor (C) as well as its Nyquist plot (b).

c) A Resistor and a Capacitor in Series

In this more complex case, when the voltage E is applied , it is always the sum of the potential

drops across all the individual components in that circuit. Therefore:

$$\vec{E} = \vec{E}_R + \vec{E}_x \qquad (200)$$

$$\vec{E} = \vec{I}\,(R - jX) \qquad (201)$$

$$\vec{E} = \vec{I}\,Z \qquad (202)$$

The reciprocal of the impedance (Z) is the admittance (Y), analogous to conductance in d.c. theory, $Y = 1/Z$. thus the voltage is linked to the current, through the vector Z, called impedance.

$$Z = R - j\,X \qquad (203)$$

$$|Z| = \sqrt{R + X} \qquad (204)$$

The following Fig.33 illustrates the relationships in the above mentioned case.

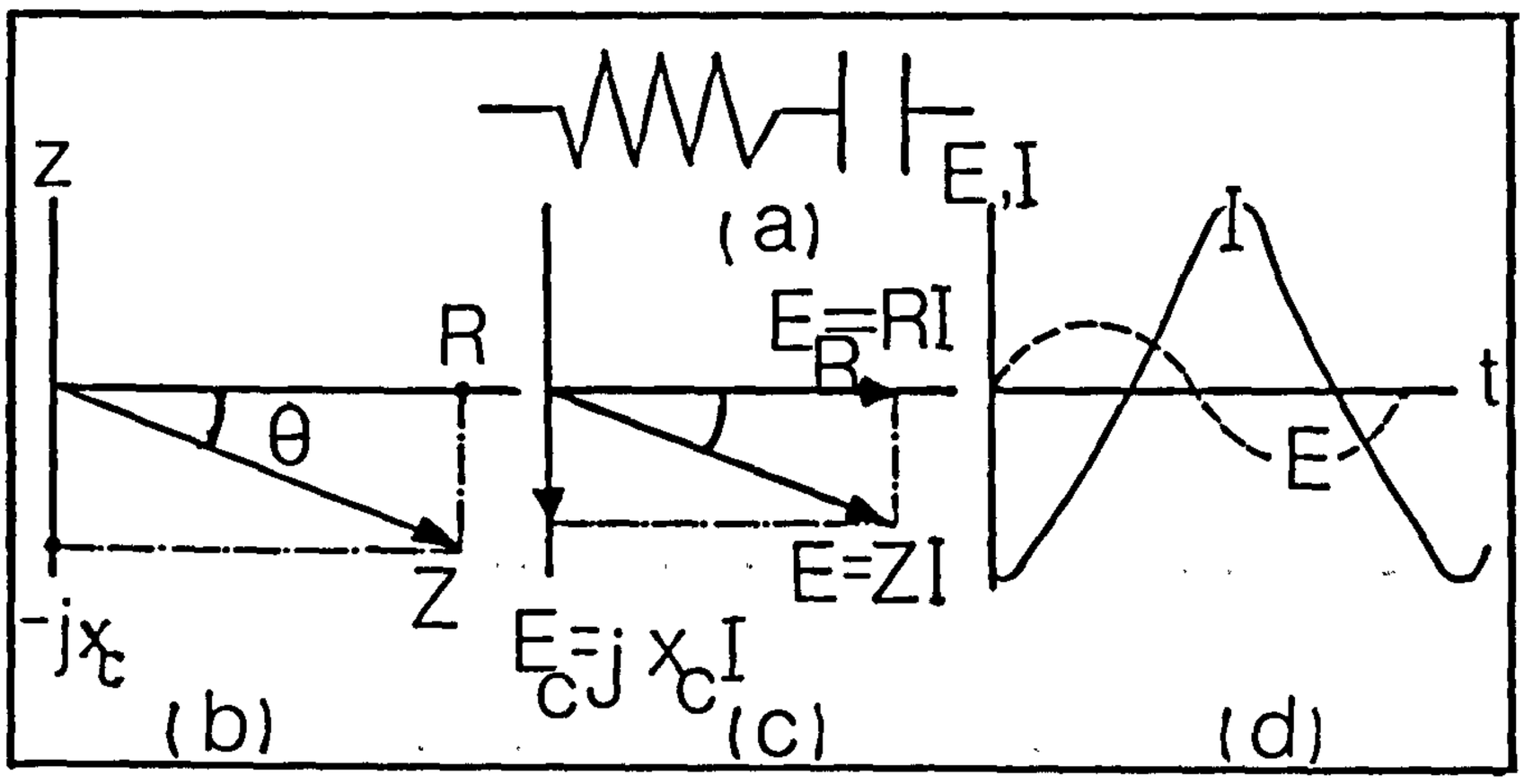

Fig.33 Phase (d),vector (c),Nyquist (b) diagrams and the schematic representation of a simple resistor-capacitor circuit.

There are several comprehensive overviews on this subject[288-293].However here attention is concentrated on the available data analysis techniques relevant to the current investigation.

2.9.6.3.Equivalent Circuit of Electrode/Electrolyte Interface in Electrochemical Problems

An electrochemical system may be compared with an electrical system in which the basic electrical components represent the different parts of the interface.This was first recognized by Randles [294] who was able to relate an electrode reaction to the form of circuit impedance consisting of impedances resulting from the charge transfer and the mass transfer processes involved.This analysis needs four components; one capacitor (C_{dl}) to represent the capacitance nature of the double layer formed on the working electrode, and three resistors to represent the charge transfer (R_{ct}).Mass transfer resistance (Z_W) Warburg (impedance), and a solution resistance (R_Ω). These are usually combined as a "Randles Equivalent Circuit" [290] as shown below .

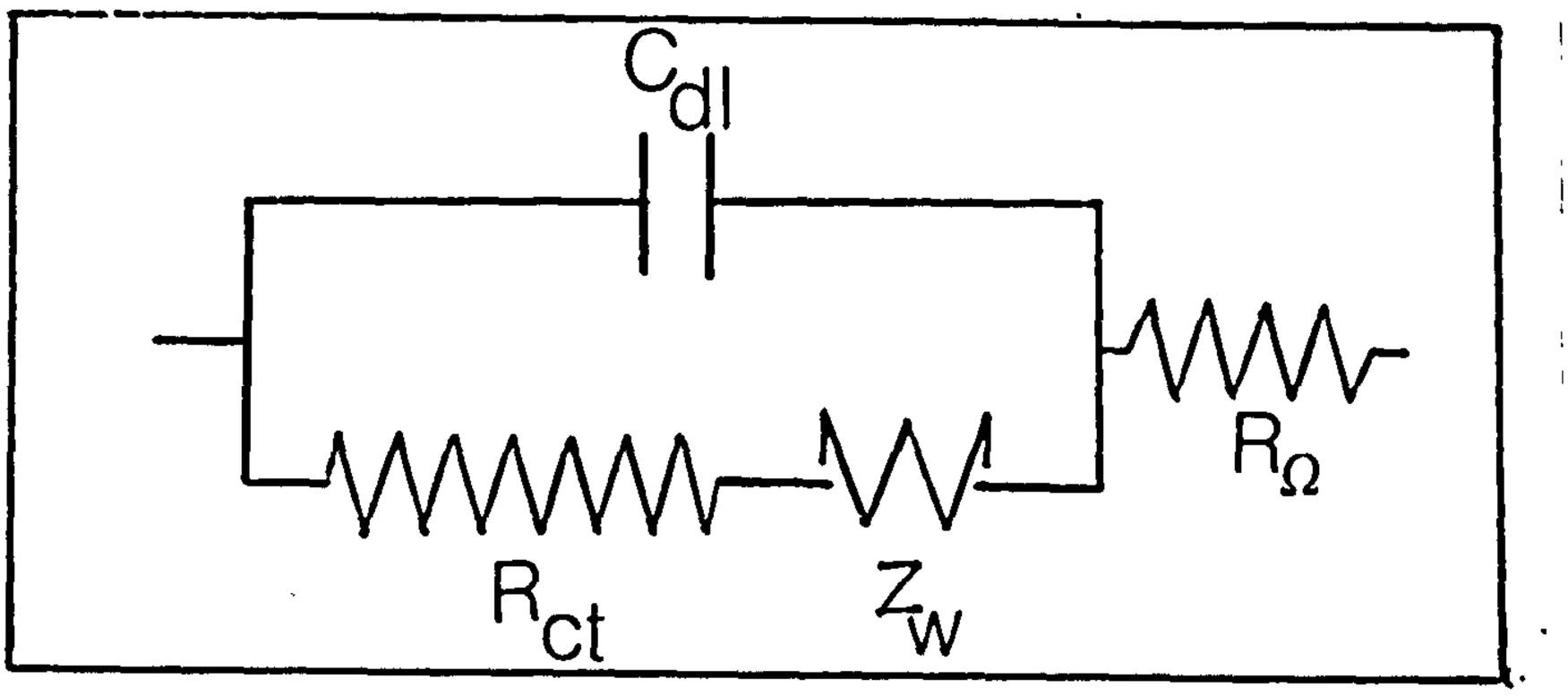

Fig.34 Typical Randles equivalent circuit

The electrical elements considered are as follows:

(I) The Ohmic Resistance (R_Ω)

The ohmic resistance of a system consists of a combination of the solution resistance as well as the resistance of the connecting leads and the metal electrode used. However, the ratio of the resistances of the metallic electrode and the leads , to that of the solution is extremely small and thus they could be neglected in comparison to the solution's resistance. In the Randles circuit, this is represented as a simple resistance (R_Ω).

(II) The Double Layer Capacitance (C_{dl})

Once an electrode is immersed in an electrolyte the surface forms an interface which in part consists of a double layer.This double layer, resulting from the separation of the positively and negatively charged ions on either side of Helmholtz planes act exactly like a "parallel plates capacitor".The capacitance thus generated is governed by the following factors:

a)the thickness of the double layer itself

b)the relative permittivity of the electrolyte

c)the ionic concentration of the solution

In the Randles equivalent circuit this is represented by (C_{dl})which is in series with the (R_Ω).

(III)Charge Transfer Resistance(R_{ct})

Charge Transfer Resistance could be defined as the Resistance shown on the part of the working electrode to any addition or removal of electrons, at a constant potential.

$$R = (dE/dt) \qquad (205)$$

At or near the equilibrium potential,this could be expressed as

$$R = \frac{RT}{z^2 F^2 K_o} \cdot \frac{1}{C_{ox}^{\alpha} . C_{red}^{1-\alpha}} \quad (206)$$

where R =gas constant, 8.314 kJ/mol/K

T =temperature, K

z =number of electrons involved

F =Faraday's constant, 96487 C/mol

C_{ox} =concentration of oxidising species, mol/dm^3

C_{red} =concentration of reducing species, mol/dm^3

α =symmetry factor, normally 0.5

(IV) The Warburg Impedance (Z)

The Warburg impedance represents all those impedances resulting from mass transport phenomenon. This could be the diffusion of species to and from the bulk of electrolyte towards the electrode. The impedance thus defined is given as:

$$Z = \sigma . \omega^{-1/2} - j \sigma \omega^{-1/2} \quad (207)$$

where σ =Warburg coefficient

$$= \frac{RT}{\sqrt{2Z^2F^2}} \left(\frac{1}{D_{ox}^{1/2} C_{OX}^{1/2}} + \frac{1}{D_{Red}^{1/2} C_{Red.}^{1/2}} \right) \quad (208)$$

where ω =angular frequency=$2\pi f$, rads

j =complex operator = $\sqrt{-1}$

D_{ox} =diffusivity of oxidising species in the electrolyte, cm^2/s

$D_{Red.}$ =diffusivity of reducing species in the electrolyte, cm^2/s

C_{OX} =concentration of oxidising species, mol cm^{-3}

$C_{Red.}$ =concentration of reducing species, mol cm^{-3}

R,T,z,F -have their usual meanings as described before

The total impedance in a Randles equivalent circuit shown in Fig.34 could be represented as

$$Z_F = Z_{ct} + (Z_{diff,ox} + Z_{diff,red}) \quad (207)$$

Z is also known as Faradaic impedance of the total circuit. The above equation could also be represented as $Z_F = R_{Ct} + Z_W$ (210)

The Randles equivalent circuit represents the simplest electrochemical reaction,i.e. a one step oxidation/ reduction reaction of Ox + ne ⟶ Red .The response to any perturbation on the impedance of the system as described above,may be summarized in the following two equations. Equation (211) describes the real part Z' and equation (212), the imaginary part of impedance Z'':

$$Z' = R_\Omega + \frac{R_{ct} + \sigma \omega^{-1/2}}{(\sigma \omega^{1/2} C_{dl} + 1)^2 + \omega^2 C_{dl}^2 (R_{ct} + \sigma \omega^{-1/2})^2} \quad (211)$$

and

$$Z'' = \frac{\omega . C_{dl} (R_{ct} + \sigma \omega^{-1/2}) + \sigma^2 C_{dl} + \sigma \omega^{-1/2}}{(\sigma \omega^{1/2} C_{dl} + 1)^2 + \omega^2 C_{dl}^2 + (R_\Omega + \sigma \omega^{-1/2})^2} \quad (212)$$

At high frequencies, i.e. as $\omega \longrightarrow \infty$, the Warburg impedance becomes negligible as $\sigma\omega^{-1/2}$ tends towards zero. Equations (211) and (212) could then be reduced to:

$$Z' = R_\Omega + R / (1 + \omega^2 . \tau^2) \quad (213)$$

$$Z'' = \omega . \tau . R / (1 + \omega^2 \tau^2) \quad (214)$$

(τ) shown in the above equations is termed the "time constant" of the system and shows the relaxation time response of any system. It can be shown that "τ" is related to R_{ct} and C_{dl} as:

$$\tau = R_{ct} . C_{dl} \quad (215)$$

At low frequencies the angular frequency w tends towards zero and therefore ω terms are negligible. Equations (211) and (212) will then be reduced to:

$$Z' = R_{\Omega} + R_{ct} + \sigma \omega^{-1/2} \quad (216)$$

$$Z'' = \sigma \cdot \omega^{-1/2} + 2\sigma^{2} C_{dl} \quad (213)$$

The above deductions are for the case of a simple, one step oxidation/reduction reaction.However,there are two more systems of additional complexity to be described here.

2.9.6.4.Equivalent Circuit for the Case of Adsorbed Species on the Working Electrode

The equivalent circuit, representing such a case is given in Fig.35.

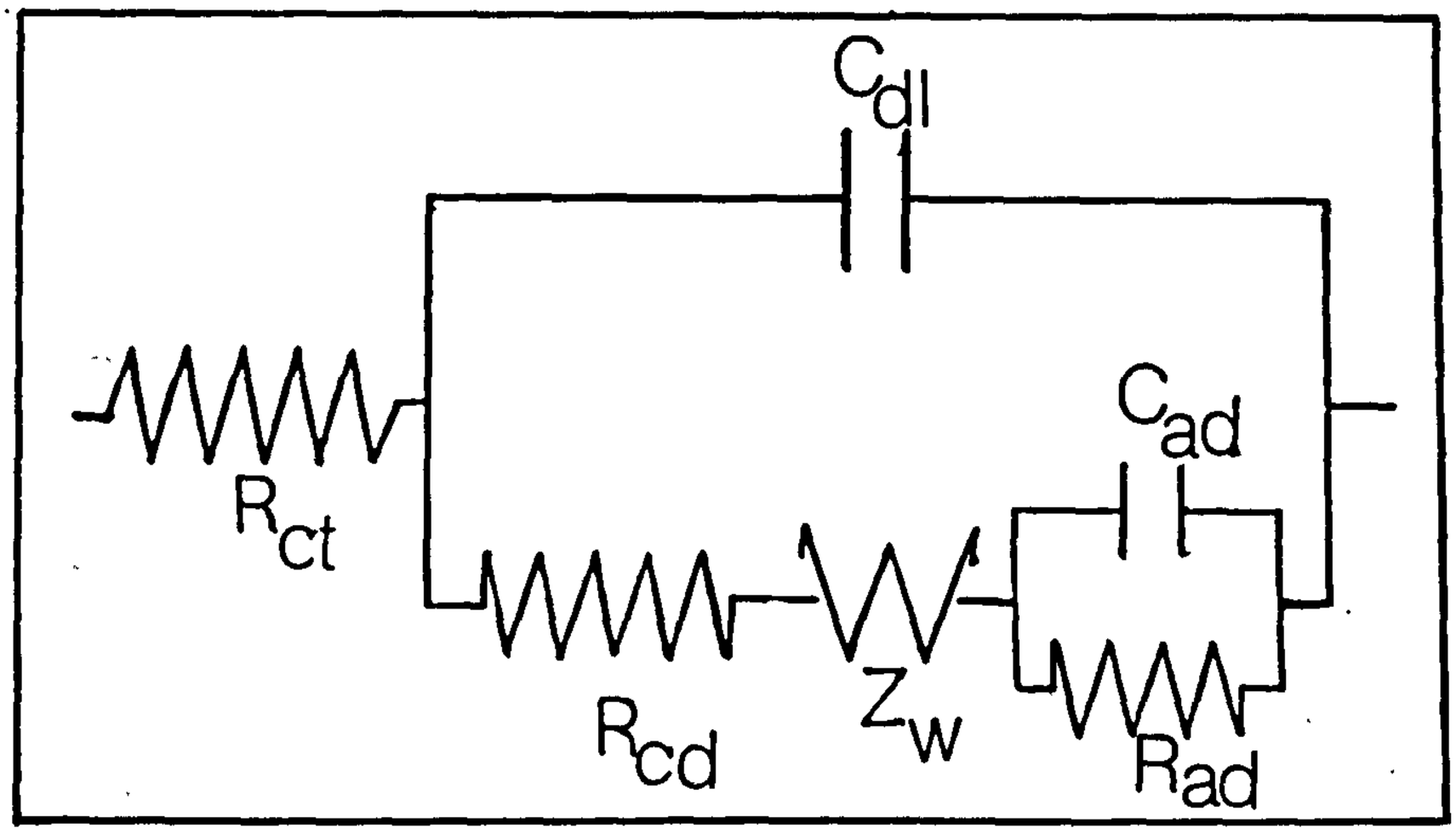

Fig.35 Schematic diagram of an equivalent circuit for an adsorbed layer formed on the working electrode.

In this representation R and C denote "adsorption pseudo resistance" and "adsorption capacitance" respectively. The two variables could be expressed[255] as:

$$R_{ad} = (RT/z^{2}F^{2}C_{ad})/K$$

$$= RT/z^{2} \cdot F^{2} \cdot K \cdot C_{ad}. \quad (218)$$

and

$$C_{ad} = z^{2}F^{2}R \quad /RT \quad (219)$$

where C_{ad}=surface concentration of the adsorbed species

R,T,z,K,F all have their usual meanings.

As will be illustrated later the effect of such changes could be represented by the Nyquist plots showing the data as semi-circles exhibiting two relaxation time constants (τ); one for the charge transfer and double layer part of the surface and the other for the pseudo RC network incorporated. These semi-circles in the Nyquist plots, fall on different sides of ordinate (Z'') and abscissa (Z'). The relationship between the τ and R_{ad} and C_{ad} is

$$\tau_{ad} = R_{ad} \cdot C_{ad} \qquad (220)$$

The above relationships show the effects of an adsorbed layer on an interfacial impedance could be arrived at using a different route. Armstrong[288] expresses the same interaction within the same equivalent circuit frame work in Fig. 39 , in terms of R_o and R_∞ which are defined as:

$$R_0^{-1} = \tau \left[n_1 F\left(\partial J_1 / \partial E \right)_{C_{ad}} + n_2 F\left(\partial J_2 / \partial E \right)_{C_{ad}} \right] \qquad (221)$$

where R_0=the additional zero frequency resistance of the system i.e. showing the C_{ad}.

n_1 and n_2=two integers resulting from the Taylor series expression

J_1 and J_2=the fluxes of formation and the disappearance of the adsorbed species

E =surface potential

C_{ad}=concentration of the adsorbed species on the surface

and $$R_\infty = \left[n_1 F\left(\partial J_1 / \partial E \right)_{C_{ad}} + n_2 \left(\partial J_2 / \partial E \right)_{C_{ad}} \right] \qquad (222)$$

with the same notation as before, except for R_∞ which denotes the infinite frequency resistance equal to the charge transfer resistance in the ordinary Randles circuit. According to Armstrong;

$$R_{ad} = - R_\infty (R_o + R_\infty) \quad (223)$$

$$C_{ad} = -R_o \tau / R_\infty^2 \quad (224)$$

2.9.6.5.Equivalent Circuit for the Film Covered Electrodes

A film formed on an electrode surface will itself introduce an impedance in the system regardless of any further interactions between it and the electrolyte. Three distinct cases may arise:

(i) Films Acting as Electrical Insulators

In such a case the film will behave as an almost pure capacitor. The equivalent circuit therefore comprises a single capacitor in series with the Warburg and the charge transfer resistances as shown in Fig.36.

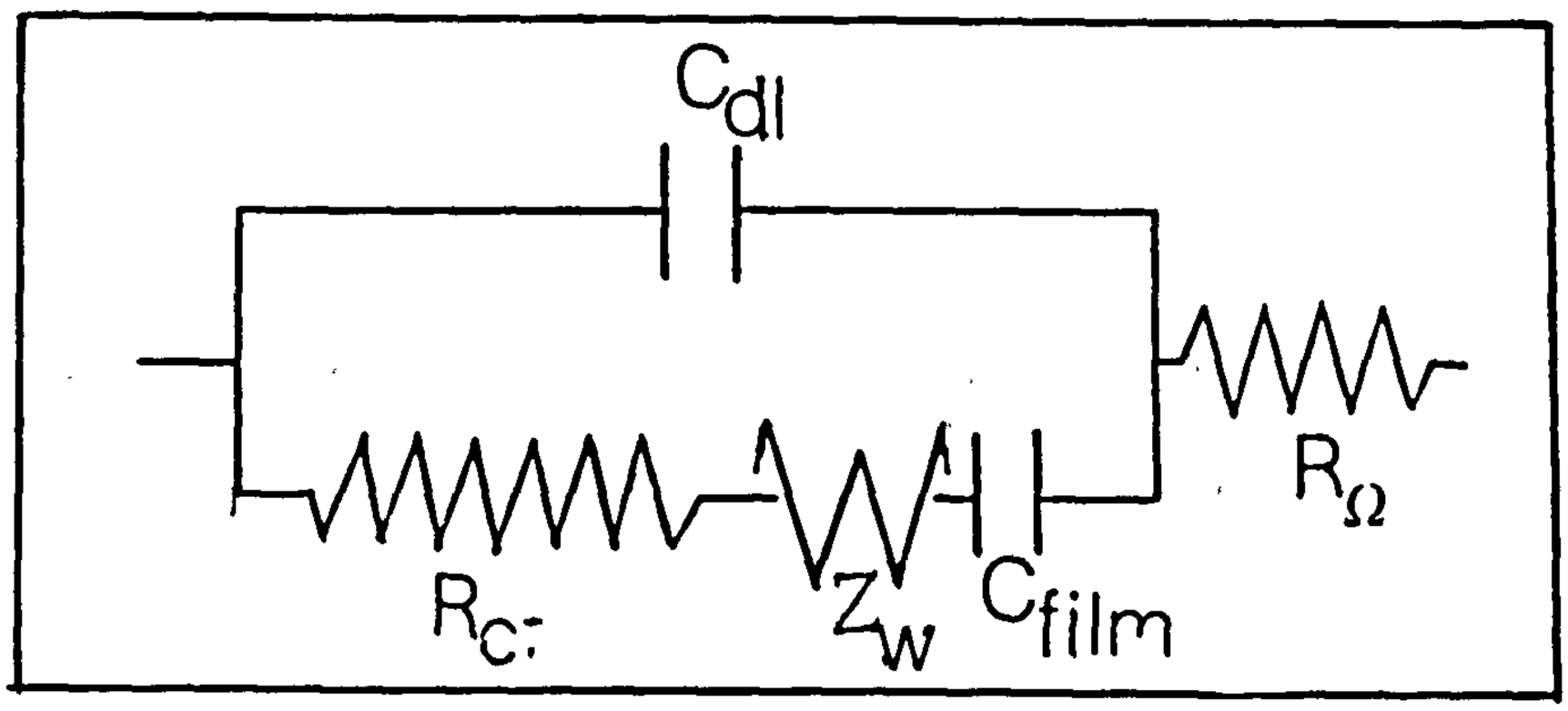

Fig.36 Equivalent circuit for a film covered electrode where the film acts as an insulator

For such a film, the relaxation time is dictated by

$$\tau = \rho . \epsilon . \epsilon_0 \qquad (225)$$

where ρ =resistivity of the film , Ω m

ϵ =relative permittivity of the film

ϵ_0 =permittivity of the vacuum.

(ii) Films Acting as Electrical Conductors

Here the film act as a pure resistance and is represented by a single resistor R in series with Z and R as illustrated in Fig.37.

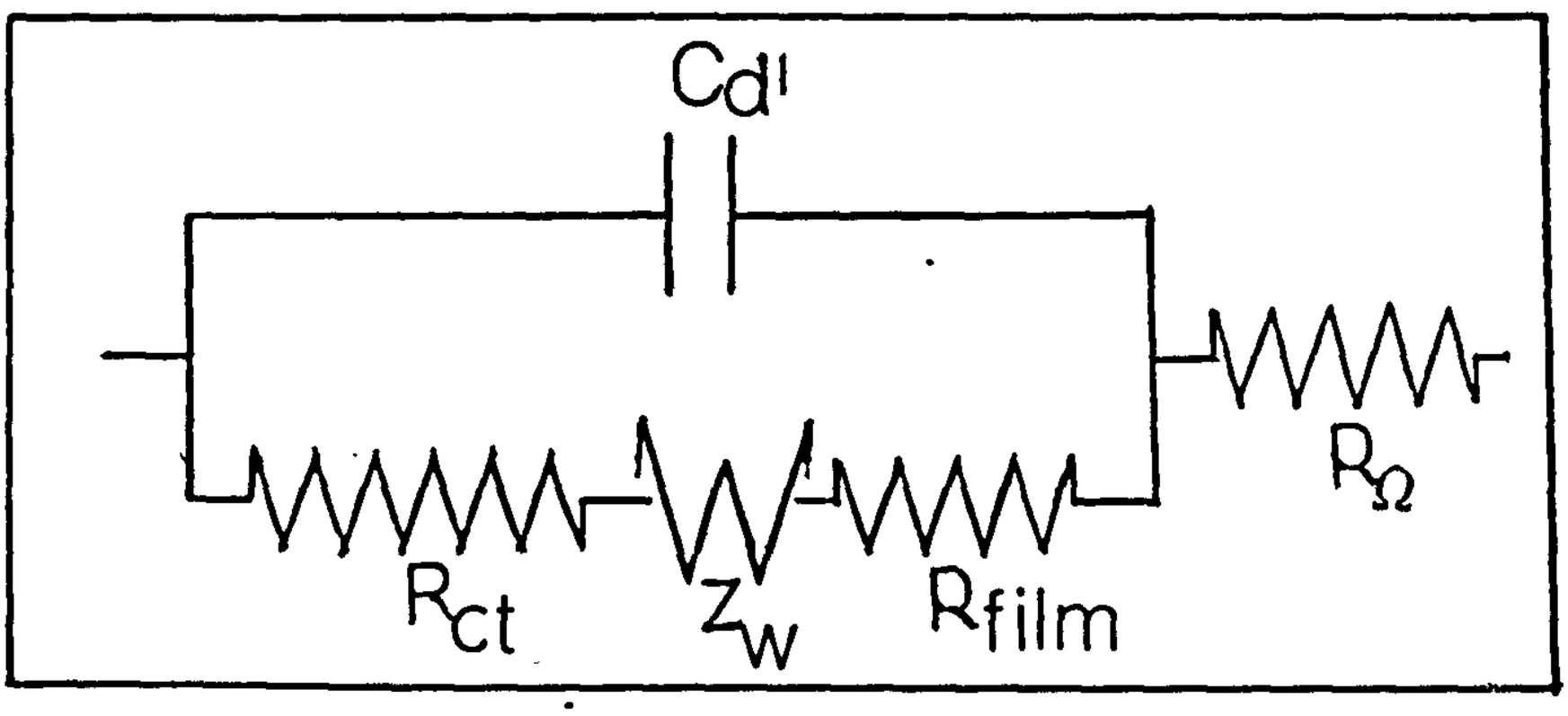

Fig.37 Schematic representation of a conductive film on a working electrode.

(iii) Films Acting as Semi-Conductors

The effect of such a surface film is somewhere in between the two previous cases and as such will be represented by an RC network. Several equivalent circuits are proposed to take into account the observed results in each case.For instance,the model proposed in Fig.38 is based on the assumption that the capacitance of the double layer is less than that of the film and also the ionic and electronic resistance of the film R

controls the current flow. The above model is observed for anodic films formed on the valve metals (V, Ti...).

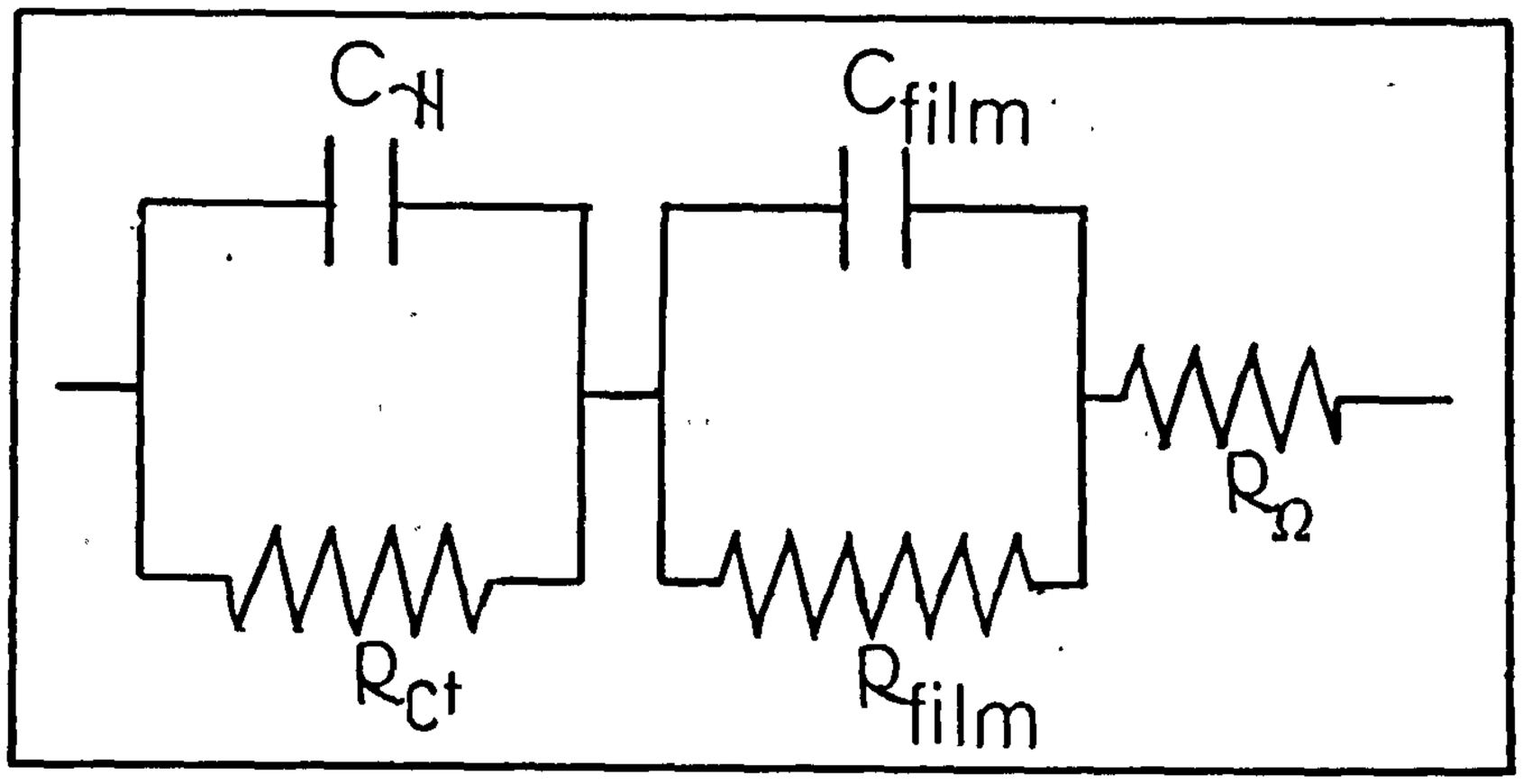

Fig.38 Schematic representation, typical of the semi-conductive anodic films on valve metals.

2.9.6.6.Graphic Representation of Impedance Data

The data resulting from the impedance experiments are best studied graphically.This enables the experimenter to eliminate the occasional spurious results, while extracting and comparing different parameters such as; τ , σ , C_{dl} , R_{ct} , R_{Ω} , R_{ad} , C_{ad} , R_{film} , C_{film} etc. from the data.The most common form of data presentation is the "complex plane","Argand"or"Nyquist" plots, all of which are synonymous for one type of plot. However,there are other forms of data presentations such as "Randles", "Cole-Cole",etc which will be discussed here.

(a) Nyquist Plots

Also known as Argand or complex plane diagrams, these are the most common forms of graphic representations of data in the literature. The data are

plotted as real and imaginary impedances so that the x-axis shows the real and the y-axis the imaginary impedance.Such plots can provide the following information as shown in Fig.39.The low frequency end of experimental results forms the right hand quarter of the semi-circle while the left hand side is the higher frequency end.The diameter of this semi-circle represents the charge transfer resistance of the process.A smaller circle indicates a faster electron exchange reaction.

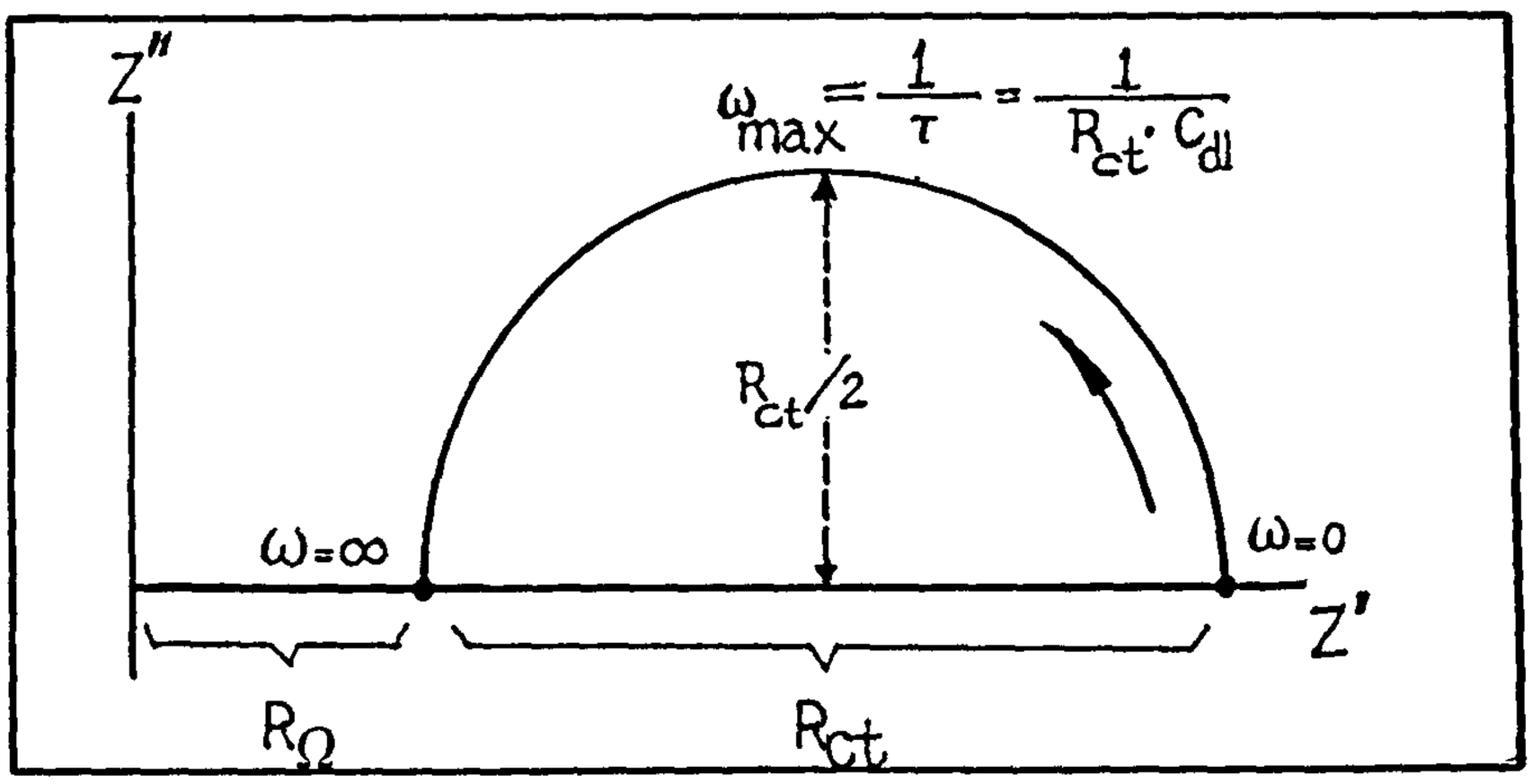

Fig.39 A Nyquist plot for the Randles equivalent circuit described in section 2.9.6.5.

The position of the high frequency ($\omega=\infty$) intercept of the semi-circle with the x-axis, with respect to the co-ordinate ($Z'=0$), shows the resistance of the electrode.A semi-circle whose high frequency end passes through the co-ordinate ($Z'=0$),indicates the extreme conductivity of the solution used.The low frequency approximation of the Randles circuit described before will show the effect of the Warberg impedance on

the system as a whole. This is illustrated in Fig.40 below. The combination of the two results in one plot

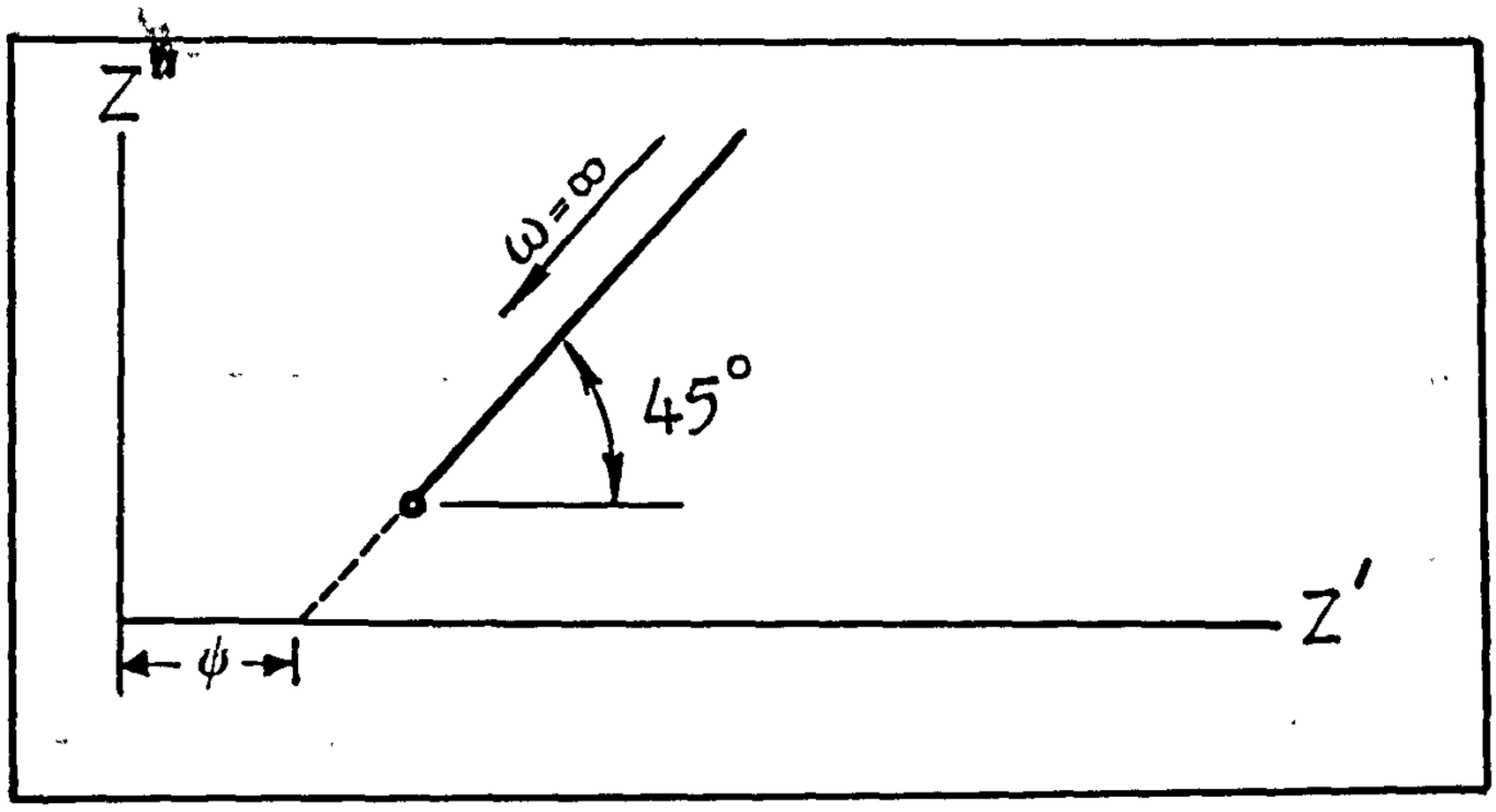

Fig.40 The Nyquist plot for the short frequency approximation of a Randles equivalent circuit.

showing the effect of the Warburg coefficient (σ) on the shape, of the semi-circle.

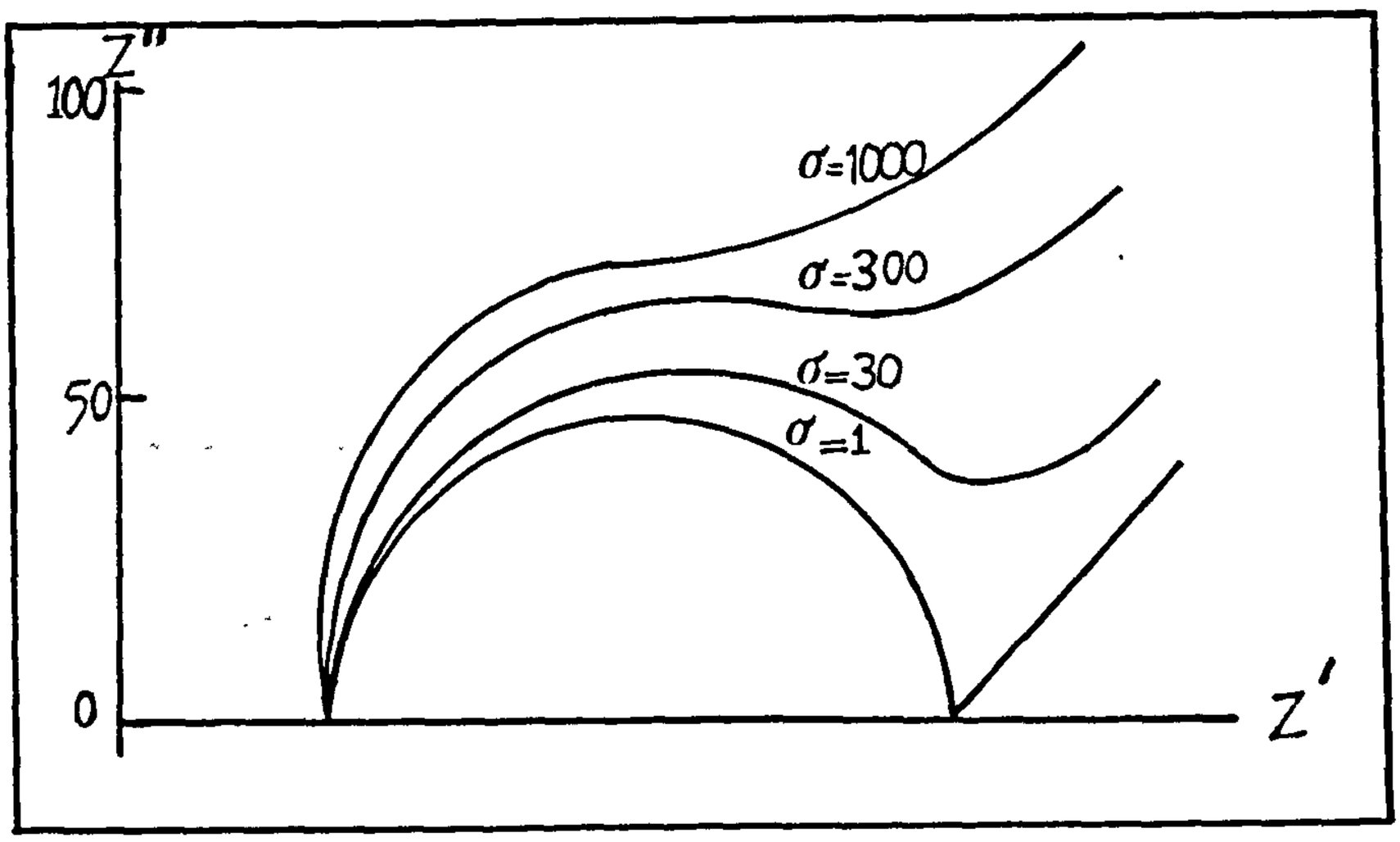

Fig.41 Nyquist plot for a simple Randles equivalent current whose Z is varied to give the σ values shown. R_{Ω} =20 $m\Omega\,m^2$ R_{ct}=100 $m\Omega\,m^{-2}$, C_{dl}=0.01 mF m^{-2} are constant.

(b) Randles Plots

As many of the variables of interest such as Warburg impedance are functions of,therefore plots of Z'and z'vsωcould reveal the mechanism of the electrode

reactions. Fig.42-47(below) show the Randles plots for different components of a Randles equivalent circuit as well the case of adsorbed species and film formation.

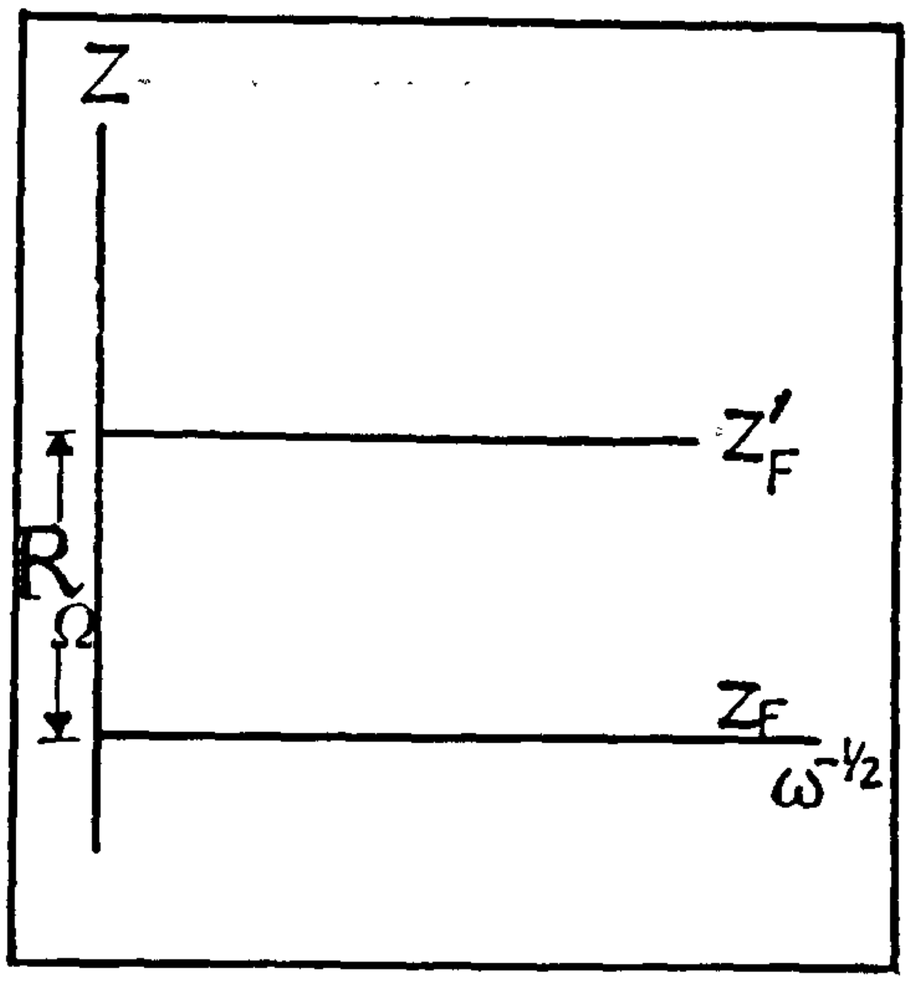

Fig.42 Charge Transfer controled system

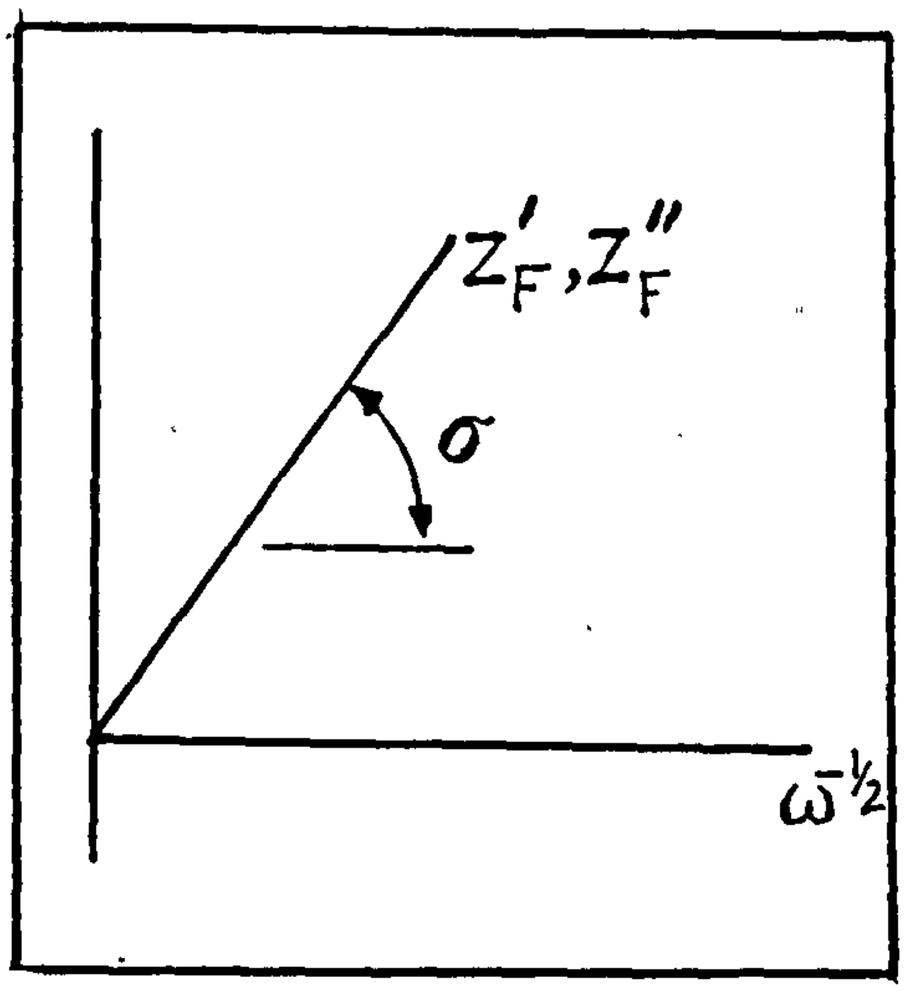

Fig.43 Warburg Impedance controlled system

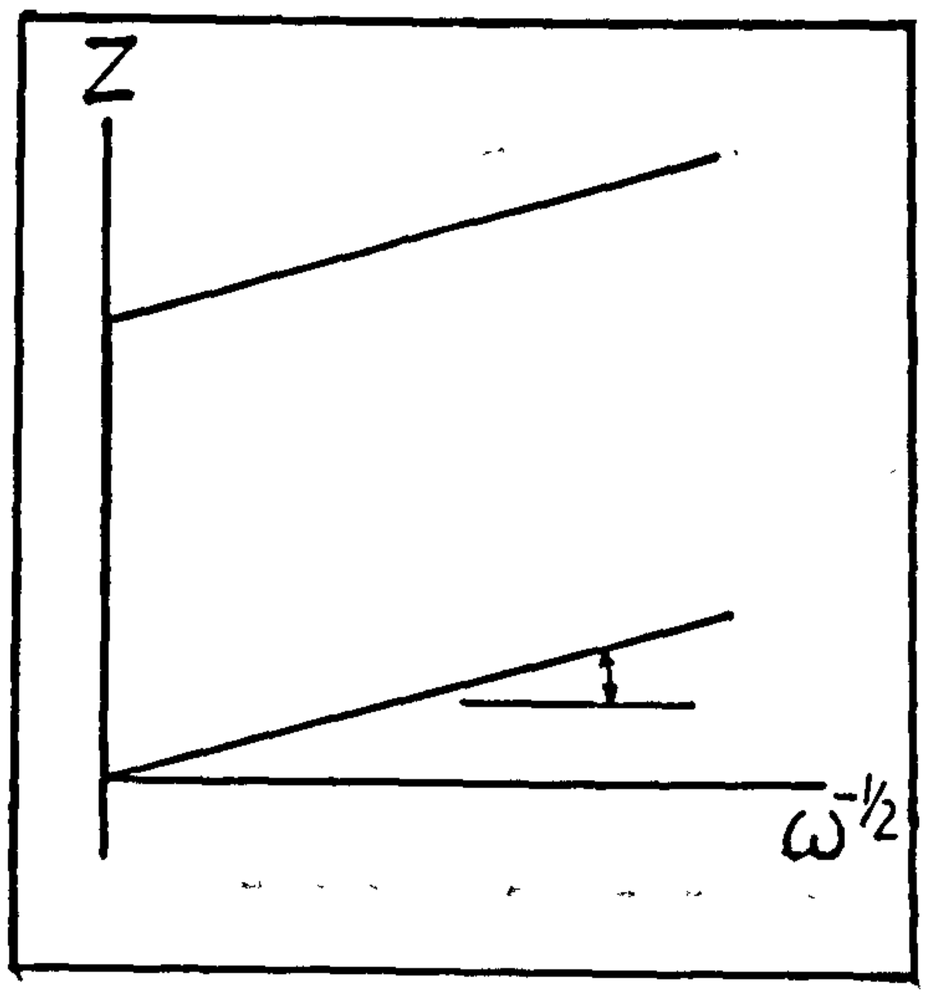

Fig.44 Charge Transfer & Warburg Impedance controlled system

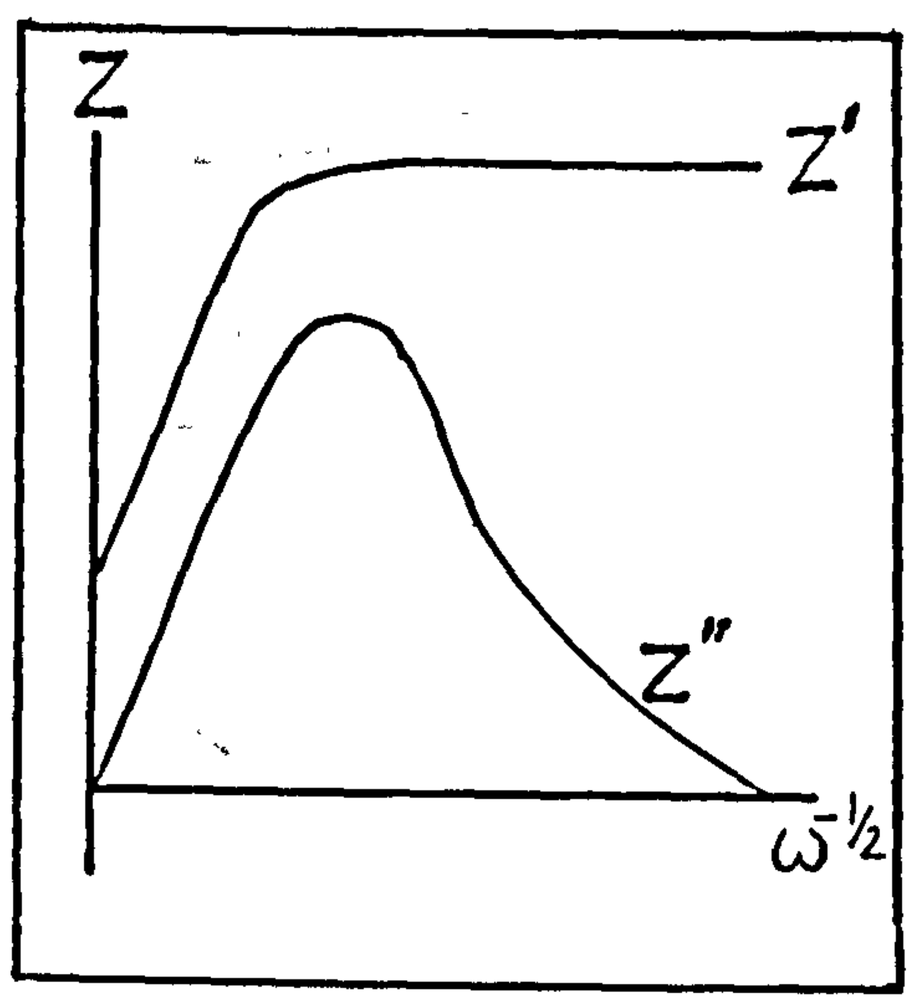

Fig.45 Complete Warburg Impedance & Charge Transfer controlled system

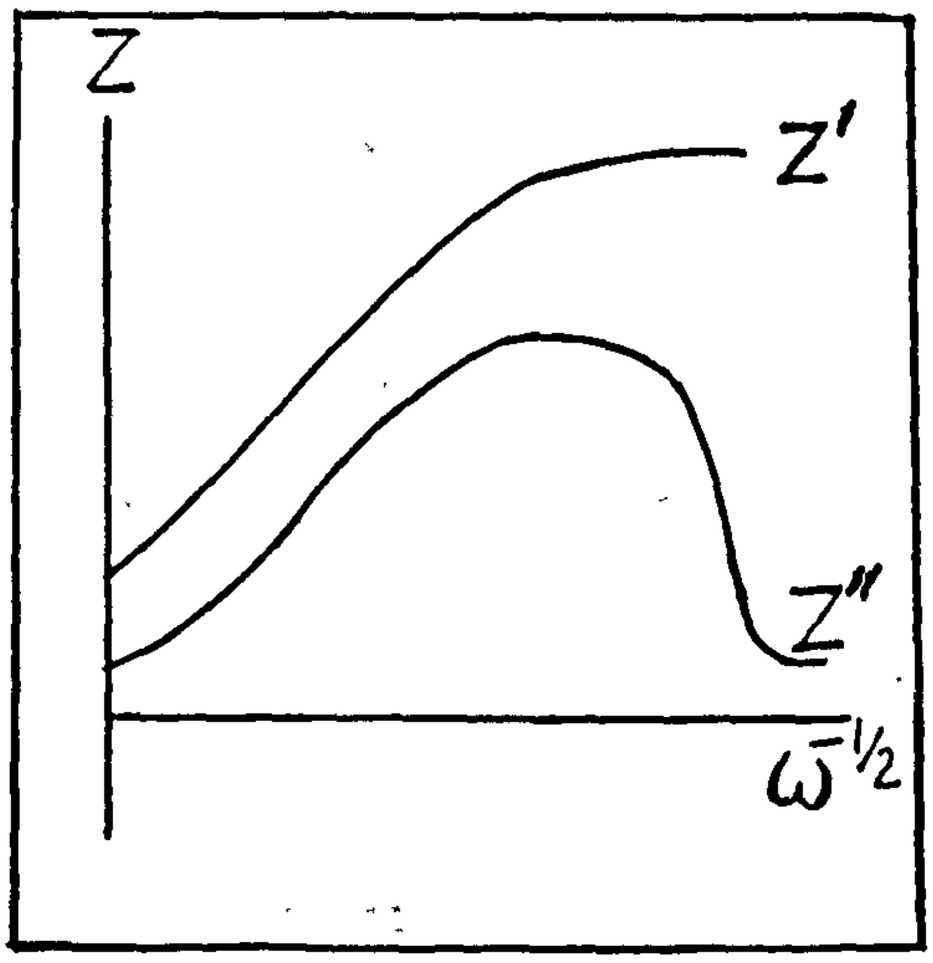

Fig.46 Charge Transfer system with pseudo RC.

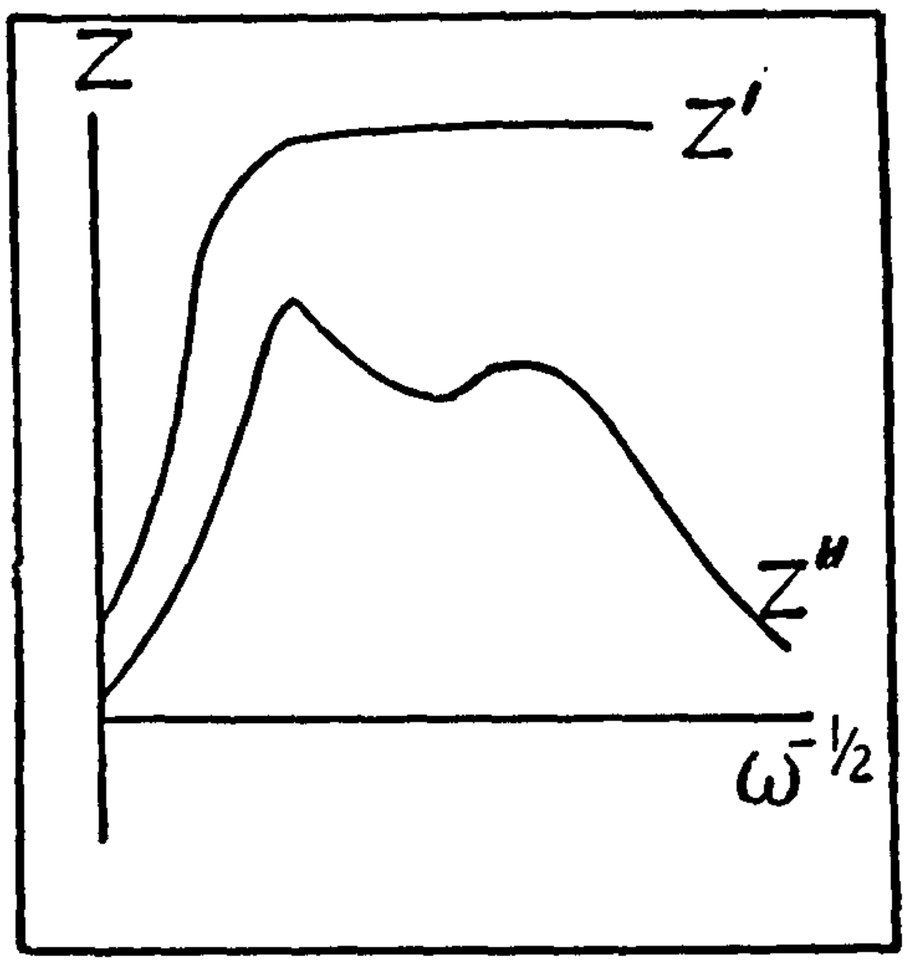

Fig.47 Warburg Impedance & Charge transfer controlled system with pseudo RC.

(c) Plots of Log Z vs Log f

Fig.48 illustrates the semi-conductive film model discussed previously, together with a logZ vs Log f plot associated with it. It is evident that many more parameters could be extracted from these plots than the previous one. However, these are complementary rather than mutually exclusive.

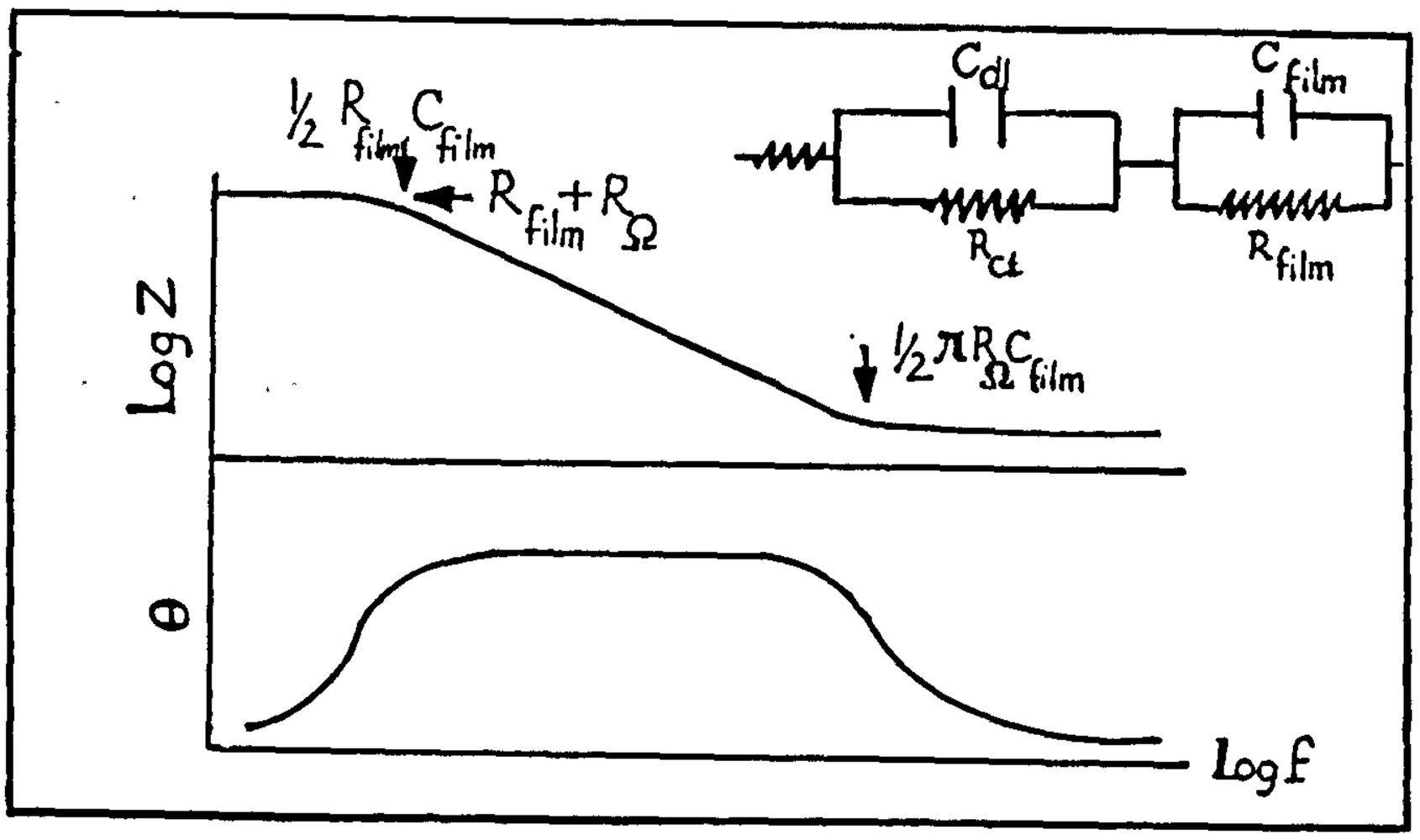

Fig.48 An illustration of Log Z vs Log f plot for the semi-conductive film model shown before.

(d) Plots of Z' vs $\omega Z''$

By plotting (Z') as ordinate and $\omega Z''$ as abscissa, a straight line will result whose gradient renders the value of (τ), the system relaxation time. The intercept of this line on the Y-axis gives $R_\Omega + R_{ct}$. The high frequency part of the plot renders an asymptote to R_Ω.

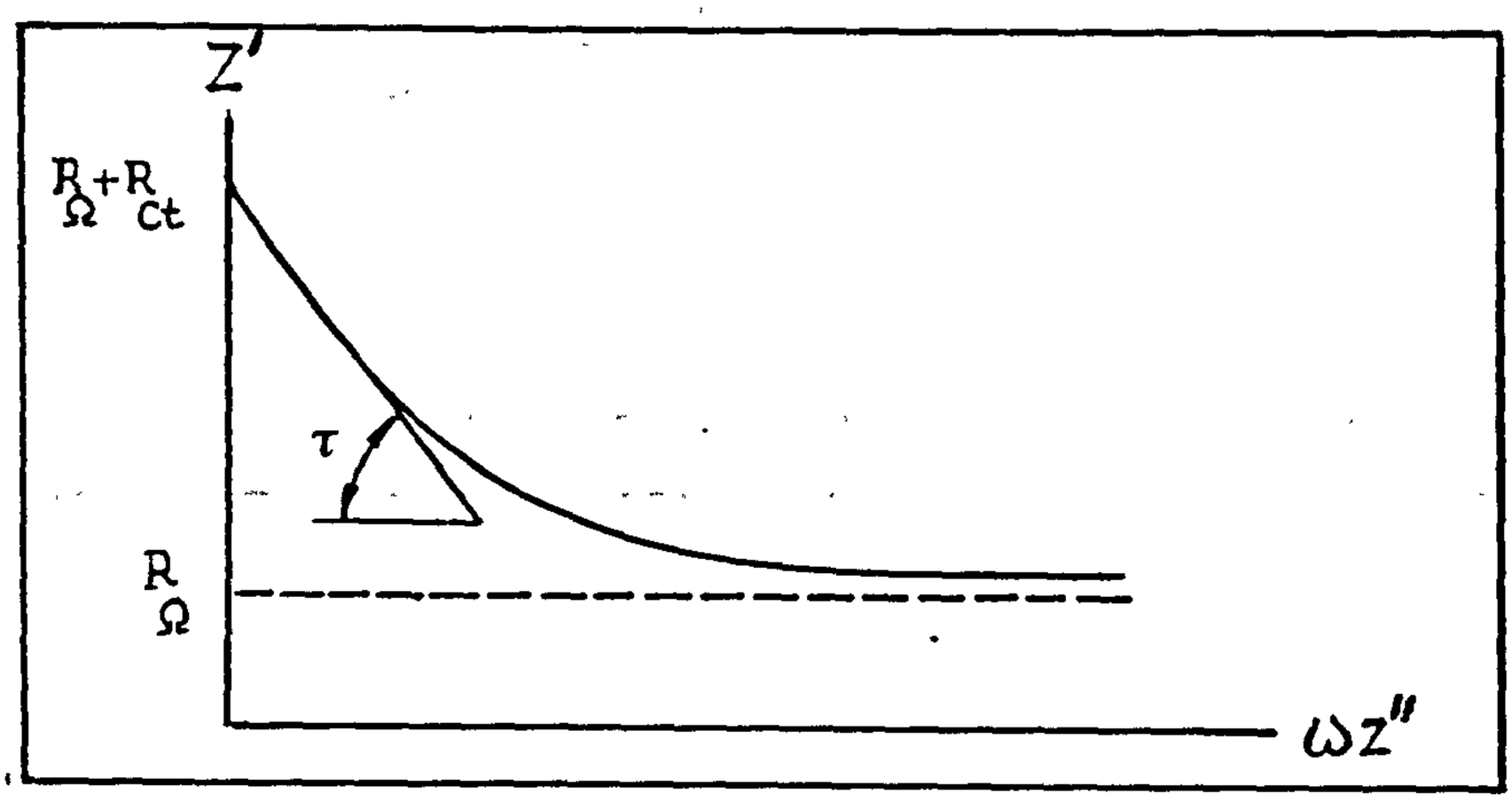

Fig.49 Schematic diagram showing a typical Z' vs $\omega Z''$ plot

(e) Plots of Y'' vs $\omega^{1/2}$

A plot of Y'' (imaginary part of admittance) as ordinate versus ω as abscissa results in a straight line. The gradient of this line renders the value of (C_{dl}).

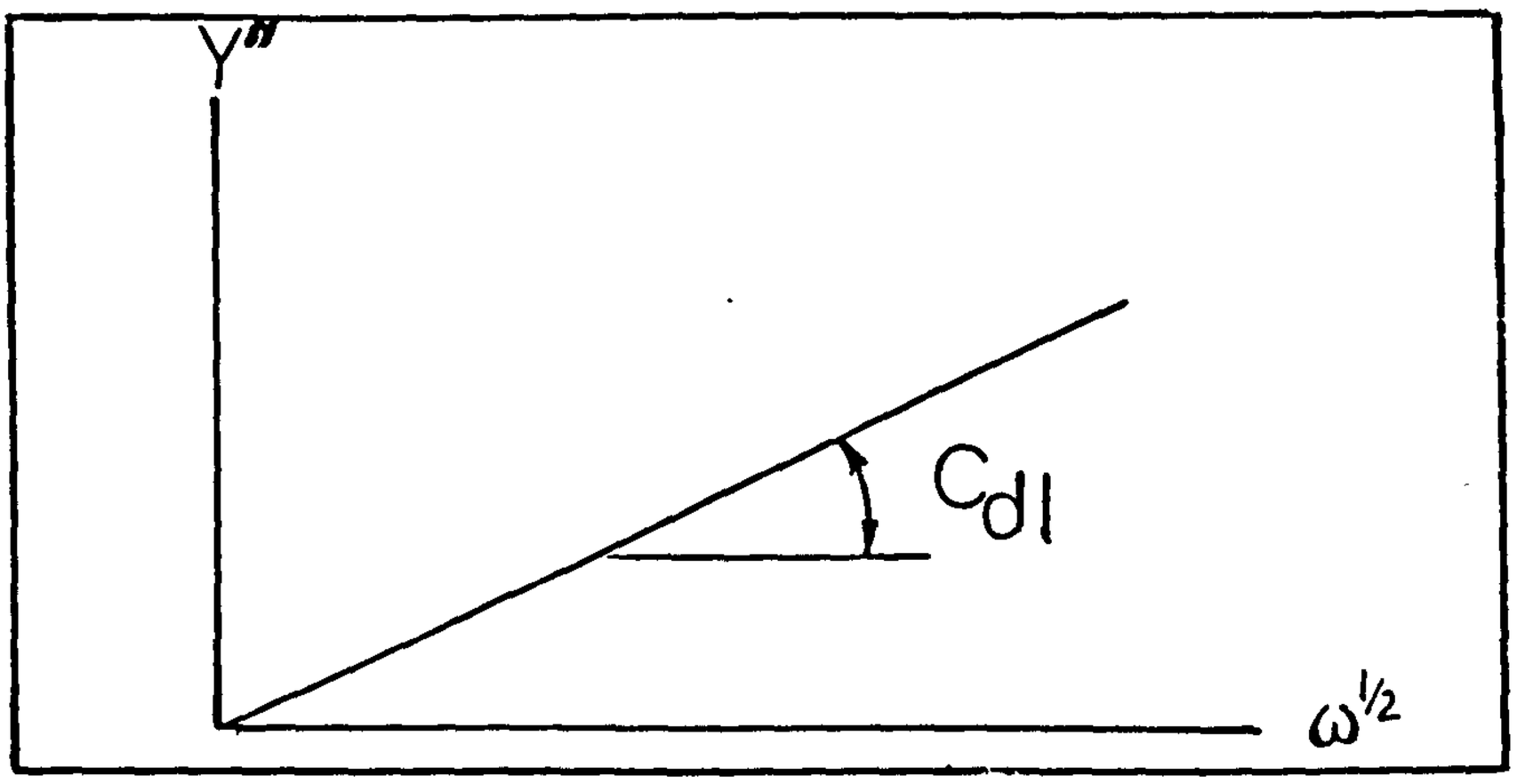

Fig.50 Typical Y'' vs $\omega^{1/2}$ plot

(f) Plots of ω / y' vs $\omega^{1/2}$

Such a plot results in a straight line at high frequencies. The gradient of this plot will be R_Ω and the extrapolated intercept on the Y-axis gives the σ, the Warburg coefficient.

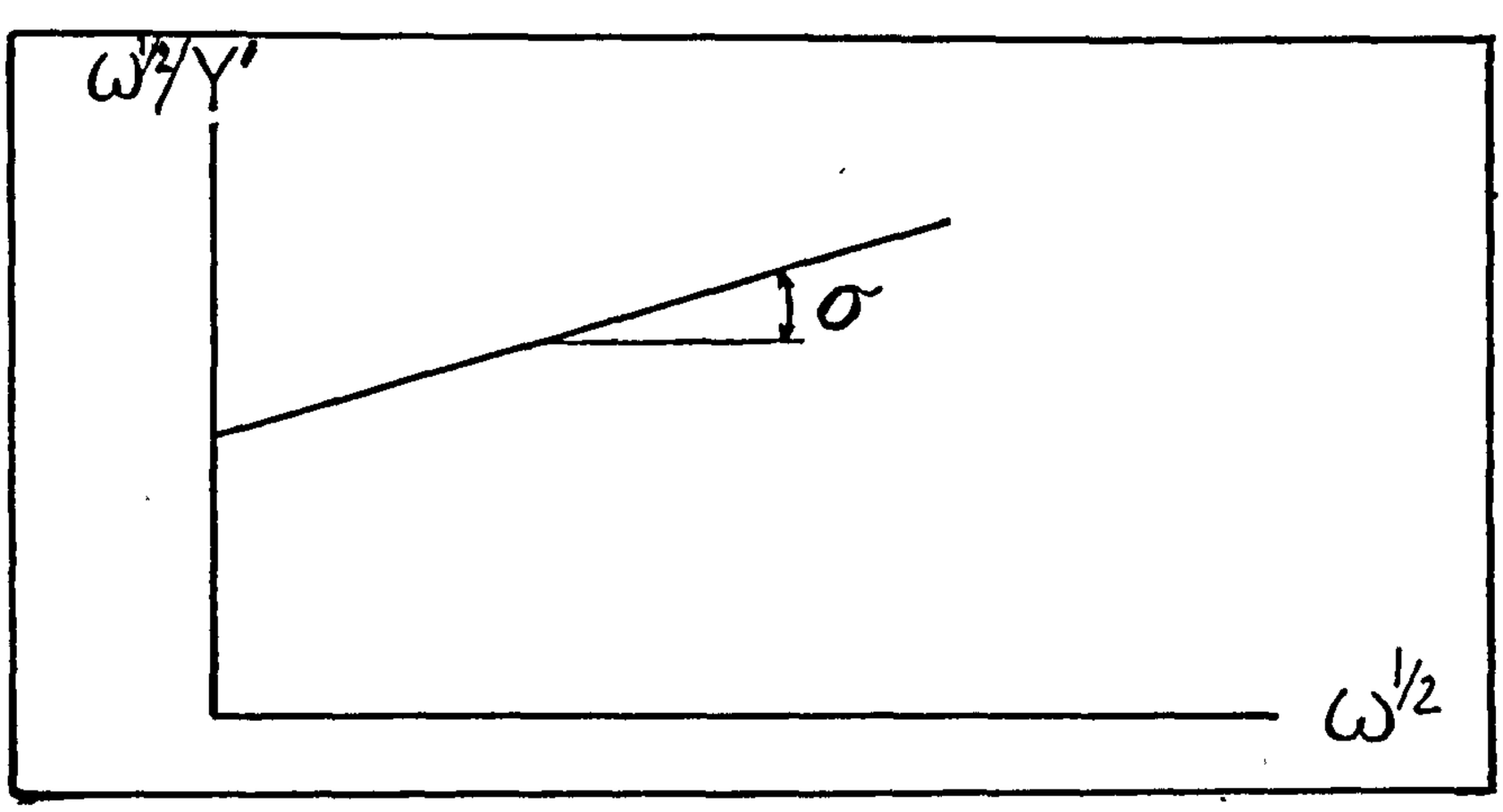

Fig.51 Typical plot of ω/Y' vs ω

2.9.6.7.Anomalous Results in AC Impedance Experiments

Ideal electrical behaviour in actual electrochemical systems based on such assumptions is not always observed. Deviations in the typical curves described above therefore have to be considered.

The discrepancies observed in the Nyquist plots are depressed semi-circles and oblonged or deformed curves[296,297]. These could be explained in terms of a variable system relaxation time (τ). The corollary of the arguments for such cases is that any depressed or elongated semi-circle could be represented by a circle whose centre has been pushed below the X-axis. The angle formed between this real centre and the intercept

of the semi-circle on the X-axis is termed "depression angle"(β) from which a depression factor is calculated.

$$\gamma = 2\beta / \pi \qquad (226)$$

In the cases where finding the real circle is difficult, a different parameter could be utilized for calculation of as follows:

$$\beta = 90 - 2\lambda \qquad (227)$$

where (λ) is the angle between ω of the semi-circle and the intercept of the semi-circle on the X-axis as shown in Fig.52.

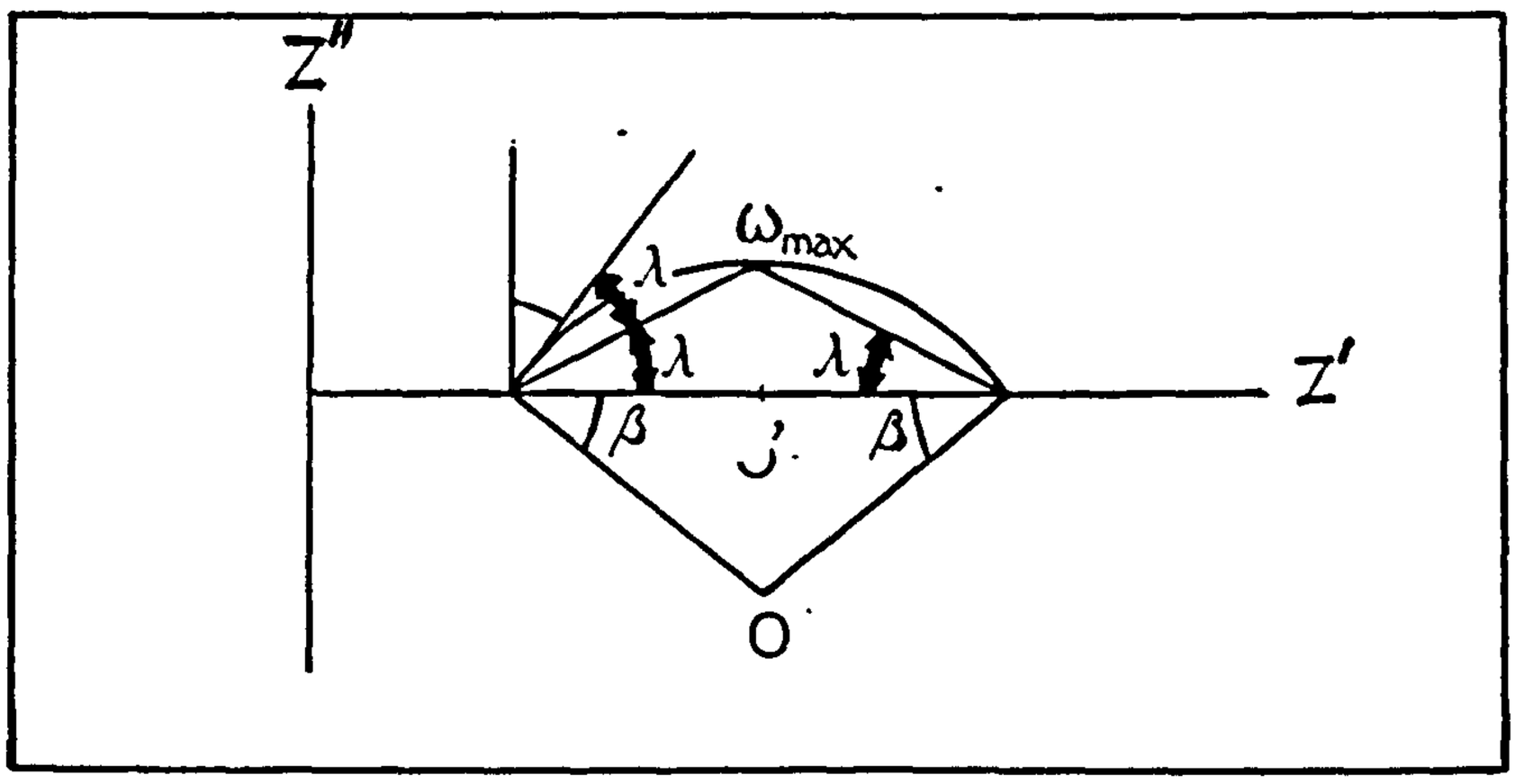

Fig.52 Schematic representation of a "depressed semi-circle due to non-linearity of the electrochemical system.

The corrections for non-ideal behaviour in the case of Randles plots are graphical. The following three cases summarize the more common deviations together with their corrections .

(A) Plots of Z' and Z'' vs $\omega^{1/2}$

The usual analysis of results based on the intercept of a straight line is uncertain as the line

bends towards zero when ω tends towards infinity. Fig. 53-a and Fig.53-b show the bent section and also the correction applied.

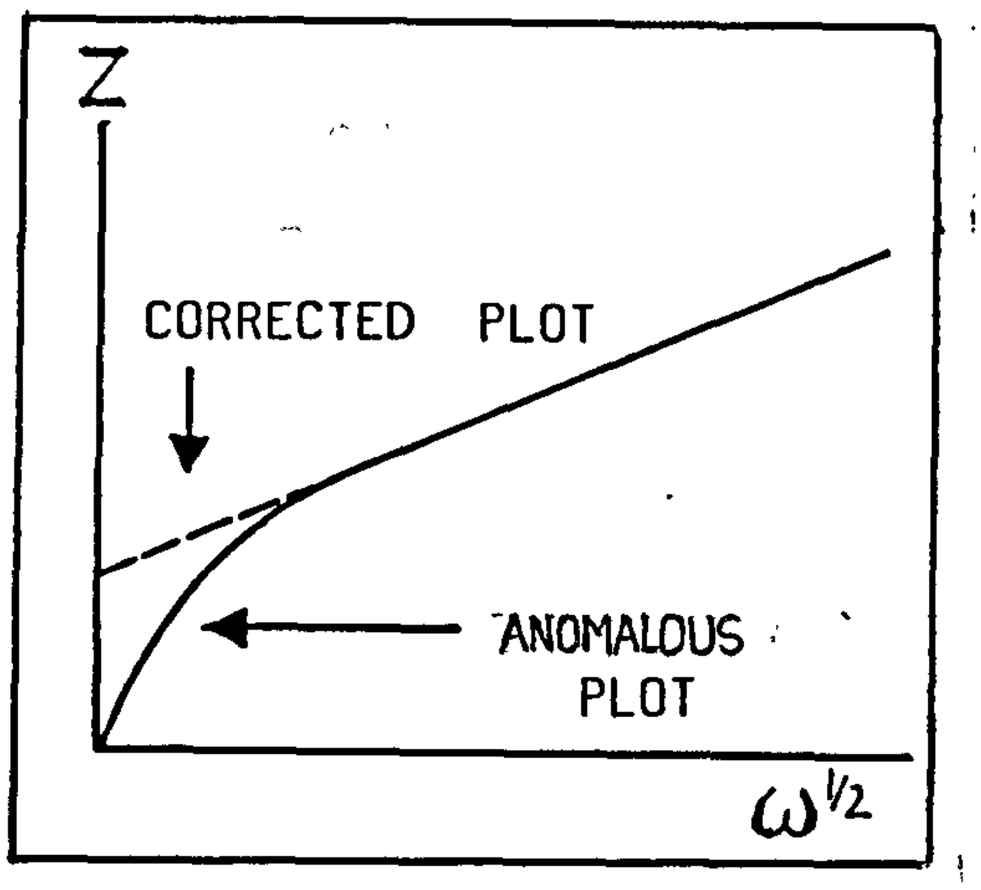

Fig.53-a Typical Z′ vs ω curves.

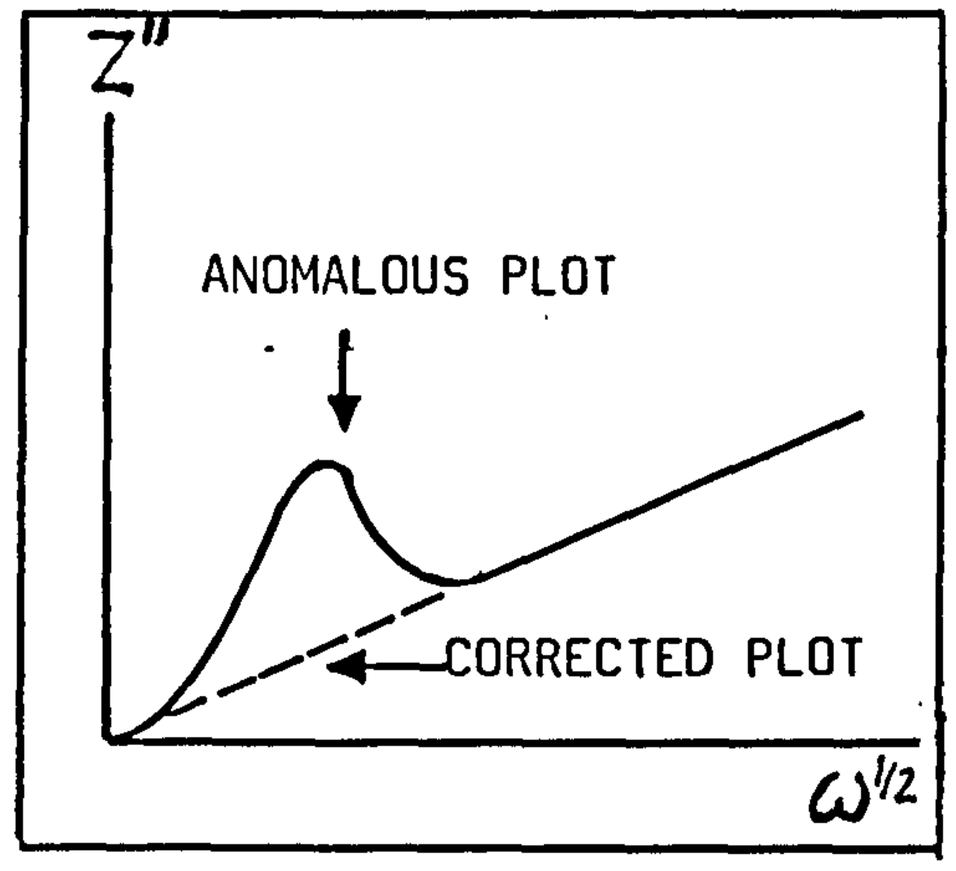

Fig.53-b Typical Z″ vs ω curves.

(B) Plots of Y″ vs ω

Deviations at lower frequencies represent depression effects.These could be eliminated by extrapolating the straight line to the centre as shown in Fig.54.

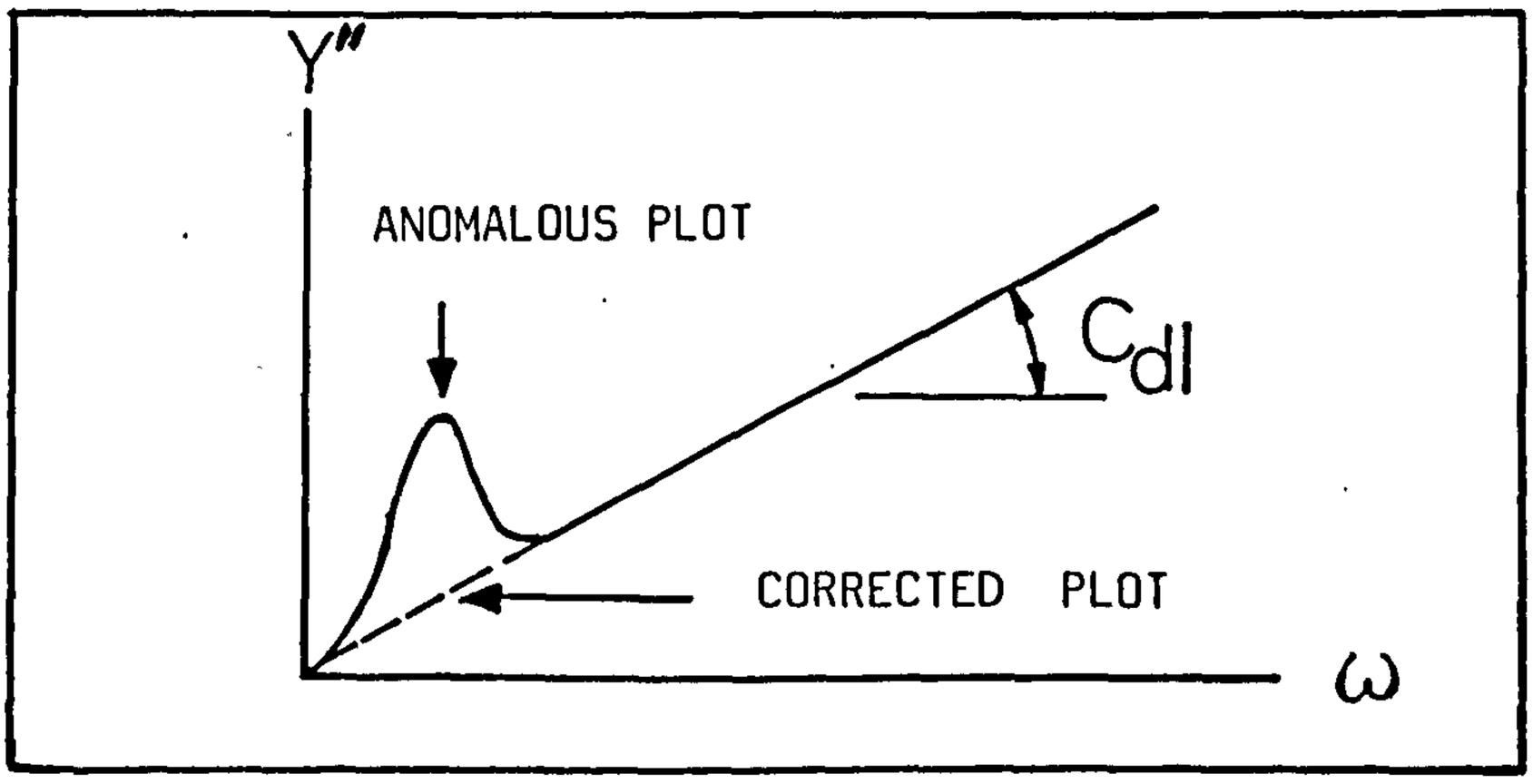

Fig.54 Non-linear behaviour of Y″ vsω plots.

(C) Plots of Z' vs. $\omega Z''$.

The discrepancy is shown at the lower frequency range in the form of an asymptote to the Y-axis, ($Z''=0$). This makes the evaluation of the $(R_\Omega + R_{Ct})$ difficult and could be remembered if the straight part of the curve is extrapolated to ($\omega Z''=0$).

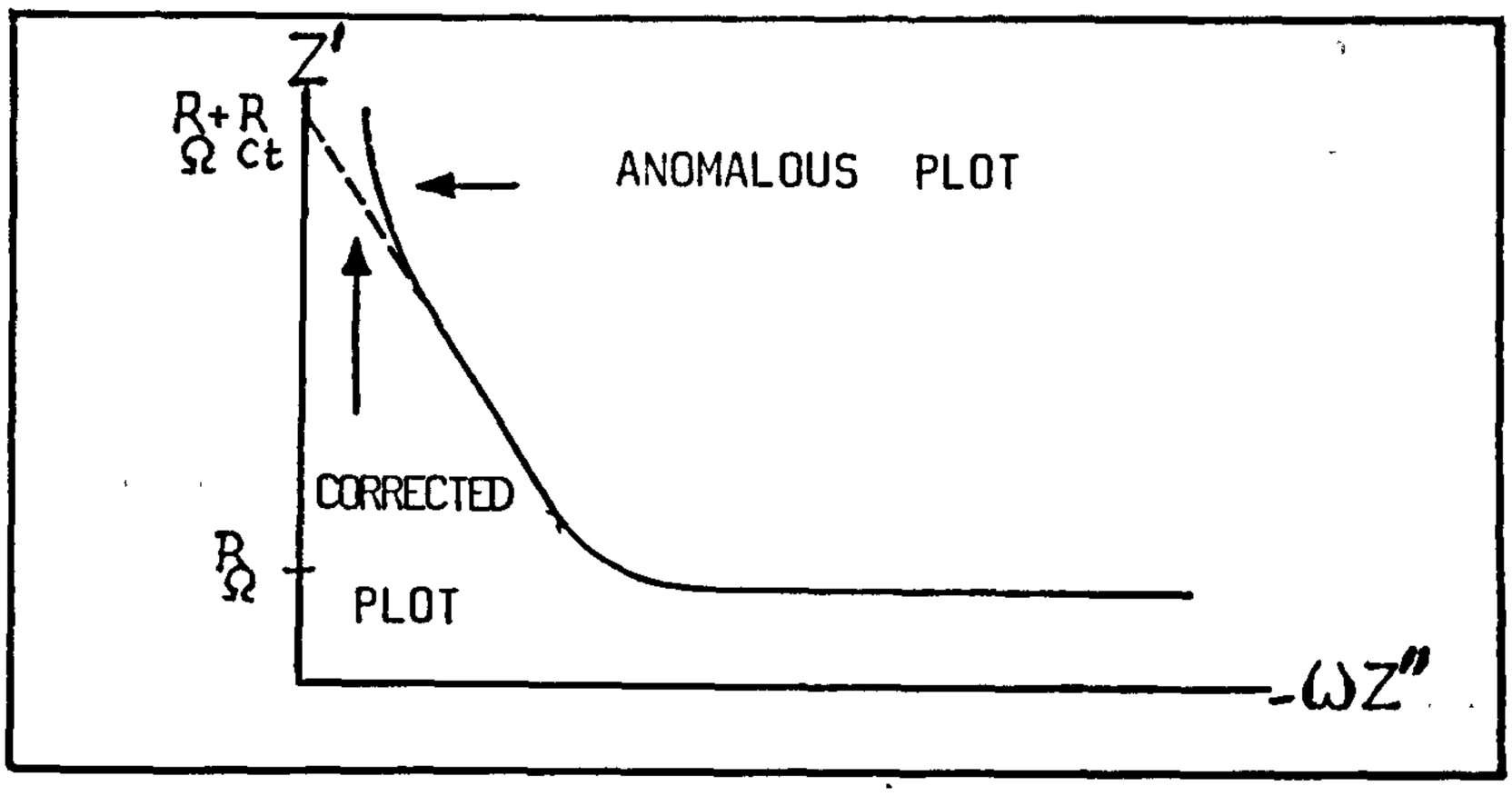

Fig.55 The anomalous behaviour of Z' vs $\omega Z''$ curves with the necessary corrections.

2.9.6.8.The Physical Interpretation of AC Impedance Data

At the high frequency end of the spectrum i.e. between 10 Hz and 10 kHz, the electromagnetic wave associated with the AC signal interacts with the system and shows the effect of the double layer as well as the charge transfer process involved. The interaction causes the relaxation of the double layer as a result of momentary reorientation of the molecules in that layer i.e. the effect of the applied potential perturbations on the orientation of the adsorbed solvent molecules and excess ionized species is to flip over and rearrange them. At very high frequencies, the wave form passes through the double layer, before the relaxation time of the previous switch in orientation

could take place. In such a case, this wave form does not lose any energy interacting with the double layer and as a result, little data is deduced. At the lower end of the frequency band, the wave form resembles that of a DC current and is effectively arrested in its interaction with the membrane. Therefore the frequency at which the relaxation of the double layer can interact must correspond to its natural relaxation time as indicated by the time constant for the system, .

Regarding the Warburg impedance, one could readily show that one needs the lower frequency domain, to be able to demonstrate the interactions of migrating ions. The effect is such that at higher frequencies the stream of charge carrying ions could not respond to the rapid changes expected from them in their motion and therefore they do not absorb any energy from the potential waves. However, as the frequency is lowered i.e. to less than 1 Hz, the ionic species start to interact with the applied wave form since they now have enough time to respond to the change of direction required of them. At even lower frequencies, near zero, the Warburg impedance acts more or less like a true resistance as the effects of ionic diffusion on the imaginary component becomes progressively less pronounced.

Both the desorption and film formation processes are best identified at lower frequencies. However, since the adsorption interacts at a slightly

higher part of the frequency band than the Warburg does, these effects could be studied in the same system. The importance of AC impedance parameters is that they can be used to determine not only the mechanistics of a system but its kinetics also. Delevie [298] shows that using the ratio of (R_Ω / σ), it is possible to ascertain whether the system is charge transfer or diffusion controlled. In general, the following boundary lines could be defined:

if $R_\Omega / \sigma > 10$	the process is charge transfer controlled
if $R_\Omega / \sigma < 0.1$	the process is diffusion controlled
if $R_\Omega / \sigma = 1$	the process is under mixed control,i.e. both charge transfer and diffusion control

The above technique is used in the present project and the results are discussed in chapter 4.

3.....EXPERIMENTAL

3.1.....INTRODUCTION

The thrust of the experimental work in the present study has been through the well-established [23-25,189,192-194] electropermeation technique.As has been shown in the previous sections , this method is modified in order to derive maximum benefit from its neglected potential.

Other methods used to complement the electrochemical studies included: AC impedance measurements which was successfully utilized to refute a claim encountered in the literature [299] according to which, an iron membrane surface can not be adequately "reduced" through cathodic polarization even after long times.

Using the above technique, it was possible to reproduce the impedance of bare iron in an acid medium after short reduction times.Other techniques used were Inductive Coupled Plasma Spectroscopy,ICPS as well as a new approach in the electrochemical studies of hydrogen in metals which the author refers to "three dimensional permeation technique".

Within each category different variables were changed so that different aspects of the research as

seen from the author's viewpoint,are covered and the aims of the project are advanced. Supporting techniques such as electropolishing, electron microscopy and X-ray analysis of the passive layers were used but are not dealt with in detail in this chapter as they are of ubiquitous application.

Materials in the present project fall within either the electrolytic media or membrane metals. The former was sodium hydroxide solution of 0.10 mol/l strength through out and the latter, Armco iron (99.9% pure) in all the thin membrane experiments; and mild steel of known composition for the 3-D permeation studies.

3.2....TECHNIQUES EMPLOYED

3.2.1..ELECTROPERMEATION TECHNIQUE

In the present investigation, the electrochemical method was employed for permeation studies of hydrogen through iron membranes. The electrolytic permeation experiments on iron specimens in itself is quite old, dating back to 1860 when Graham[300] showed the effect of cathodic charging of iron samples.He showed This to lead to the establishment of a hydrogen flow (flux) across the membranes used, which was shown to be reversible i.e. by anodic polarization,

the same membrane could be depleted from the hydrogen previously deposited in it.

Bodenstein [49] was the first to investigate the overpotential/current problem using what one could call an elementary version of the more sophisticated electrochemical apparatus to be utilized later. However the credit for the modern electrochemical permeation technique goes to Devanathan and Stachurski [23] who worked on the properties of hydrogen in iron, using what is known as the permeation technique. The prime advantage of the method is in the instantaneous rate of transport of hydrogen it could establish and measure .

In principle, a thin film forms a bipolar electrode, one side of which is polarized cathodically so as to generate hydrogen, while the other side is maintained at a potential more anodic than that, leading to the "hydrogen reduction reaction" on the surface of the metal at the pH maintained in the solution. The primary objective of this is to facilitate and ensure the instantaneous oxidation of any hydrogen atoms reaching this surface.

The following six step process shows the general position of a hydrogen atom after generation on the cathodic side.

$$H^+ + e^- \longrightarrow (M\text{-}H_{ads.}) \rightarrow H_{abs.} \rightarrow H_{diffused} \leftrightarrow M\text{-}H_{ads} \rightarrow H^+ + e^- \qquad (228)$$

ON THE CATHODIC SIDE — ON THE ANODIC SIDE

The method used for the production of hydrogen has a bearing on the way the diffusivity and hydrogen solubility of a membrane is calculated. This has been extensively discussed in section 2.7 where the two main charging methods are differentiated as :

(a) Galvanostatic Charging

This entails a constant flux of hydrogen provided at any instant and is achieved through the use of a d.c. stabilized power source or a galvanostat. The principles here are either to operate with a large applied voltage , by using several megohms of external resistance between the cell and the power source, which minimizes the current fluctuations, or by the use of a closed feed-back system as in a galvanostat to maintain the current at the preset value through controlled variation of the potential.

The boundary conditions thus imposed result in the following equation for the concentration profile of hydrogen inside the membrane during a fast decay[194];

$$C(X,t)=C\ (1-X/L)-C\sum_{n=0}^{\infty}\operatorname{erfc}\left(\frac{2nL+X}{2\sqrt{Dt}}\right)+C\sum_{n=0}^{\infty}\operatorname{erfc}\left(\frac{2L(n+1)-X}{2\sqrt{Dt}}\right) \qquad (229)$$

or in terms of "flux" during the decay phase:

$$J_t/J_\infty=1-\frac{4}{\pi}\sum_{n=0}^{\infty}\frac{(-1)^n}{(2n+1)}\exp\left[\frac{-(2n+1)^2\pi^2 Dt}{4L^2}\right] \qquad (230)$$

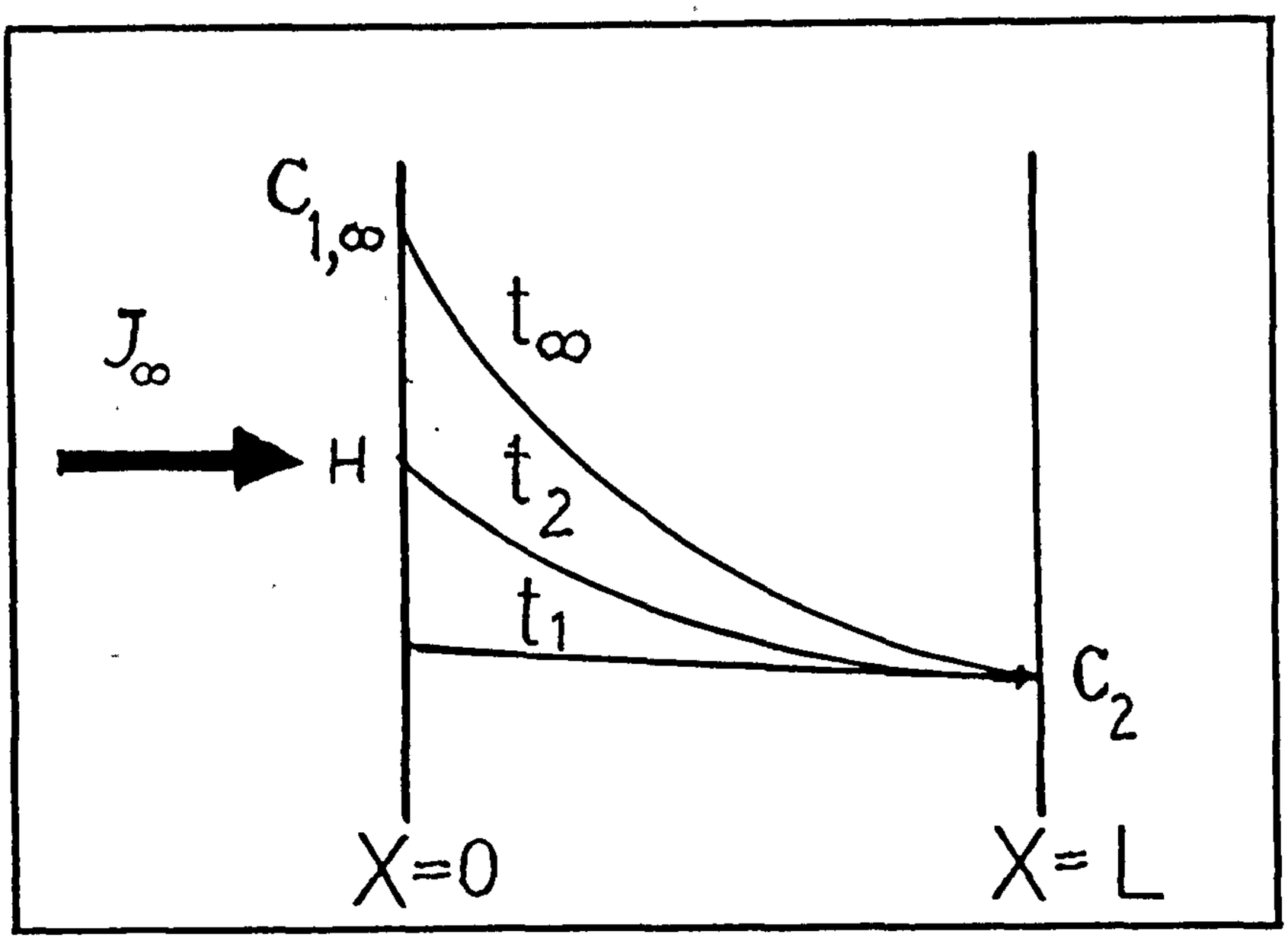

Fig.56 Schematic representation of the galvanostatic charging of a thin membrane. The attainment of the concentration is not instantaneous.

(b) Potentiostatic Charging

The regime imposed here is based on the maintenance of a constant potential across the charging side of the bi-electrode,through the controlled variation of current between the counter and the working electrode of that half cell. Any ordinary potentiostat is capable of this task. The concentration profile inside the bi-electrode during the decay is dictated

$$C(X,t)=C_s - \frac{C_s \cdot X}{L} + \frac{2}{\pi} \sum_{n=1}^{\infty} \frac{C_s}{n} \sin\left(\frac{n\pi X}{L}\right) \exp\left(\frac{Dn}{L}^2\right) \quad (231)$$

in terms of flux at the time t,

$$J_t / J_\infty = 2 \exp(-4 \pi^2 Dt/L^2) \quad (232)$$

In both cases , there is no interference between the electrical field of one side on the other,since the electrical circuit is established between the counter electrode of one half cell and the surface of membrane facing that electrode. Since the cells are hermetically sealed, the current paths can never cross. It is obvious that such fields could not penetrate a conductive medium.

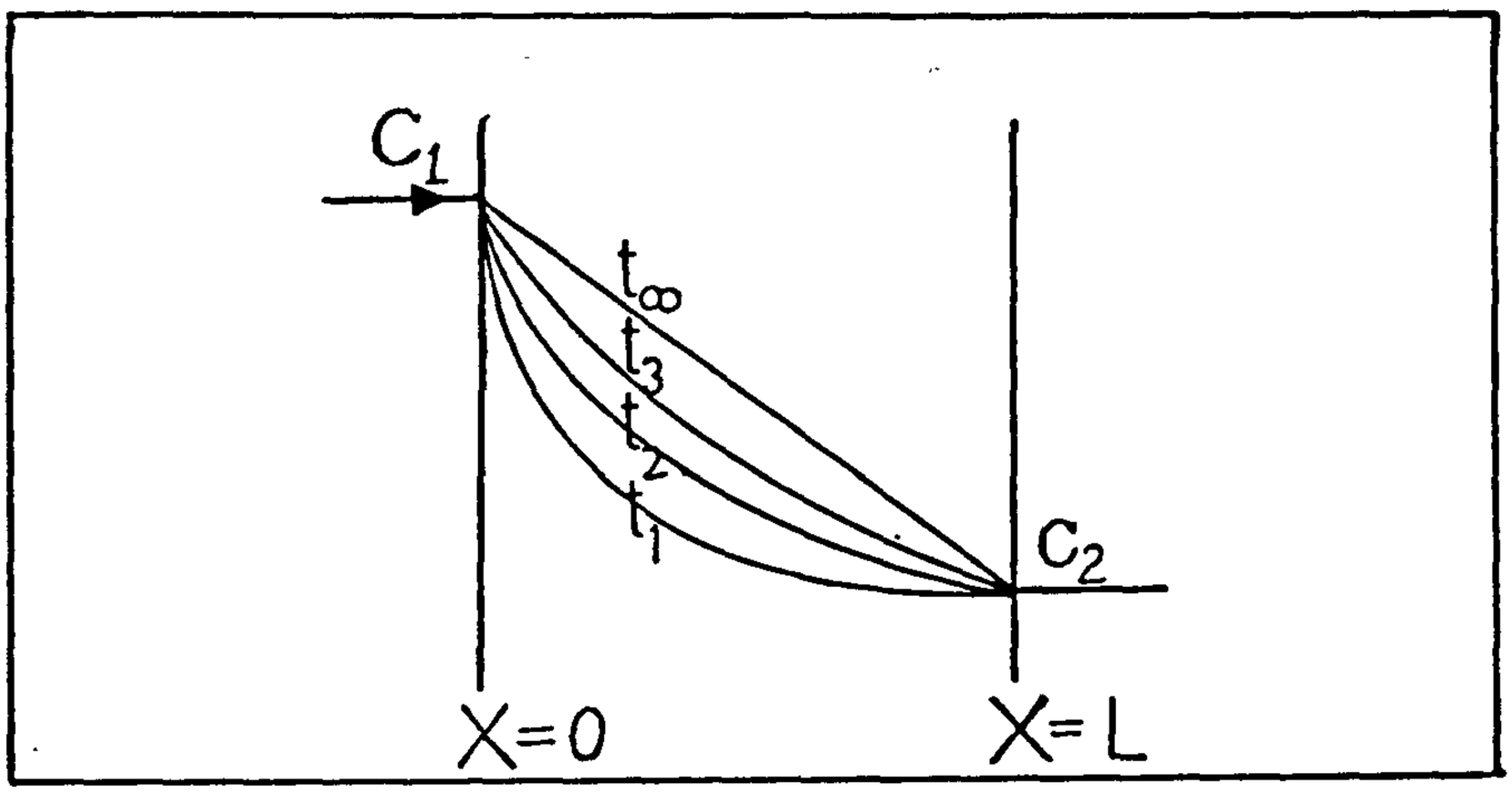

Fig.57 Graphic representation of constant potential (potentiostatic) charging of thin membranes.

3.2.1.1.Description of the Permeation Cell

Fig.58 shows the schematic representation of such a permeation double cell. One of the cells, say the left hand side unit is termed, the detection or anodic cell,while the right hand side is the charging or cathodic cell.The function of the detection cell is to provide anodic polarization conditions in which oxidation of hydrogen oxidation can take place according to equation (228).This means, any hydrogen reaching that face is instantaneously oxidized and there is no hydrogen build up on that side i.e. a zero concentration can be inferred.

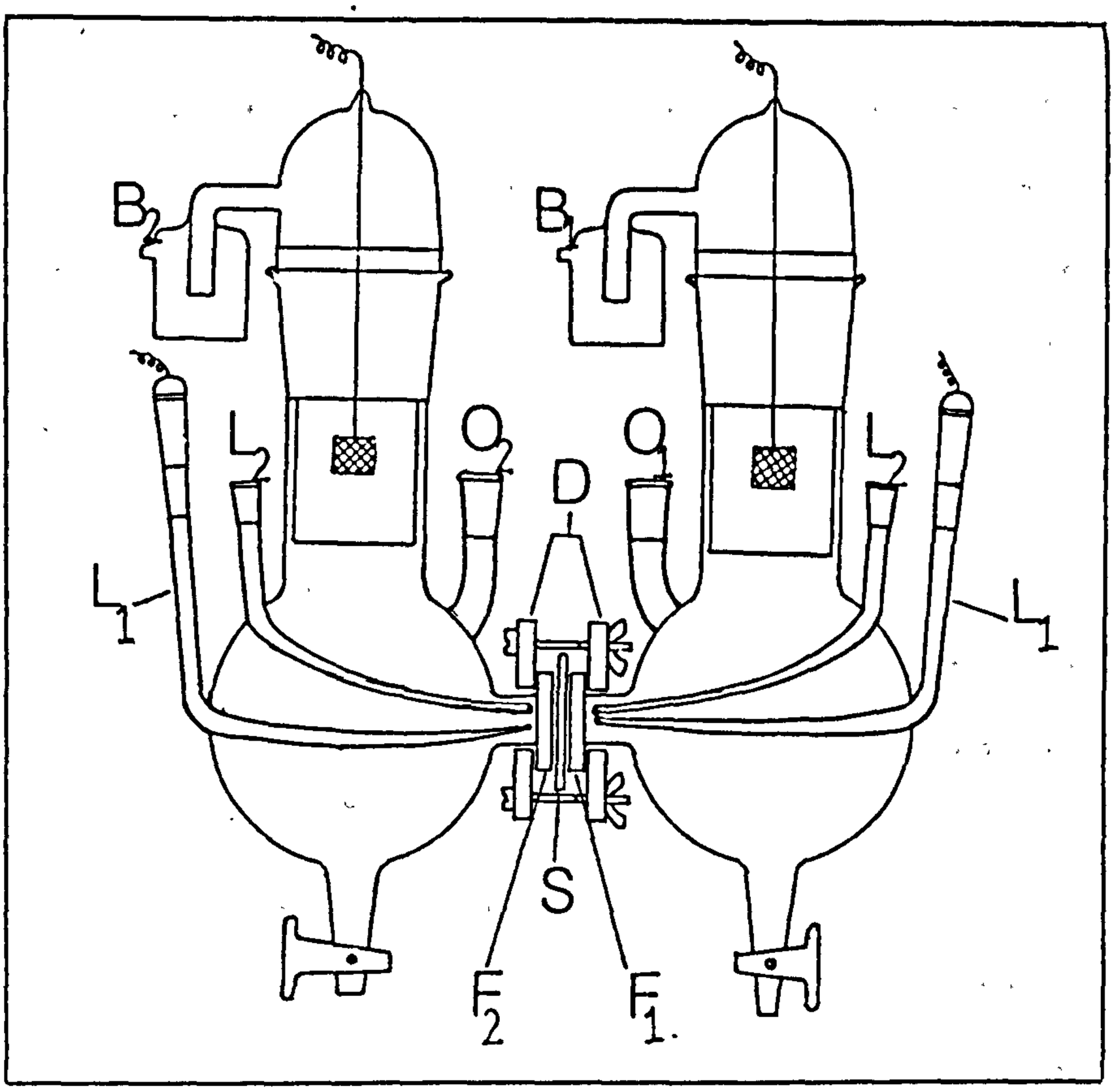

Fig.58 Schematic representation of a thin membrane permeation cell.Lettering used to denote the parts explained in the text.

The charging side provides a stream of hydrogen to the membrane by the decomposition of water molecules. This stops as soon as the charging current is terminated at source and from then on the decay phase commences.In Fig.58 Luggin capillaries L_1 and L_2 provide means of delivery of nitrogen gas near the surface of the bi-polar electrode and also a channel for accurate potential measurement of the surface. This Luggin capillary terminates not closer than 2 mm , and not more than 4 mm away from the surface. A very close Luggin would interfere with the double layer and a very distant on would not register the potential variations fast enough for potentiostatic measurements or

passivation studies. Bubblers B_1 and B_2, provide a secure escape route for the gases in the system and also act as gas locks to prevent the ingress of oxygen back into the system. Platinum gauzes C_1 and C_2, act as counter electrodes for the anodic and the cathodic cells. In the latter case, the counter is, the positive pole of the cell while in the former, the opposite is true. The openings O_1 and O_2 allow access to the electrolyte, both for separate analytical work or accurate temperature measurements. Flanges F_1 and F_2 house the sample holder in between them. This in turn provides a water tight seal between the two sides of the bi-polar electrode. The flanges are fastened together through the rubber clad clamp D which ensures a water tight seal between the two half cells. Fig.59 below shows the design of the sample holders devised in this work for the flat membrane experiments. The area exposed to the solution is a circle of 4.5 cm^2 area.

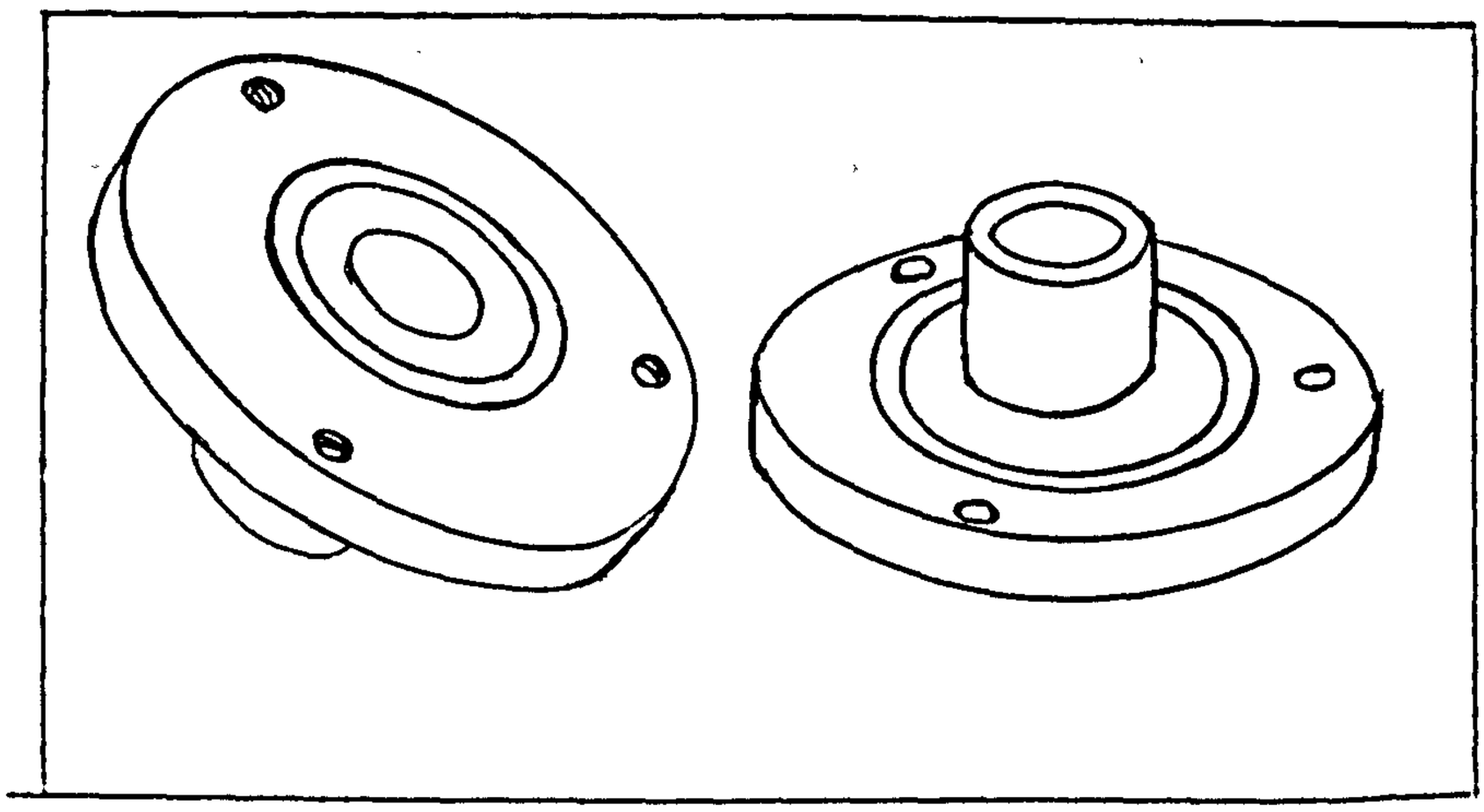

Fig.59 The design of the flat membrane sample holder for the permeation experiments.

3.2.1.2.The Electrical Circuitry and Measuring Equipment

Fig.60 shows circuit diagram of a flat membrane permeation experiment as used in the present research.

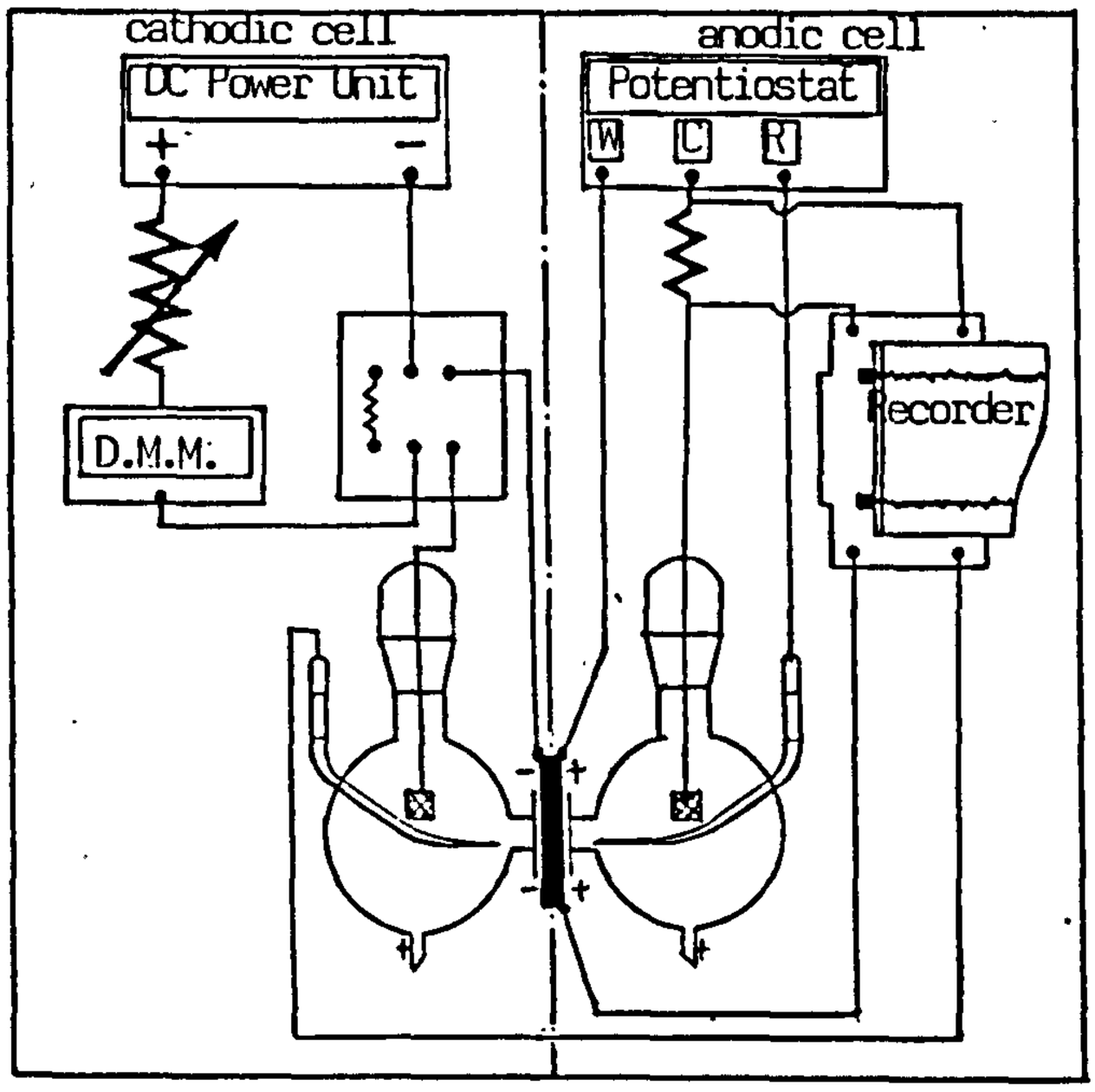

Fig.60 Schematic diagram of the electrical circuit for the flat membrane permeation experiments.

The anodic (detection) side of the membrane is maintained at a constant potential using a Wenking 70 TS1 potentiostat whose counter electrode is connected to a 5kΩ resistance and then to the counter electrode of the anodic cell. The potentiostat measures the surface potential of the membrane and compares it with its preset. Any variation of that potential is compensated by imposition of a current, which pushes the potential in the opposite direction as to restore the preset potential.

The arrival and subsequent oxidation of the hydrogen atoms causes an excess of electrons on the anodic side which is balanced by an equal current in

the opposite direction. It is this current passing through the fixed bank of resistors which is a direct measure of the number of hydrogen atoms arriving at the surface. To measure the current, the potential across a bank of resistors is measured and is recorded on a Linseis LS 52-4 two pen recorder.

The charging side is polarized cathodically at constant current using a stabilized DC power source whose output is fed into a variable resistance box. The resistance is always at the megohm level to prevent current fluctuations. The current thus generated is measured using a multi-function digital multimeter (DMM), Solartron - Schlumberger 7045, while being connected to a 20 Ω resistance in the "stand by" position of a double throw switch. A two pen recorder described previously,allowed the simultaneous recording of both the potential on the charging side, as well as the diffusion current. The equipment could provide independent full scale deflections and a fast response time. The measured diffusion current suffers from a relatively high level of noise which because of the small magnitude of the total currents involved,(μA), could be problematic.This was remedied using a stabilizing unit, comprising two 1000 μF condensers in parallel to the input side of the recorder.

The reference electrodes used were the Saturated Calomel, SCE,with a standard potential of 0.242 vs SHE at 298^{o}K. Two glassware adaptors provided

leak-proof housing for the electrodes and a means of connection to the cell.The potential of these reference electrodes was checked against a separate SCE as a diagnostic measure against the possibility of "poisoning" of them by the elements used. This happened from time to time during the work with reagents incorporating arsenic.

3.2.1.3.Materials Used

All experiments were carried out in 0.10 mol/l NaOH at pH 12.7. This electrolyte was chosen because it maintains the ferrous membrane in a stable passive state before the charging experiment and provides an opportunity to study the passivation phenomenon after termination of the cathodic polarization (decay phase). In contrast, acid media tend to corrode the metal, which leads to hydrogen occlusion in the membrane, apart from that generated by cathodic polarization.

Utmost care was taken to prevent contamination of the solutions in view of possible adverse influences on the permeation rate of hydrogen. To this end all solutions were freshly prepared and were pre-electrolysed for periods of up to 24 hours to remove any heavy elements present. During this time and throughout the duration of experiments, the electrolytes in both compartments were purged with high purity (99.999%) nitrogen gas. This prevented the ingress of oxygen which was a major source of anomalous behaviour in the system as has been observed in the

present research and in earlier work by Wach[7]. Both studies showed the depolarizing effect of O_2 on the measured rates of diffusion.

Experiments were also conducted with sodium hydroxide solutions dosed with $5x10^{-3}$ mol/l of arsenic in the form of $As_2 O_3$ to study the effects of"poisons" (elements which enhance the hydrogen occlusion in metals by interfering with the recombination step during HER) on the overall passivation process. These solutions were pre-electrolysed before the $As_2 O_3$ was added however, the purging was carried out regardless.

Some experiments used electrolytes with added EDTA(Ethylendiaminetetracetic acid) to assist the film reduction process[299]. EDTA is a known complexant for Ferric ions. As will be explained later,it was found to interfere with the film formation process; while the permeation "signature" of the experiment during the permeation phase remained the same. To avoid dust, experiments were conducted inside closed cabinets, properly earthed to prevent induced "stray currents". Membrane metal was Armco iron of 0.07±0.01 mm, 0.205±0.01 mm and 1.07±0.1 mm. The chemical composition of this 99.9% pure iron is given in Table 11.

Table 11 Composition of Armco iron used in the flat membrane permeation experiments.

CONSTITUENTS	C	Mn	Si	P	S
PERCENTAGE	0.017	0.001	0.034	0.008	0.032

The three dimensional experiments were conducted using a 6.5 mm side cube of mild steel of the following composition.

Table 12 Composition of the mild steel used for the 3-D experiments.

CONSTITUENTS	C	Mn	Si	P	S
PERCENTAGE	0.2	0.8	0.06	0.06	0.03

3.2.1.4.Heat Treatment of the Metal Samples

Material used in this study were vacuum annealed up to 8 hours at 800 C in a vacuum furnace. The vacuum furnace comprised a silica tube connected to a vacuum train, made up of a rotary pump (Metrovac Dr1-K) backed by a diffusion pump (Edwards, Speedivac QSB2). The two pumps could achieve a 10^{-6} Torr vacuum level which was adequate for the purpose of this study. However as an additional precaution, all annealing were carried out with degreased shavings of Ti which acted as "getter".

The temperature control of the slide on furnace was $\pm 2^{\circ}C$. The samples were positioned inside the silica tube and when a minimum pressure of 10^{-5} Torr was achieved, the furnace was switched on to reach the temperature, at a slow rate to prevent rapid degassing of the samples.

3.2.1.5.Surface Preparation of the Membrane

Surface preparation is of fundamental importance in diffusion studies, as discussed previously. In

all flat membrane experiments, the surface was cleaned with acetone and then degreased in a vapour degreasing unit containing trichloroethylene. This was continued as long as necessary, so that a successful water-break test could be conducted on the surface. The membranes were then electropolished in a solution containing:

200	g	Cr_2O_3,
1000	ml	acetic acid concentrated
40	ml	distilled water

the mixture was heated for an hour at 65C to help dissolution of Cr_2O_3 . The voltage applied for electropolishing was between 20 to 30 V . This solution needs to be kept at 18°-20° C for optimum effect. Removal of around 10-15 μm from either side was achieved after this period. This ensured the removal of the defect rich layers of the surfaces.

3.2.1.6.Plating Procedure for the Anodic Surface

The anodic surface of every membrane was plated with Pd in order to satisfy these requirements

(1) Prevention of Passivation

As the anodic potentials used are above the rest potential of iron in NaOH solution of pH 12.7 this will lead to the passivation of the surface, rendering it impermeable to hydrogen.

(2) Neutrality in the Kinetics of the Membrane

Any physical barrier used to prevent corrosion should not itself hinder the diffusivity of migrating hydrogen atoms. Pd is the only metal which at room temperature

can dissolve all the hydrogen generated at low to moderate current densities on it [301] and also having a high diffusivity coefficient of $3x10^{-5}$ cm^2 s^{-1}[302] would not impede the passage of hydrogen through it.

(3) Neutralization of Surface Imperfections

As has been discussed , surface defects are inevitable features of cold-work and hence any preparation which could alleviate or at least reduce this,is useful. Pd plating establishes epitaxial growth patterns which cover faults on the surface[117].

(4) Facilitating the Desorption of Hydrogen

Desorption of hydrogen from iron, especially in the atomic form and at low activities, is slow. The same process occurs much more rapidly on a Pd bed and therefore, a coating of Pd would ensure that the diffusion process within the test membrane is the rate determining step rather than the desorption step. There are many plating procedures suggested and used for the plating of thin layers of Pd as well as Ni which has been used by some workers[307].In the present study the plating bath in Table 13 was successfully used in forming an adherent and clean deposit which could withstand the empirical Sellotape test, as proof of coherent as well as adherent strength.,

Table 13 Composition of Pd plating bath.

CONSTITUENT	COMPOSITION
PdCl	60 g/lit
NaOH	180 g/lit

The resultant mixture must be boiled with a few drops HNO3 and HCl for several hours to dissolve all the palladium. The solution is then stored in air tight containers for future use. The plating current is 16 mA cm^{-2} for the first 30 seconds and 8 mA cm^{-2} for a further 270 seconds. The plating solutions must then be drained for further use.

3.2.1.7.Procedure for Flat Surface Experiments

Securing the membrane holder between the flanges(F_1 and F_2) with the aid of rubber cladded clamps, provides a water seal between the two cells of Fig.58. The cells are ready to be filled with the test solution. The clamping must be done diagonally to avoid over straining of the cells.

At this point, a high potential was applied to the anodic side of the membrane in order to remove as much hydrogen as possible from the anodic surface of the working electrode. This is the hydrogen generated mostly during the plating procedure. The membrane can now be charged at the desired current density.

The potentiostat, connected to the anodic side, is set at a potential of -300 mV vs SCE to facilitate the ionization of hydrogen atoms reaching that side. The hydrogen permeation current on the anodic side due to the oxidation of permeating hydrogen is monitored on the chart recorder until a steady state is observed. Change of charging current from $I_{C1} \longrightarrow I_{C2} \longrightarrow I_{C3}$ results

in a multi transient experiment while straight termination of the current leads to a "decay" transient.

Duration of the charging phase was fixed at 2.5 hours but the decay phase was followed up to 12 hours and exceptionally to 170 hours after the termination of charging in certain high current experiments.A fresh membrane was used for each experiment. However,at low to medium current densities, there was no evidence of damage to the substrate after several experiments. The temperature units were controlled within ± 2°C .

3.2.2...THREE DIMENSIONAL EXPERIMENTS

While pursuing the flat membrane experiments, it became clear that the assumption of unidirectional diffusion, so valid for thin electrodes,is distorted as the membrane thickness is increased. Hence the need for an experimental arrangement which allowed the instantaneous monitoring of hydrogen atoms permeating a thick specimen became apparent.The following is the account of each successive step in this part of the project leading to a different design which incorporated these improvements.It was decided from the outset, that an experiment capable of investigating the hydrogen activity on four sides of a cube is quite adequate to give a comprehensive picture of the conditions in membranes charged with hydrogen. The top

and the bottom side of the cube were specified for the provision of electrical contacts in the case of the former and a positioning base in case of the latter. The first attempt at finding a solution to the problem resulted in the design of Fig.60. The problem of very long periods of charging called for thicker membranes

_ was tackled here through the use of a small cube, 4 mm side. A Perspex cube in which a 4 mm side cube cavity was machined held the sample in place. The use of such a small cube meant that no commercial O-rings were available.Therefore, thin but resistant "washers" for water sealing were fabricated. Numerous attempts at different materials from natural rubber to a variety of man-made polymers such as PVC and PTFE were made without success as all the gaskets made showed signs of leakage.

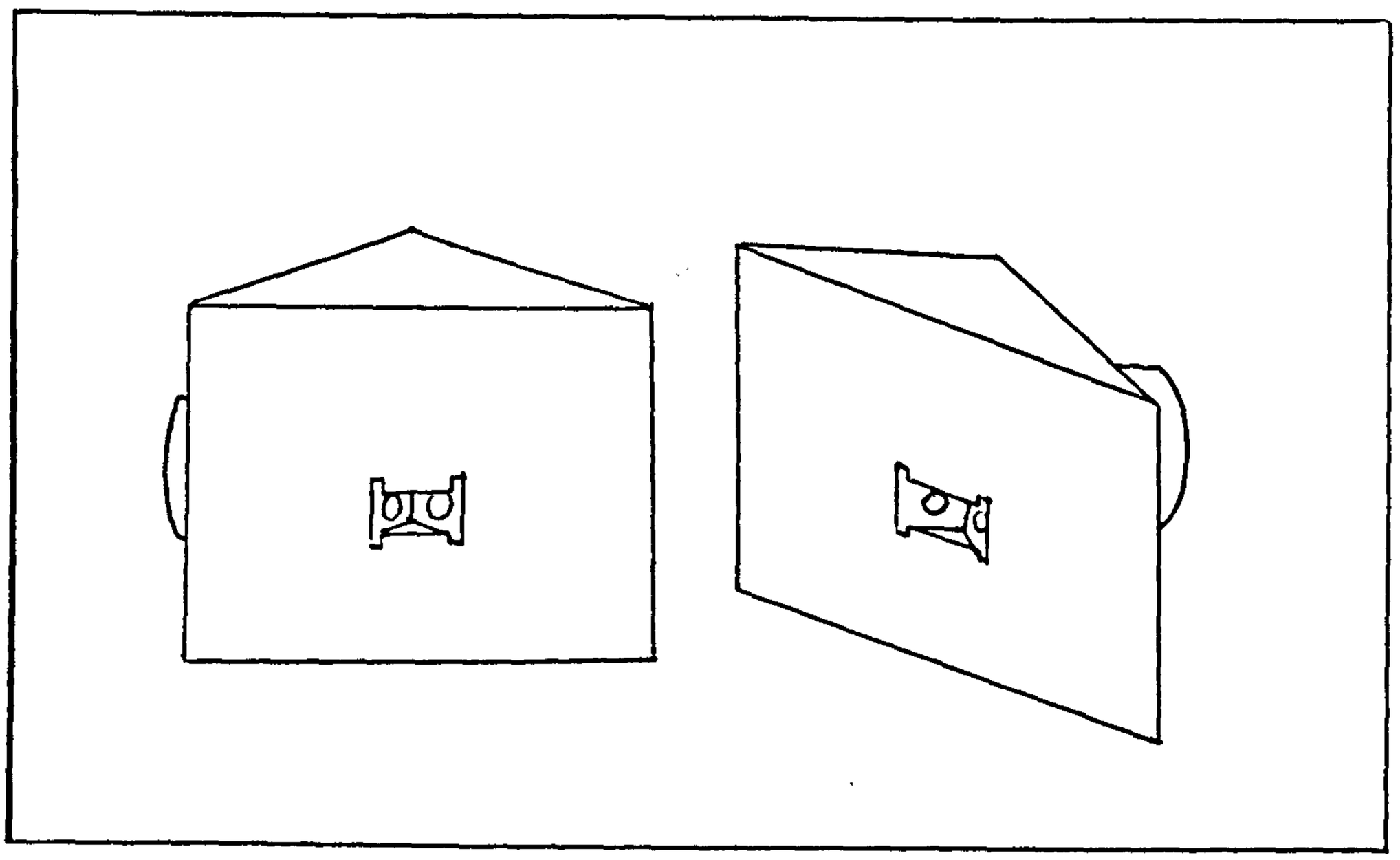

Fig.60 Schematic representation of the first attempt at making a three dimensional sample holder.(model A)

The general conclusion from these tests was that a 4 mm cube was too small to allow a satisfactory water seal against NaOH. Also, it became clear that hydrogen bubbles generated during charging coalesce and cover the surface. Fig.61 shows model B holder in which the cavity was enlarged to accept a 5mm side cube, and introduction of 4 risers to allow the circulation of the electrolyte by the use of a pump.

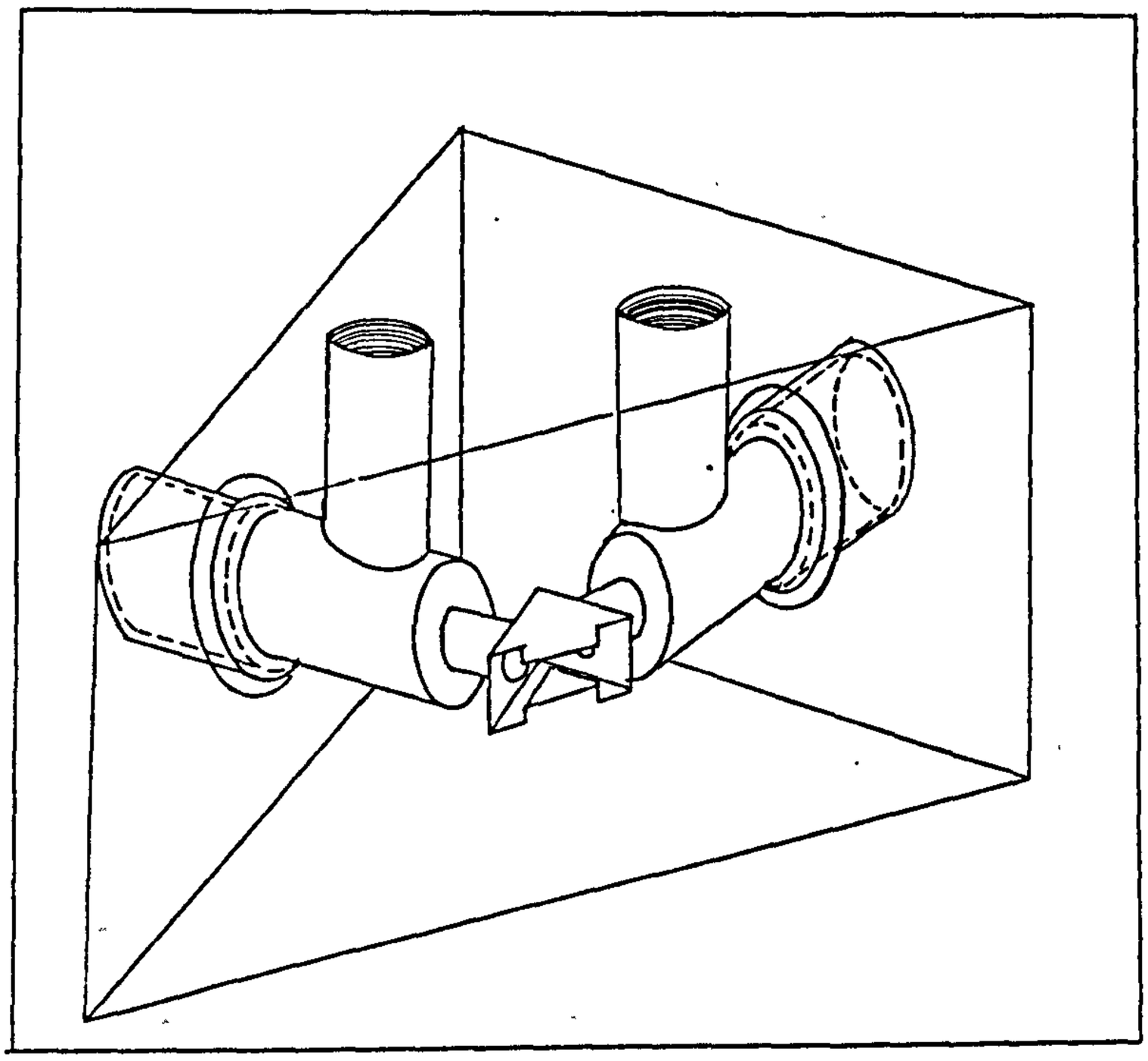

Fig.61 Sample holder Model B incorporating improvements

As the above problems persisted, another unit was constructed.The aim being the provision of a water seal and improved handling of the sample holder as the previous models could take up to 45 minutes to assemble (Fig.62).The use of an even larger cavity increased the dimensions of the sample to 5.5 mm and positioning the risers at an angle simplified the assembly procedure as they allowed more room for the rubber tubings.This idea

abandoned later as the frequent breakage of these risers counteracted any benefits achieved.

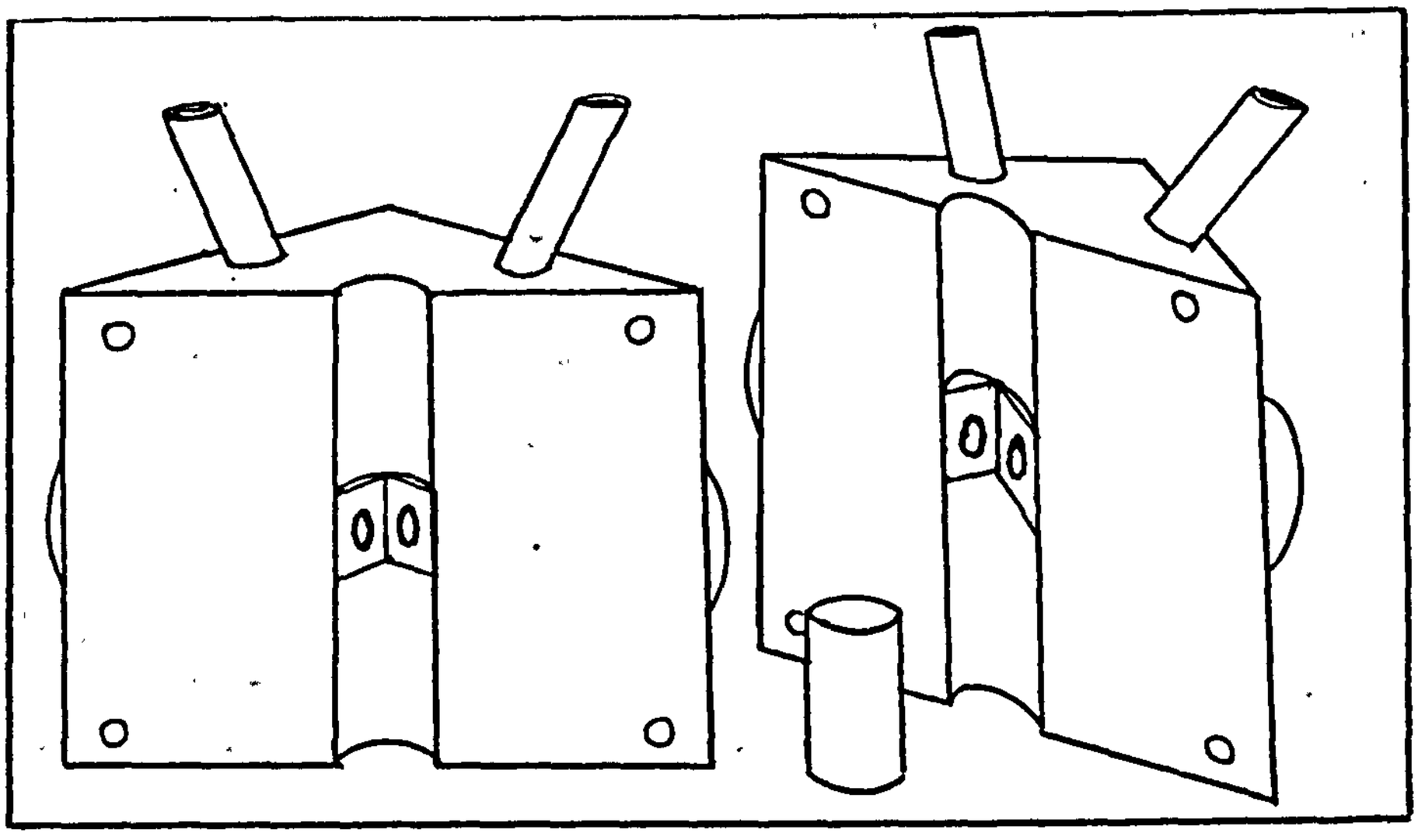

Fig.62 The pictorial representation of Sample holder Model (c).

Figures 63 shows the extent to which the size of the cavity was enlarged, after the previous models proved unsuccessful. Although, on occasions, the sample holders worked, their unreliable nature necessitated a totally new approach. Fig.64 illustrates the overall circuitry of the three dimensional experiments.

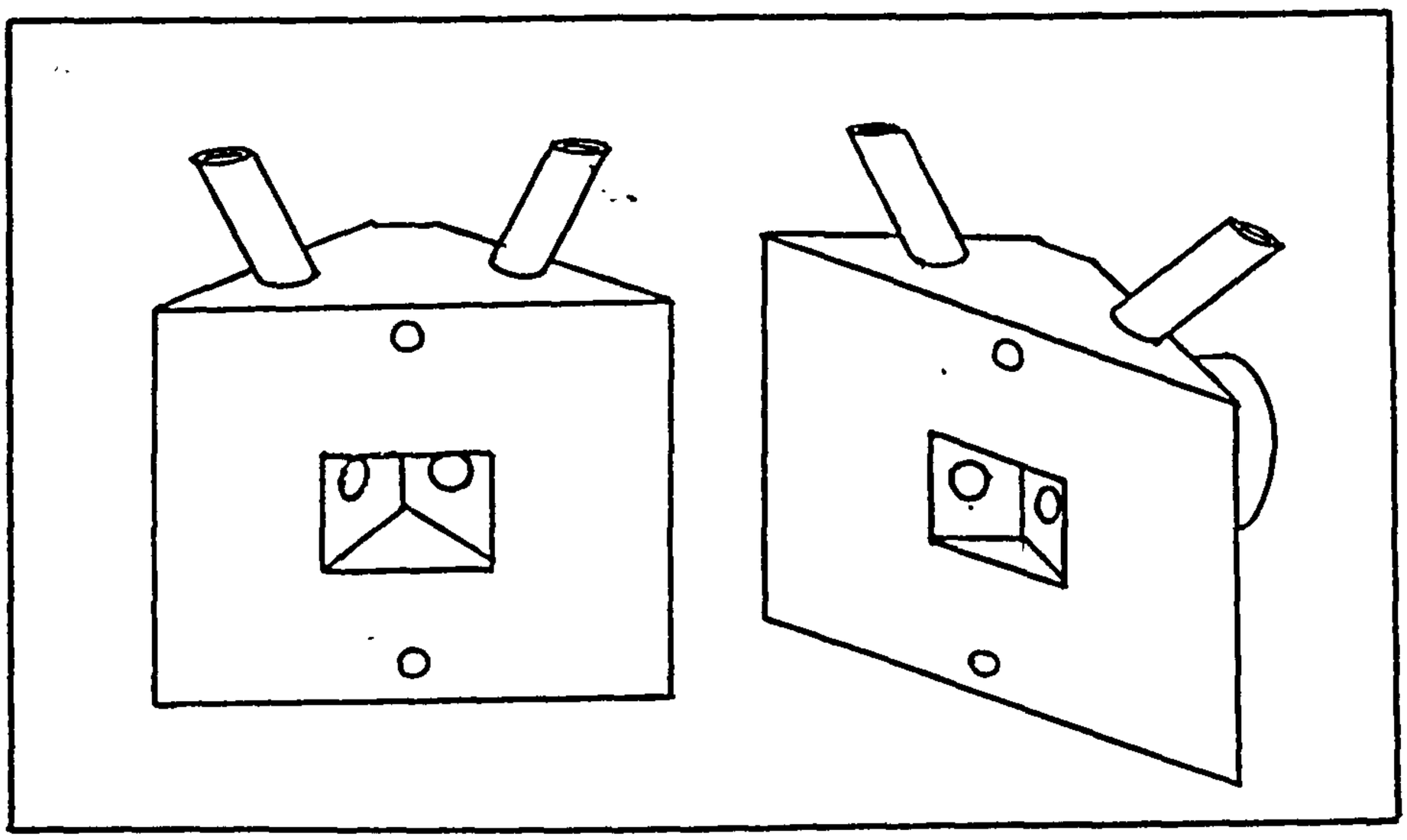

Fig.63 Sample holder Model D

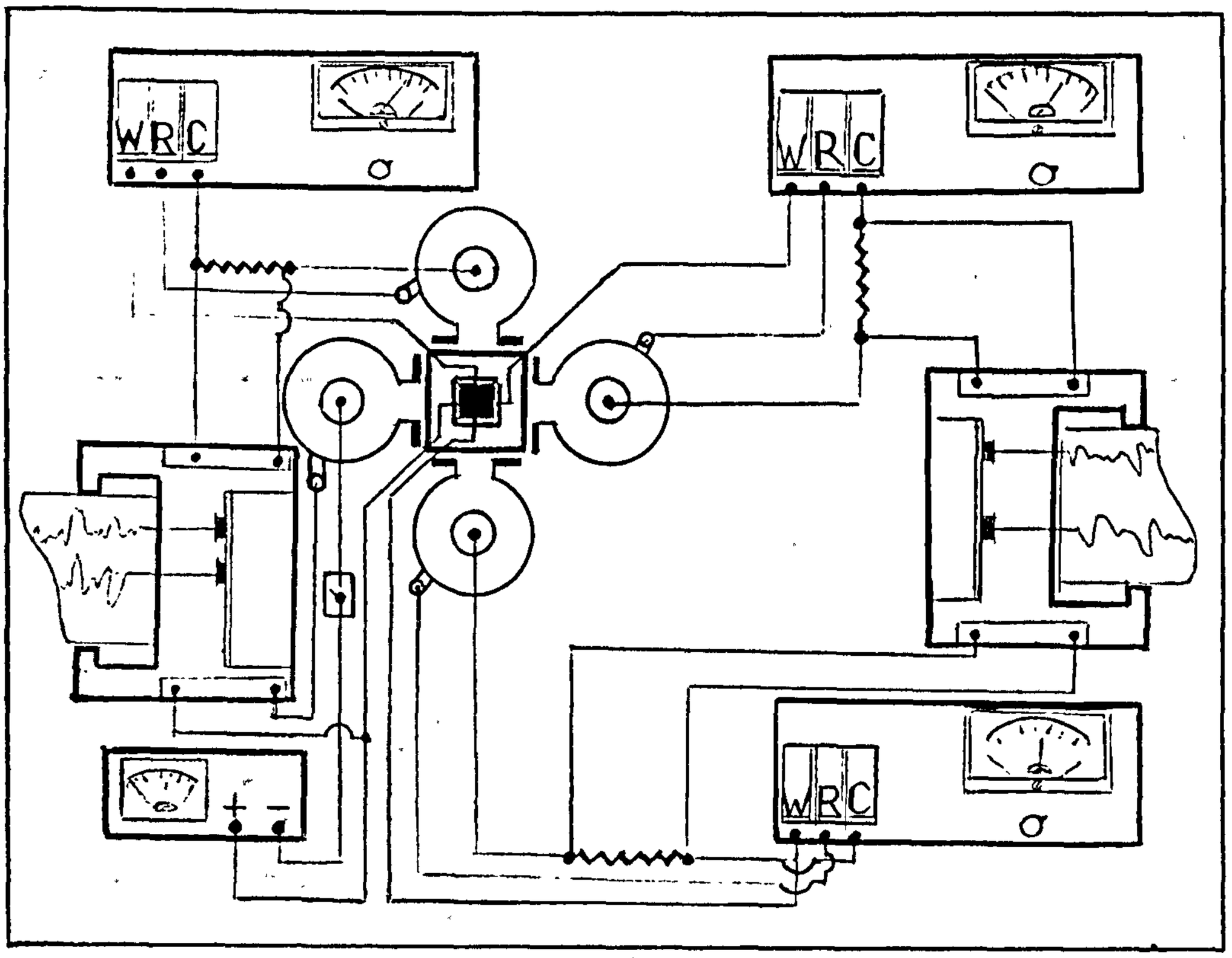

Fig.64 Pictorial representation of the the electrical circuitry for the three dimensional experiments.

The common solution to any gas or electrolyte seal has been the screw type seal. This is based on a multi-level fastening which is tapered at a 45 angle from one junction level to another. The inherent strength of this design is the possibility of several sealing junctions backing one another, resulting in a hermetic seal.

As is evident from Fig.65, O-ring (a) with an internal diameter of 2mm has the task of sealing the side in contact with it. This was made much easier in this case by the use of standard O-rings . To ensure an absolutely tight seal, silicone-rubber paste was spread around the O-ring and the fastening screwed into place. The joint is then left to harden thereby provide

additional barrier to electrolyte seepage. These modifications provide a final satisfactory design for the 3-D sample holder and cell.

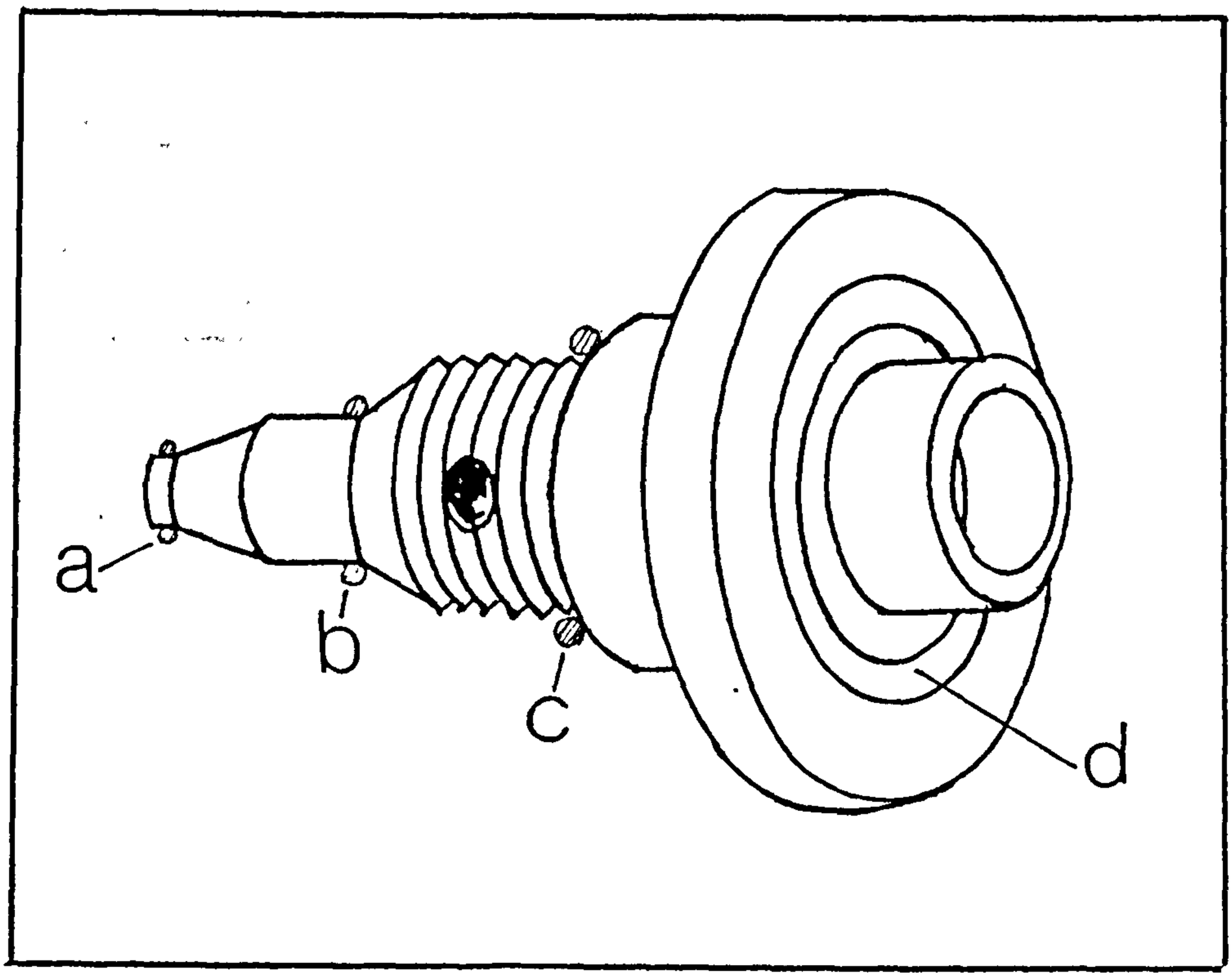

Fig.65 The pictorial representation of fastenings used in the screw on design. O-rings a, b, c and d represent the four different levels of sealing .

Once in place, the surface of one of the three sides is galvanostatically polarized to generate hydrogen while the other three faces will be potentiostatically controlled ,provides the right thermodynamic conditions for hydrogen ionization. These faces are Pd-plated in the same way as described elsewhere. Figure 65 shows the base designed for receiving the screw on fasteners and Fig.67 illustrates the sample holder with the fasteners in place.

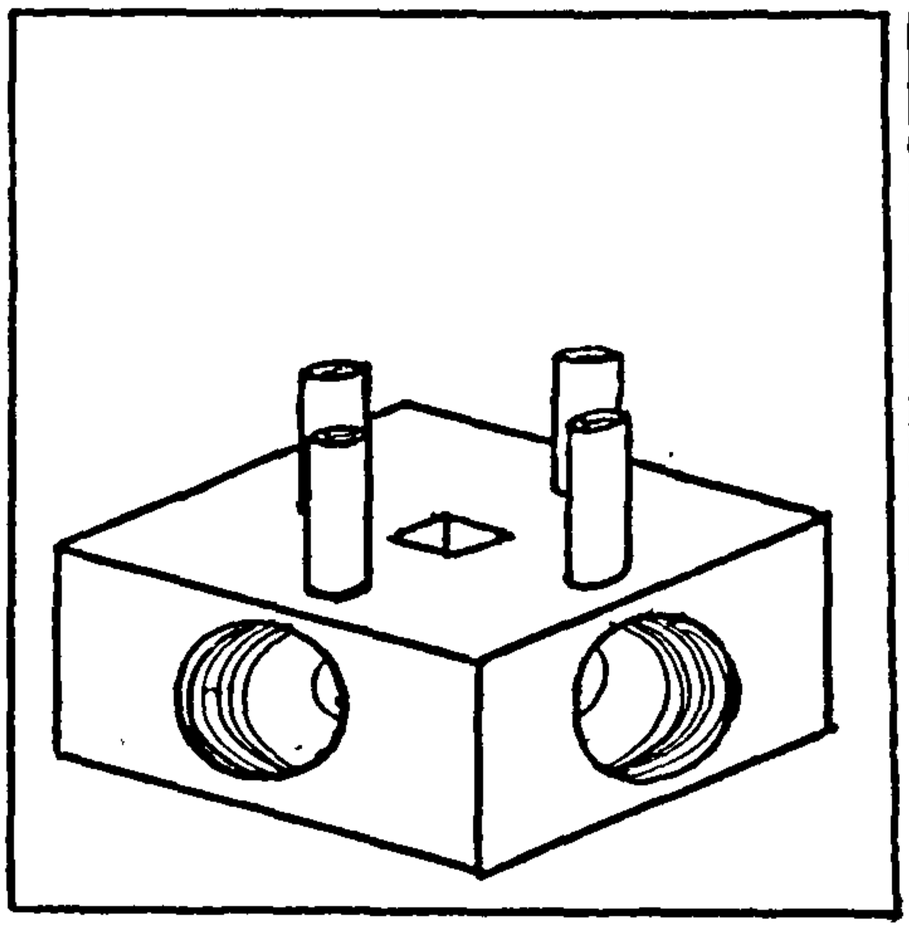

Fig.66 The base for the screw on design.

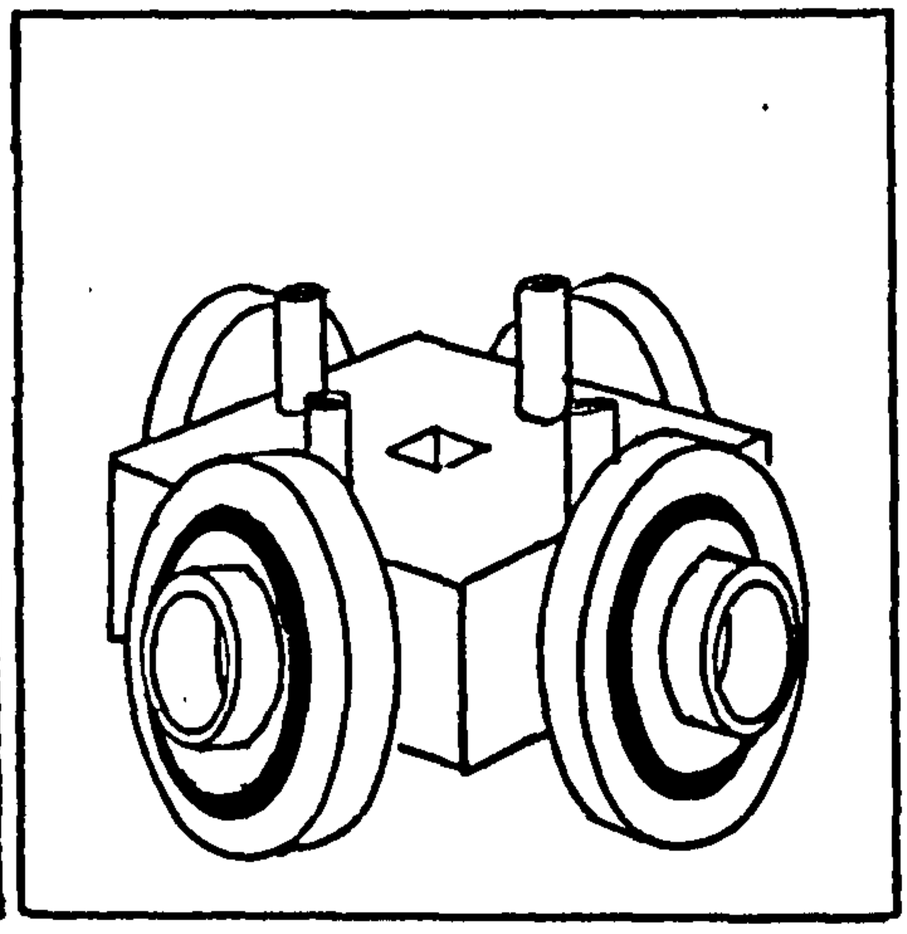

Fig.67 The pictorial representation of assembled sample holder.

3.2.3...AC IMPEDANCE TECHNIQUES

While permeation experiments are best suited for the study of large deviations from equilibrium as described in the previous section, passivation studies do not lend themselves easily to these techniques . To study the mechanism as well as kinetics of such processes there is a need for these to be done in situ and with as little disturbation to their real or quasi-equilibrium state. The AC impedance technique as the main non-optical surface analysis method was used in an attempt to investigate passivation phenomenon. The technique is based on the principle that most passive films are non conductive or semi-conductive.However, the same films interact with the wave form of an AC current and this exchange of energy can be observed and measured with a sensitive detector.

In the present experiments the working electrode of a charging cell (cathodic) cell as described before was monitored using an AC impedance equipment comprising a potentiostat and a lock in amplifier. An IBM PC logged all the results and produced hard copy . The higher frequencies applied were resolved using Fast Fourier Transformation(FFT). The following diagram represents how this is achieved. Experiments were carried out on a freshly prepared sample from the rest potential followed by film reduction,leading to hydrogen generation.The reverse of the above was also followed during the decay phase,after the termination of charging current.In order to follow the process of film formation,the surface potential was arrested and FFT and simple "lock in" measurements were performed on the passivating surface

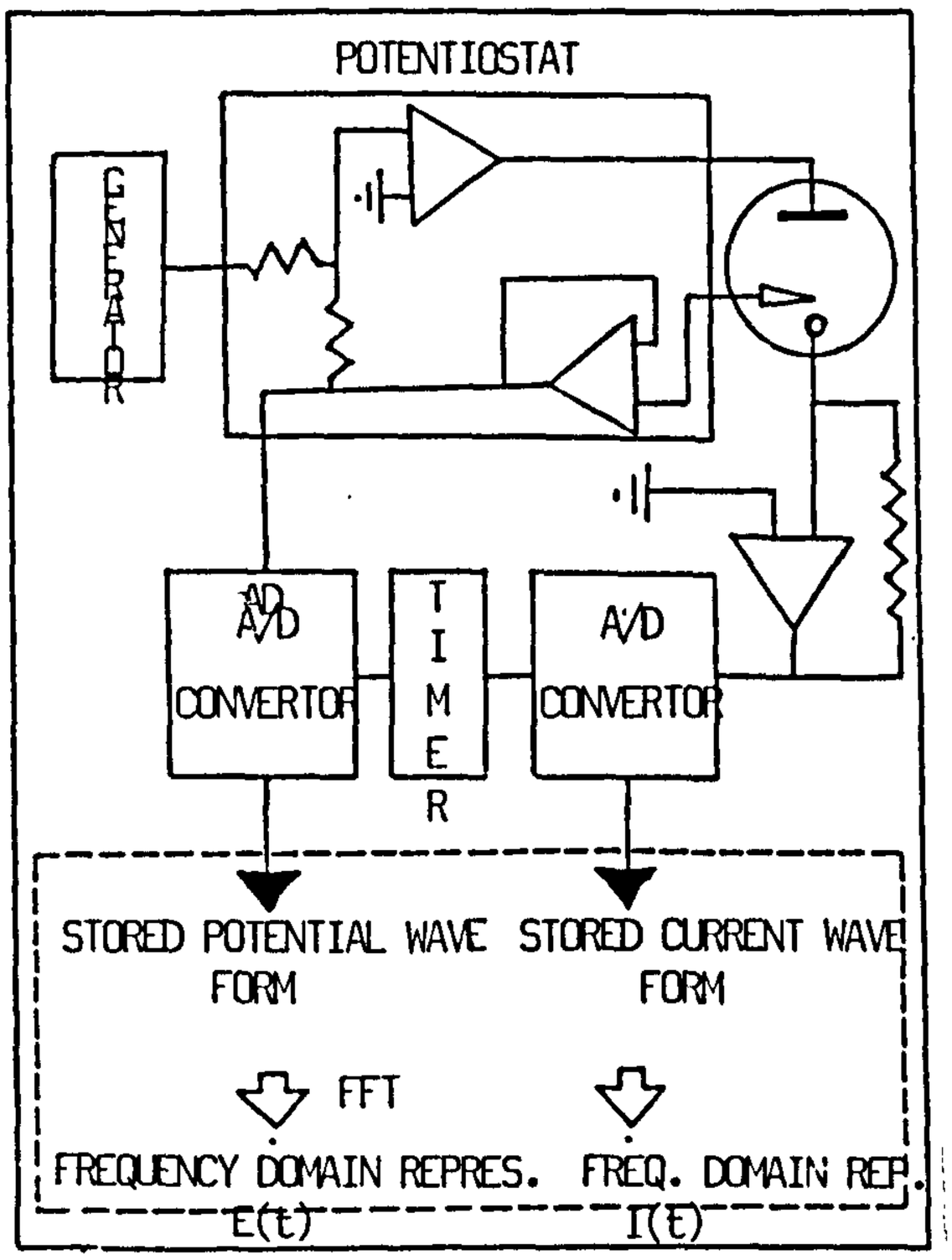

Fig.68 Schematic diagram showing apparatus and data processing steps in on-line Fourier analysis of AC impedance measurements.

Although the FFT shortens the time needed for high frequency measurements, nonetheless, the overall time scale remained large for covering a meaningful range of frequency. This meant that the effect of hydrogen at shorter times was not ascertained while potential was being fixed and AC impedance measured, more of the hydrogen was lost from the membrane through the usual process of diffusion. This, as has been shown in later sections has a profound effect on the surface phenomena The loss of hydrogen was not so problematic at the longer times as the rate of change of potential was much less.The data retrieved from the PC was interpreted using the models available in the literature (section 2.9.7) .

3.2.4...INDUCTIVELY COUPLED ARGON PLASMA (ICAP) ATOMIC EMISSION SPECTROSCOPY (AES)

Atomic emission spectroscopy has for a long time been the standard for routine analysis in many fields. A minute part of the sample is vaporized and then excited to the point of light emission. This may be done in a variety of ways, including spark, laser, plasma or as in the present case, an induced coupled argon plasma. Since each element produces a series of spectral lines of specific wavelength, characteristic of that element, the identification of each element from the study of the position of the lines generated is possible. Determination of the quantity of each element is also possible according to the intensity of the lines in an unknown sample compared to a standard.

For the purpose of these experiments , samples of 2-3 ml were drawn in quick succession from the cathodic cell using a very long needle and syringe. The timing of each withdrawal was chosen to cover broadly, the important points in the potential-time curves as described in the following section. The total ferric content of the samples provided and a such no effort were made to prevent the oxidation of ferrous ions to the ferric ions. The limit of sensitivity of the technique was 0.010 ppm and the results below this limit contain a large degree of uncertainty.

3.2.5...SCANNING AND TRANSMISSION ELECTRON MICROSCOPY

Scanning electron microscopy (SEM) was used to examine the morphology and the integrity of surface Pd deposit. The system used was a Super Mini-Sem scanning electron microscope at an accelerating voltage of 15 keV . Additional information as to the composition of the surface deposits was provided by the "Energy Dispersive X-Ray Analyser" System 4.

The transmission electron microscope (TEM) was used to characterise the surface film. A carbon replica from the film detached from the surface was made and then cut to small pieces. These pieces collected on a fine gauze,are placed inside a gelatin capsule and then positioned in the vacuum chamber of the TEM. The intensity and the position of the lines generated are compared to those available in the index books leading to the identification of the compound.

4.....RESULTS

4.1....INTRODUCTION

In this section, the data obtained throughout this work will be discussed in five different categories.

1 - the thin membrane permeation experiments

2 - the electrode potential measurement experiments

3 - atomic emission spectroscopy studies

4 - the three dimensional permeation experiments

5 - AC impedance results.

Hydrogen-related experiments are notorious for the wide scatter of results[117]. In the present work, scatter in the results was observed which has been reported accordingly. However, this is believed not to be greater than normal.

As this work is mainly concerned with the surface properties of iron membranes,the majority of the results were obtained from experiments devised specifically, to throw light on such aspects. The results obtained are presented in the subsequent subsections.

4.2.....HYDROGEN PERMEATION EXPERIMENTS

Hydrogen permeation experiments form a major part of this work. Table 14 represents the compiled data from these experiments. Permeation experiments were carried out on three different membrane thicknesses (0.07, 0.205, 1.07 mm) at 25° C. Further experiments were conducted on the 0.205 mm thick membranes at 19° C, 30° C, 45° C and 65° C. The permeation flux (i_∞ , $\mu A cm^{-2}$) results are plotted against the charging current density (i_c) in Figures 69 and 70. As is shown, the permeation current increases as the CCD is raised.

The effect of temperature on permeation flux is evident from these figures which show increase in i as the temperature goes up from 19° C to 65° C. Fig.71 shows the efficiency of the experiments as defined by $\epsilon = (i_\infty / ic) \times 100$ .The decrease in is in line with the observed decrease in permeation flux by Daft [190]. The dependency of permeation flux on CCD has ben shown by other workers [104,305] and our results confirm it.

The 4th column of Table 14, are the relaxation times for the experiments upon the termination of charging current (t_d).These time constants were used when calculating diffusivity coefficients from the formula: $D = L^2 / (\pi^2 t_d)$ (233)
The results of these calculations are tabulated in the last column of Table 14.

Table 14 The results of permeation experiments conducted on different thickness membranes at 25 C temperature and on uniform thickness membranes at various temperatures.

MEMBRANE THICKNESS AND TEMP.	i_c ,μAcm^{-2}	i_∞ ,μAcm^{-2}	$\epsilon = i_\infty / i_c$	t_d ,s	D ,cm^2 s^{-1}
	2.4	1.88	78.30	1.26	3.94E-6
	12.0	4.93	41.08	1.04	4.77E-6
0.07mm	24.0	9.03	37.60	0.95	5.22E-6
25° C	120.0	15.20	12.60	0.80	6.20E-6
	482.0	20.50	4.25	0.51	1.08E-5
	2.4	0.12	5.00	316	3.70E-6
	12.0				
1.07mm	24.0	2.10	2.10	205	5.71E-6
25° C	120.0	1.73	1.40	115	1.02E-5
	482.0	3.56	0.70	50	2.33E-5
	2.4	1.32	55.00	7.09	6.09E-6
0.205	12.0	1.85	15.40	3.90	1.09E-5
mm	24.0	3.27	13.60	2.98	1.43E-5
25° C	120.0	10.09	8.40	1.77	2.44E-5
	482.0	18.20	3.80	1.16	3.66E-5
	2.4	1.08	45.20	15.48	2.75E-6
	12.0	1.61	13.50	4.62	1.49E-5
0.205	24.0	2.82	11.80	3.70	1.15E-5
mm	120.0	7.18	6.10	2.21	1.92E-5
19° C	482.0	14.70	3.20	1.67	2.55E-5
	2.4	1.52	63.30	8.18	5.20E-6
	12.0	2.78	23.20	3.40	1.25E-6
0.205	24.0	6.04	25.20	2.97	1.43E-5
mm	120.0	12.42	10.40	1.93	2.20E-5
30° C	482.0	19.68	4.10	1.21	3.50E-5
	2.4	1.71	71.20	5.13	8.30E-6
	12.0	3.20	26.60	2.66	1.60E-5
0.205	24.0	6.91	28.80	2.13	2.00E-5
mm	120.0	12.96	10.80	1.31	3.25E-5
45° C	482.0	24.50	5.00	1.16	3.65E-5
	2.4	1.92	80.50	3.40	1.25E-5
	12.0	5.06	42.20	1.91	2.25E-5
0.205	24.0	7.83	32.60	1.37	3.10E-5
mm	120.0	15.60	13.00	0.89	4.80E-5
65° C	482.0	30.10	6.20	0.79	5.40E-5

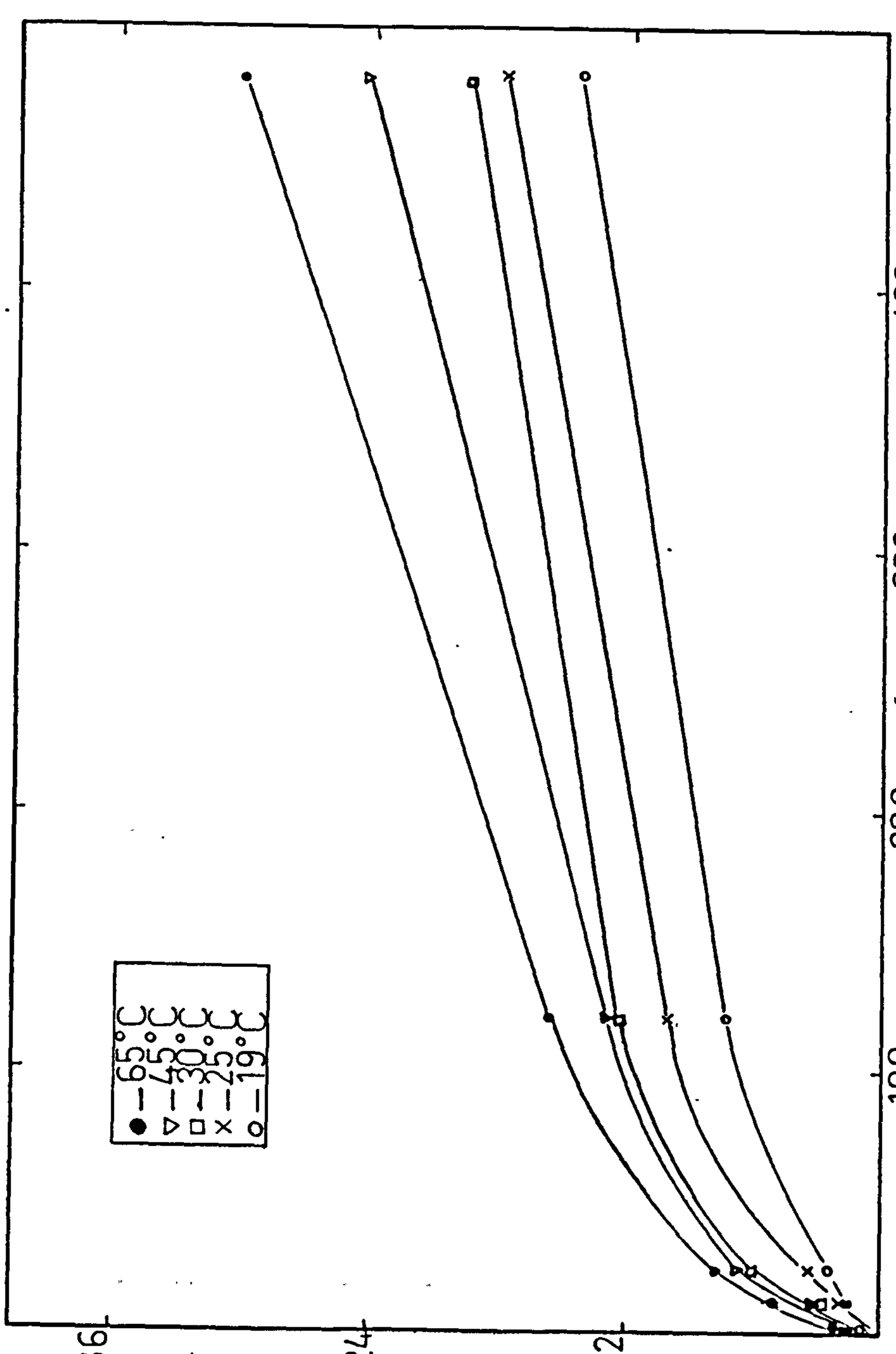

Fig.69 The permeation/charging current density relationship for experiments conducted on 0.205mm thick membranes at different temperatures.

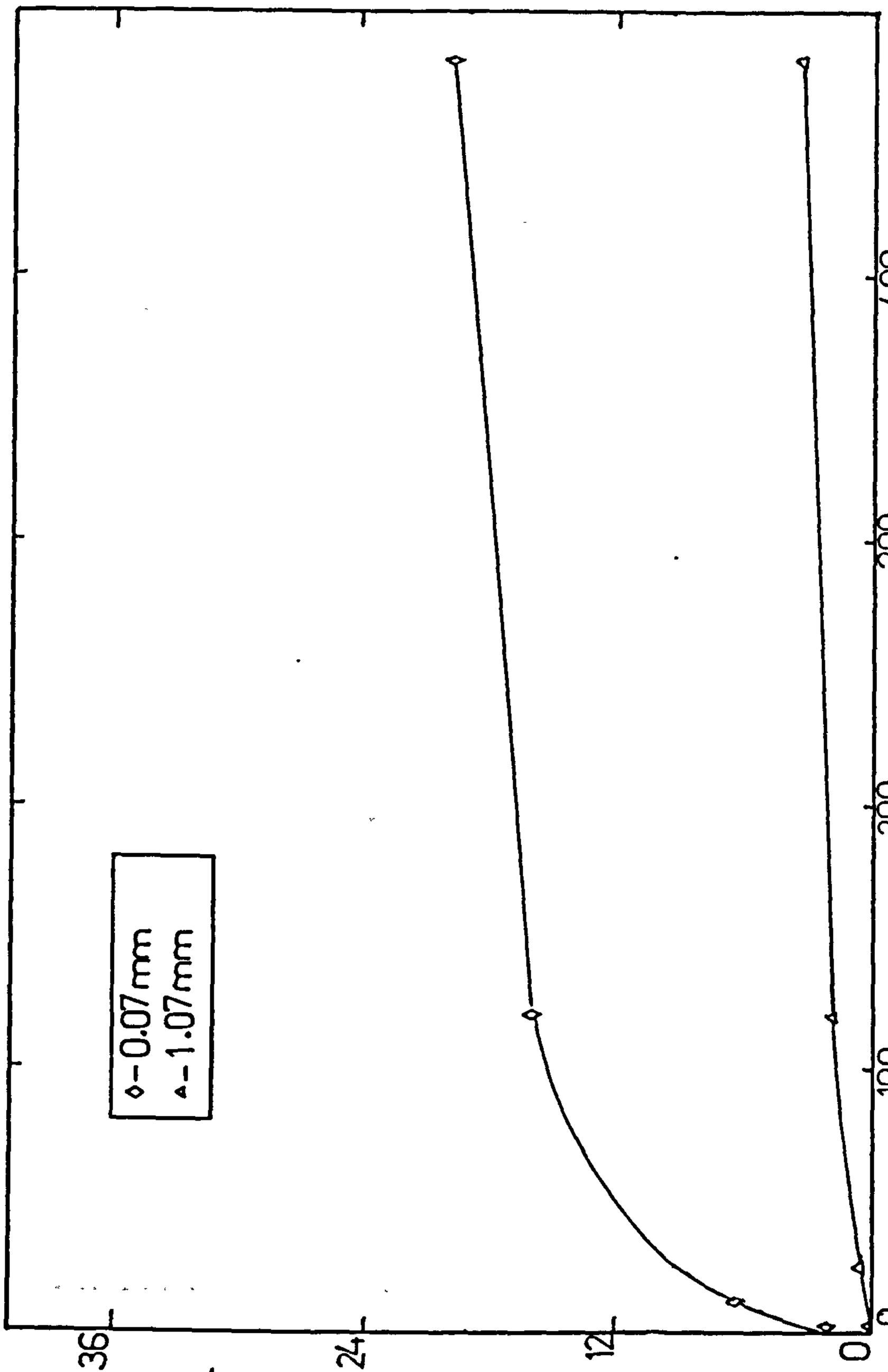

Fig.70 The permeation/charging current density relationship for experiments conducted on membranes of different thicknesses at room temperature.

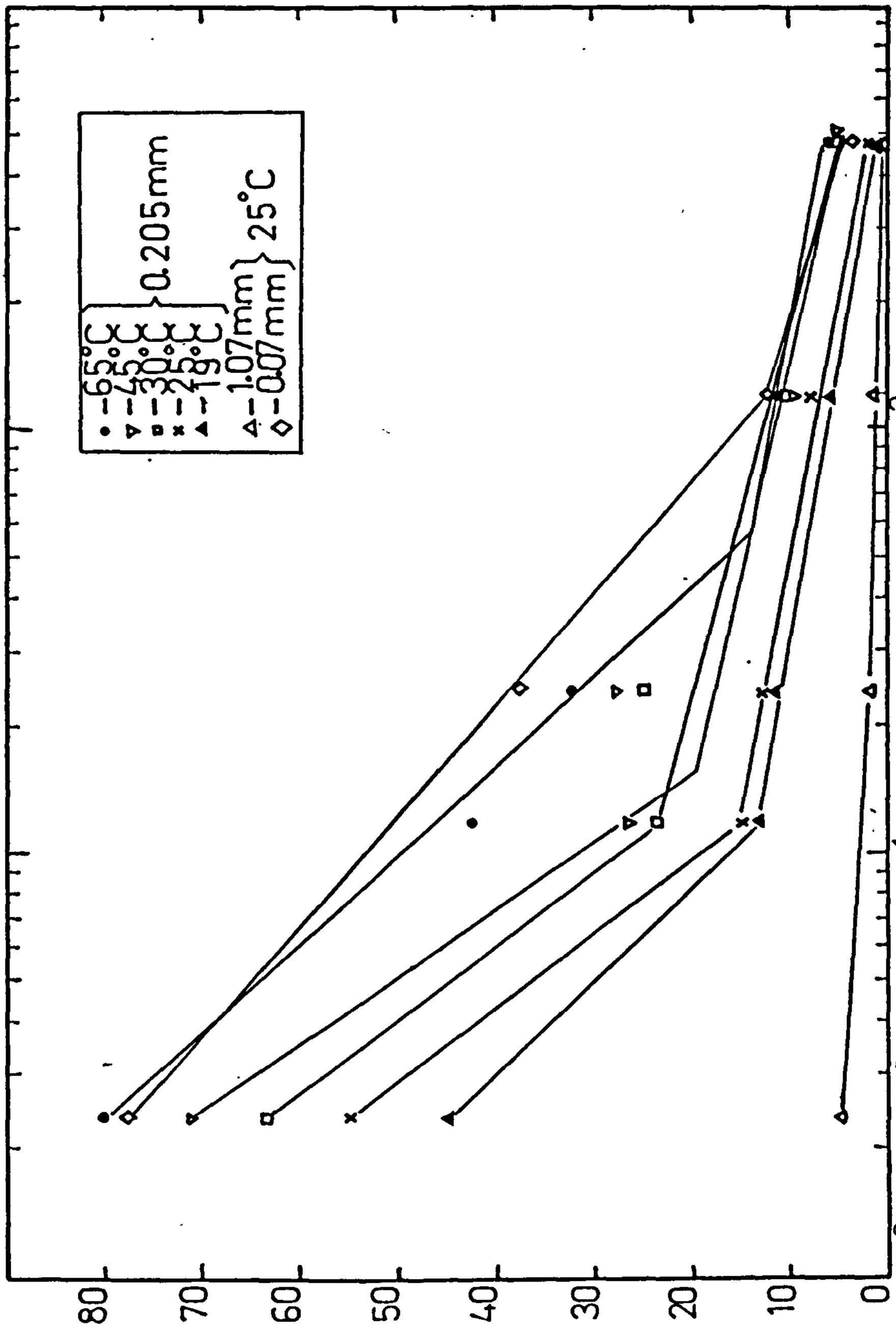

Fig.71 The efficiency of charging current densities used for experiments at different membrane thicknesses and temperatures.

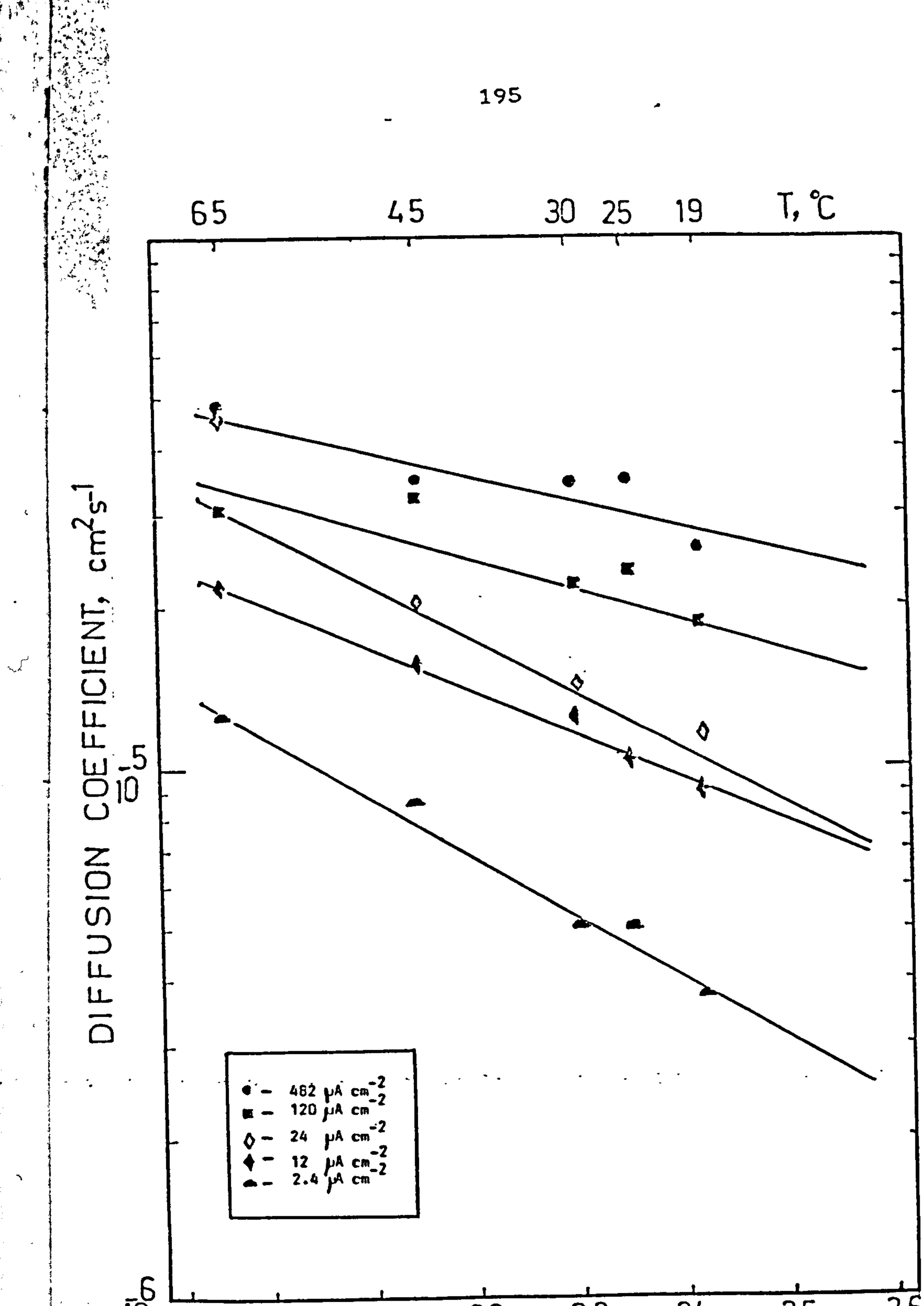

Fig.72 Diffusivity versus the reciprocal of temperature plots for different charging current densities. Least Means Square analysis of data has been used to form the plots.

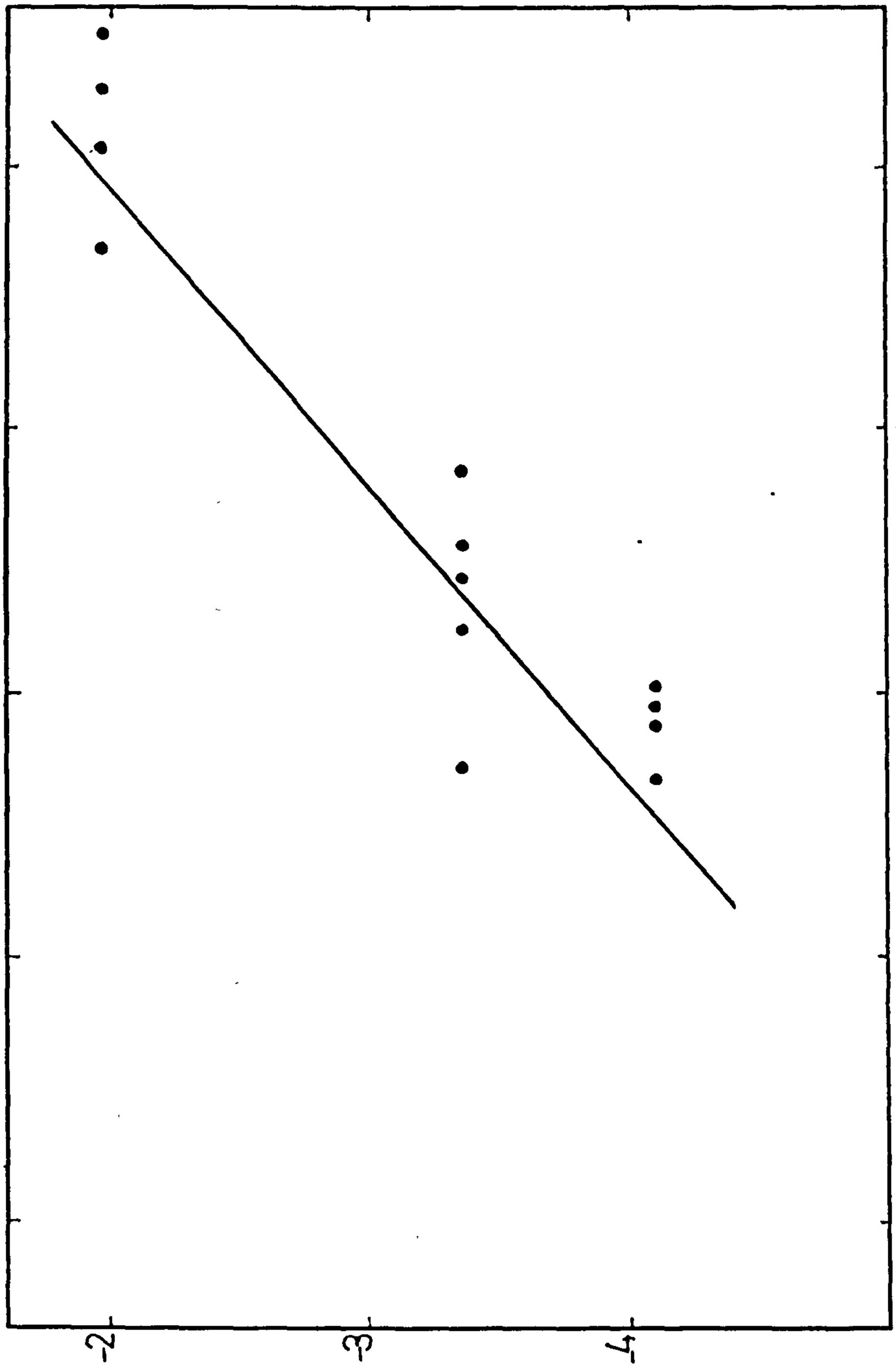

Fig.73 The plot of Log L^2 against Log t for calculation of lattice diffusivity D .

The dependency of these diffusivity values on the charging current is well documented [16,157,306-308]. Fig.72 illustrates the diffusivity versus the reciprocal of temperature plots for different charging currents used in this work.The relationship between D and 1/T follows an Arrhenius type equation such as $D=D_0 exp(E_D/RT)$.The value of D_0,the pre-exponential factor could be calculated from the intercept on the ln D axis of the plots in Fig.72 when 1/T tends to zero. The activation energy term, E_D, is calculated from the slope of the curves. These results are tabulated in Table 15 below.

Table 15 The calculated values of D and E_D for different charging current densities.

i , μAcm^{-2}	2.40	12.00	24.00	120.00	482.00
E_D , kJ/mol	28.08	25.75	25.87	9.01	10.26
D_0 , $cm^2 s^{-1}$	3.50E-1	4.01E-1	4.26E-1	8.37E-4	9.74E-4
D , $cm^2 s^{-1}$	4.16E-6	1.22E-5	1.24E-5	2.20E-5	3.22E-5

The E_D /kJmol^{-1} is a measure of ease with which hydrogen atoms could move about in the membrane. For charging current densities above 120 μA cm^{-2} there is good agreement between the activation energies calculated from this work and other reliable published data[117]. The calculated diffusivities at 298 K as shown in the last column of the Table 15, illustrating the "concentration dependence diffusion" phenomenon.

This concentration dependence is the result of the effective saturation of the internal trapping sites, as has been explained in Chapter 2. The decrease

in activation energy from 28.08 kJ/mol for the diffusion process at the low CCD of 2.4 μAcm^{-2} to 10.26 kJ/mol for the CCD of 482 μAcm^{-2}, is evidence for the ease with which the hydrogen atoms could traverse the membranes in the latter case.

The effects of concentration dependent diffusivity could be avoided if the fundamentally thickness independent relaxation time (t_d), for the membranes of different thickness is plotted against the square of the membrane thickness [218].

Fig 73 shows the plot of Log L^2 versus Log t; The intercept on the Y-axis of which gives the value of the lattice diffusivity for these experiments as $2.67x10^{-5}$ $cm^2 s^{-1}$.Although this is slightly less than the reported hydrogen diffusion coefficient values in iron, it is in general agreement with most recent published data[117].

A test for ascertaining that the lattice diffusion is the rate-determining step in any permeation experiment is to plot the reciprocal of permeation current against the thickness.This should pass through the origin[16,203,219]. Fig.74 effectively shows this for the membranes used in this work.

4.3.....POTENTIAL MEASUREMENTS

These measurements were carried out in three different forms

(a) During the decay phase of hydrogen permeation experiments

(b) In experiments devised solely to show the effects of effusing hydrogen on the passivation

(c) The potential measurements in the presence of EDTA and As_2O_3 .

Figs.75 to 81 show the potential decay curves vs time. A feature of these measurements was the very long periods of follow up of the potential . This revealed a special pattern of successive breaks whose corresponding potentials and times identified the surface reactions in progress. Table 16 tabulates these breaks as t_1 , t_2, t_3 and t_4 together with their corresponding potentials for experiments conducted at temperature range 19°-65° C and on membranes of 0.07, 0.205 and 1.07 mm thick. As is evident, the steady state potential of the surface, E_{ss} and hence the relevant overpotential becomes more negative as the CCD increases. Several papers in the literature have shown such relationship between CCD and the overpotential in Pd and Fe[302,309-312].

In the present work the following procedure was adopted for calculating the true overpotential of the membrane. As it will be shown later, iron in 0.1N NaOH has a strong propensity for passivation. Therefore the only true overpotential which shows the difference between the potential of the film-free surface and the steady state potential of the same membrane is obtained only by extrapolating the first plateau of E-Logt curves to zero time as shown in Fig 75. The values of η thus calculated are shown in Table 16.

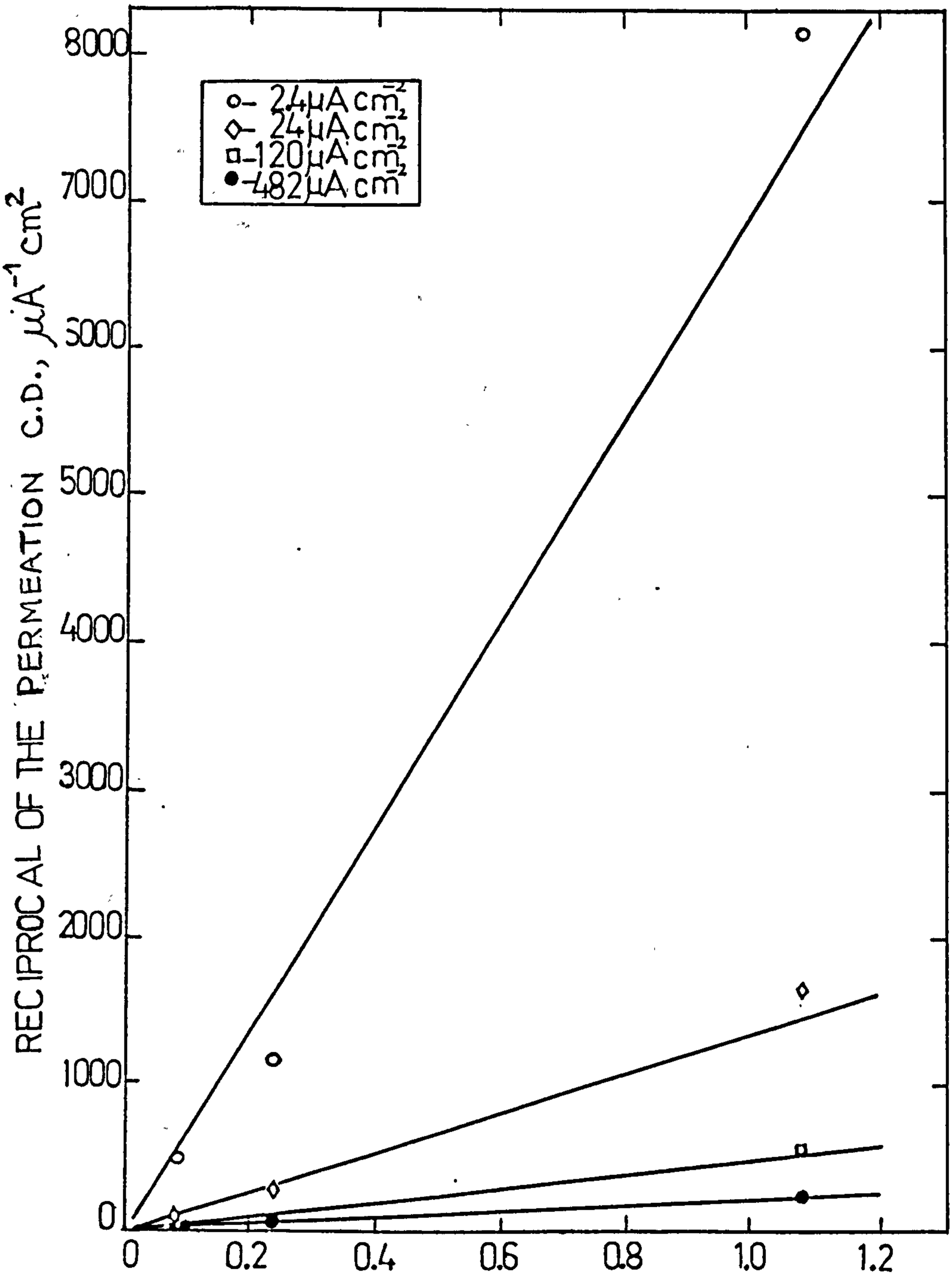

Fig.74 The plots of reciprocal of permeation current density against membrane thickness crossing through the origin illustrating that the rds in the observed permeation experiment is the lattice diffusion.

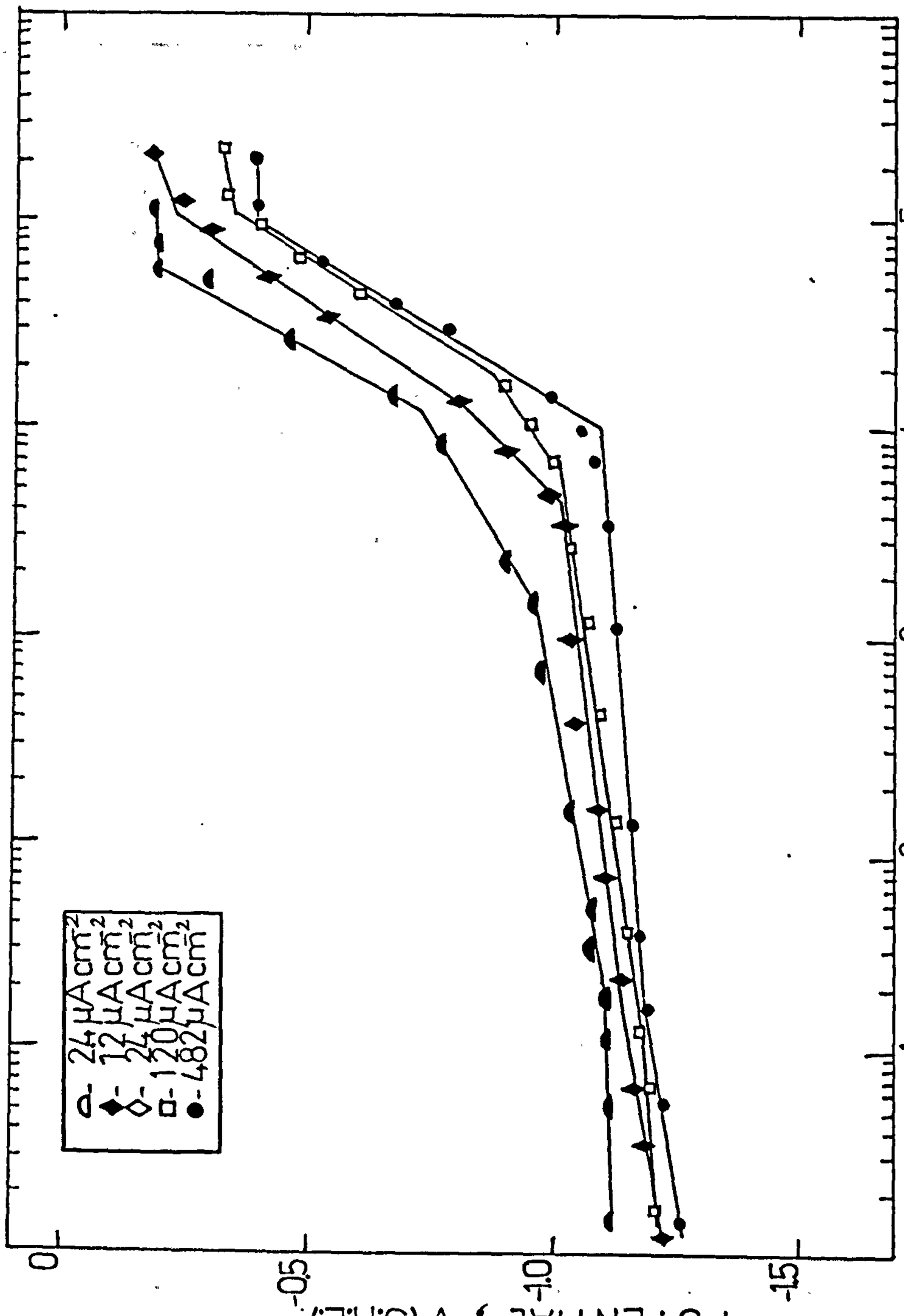

Fig.75 Plots of potential vs time during decay part of the experiments conducted at 25 C at different CCDs on 0.07 mm thick membranes.

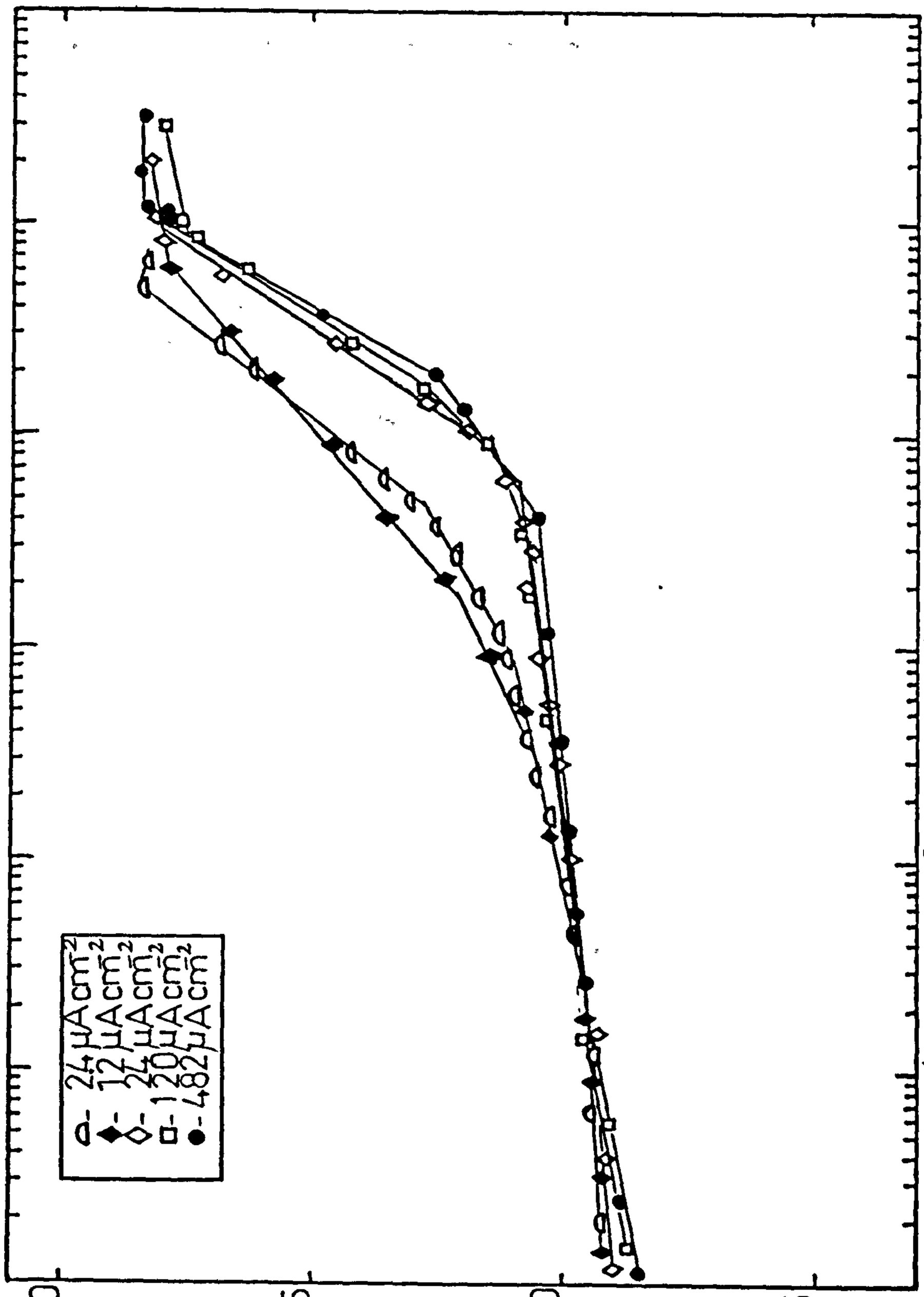

Fig.76 Plots of potential vs time during the decay part for the experiments conducted at 25° C at different CCDs on 0.205 mm thick membranes.

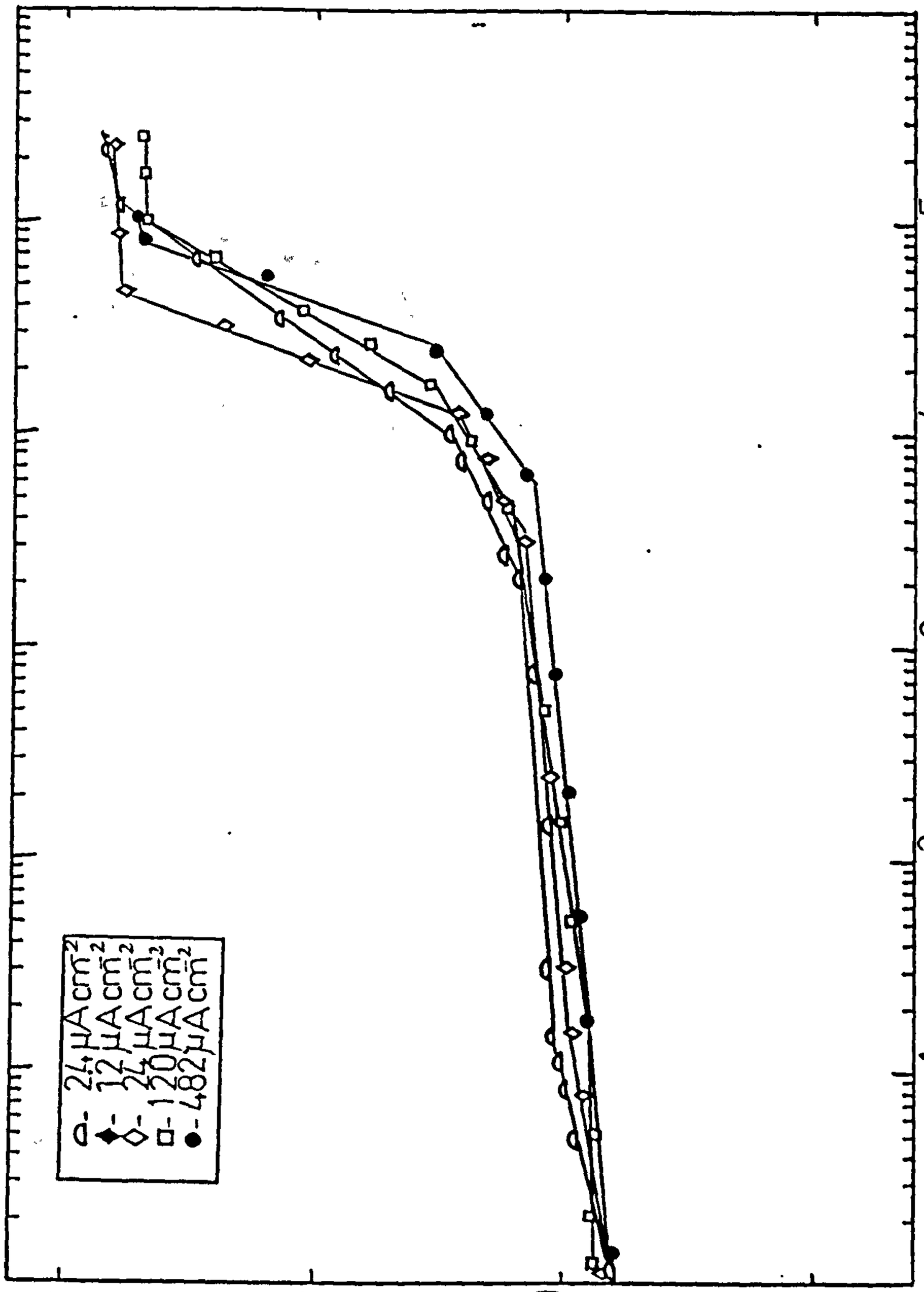

Fig.77 Plots of potential vs time during the decay part of the experiments conducted at 25 C at different CCDs on 1.07 mm thick membranes.

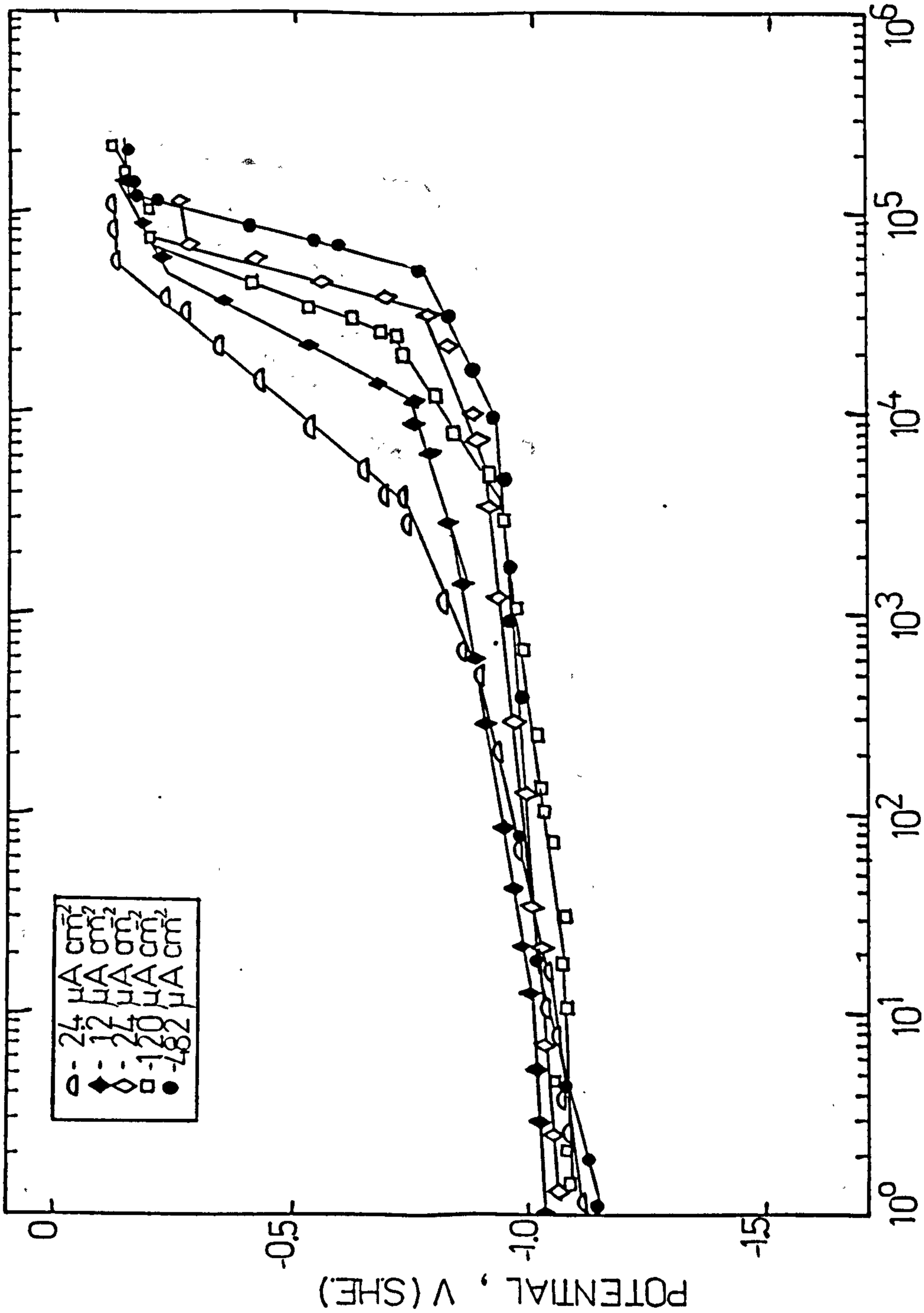

Fig.78 Plots of potential vs time during the decay part of the experiments conducted at 19 C at different CCDs on 0.205 mm thick membranes.

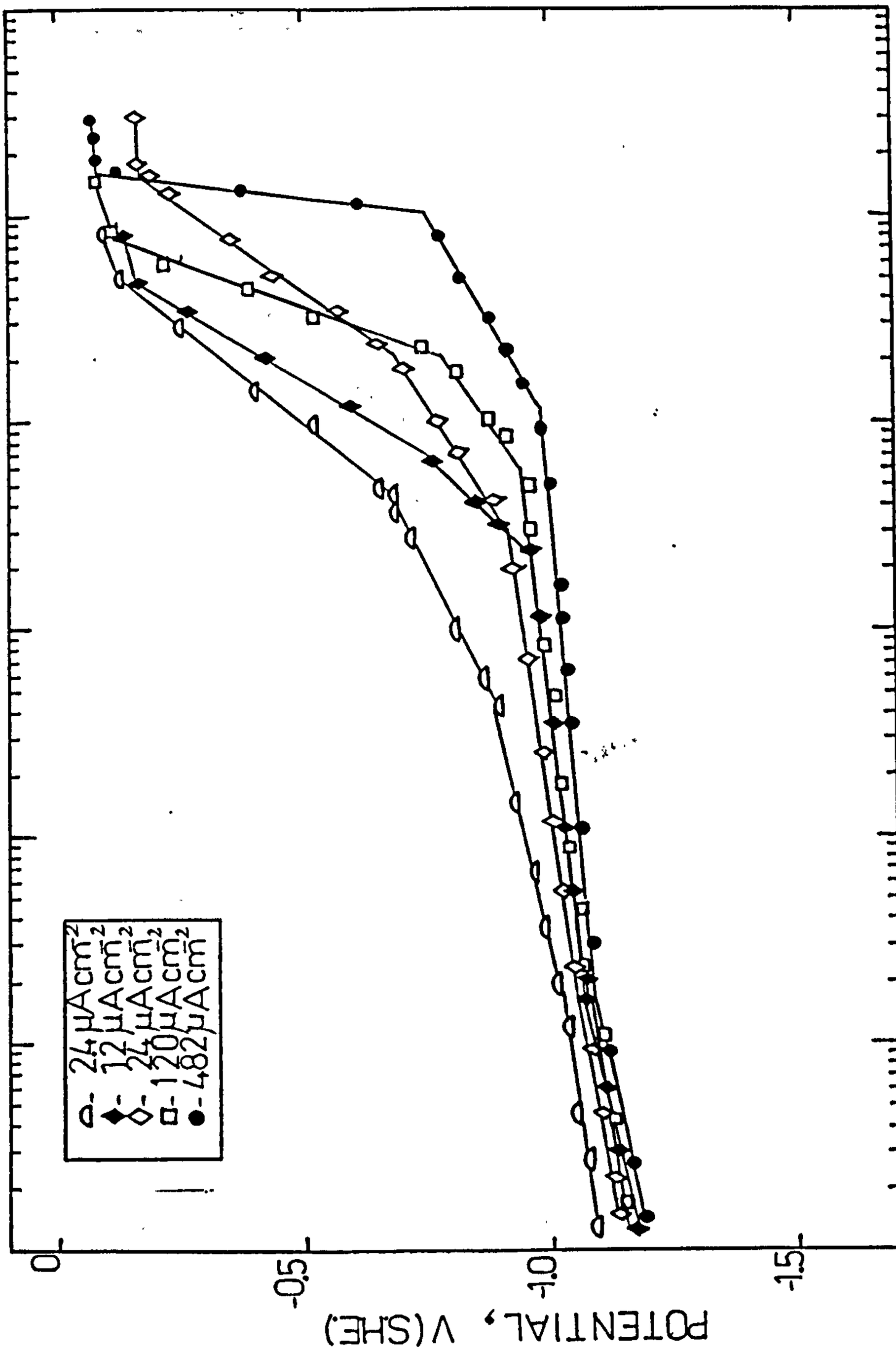

Fig.79 Plots of potential vs time during the decay part of the experiments conducted at 30 C at different CCDs on 0.205 mm thick membranes.

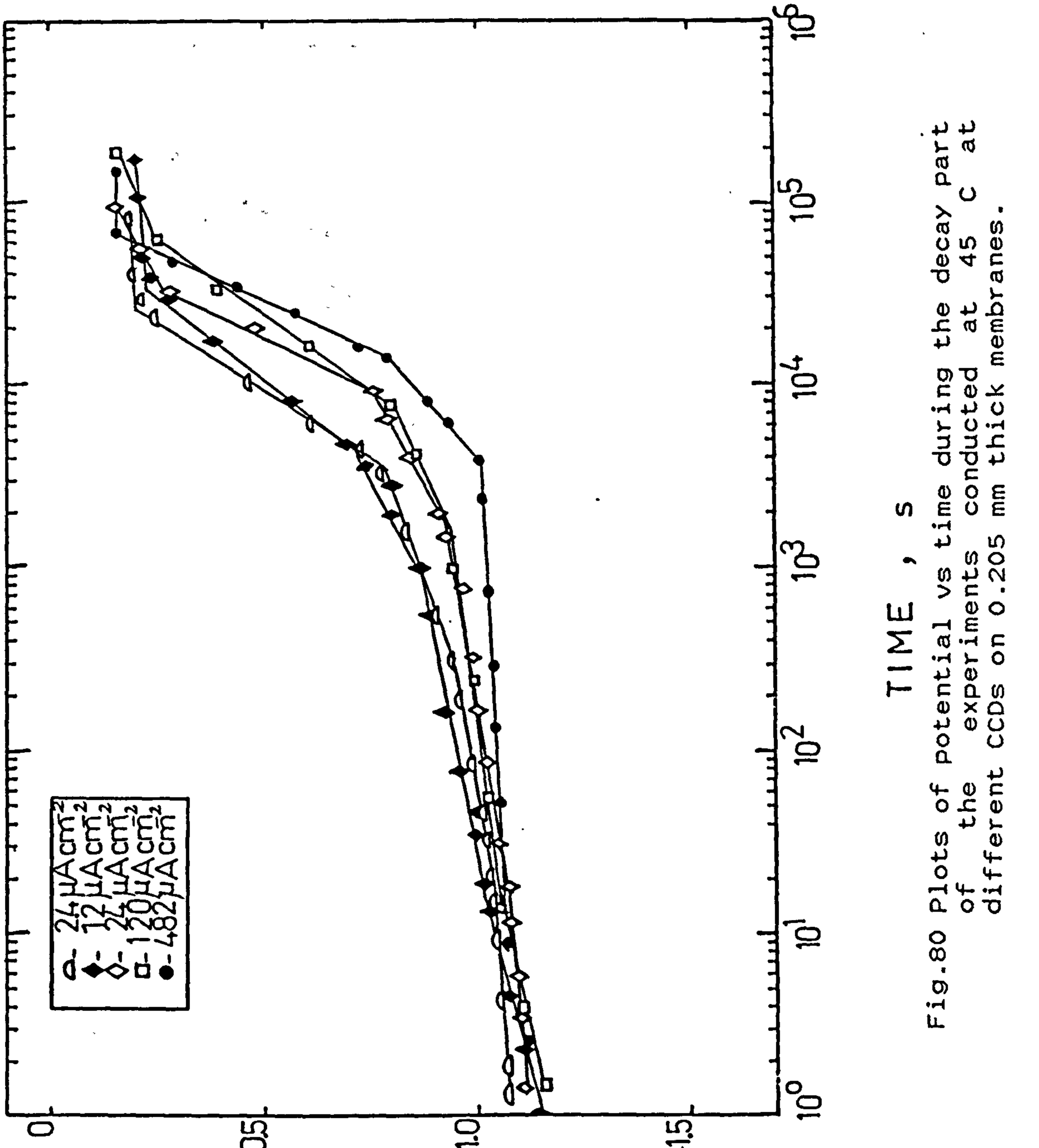

Fig.80 Plots of potential vs time during the decay part of the experiments conducted at 45 C at different CCDs on 0.205 mm thick membranes.

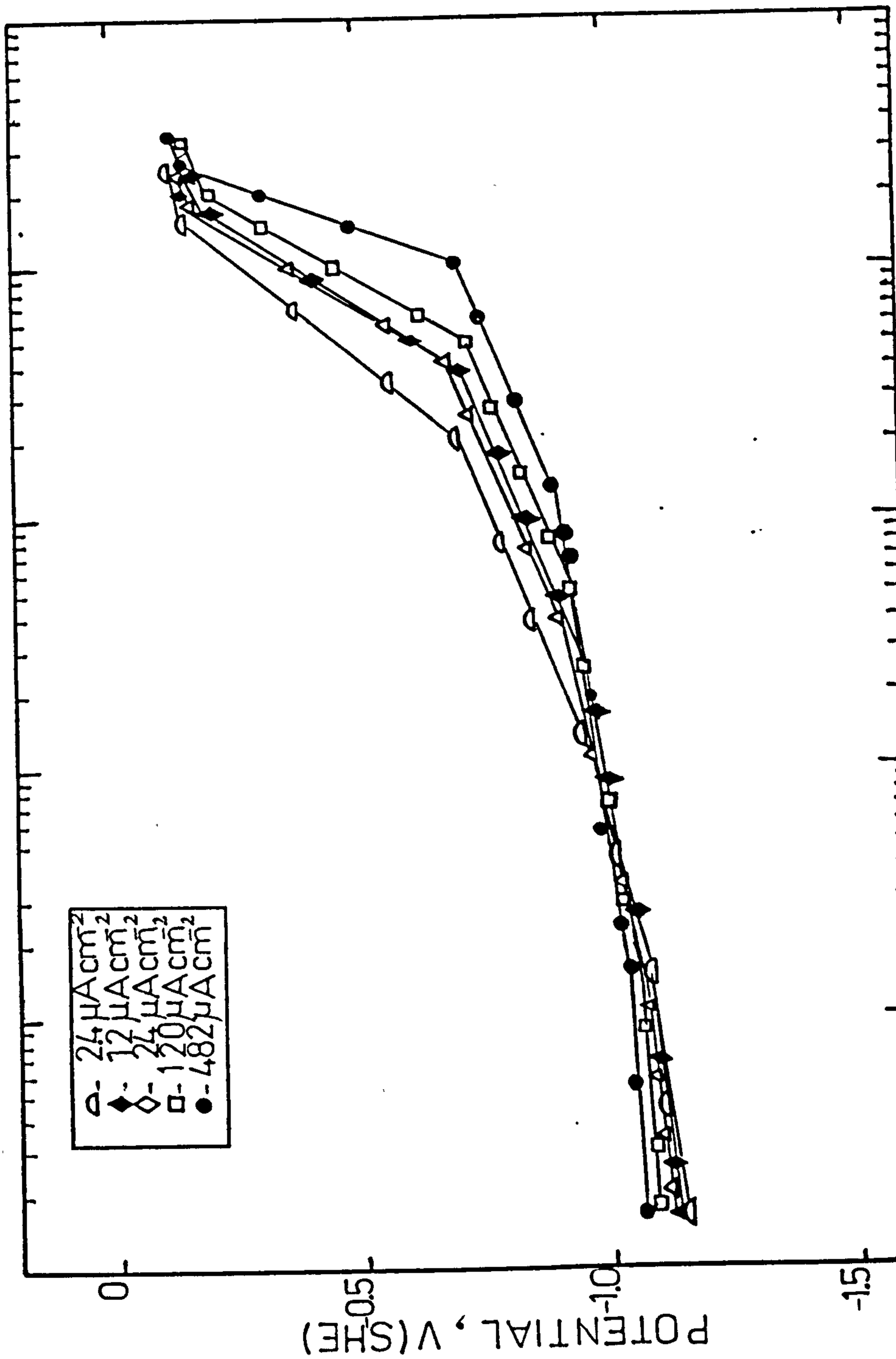

Fig.81 Plots of potential vs time during the decay part of the experiments conducted at 65 C at different CCDs on 0.205 mm thick membranes.

Table 16 The data pertaining to the effusion experiments shown in Figs.75 - 81.

MEMBRANE THICKNESS AND TEMP	i_c μAcm^{-2}	t_1 s	$-\eta_1$ V	$-E_1$ V	t_2 s	$-E_2$ V	t_3 s	$-E_3$ V	t_4 s	$-E_4$ V
	2.40	19	0.240	1.067	1350	0.970	11500	0.720	7500	0.180
	12									
0.07mm	24	18	0.288	1.062	4200	0.980	13000	0.780	12E4	0.150
25° C	120	18	0.308	1.080	7000	0.900	18000	0.740	10E4	0.220
	482	15	0.355	1.070	9000	0.910	23000	0.750	8E4	
	2.40	10	0.050	1.065	2100	0.940	10000	0.770	11E4	0.100
	12									
1.07mm	24	16	0.085	1.042	3300	0.920	12500	0.780	55E3	0.100
25° C	120	16	0.152	1.048	4500	0.880	17000	0.720	10E4	0.150
	482	18	0.160	1.035	5500	0.940	22000	0.760	8E4	0.150
	2.40	17	0.205	1.015	850	0.890	4600	0.730	68E3	0.150
0.205	12	18	0.225	1.050	400	0.920	1800	0.760	55E3	0.200
mm	24	18	0.240	1.055	2500	0.930	7000	0.820	62E3	0.170
25° C	120	18	0.262	1.078	5000	0.930	15500	0.740	10E4	0.230
	482	14	0.288	1.072	4100	0.950	21000	0.750	11E4	0.150
	2.4	20	0.210	1.045	550	0.880	3600	0.740	58E3	0.120
	12	18	0.220	1.020	2200	0.840	12000	0.760	50E3	0.250
0.205	24	18	0.235	1.035	4000	0.920	25000	0.770	54E3	0.200
mm	120	18	0.275	1.080	6000	0.990	24000	0.730	95E3	0.180
19° C	482	16	0.290	1.050	10E3	0.920	55000	0.750	14E4	0.150
	2.40	12	0.190	1.035	400	0.910	3800	0.690	40E3	0.120
	12	15	0.220	1.045	2200	0.980	6500	0.760	48E3	0.150
0.205	24	18	0.230	1.050	2900	0.930	20000	0.690	13E4	0.170
mm	120	17	0.255	1.070	6000	0.920	21000	0.770	75E3	0.150
30° C	482	18	0.270	1.080	12E3	0.970	10E4	0.750	16E4	0.080
	2.4	16	0.165	1.070	500	0.940	3400	0.770	40E3	0.190
	12	16	0.212	1.030	950	0.850	4900	0.700	30E3	0.200
0.205	24	18	0.225	1.070	1600	0.920	8580	0.750	38E3	0.190
mm	120	15	0.240	1.040	1700	0.950	9000	0.780	60E3	0.230
45° C	482	17	0.260	1.070	3000	1.010	14000	0.790	76E3	0.150
	2.4	16	0.150	1.040	220	0.950	400	0.700	17E3	+0.150
	12	16	0.160	1.050	180	0.940	300	0.700	16E3	+0.175
0.205	24	17	0.185	1.030	230	0.900	248	0.695	13E3	+0.150
mm	120	15	0.210	1.050	700	0.920	675	0.720	20E3	+0.200
65° C	482	17	0.235	1.040	2150	0.900	11000	0.705	18E3	+0.150

The time for attainment of the potentials E_1,E_2,$E_3$and E_4 are plotted against the charging current density in Figs.82-86. The lowest line represents the results of the first break (t_1) at different CCD's.Subsequent lines correspond to t_2,t_3, and t_4 breaks respectively. Fig.82 shows the decay phase potential measurement results from membranes of different thickness at room temperature . The relationship between the decay times and the CCD is a linear one , showing increasing decay times for thicker membranes at constant CCD.

The overall effect of higher diffusivity at higher temperature is detected through the progressive shift of t_2, $t_3$and $t_4$to shorter times.There is no useful inferences to be made from the slopes of these lines as there does not seem to be a detectable set pattern, apart from the general trends shown. The independence of the time to reach E_1 from CCD, is evident from all five figures.From this a value of 16±1 seconds is calculated for t,regardless of the thickness or temperature. The lower end of this time relates to high temperature experiments and vice versa, indicating an electrochemical reaction sensitive to temperature variations. This will be shown to be a nucleation process for the passivation phenomenon. Lines,t_2 andt_3 in all five plots are strongly influenced by hydrogen concentration in contrast to the lines fort_1 and $t_4$which show a remarkable independence towards it.Although the t_4 line shows a slight variation with CCD,this is thought to be as a result of film thickening and not a direct influence from hydrogen.

The overpotentials calculated from Figures 75 to 81 are plotted against Log i_c in Fig.87. These Tafel slopes are 0.06 V/decade which is in good agreement with the value suggested by Bockris et al[189] and Daft [190] for such plots.The surface potential of the electrode is expected to be temperature dependent on account of a temperature term in the Tafel equation. However the fact that at the same current density the thicker membranes attained more noble surface potentials and therefore smaller overpotentials was unexpected.

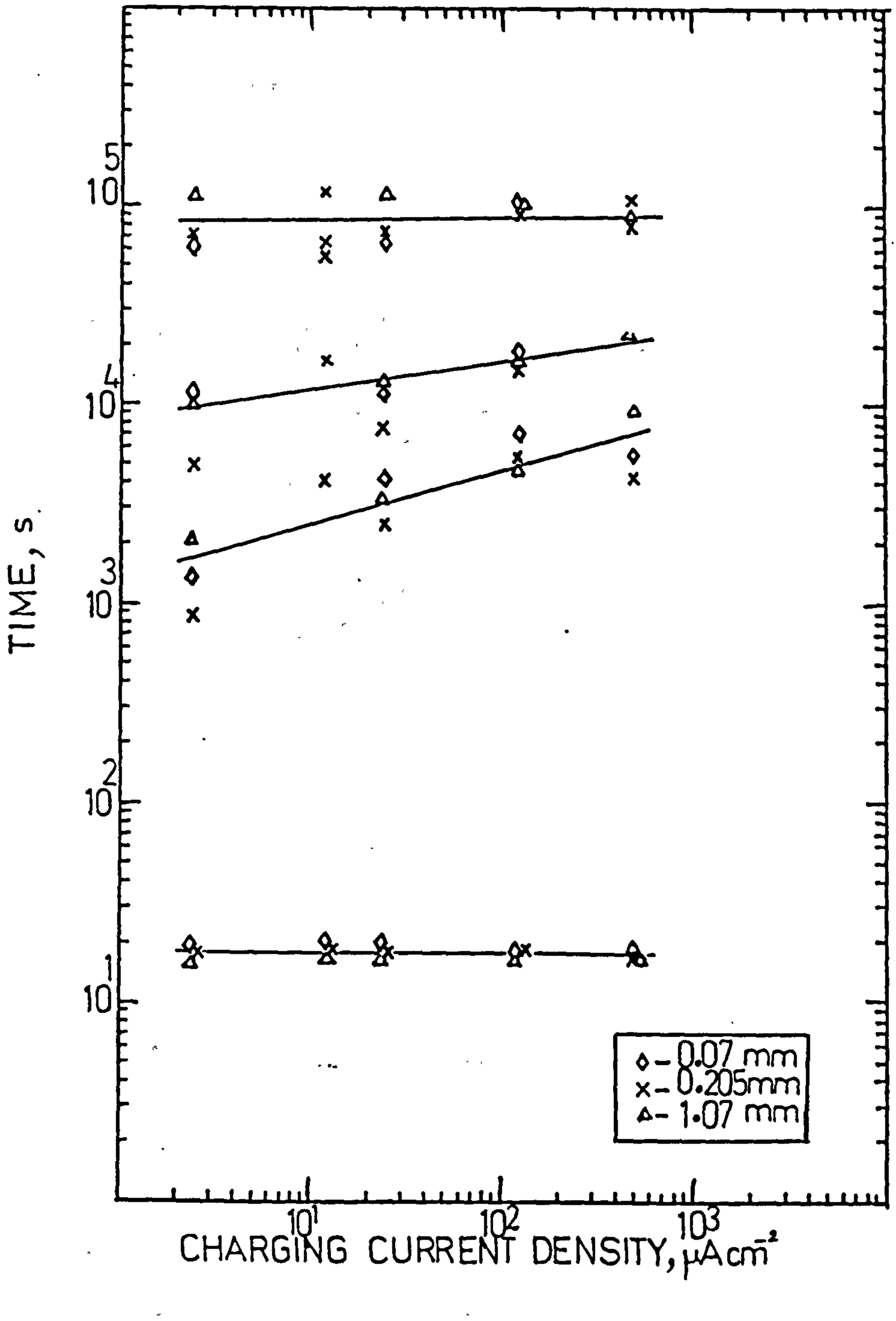

Fig.82 Time to attain the E_1, E_2, E_3 and E_4 potentials in E - Log t curves, plotted against the CCD for membranes of different thicknesses at 25° C.

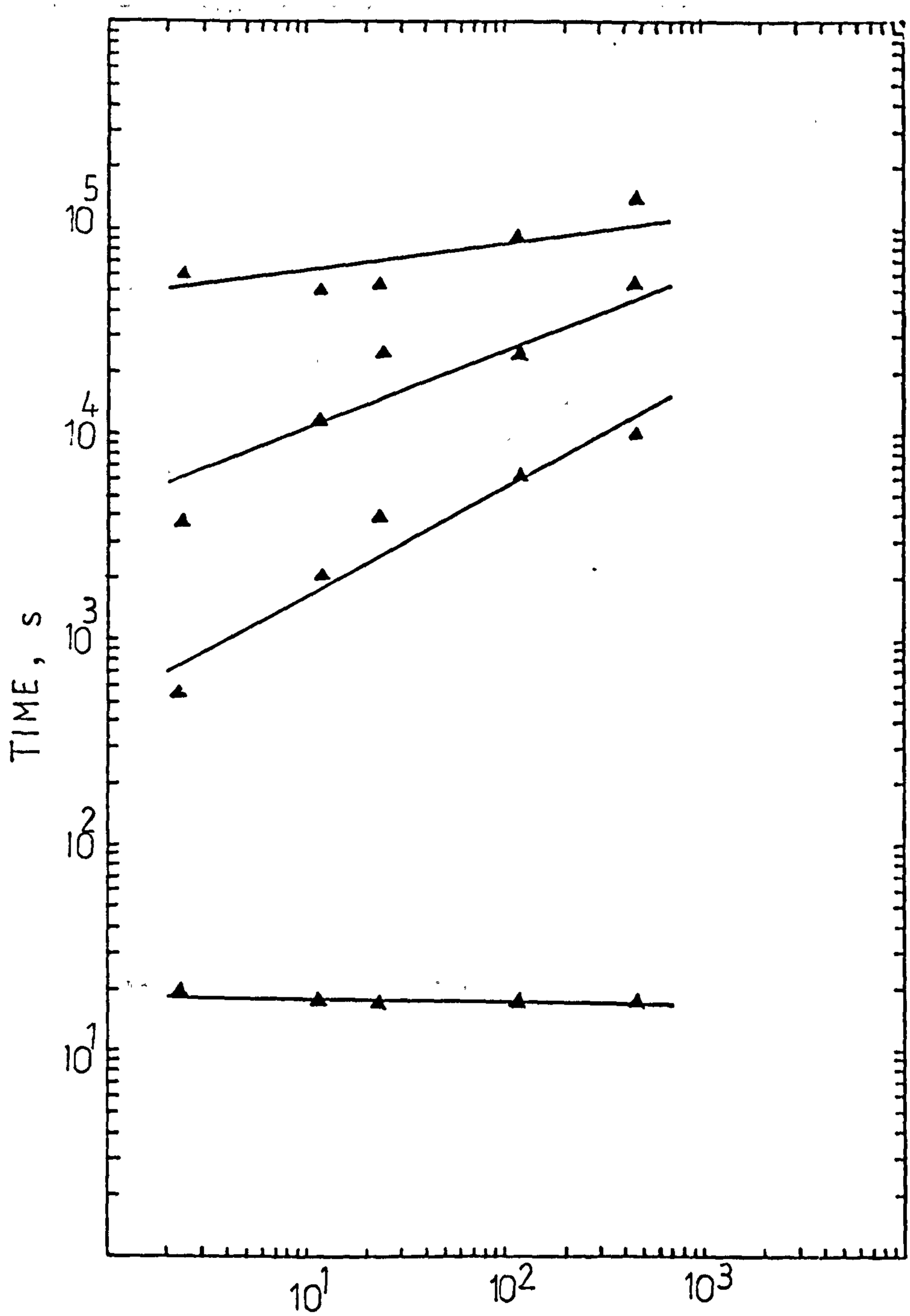

Fig.83 Time to attain the E_1 ,E_2 ,E_3 and E_4 potentials in E - Log t curves plotted against the CCD for 0.205 mm thick membranes at 19°C.

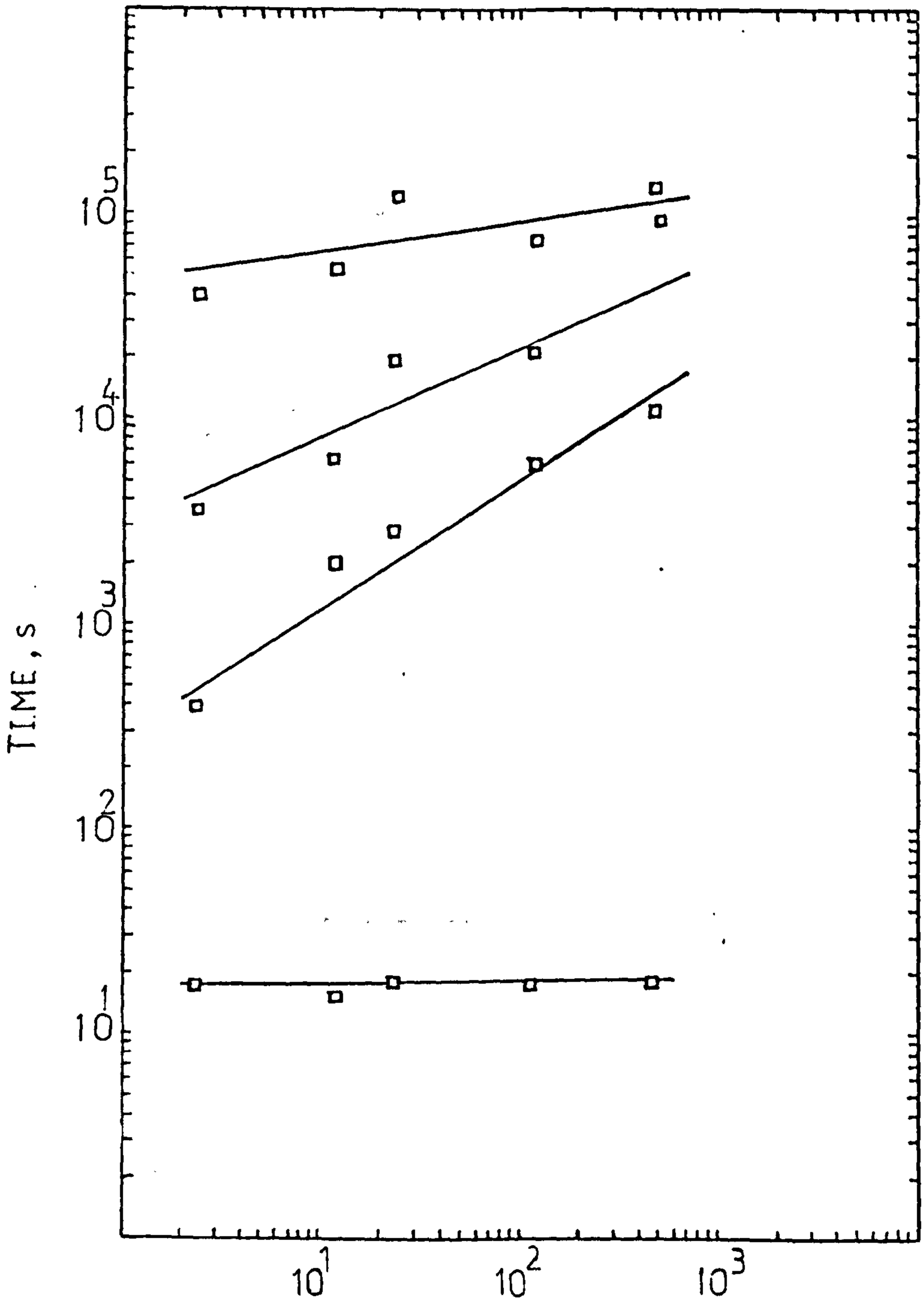

Fig.84 Time to attain the E_1, E_2, E_3 and E_4 potentials in E - Log t curves, plotted against the CCD for 0.205 mm thick membranes at 65°C.

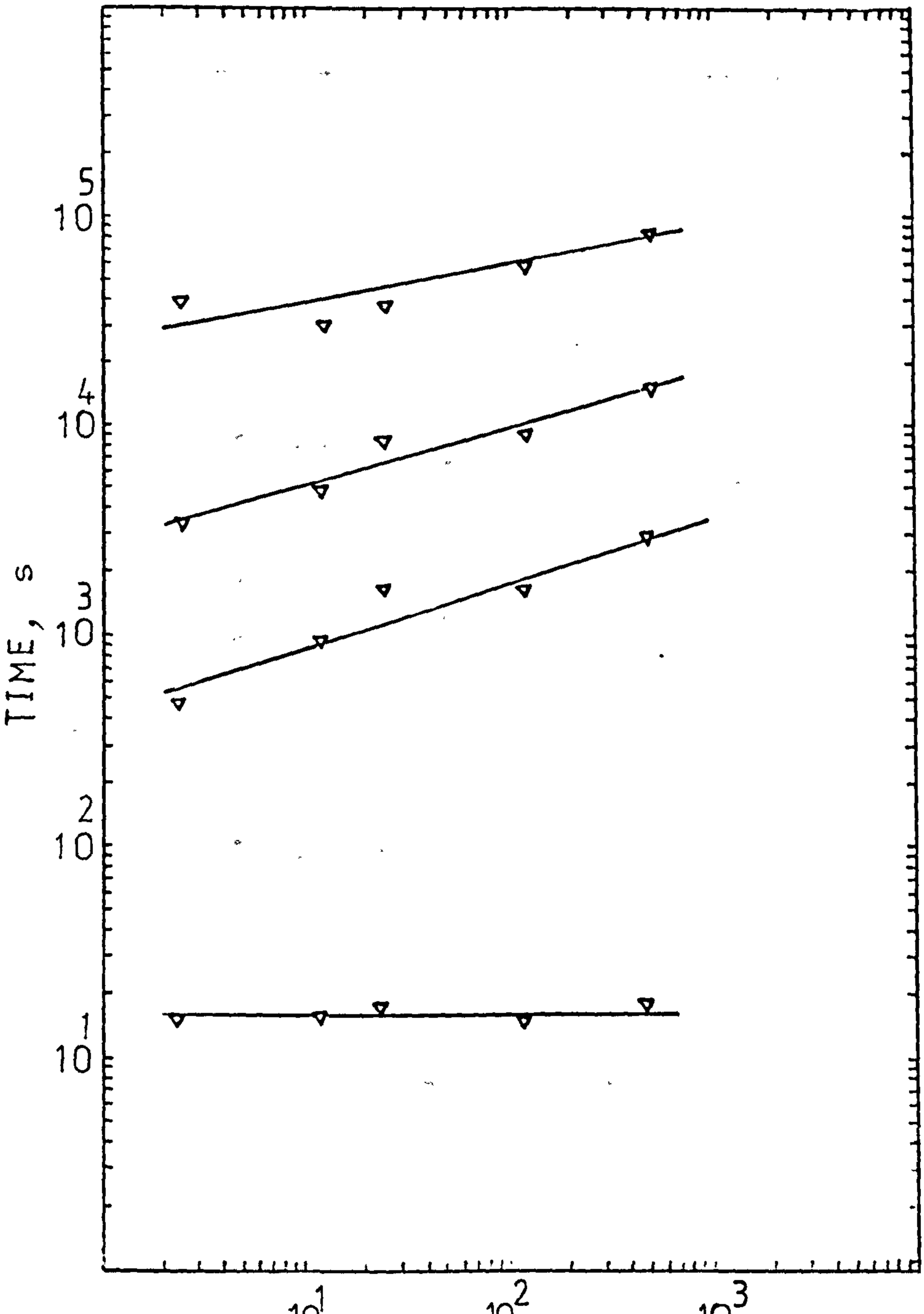

Fig.85 Time to attain the E_1, E_2, E_3 and E_4 potentials in E - Log t curves, plotted against the CCD for 0.205 mm thick membranes at 45°C.

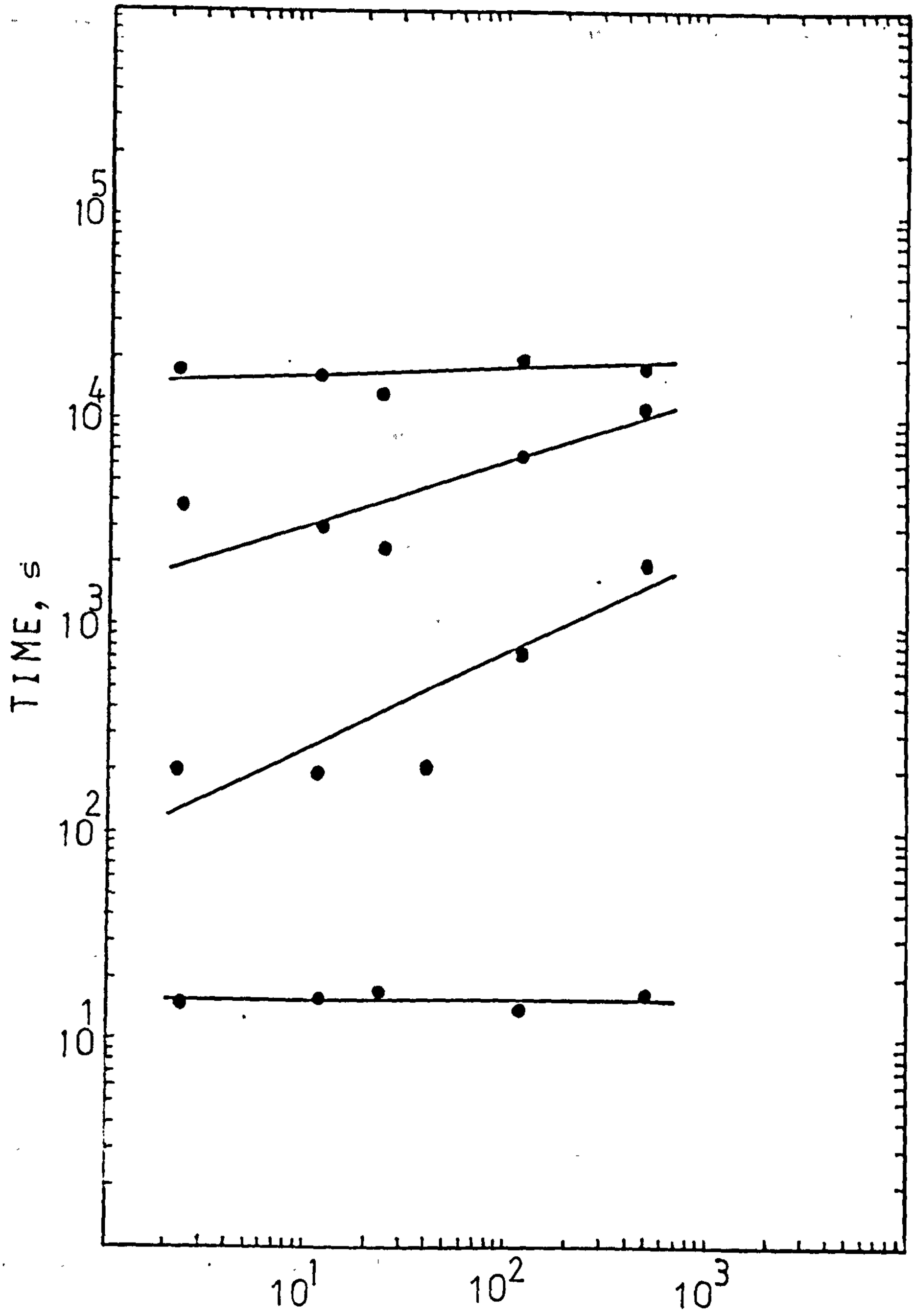

Fig.86 Time to attain the E_1, E_2, E_3 and E_4 potentials in E - Log t curves, plotted against the CCD for 0.205 mm thick membranes at 30°C.

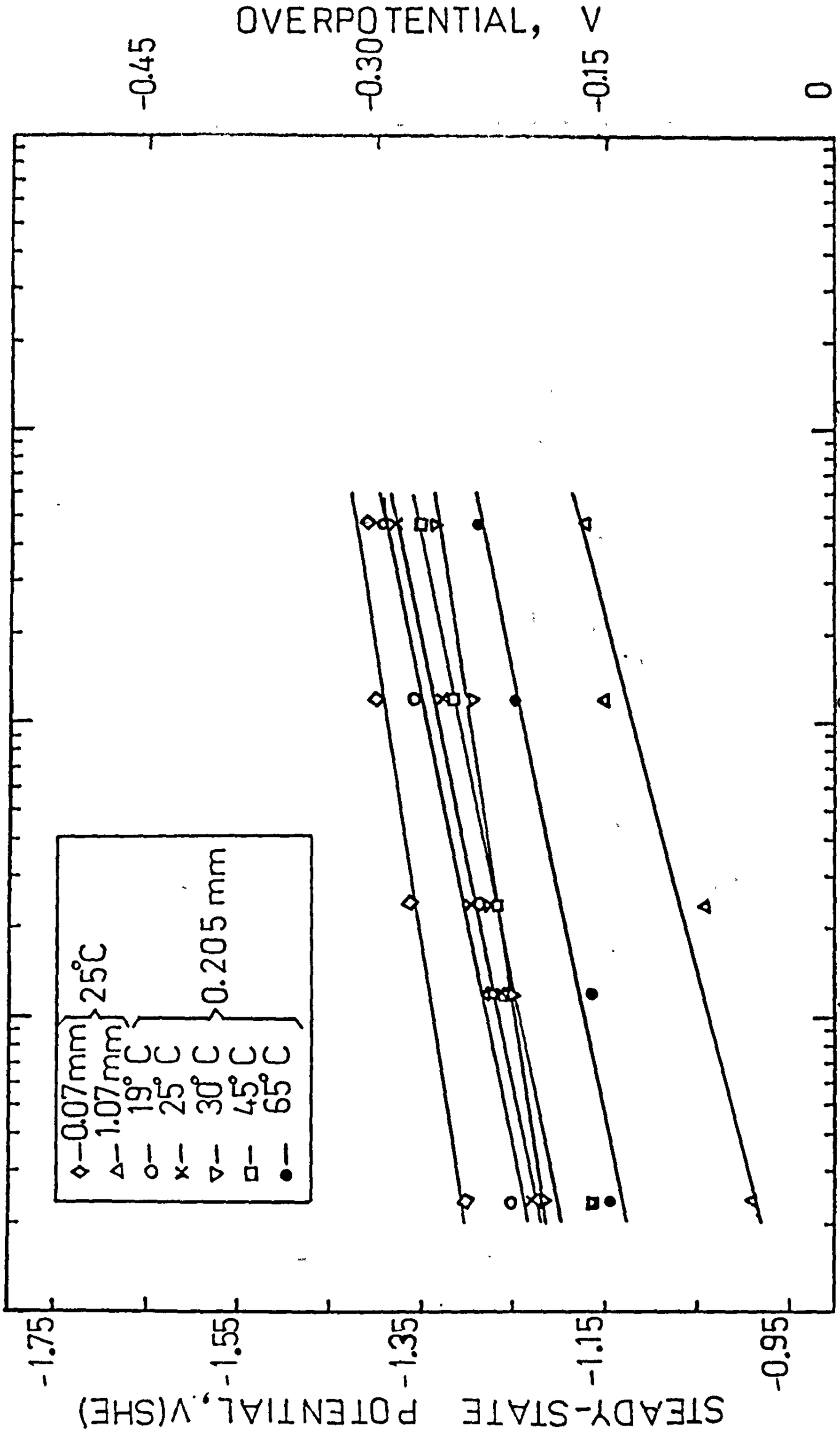

Fig.87 Tafel plots for hydrogen charging experiments at different temperatures and membrane thicknesses.

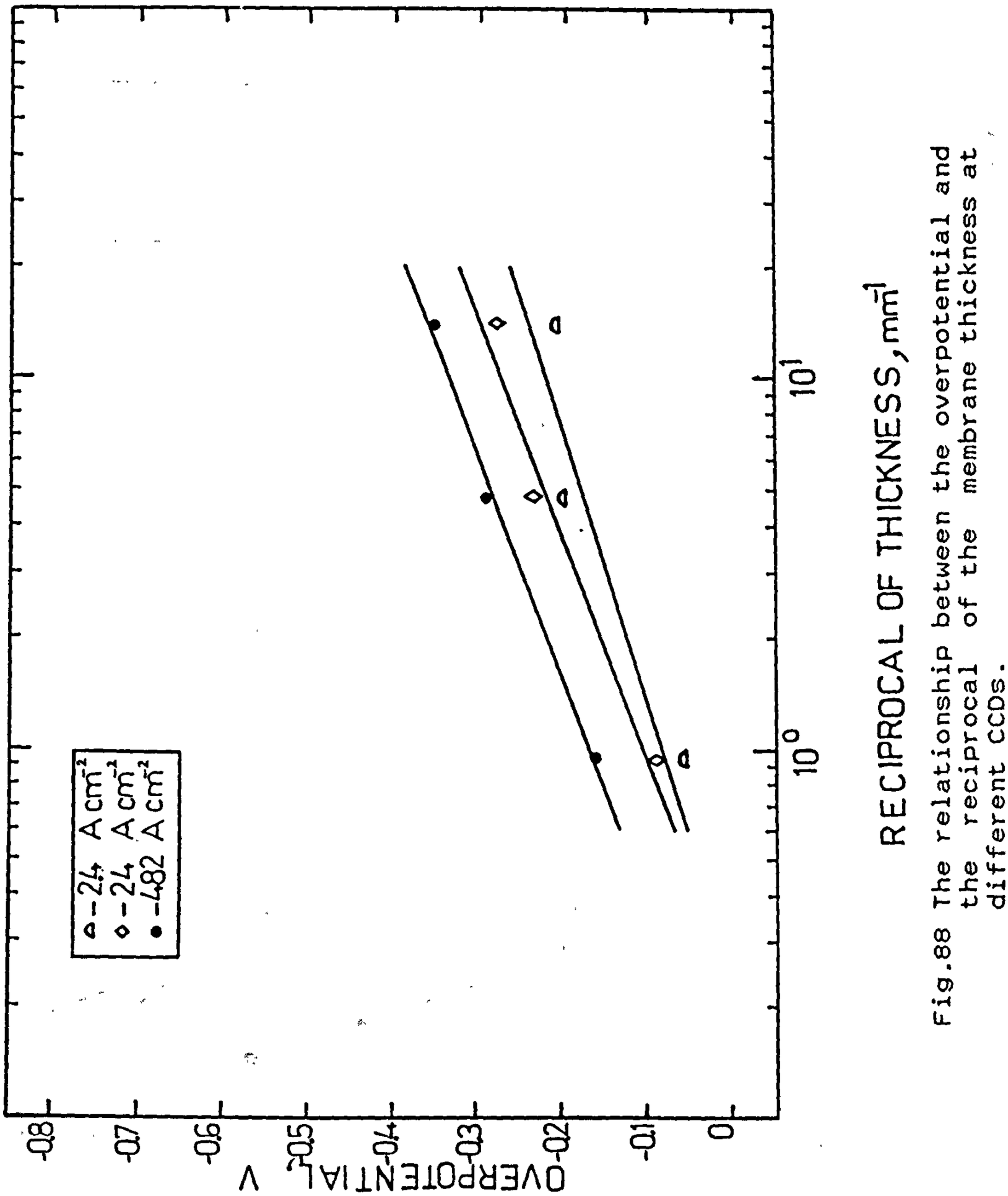

Fig.88 The relationship between the overpotential and the reciprocal of the membrane thickness at different CCDs.

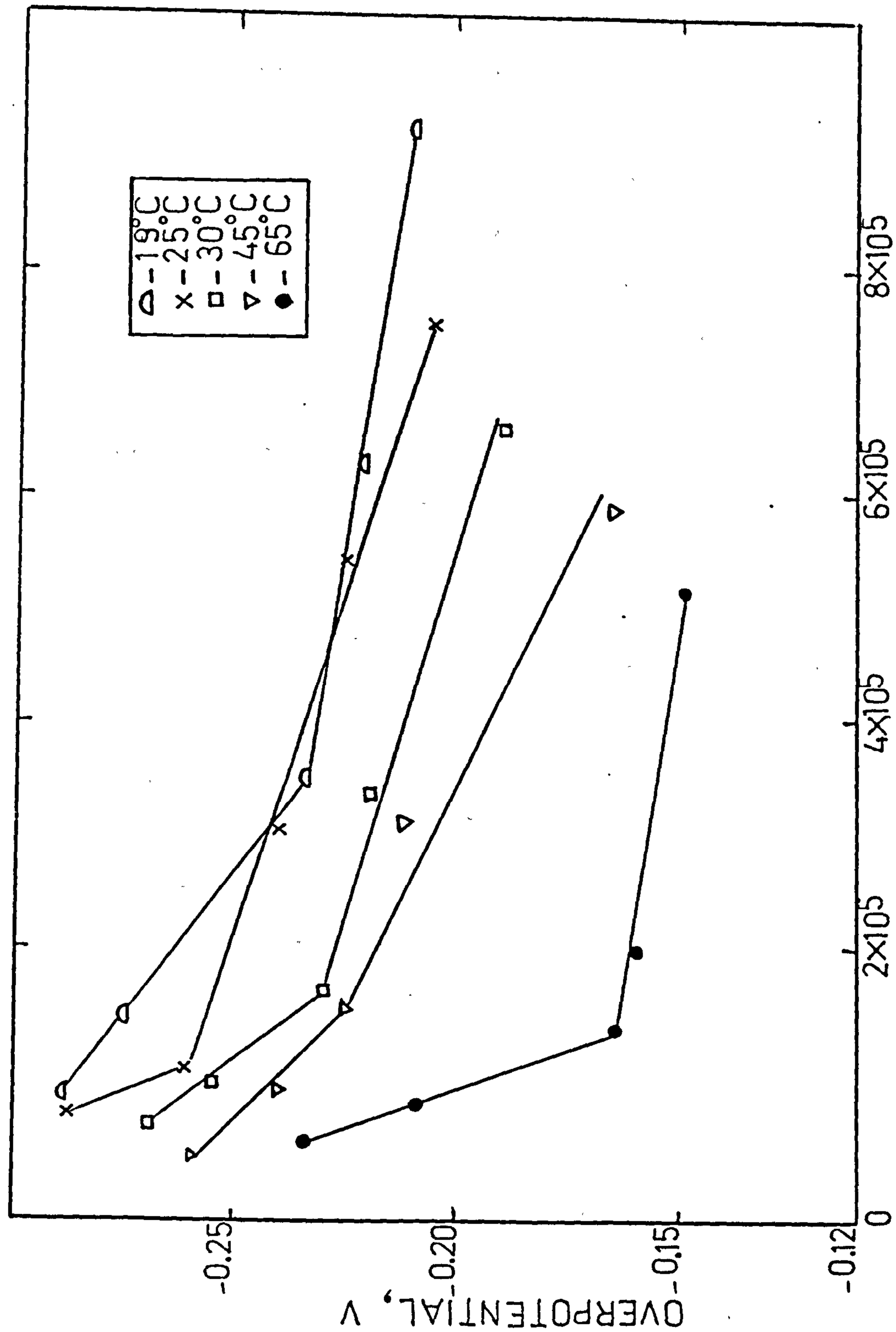

Fig.89 The relationship between the overpotential and the reciprocal of permeation current density for experiments at different temperatures.

Fig.88 is the result of investigating the effect of membrane thickness on overpotential. The fact that the results of all nine experiments illustrated in this figure follow the same trend compensates for the lack of experimental points. The three lines shown in Fig.88 clearly show the room temperature dependence of η on the reciprocal of thickness. Also the similarity of the slopes i.e. -0.13, -0.12 and -0.125 V/decade indicates that a common mechanism is responsible for this dependency at the low as well as higher CCD's. A mathematical analysis of this phenomenon will be presented in the subsequent Chapter.

Fig.89 depicts the relationship between the overpotential and the reciprocal of steady state permeation currents.The effect of temperature is evident by the shift of the curves to more negative overpotentials, as the temperature is lowered. The overpotential becomes more negative with increasing CCD and the steady state permeation current rises. A qualitative analysis of this phenomenon will be discussed in the subsequent sections.

Fig.90 illustrates the effect of temperature on overpotential. The overpotential becomes less cathodic, as the temperature is raised. This will be shown to be the result of changes in hydrogen coverage which leads to change in surface potential. The scatter in results is due to slight variations in temperature, membrane thickness or internal defect concentration which in

turn influence the movement of hydrogen and, therefore, affect the surface coverage.Fig.91 shows the effect termination of the CCD has on the permeation current, recorded on a 1.07_mm thick membrane. The permeation actually increased as the steady state permeation was interrupted .An increase of 6-10% was observed which is interpreted as strong evidence for the effect of electrical field on the protonic hydrogen just inside the membrane. The reason this phenomenon was not detectable in thinner membranes is that the very fast relaxation time (t_d), obscure the rather small effects of the field.

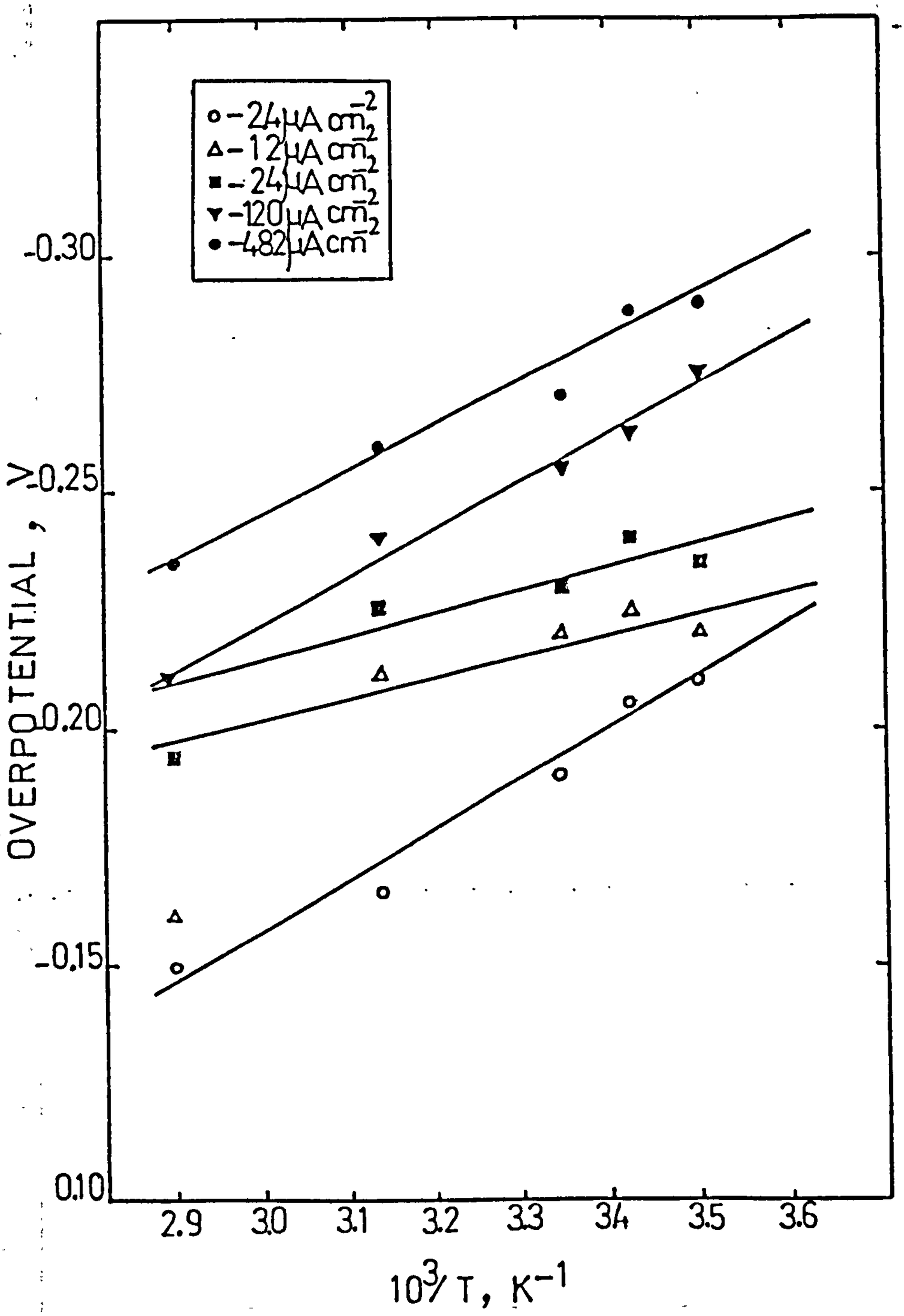

Fig.90 The relationship between the overpotential and the reciprocal of temperature for experiments at different CCDs.

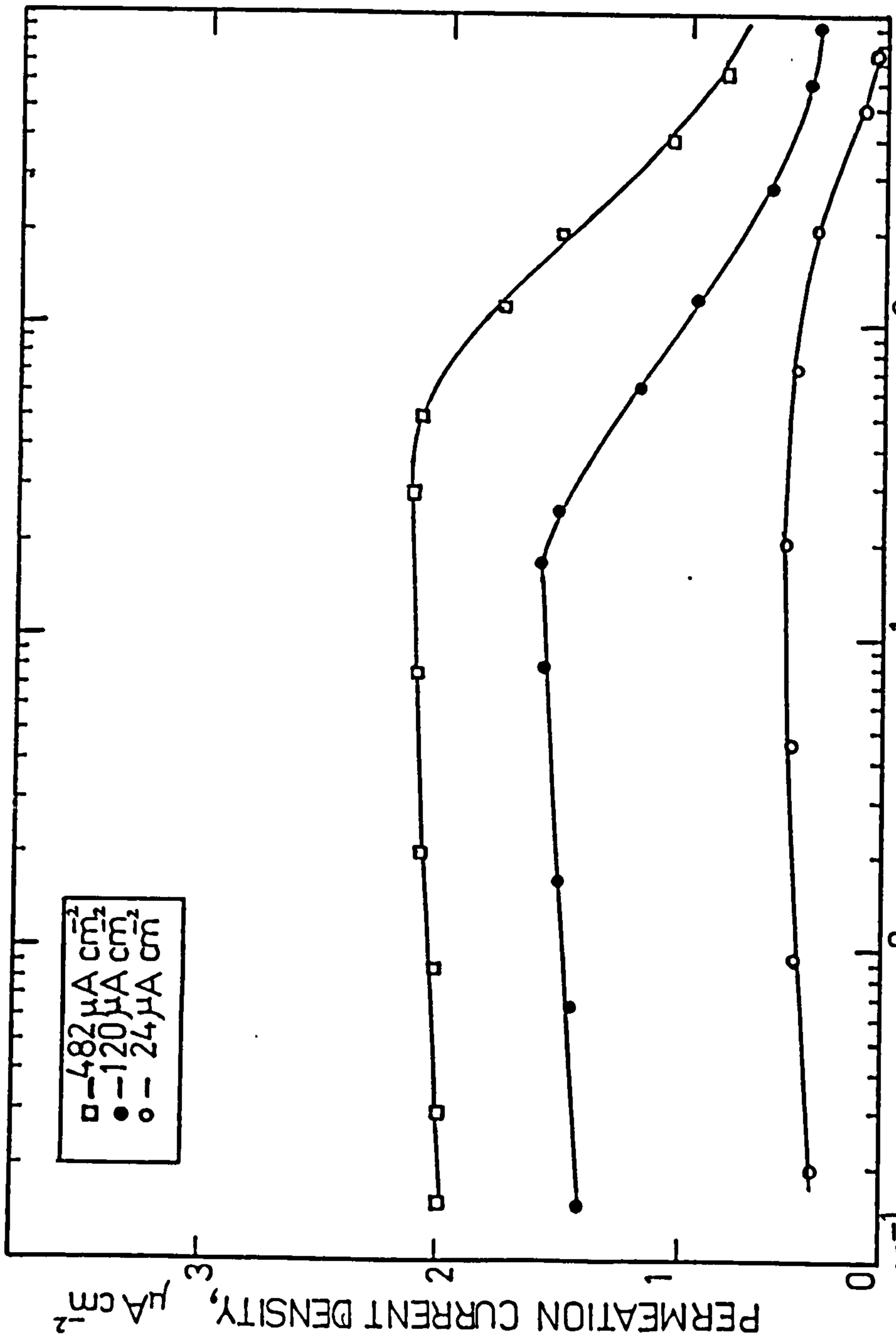

Fig.91 The effect of field on hydrogen permeation as shown by the slight increase in permeation flux after the termination of CCD for 1.07 mm thick membranes.

4.4.....EXPERIMENTS SHOWING THE INFLUENCE OF HYDROGEN ON PASSIVATION

These experiments were specifically designed to elucidate the part played by hydrogen during the passivation phenomenon.Figures 92 and 93 are the result of an experiment on the reducing effect of protonic hydrogen. A membrane was placed in the permeation cell. However,neither palladium plating nor the potentiostatic control of the anodic side was applied. Oxygen purging by bubbling nitrogen through both compartments of the cell was carried out. The potentials of both faces of the electrode were monitored separately.

Fig.92 shows the effect,applying a CCD of 12 μAcm^{-2} on one side of the membrane, had on the open circuit potential of the other side.Charging was carried out for more than 200 hours. The changes in the potential of the "monitored side" shows four different plateau at -0.40 V, 0.50 V vs SCE , which do not correspond to the potential of any known surface film on iron, and -0.62 and-0.90 V vs SCE which are close to the E_3 and E_2 in the potential decay experiments. Fig.93 illustrates the data from an experiment under identical conditions except for the charging current which was increased to $30\mu Acm^{-2}$. The effect is the shortening of the time required for the monitored side to attain the final potential of -0.982 V vs SCE. While the time taken for the experiment at 12 μAcm^{-2} to attain the final potential of 0.960 V vs SCE was in excess of 250 hours, the same potential was reached in the second

experiment in only 70 hours. The clear relationship between the activity of hydrogen in the membrane and its surface potential is evident.

Fig.94 shows the potential of the surface of a membrane, charged at 24 μAcm^{-2} and then increased in succession to 48 μAcm^{-2}120 μAcm^{-2}, 240 μAcm^{-2} and finally 500 μAcm^{-2}.The time taken for the potential to reach the same E value was the same as before but, once this potential was attained using the 24 μAcm^{-2},the current was raised to 48 $\mu Acm^{-2}$and was maintained for more than 24 hours before it was stepped up to 120 $\mu Acm^{-2}$and the potential of the "monitored side." was recorded.Once the rate of change in the surface potential stabilized, the current was increased to 240 μAcm^{-2}.

The time that the membrane was maintained at this current density was prolonged in a last attempt to increase the activity of hydrogen inside the membrane and observe change in the open circuit potential of the monitored side.The CCD of 500 μAcm^{-2} for a period of 20 hours was later attempted and the resulting potential of the monitored side recorded. Greater current densities, resulted in a tarnished surface of brown deposit which markedly reduced the conductivity of the membrane.The charging current dropped to one tenth of the previous value due to increased circuit resistance. The open circuit potential of the surface throughout the experiments at current densities above 48$\mu Acm^{-2}$was constant and equalled -0.98 V vs SCE.

It seems that the activity of hydrogen is insufficient to remove the oxide layer formed immediately on the electrode surface.To elucidate the difference between the properties of the air-borne films and those formed in an aqueous solution, an experiment was conducted in which the both sides of the membrane were reduced cathodically at a CCD of 24 μAcm^{-2} for 360 minutes. However, at the end of this period the charging current on both sides was switched off, allowing the potential to float freely. When a potential, slightly above -0.70 V vs SCE was registered on both sides, the current on one side only, was re-established. This caused the surface potential of the monitored side to drift slowly back to a more negative value, indicating a depassivation process. The results of these experiments are shown in Fig.95 .

The steady state potential of -1.05 V vs SCE on this face was registered after only 2-3 hours. This potential corresponds to E_1 break in the E-Log t curves and is strong proof for the different structure of the air-borne passive films from those formed in alkaline solutions.

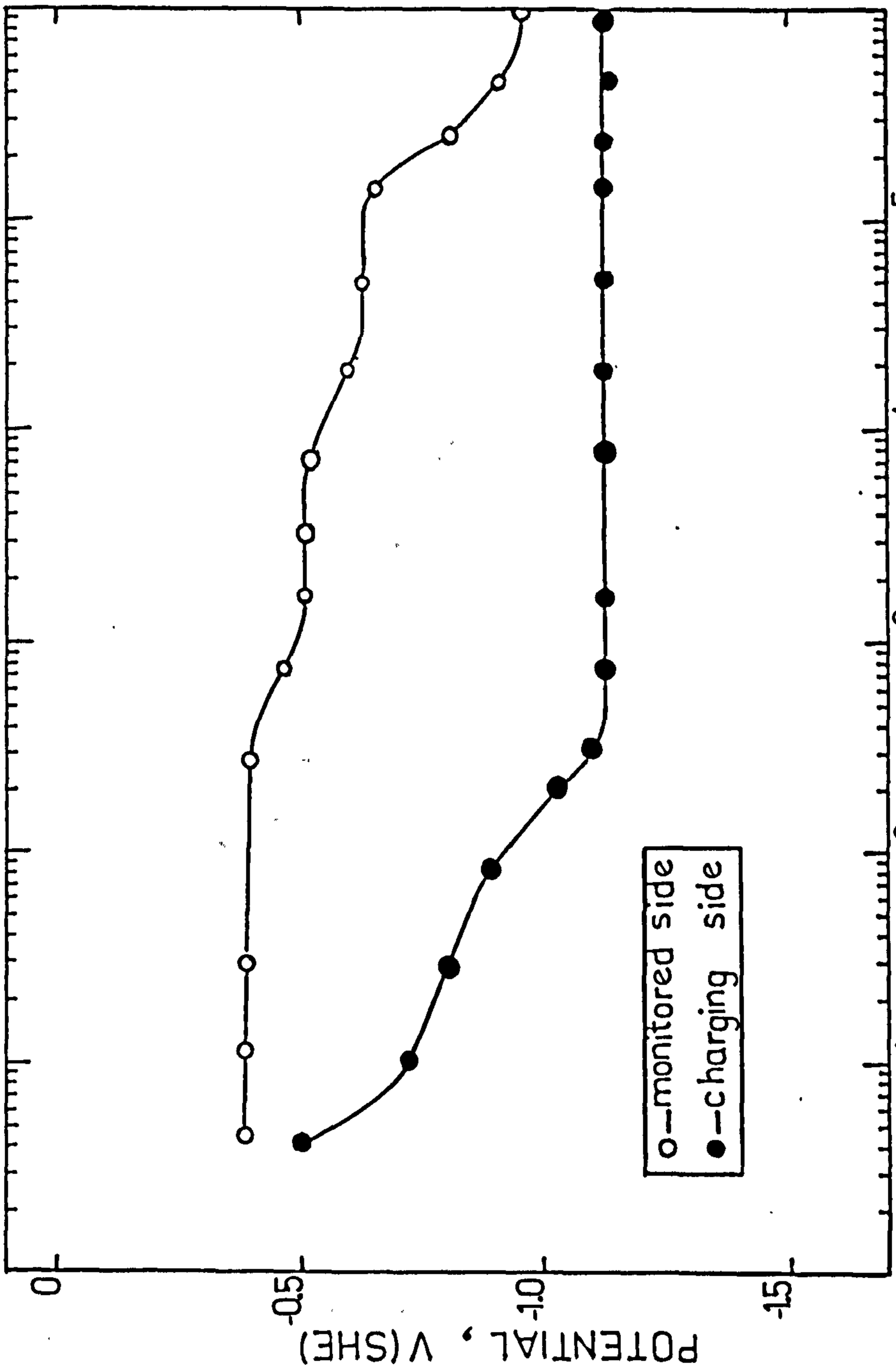

Fig.92 Potential measurements on the monitored side of a membrane charged at 12 $\mu A\ cm^{-2}$.

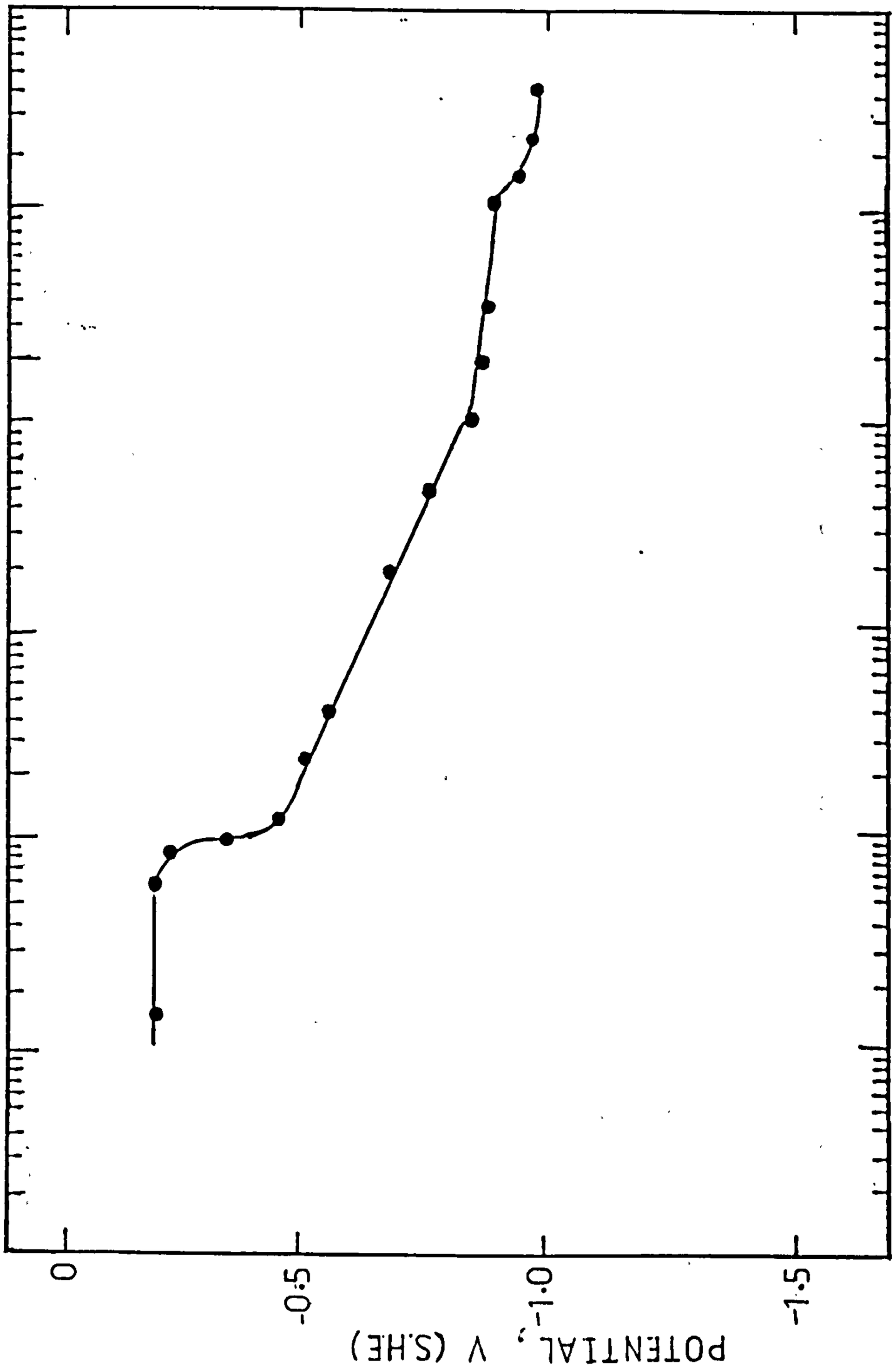

Fig.93 Potential measurements on the monitored side of a membrane charged at 30 $\mu A\ cm^{-2}$.

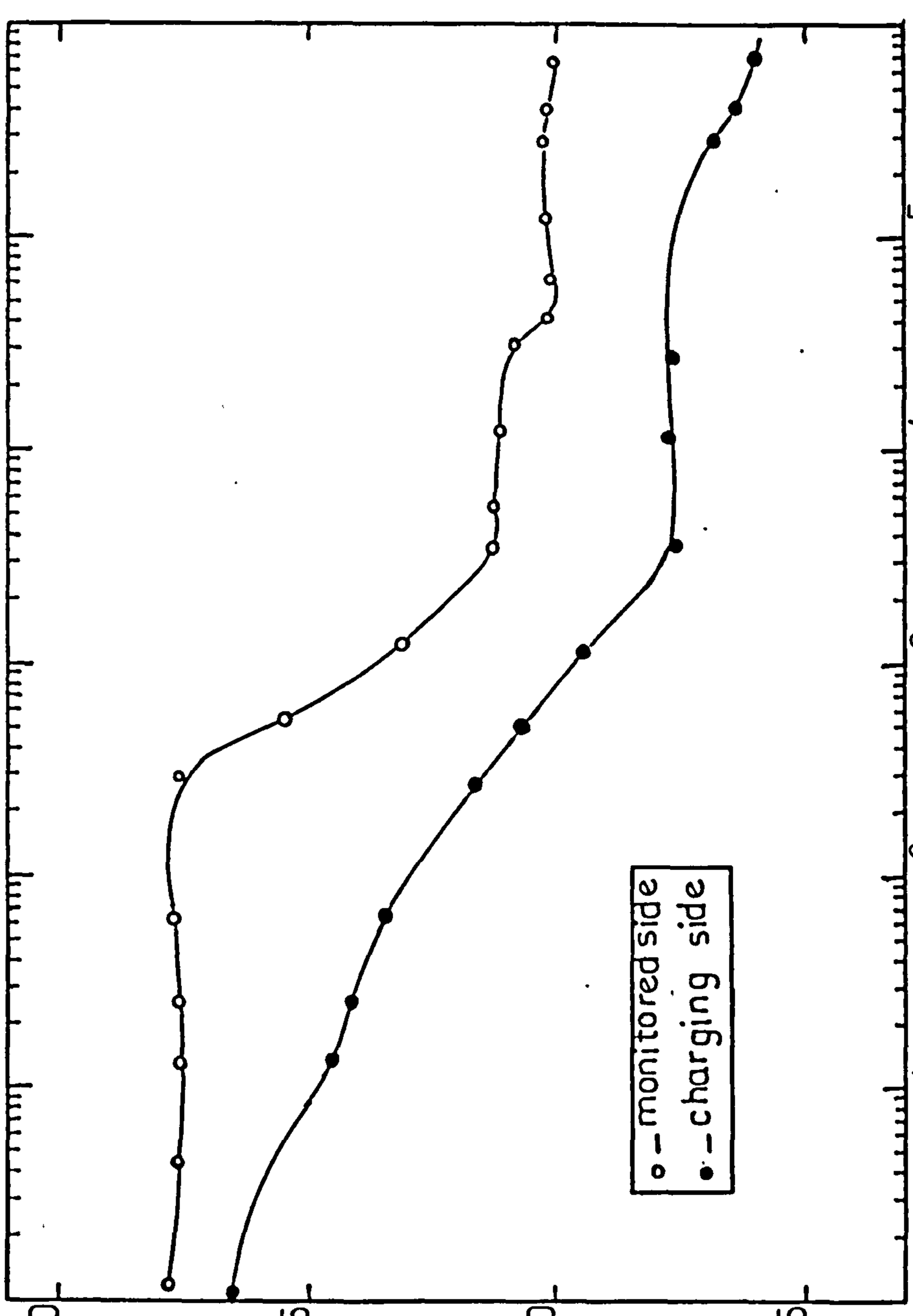

Fig.94 The effect of progressive increase in CCD on the surface potential of the monitored side.

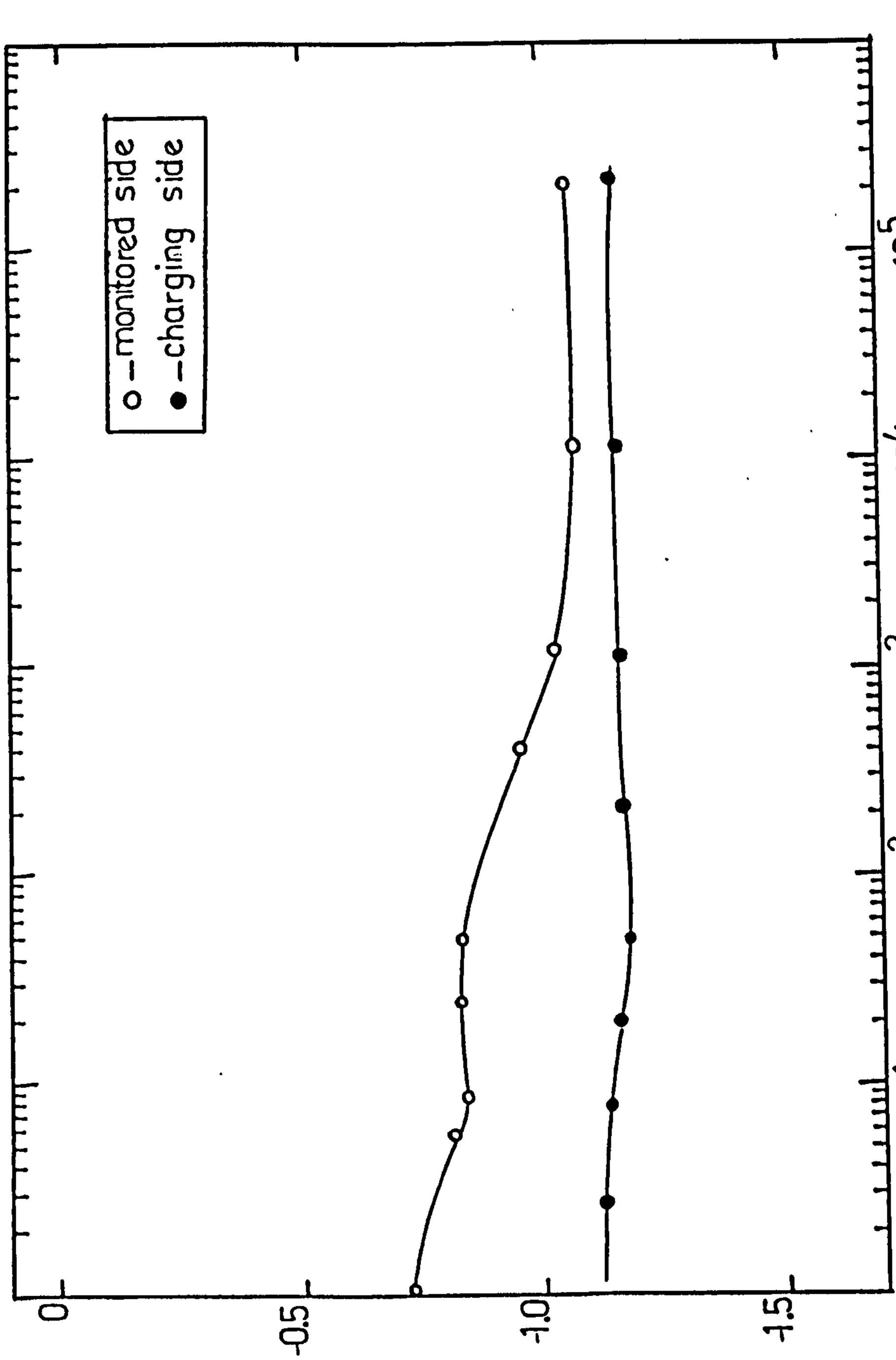

Fig.95 The effect of hydrogen on a film formed in 0.1 N NaOH solution. The CCD used is 12μA cm^{-2}.

4.5.....POTENTIAL MEASUREMENTS IN THE PRESENCE OF ADDITIVES

Addition of EDTA has been recommended in the literature [299] as the only means of producing a film-free surface on iron in NaOH through cathodic reduction. The contradictions associated with this claim are adequately dealt with in the discussion chapter. However, to evaluate this claim, a series of experiments was conducted in NaOH solutions,dosed with 0.1 M EDTA.The aim was to see if EDTA could be a useful reagent in passivation studies in a film reducing capacity. Also, the effect of the EDTA molecules on normal passivation process was .investigated in these experiments. The experiments conducted showed little increase in permeation currents of a membrane charged at a CCD of 1 mA cm^{-2}.

As it will be shown later ,the unaffected permeation current demonstrates that, contrary to these suggestions no change in the I_{∞} could be observed at these non-destructive CCDs ,because the source of increases in Zakroczymski et al [299] experiments is totally different.Furthermore,the decay phase potential measurements on such membranes showed that E - Log t curves were affected in a way that only one break could be observed at -1.01 V vs SCE . This break was attained in only 42 s ; after termination of current which suggests the adsorption of part or whole of the EDTA molecule on the surface. Also EDTA is known as a complexant for Fe^{3+},thus explaining the levelling of the

curves. As no ellipsometric facility was available to the author, direct evidence of the film free state of the surface was not available.However, the AC impedance measurements presented in this section and discussed later, corroborate the assumption that the surfaces used were as film-free as a freely corroding iron electrode in H_2SO_4. No further use was made of EDTA in the present work. Potential-time results from these experiments are presented in Fig.96 .

The role of poisons as promoters of hydrogen entry into iron is well known[313]. In an attempt to demonstrate the effect of hydrogen concentration inside the membrane on passivation,a permeation experiment was carried out and the permeation current recorded. Then, using the same CCD , and after adding As_2O_3 to the electrolyte, the experiment was repeated. Although the As^{3+} proved a very effective promoter of hydrogen entry, the results of E-Log t plots were unexpected.

Fig.97 shows the effects of using $3.0x10^{-3}$ mol/l As_2O_3 on the potential measurements during the decay phase. The surface potential seemed quite slow to change and there are no sharp changes of slope as is the norm in E-Log t curves.The reason seems to be the adsorption of As on the active sites for hydrogen effusion leading to a different passivation process. No further experiments using this or other promoters (poisons) were carried out.

4.6....INDUCTIVELY COUPLED ARGON PLASMA ATOMIC EMISSION SPECTROSCOPY

The aim of these experiments was to evaluate the possible levels of ferrous and/or ferric ion in the solution during the passivation process. Analyses were carried out on 2 cm^3 samples, withdrawn from the solution in quick succession after the termination of CCD. These were then injected into the ICAP instrument and the spectrum compared to the standard. Two such experiments were conducted, the results of which are presented in Table 17.

Although the limit of accuracy of this technique was 0.001 ppm,no significant amount of Fe^{3+}/Fe^{2+} was detected in these experiments. The values reported in Table 17 should be regarded critically,because they all fall very close to the limit of accuracy of the technique.

Table 17 The total concentration of Fe ions in the solution close to the membrane during the passivation process.

	SAMPLE NO.1											
	1	2	3	4	5	6	7	8	9	10	11	12
Experiment 1												
CONC./10^{-3} ppm	20	4	7	8	9	3	5	5	3	1	1	2
Experiment 2												
CONC./10^{-3} ppm	20	10	100	7	5	7	3	1	1	1	2	2

	SAMPLE NO.2								
	13	14	15	16	17	18	19	20	21
Experiment 1									
CONC./10^{-3} ppm	1	1	1	3	11	1	7	1	2
Experiment 2									
CONC./10^{-3} ppm	1	3	5	1	-	-	-	-	-

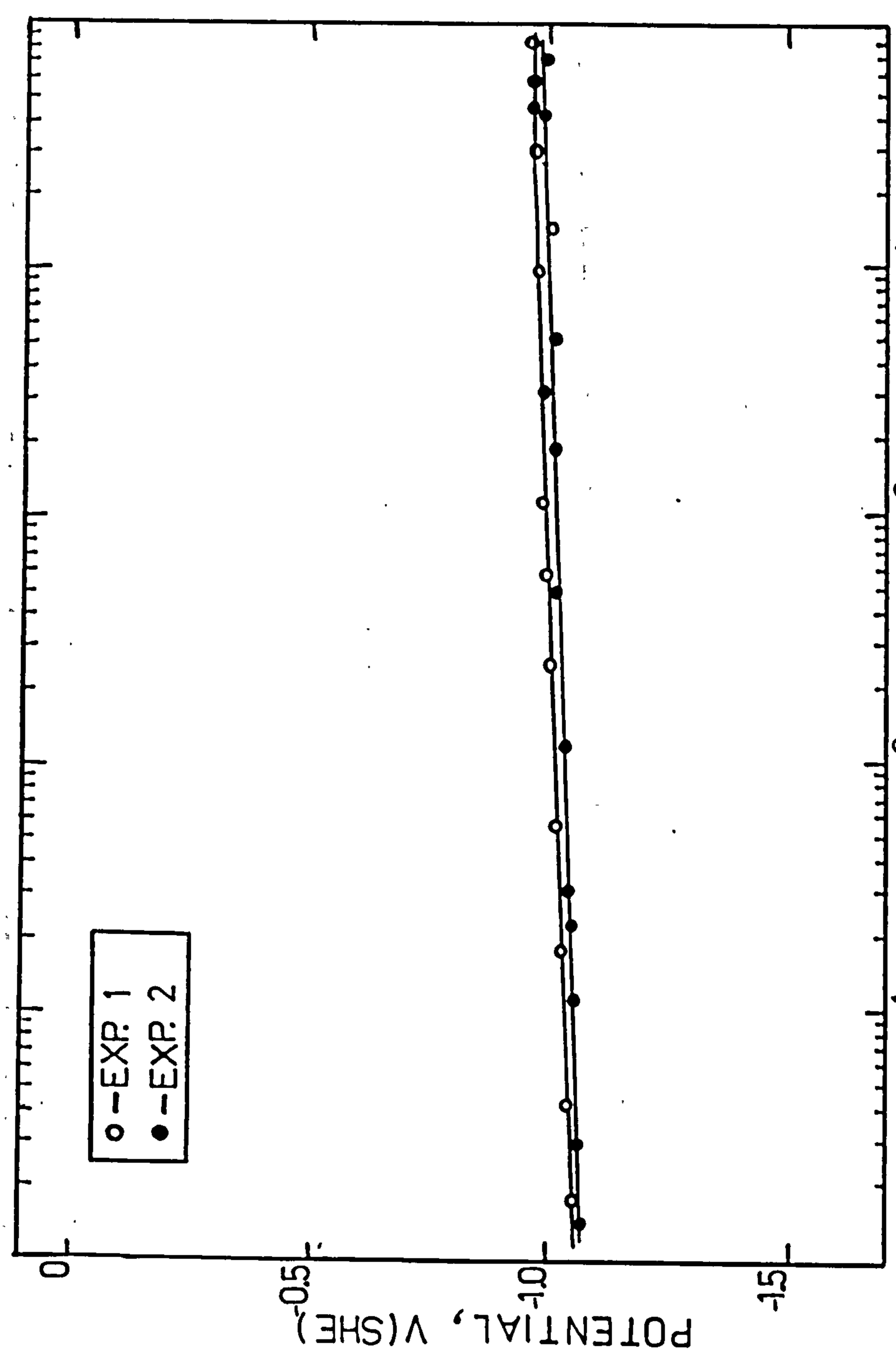

Fig.97 The surface potential of a membrane during the decay phase after the addition of $3x10^{-3}$ mol/l of As_2O_3 as a promoting agent. ($i_c = 24\ \mu A\ cm^{-2}$).

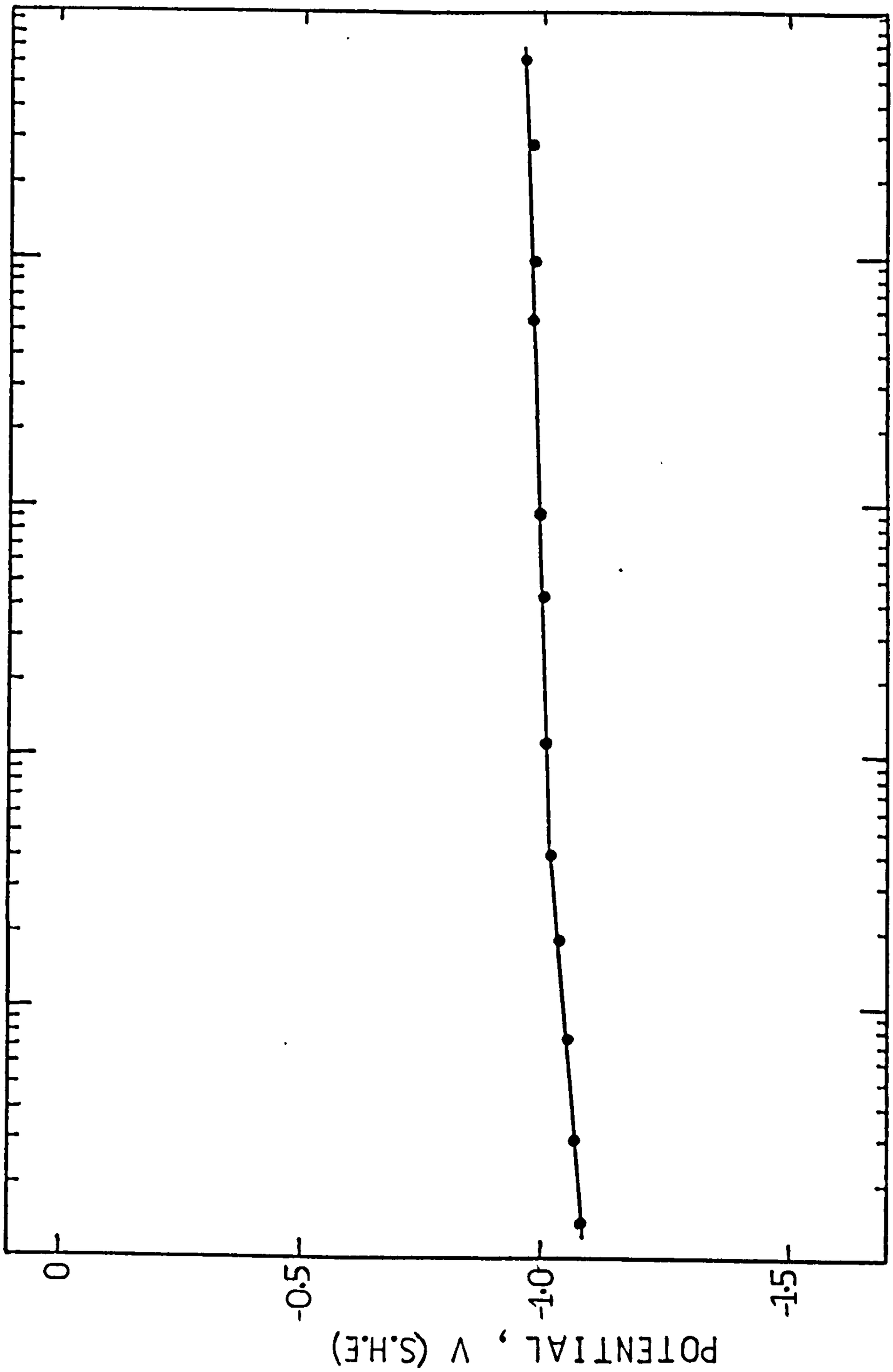

Fig.96 The effect of EDTA on the potential decay of an iron membrane charged at 24 $\mu A\ cm^{-2}$.

4.7.....RESULTS OF THE THREE DIMENSIONAL EXPERIMENTS.

These results are shown in Figures 98-100. Early on in these experiments, it became clear that the usual range of charging currents used on the flat membranes were unsuitable for a cube,6.5 mm side. This was because the time needed for the saturation of the membranes proved impracticably too long. It was also observed that the permeation current at these lower charging currents would suddenly collapse; perhaps as a result of a new trapping site opening up or the equilibrium between the lattice hydrogen atoms and those in traps, changing towards more entrapment.

To prevent this flux collapse which could happen in any one of the faces, long periods of further charging were needed. Therefore, to avoid this problem, a high charging current regime was adopted in which the charging current densities in excess of 50 $mA\ cm^{-2}$ were employed. The reproducibility of the results was enhanced and the instances of sudden collapse of permeation current minimized. The theoretical basis for the treatment of the results in accordance with the boundary conditions of these experiments, is explained in Appendix 1.

To calculate apparent diffusivity, the concept of the total flux F(t) has been utilized:

$$F(t)=\frac{b^2.c.C_o}{\pi(t)^{1/2}}\left[1-\exp(-a^2/t)\right]+\frac{b.c}{81}\cdot\frac{C_o}{(\pi t)^{1/2}}\left[1+\exp(-\frac{4a^2}{t})\right] \quad (234)$$

In part of F(t), it is possible to introduce:

$\frac{i_1^\infty + i_2^\infty + i_3^\infty}{zF}$ where i are the permeation currents recorded from the three faces of the cube under anodic polarization. For the experiments depicted in Fig.98, the corresponding values at t=5,000 s are as follows:

$$D=\frac{b^2c}{(\pi t)^{1/2}}.\frac{i_1^\infty + i_2^\infty + 2i_3^\infty}{i_1^\infty + i_2^\infty + i_3^\infty}\left[1-\exp(-\frac{a^2}{t})+\frac{1-2\exp(-4a^2/t)}{81}\right] \quad (235)$$

$$D=\frac{(0.64)^3\ 270\times10^{-6}}{[\pi(5000)]^{1/2}\ 245\times10^{-6}}\left[1-\exp(-\frac{0.64^2}{5000})+\frac{1-2\exp(-0.64^2\times4/5000)}{81}\right] \quad (236)$$

$$D=2.044\times10^{-5}\ cm^2\ s^{-1}$$

The above value obtained from the proposed mathematical model, corresponds well with the thin membrane experiments. The points to be made about these experiments is,that any meaningful calculation of diffusivity could only be made if hydrogen saturation of the membrane is achieved.

Potential measurements were conducted during the decay phase,but at the high charging currents used, the formation of a black/blue surface film was observed This film comprises mechanically removed iron particles redeposited on the surface. These form highly active sites which react with water molecules to form different oxide/hydroxides with varying degree of water incorporation.

The potential decay was fast and the breaks did not correspond to any found in other experiments. Fig.100 shows that during the decay of the permeation, the flux increased slightly after the termination of the charging current. It is believed an electrical field influences the movement of protonic hydrogen in an opposite direction to the flux.

The reason why this phenomenon is observed, only in the thicker membranes is that the relaxation time for the lattice is long enough for the hydrogen wave traversing the membrane to reach the other side. This wave bears the information about the changes in the cathodic face conditions i.e. the absence of the electric field.By contrast, the wave passing through thin membranes reaches the opposite side and starts the decay before the changes in the flux due to the field effect could be detected.

The 3-D experiments were modified in several ways to establish the effects of field; such as the switching off the potentiostat on the side adjacent to the charging side or the one controlling the opposite to it. However, no detectable variation in the fluxes were recorded to show the dependence of the effect field on entry side, from the exit side's boundary conditions.

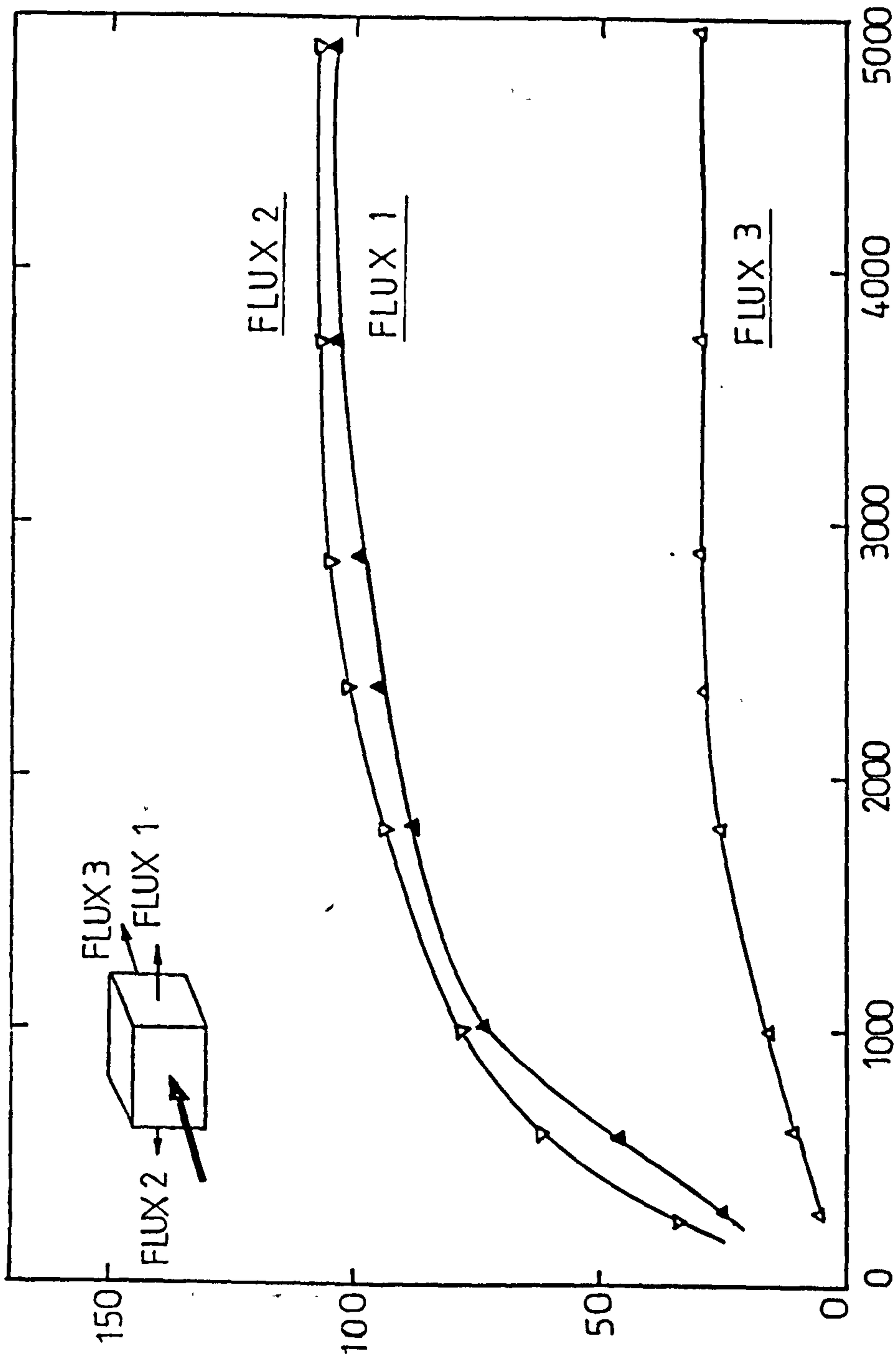

Fig.98 Permeation flux (i_∞, $\mu A\ cm^{-2}$) on the three monitored faces of the cube in the 3-D experiments at a CCD of 146.5 mA cm^{-2}.

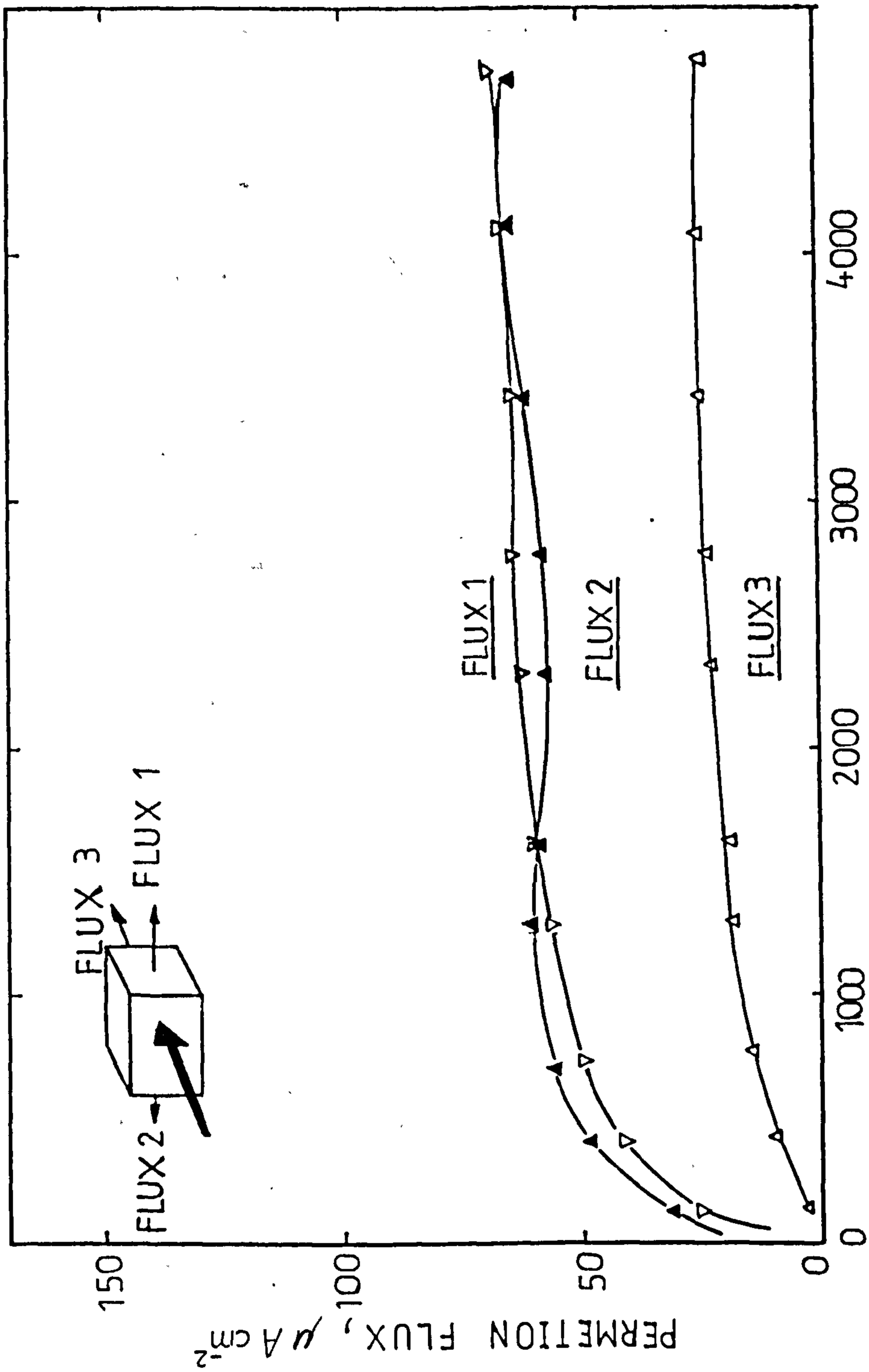

Fig.99 Permeation flux (i_∞, μA cm^{-2}) on the three monitored faces of the cube in 3-D experiments at a CCD of 53.5 mA cm^{-2}.

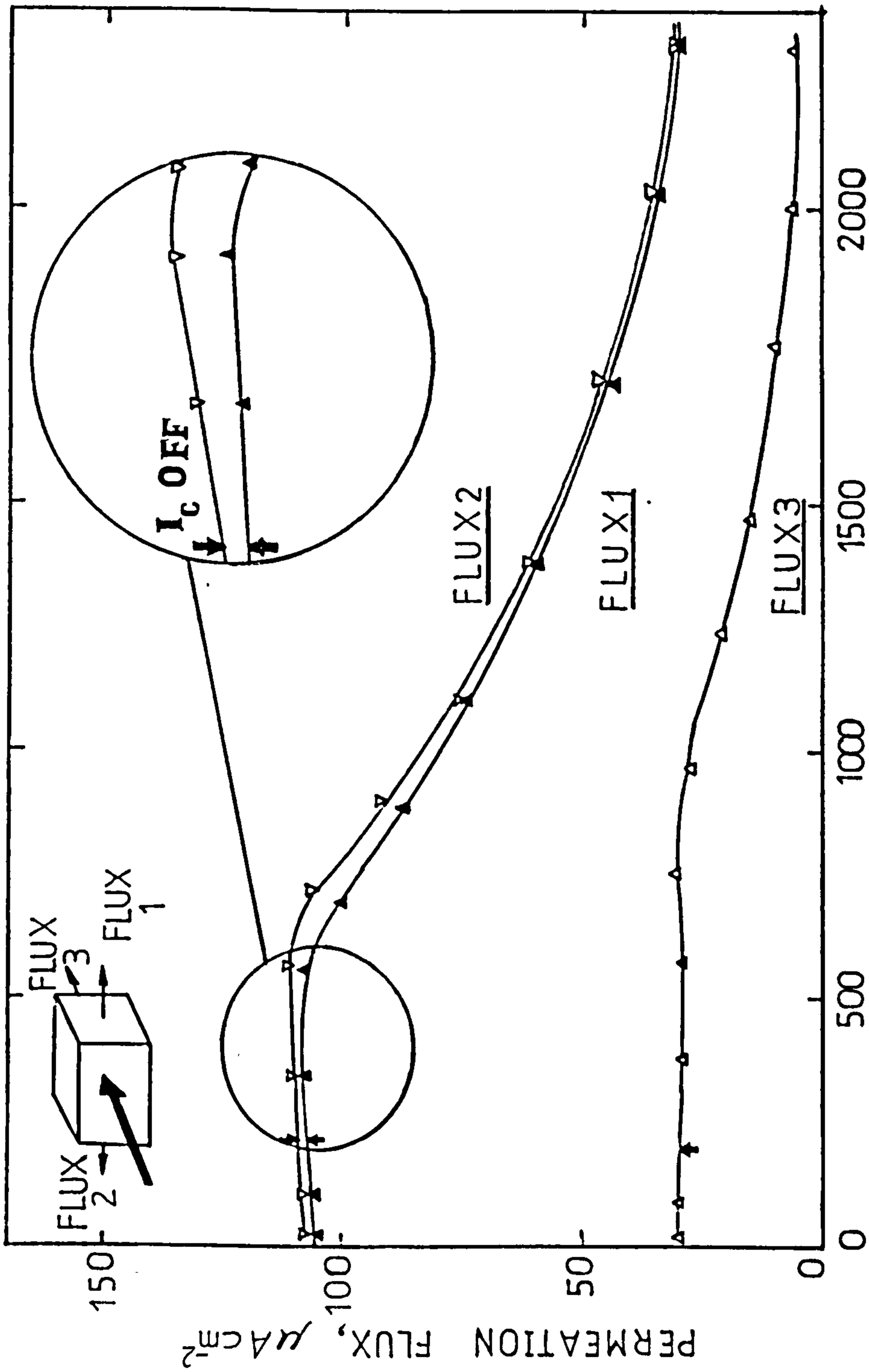

Fig.100 permeation flux during the decay part of a 3-D experiment at a CCD of 146.5 mA cm^{-2}. The inset shows an enlarged view of the decay section of the curve just after the termination of current

4.8.....AC IMPEDANCE MEASUREMENTS RESULTS

These experiments were performed to elucidate the film formation mechanism on iron in alkali solutions. The results of these experiments are plotted in four different ways i.e. Log|Z| vs Log f , Z' vs $\omega^{-1/2}$ and Z'' vs $\omega^{-1/2}$ and Z' vs $-\omega Z''$ in Figures 101-115. These plots lend themselves to calculation of one or more characteristic factors of the passive film.For instance Z' vs ω and Z'vs $\omega^{-1/2}$ could be used to elucidating mechanisms which control the complex electrochemical reactions occurring on the electrode while Z' vs $-\omega Z''$, is best suited for calculation of R_{ct} which shows ease with which electrons could traverse metal/electrolyte interface.

Plots ofLog Z vs Log f could be used to demonstrate the resistance of electrolyte used. The results thus gathered are tabulated in Table 18. As the results obtained from the first experiment at -1.020 V vs SCE show, the charge transfer resistance of the membrane at this cathodic potential is only 150 Ωcm^2. The reported impedance of iron at the pH=0 and a potential of -1.00 V vs SCE has been reported as 120 Ωcm^2[244].The examination of this point on the Pourbaix diagram indicates a film-free surface in the immune zone, while the impedance measurements of corroding pure iron in de-oxygenated 1 mol/l H_2SO_4 gives a value of 30 Ωcm^2 for the charge transfer resistance[249].It is the opinion of the author that under alkaline conditions ,the value of the surface impedance could be

safely interpreted as film free surface entering the passivation process.

Table 1 Compiled Results From AC Impedance Experiments

		Lg Z vs Lg f	Z' vs $w^{-1/2}$	$\angle'$ vs $w^{-1/2}$	$\angle'$ vs $-w\angle''$
Exp.	σ		110.0		
Pot.	R_Ω	12.5	12.5	12.5	12.0
-1.020	R_{ct}	159.3	159.5	-	161.0
vs SCE	C_{dl}	2.3E-3 F	-	-	-
Exp.	σ		425.0		
Pot.	R_Ω	20.0	14.0	13.0	17.0
-1.000	R_{ct}	1975.2	-	-	1756.8
vs SCE	C_{dl}	1.6E-3 F	-	-	-
Exp.	σ		2375.0		
Pot.	R_Ω	17.8	20.0	18.0	-
-0.617	R_{ct}	9982.2	-	-	11826.0
vs SCE	R_{dl}	5.0E-4 F	-	-	-
Exp	σ		6430.0		
Pot.	R_Ω	11.2	12.0	14.0	14.0
-0.447	R_{ct}	14114.0	-	-	18619.0
vs SCE	C_{dl}	3.9E-4 F	-	-	-
Exp.	σ		3600.0		
Pot.	R_Ω	16.0	22.0	20.0	23.0
-0.136	R_{ct}	16471.0	-	-	16055.0
vs SCE	C_{dl}	6.3E-4 F	-	-	-

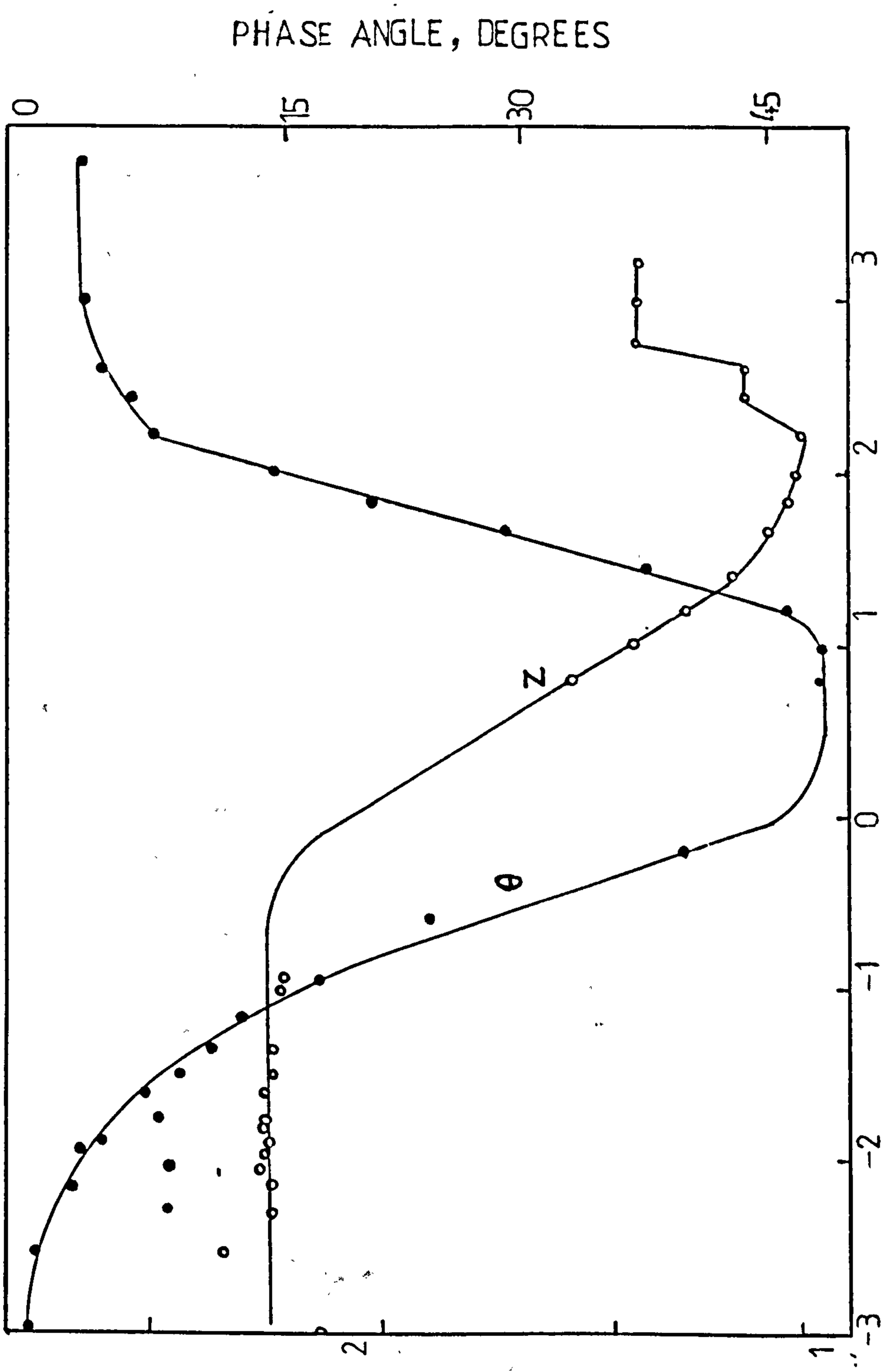

Fig.101 Logarithm of impedance and the phase angle vs the logarithm of frequency for experiment at -1.02 V (SHE)

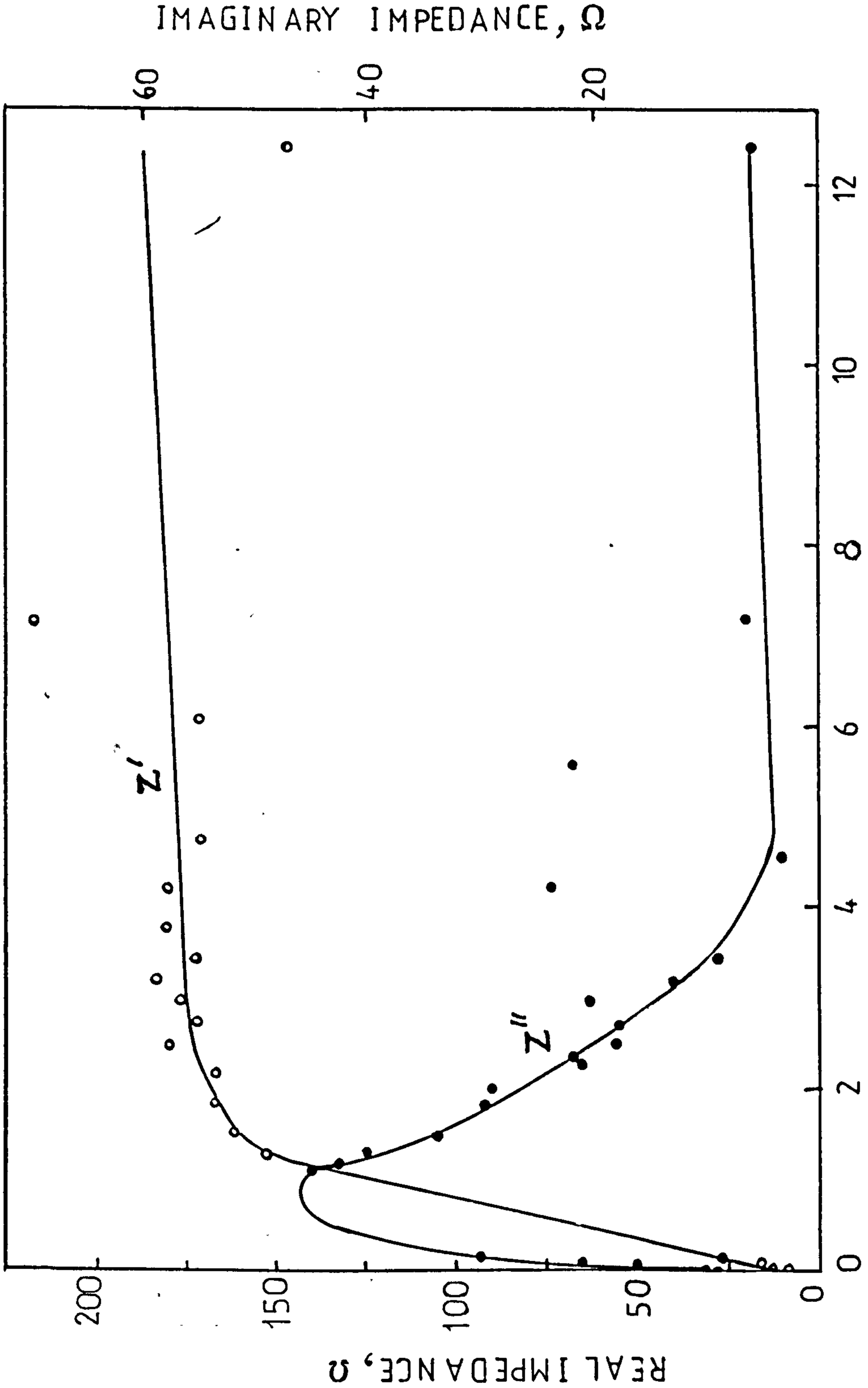

Fig.102 Real and imaginary impedance vs $\omega^{-1/2}$ plot for experiment at -1.02 V (SHE).

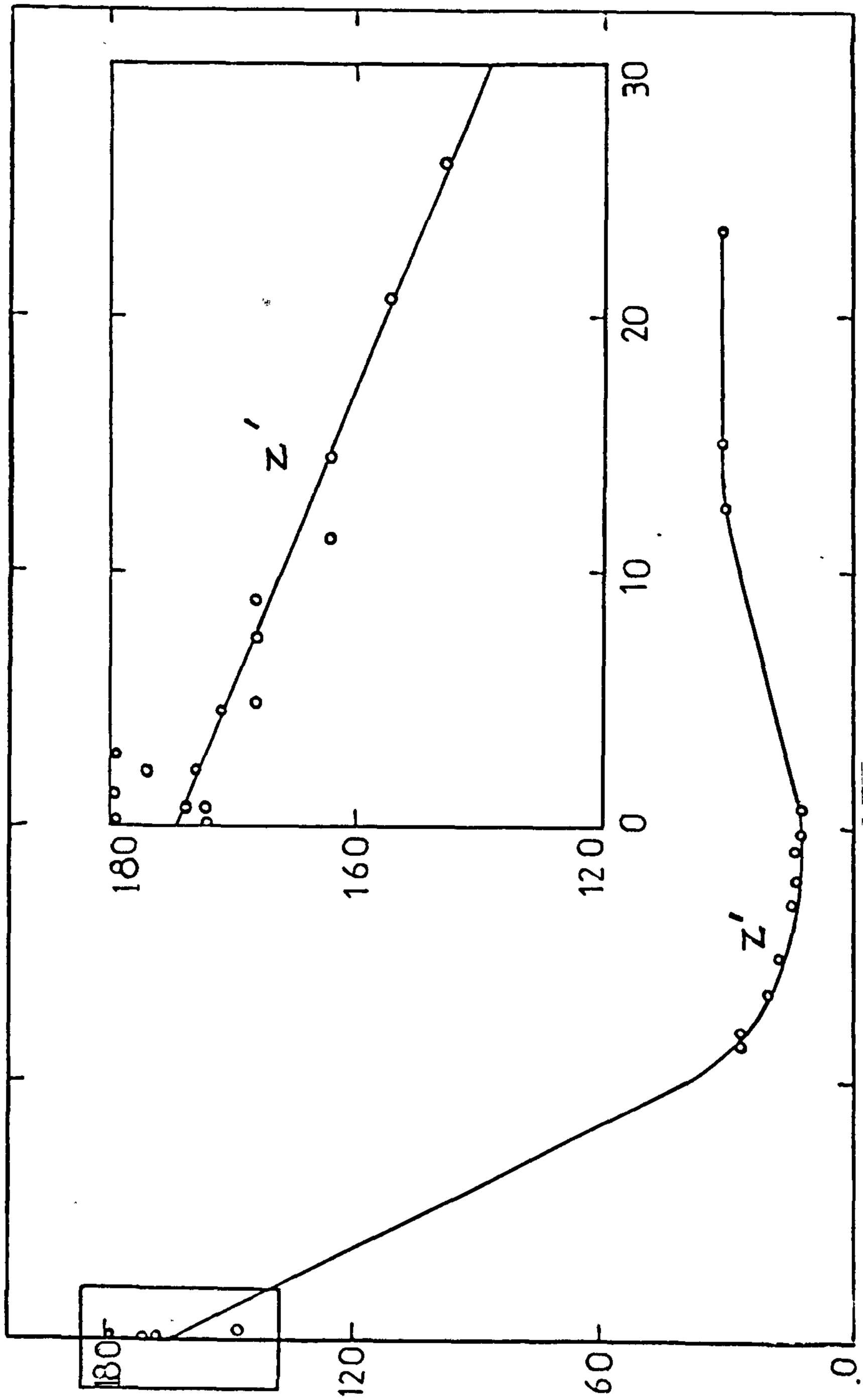

Fig.103 Real impedance vs $-\omega.Z''$ plot for experiment at -1.02 V (SHE).

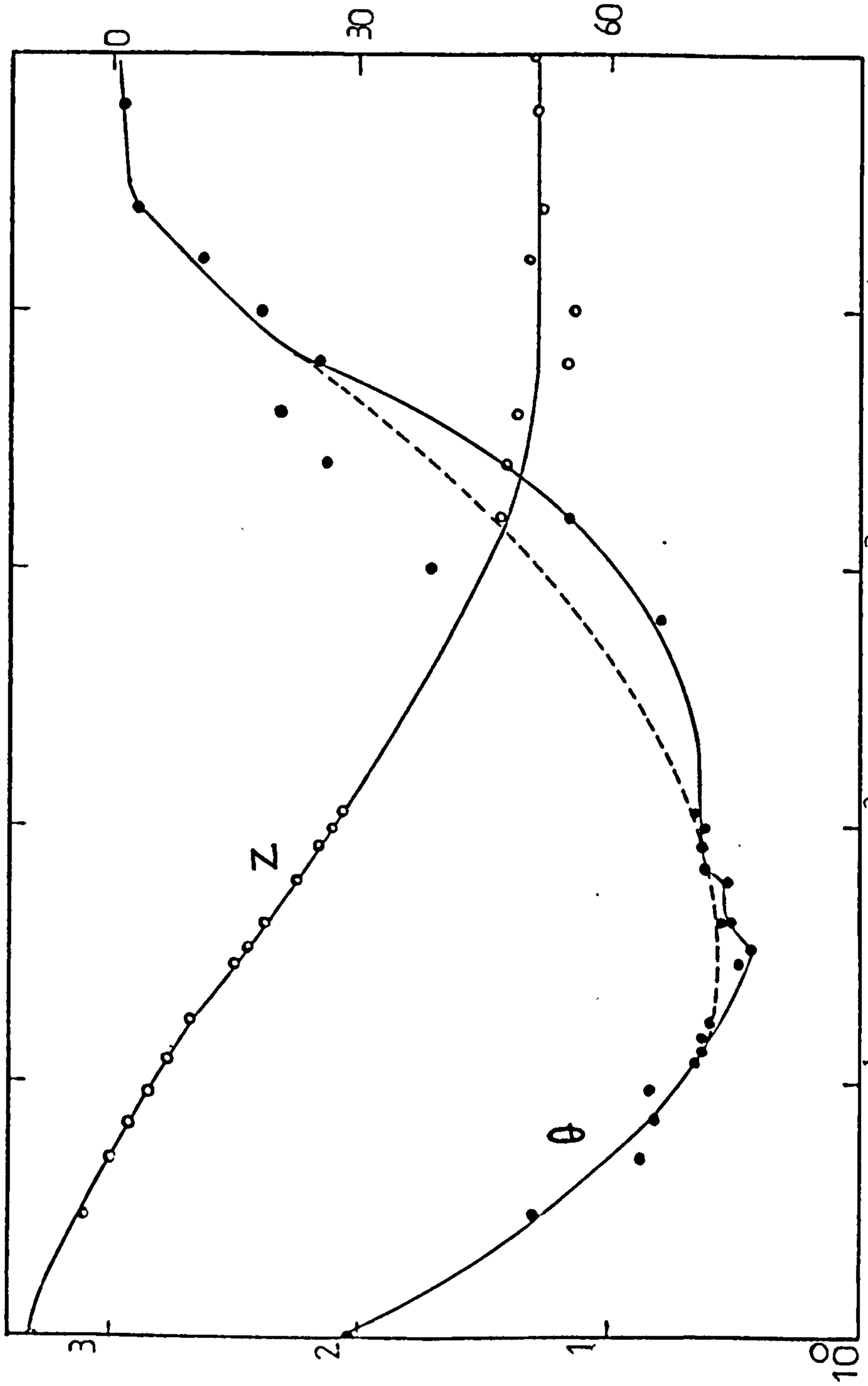

Fig.104 Logarithm of impedance and the phase angle vs the logarithm of frequency for experiments at -1.00 V (SHE).

Fig.105 Real and imaginary impedance vs $\omega^{-1/2}$ plot for experiment at -1.00 V (SHE).

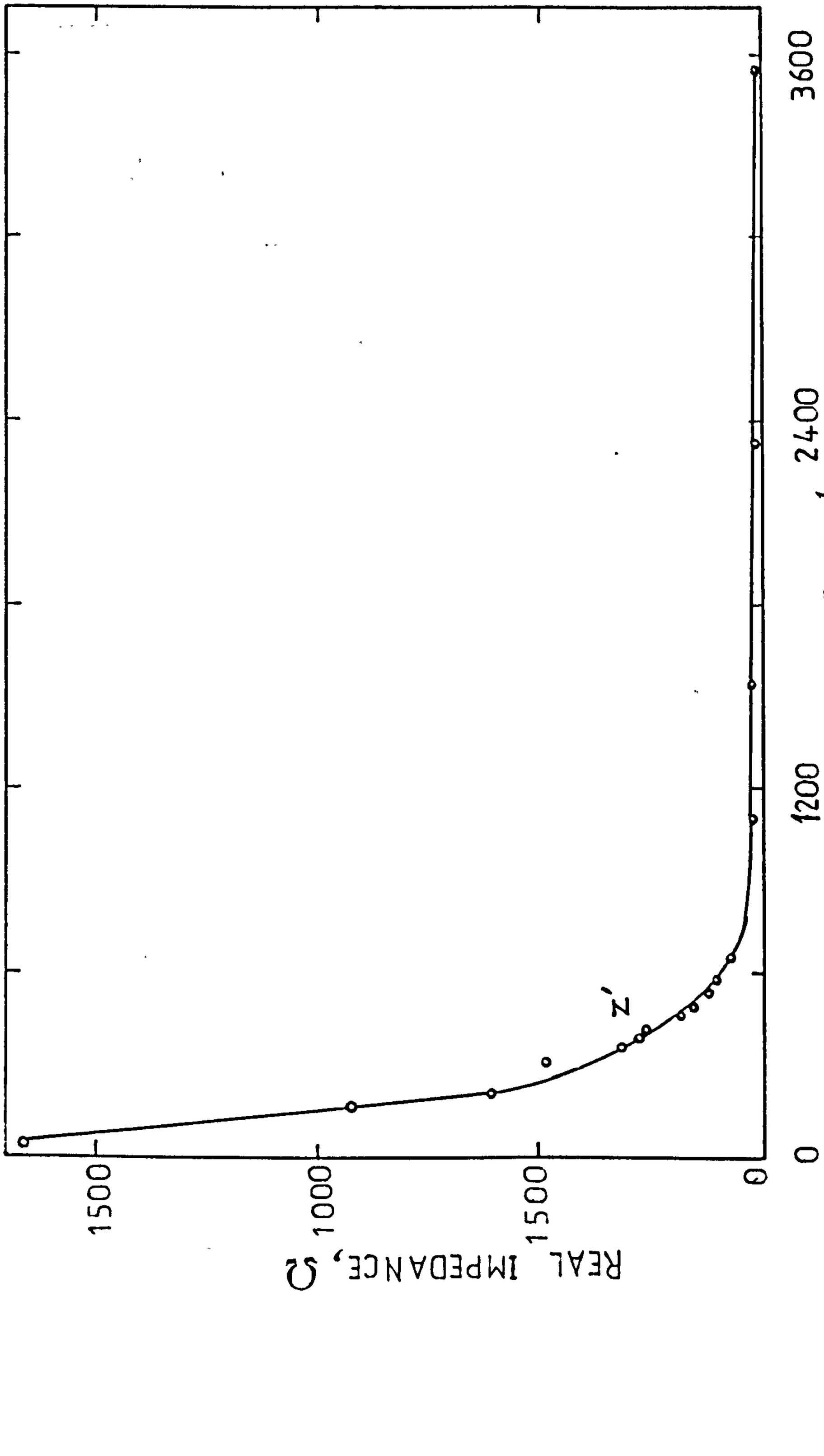

Fig.106 Real impedance vs $-\omega \cdot Z''$ plot for experiment at -1.00 V (SHE).

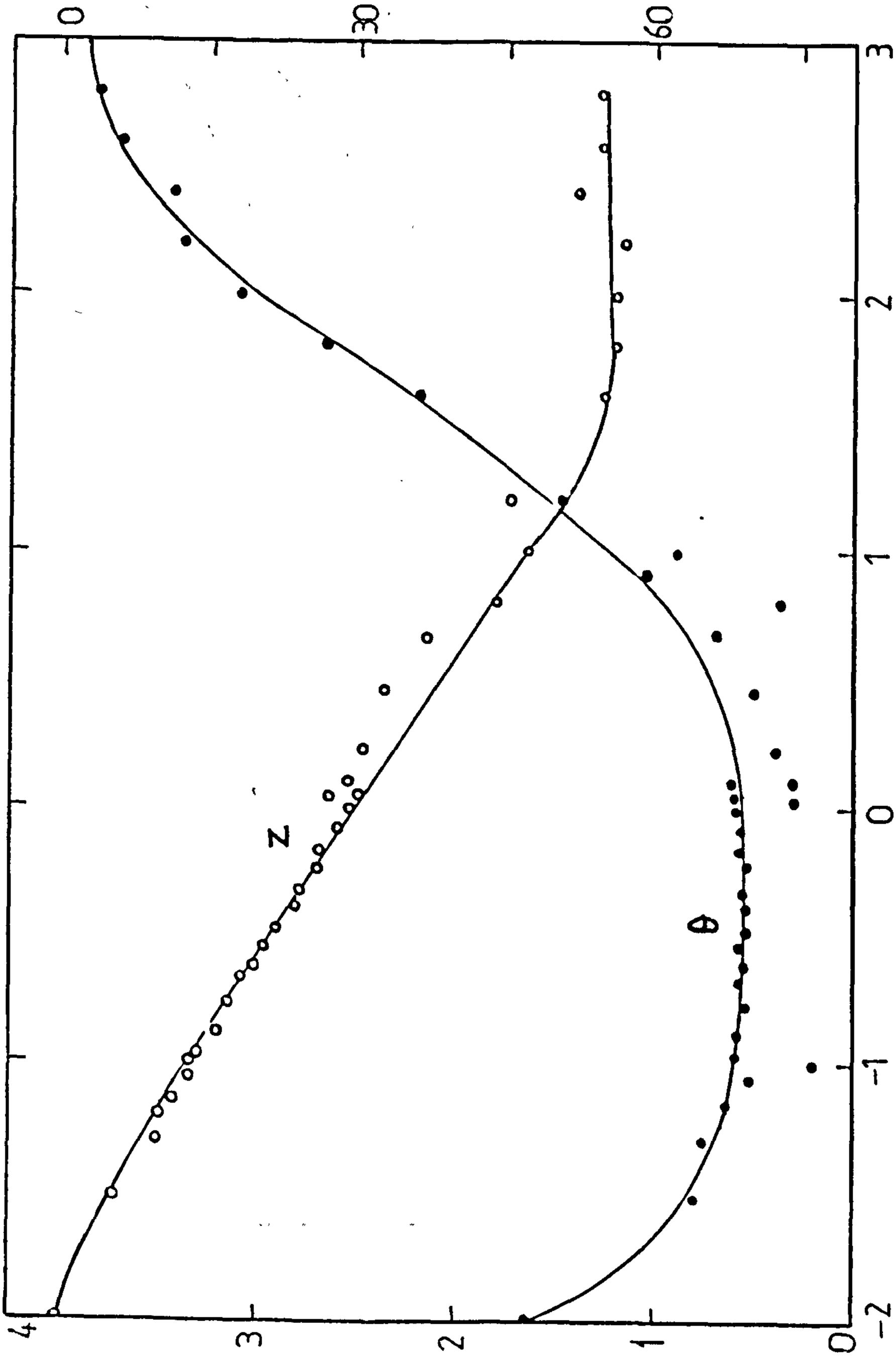

Fig.107 Logarithm of impedance and phase angle vs the logarithm of frequency for experiment -0.617 V (SHE).

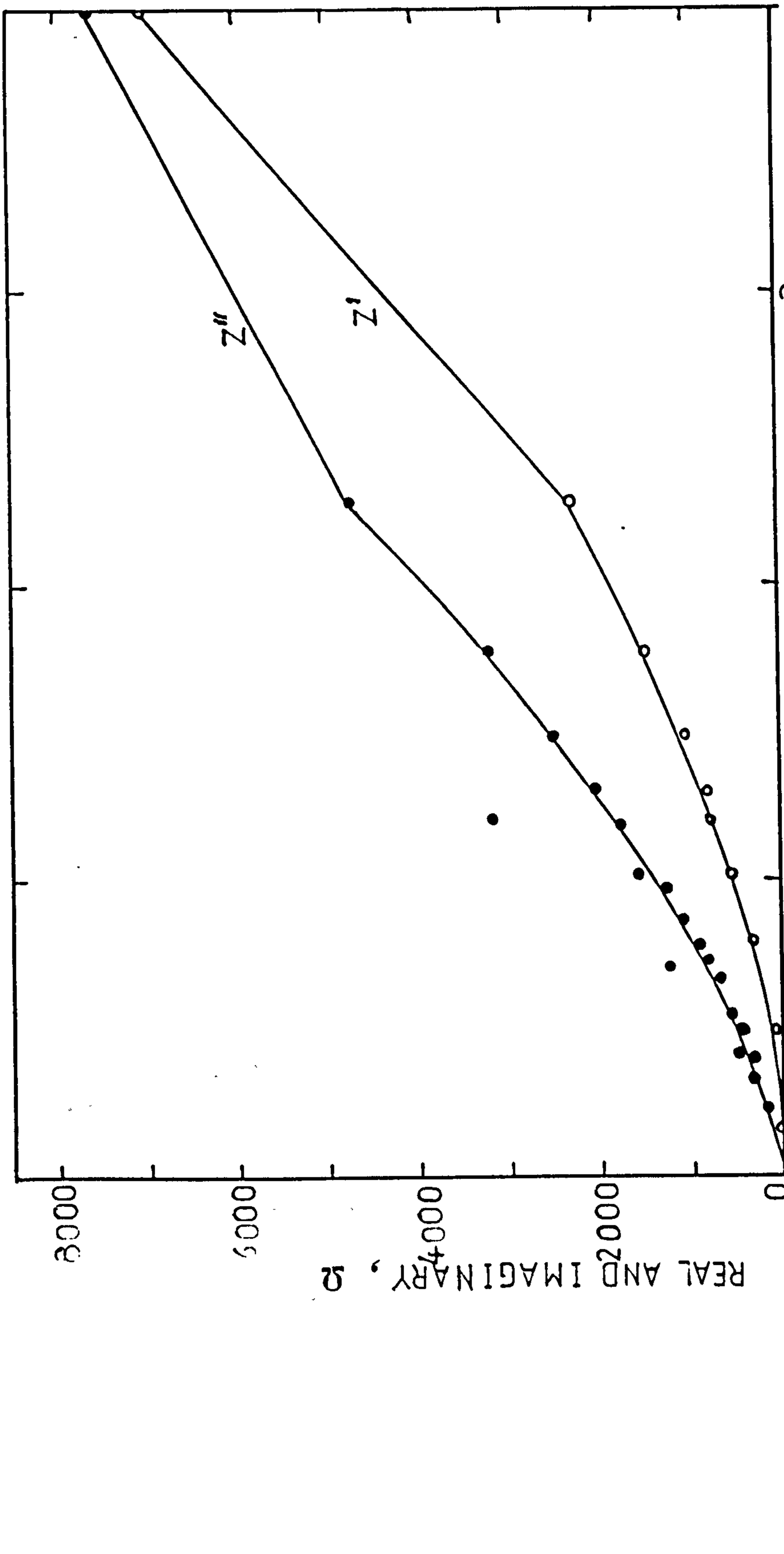

Fig.108 Real and imaginary impedances Plotted vs $\omega^{-1/2}$ for experiment at -0.617 v (SHE).

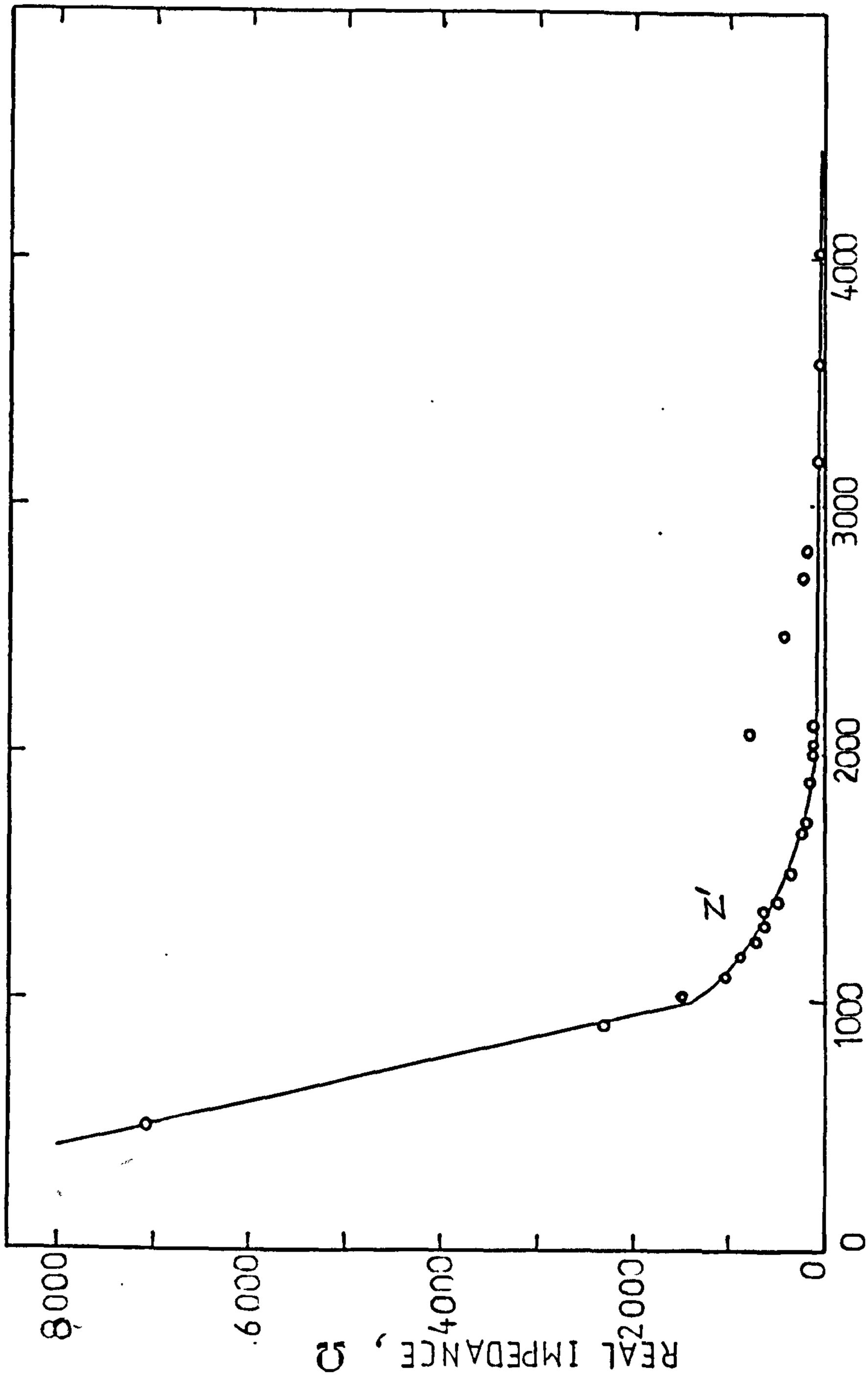

Fig.109 Real Impedance vs $-\omega . Z''$ plot
for experiment at -0.617 V (SHE).

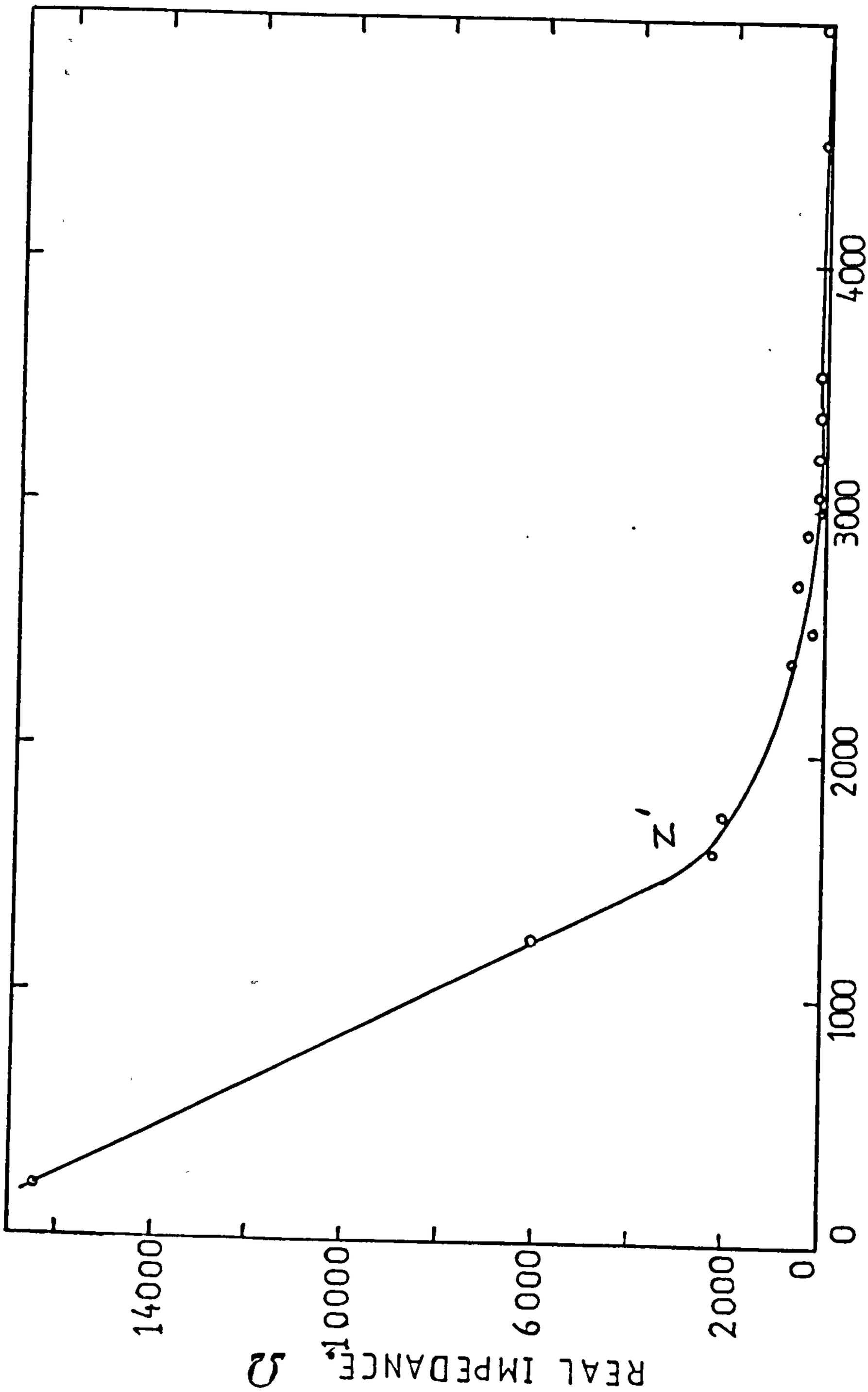

Fig.110 Real impedance vs $-\omega Z''$ plot for experiment at -0.447 V (SHE).

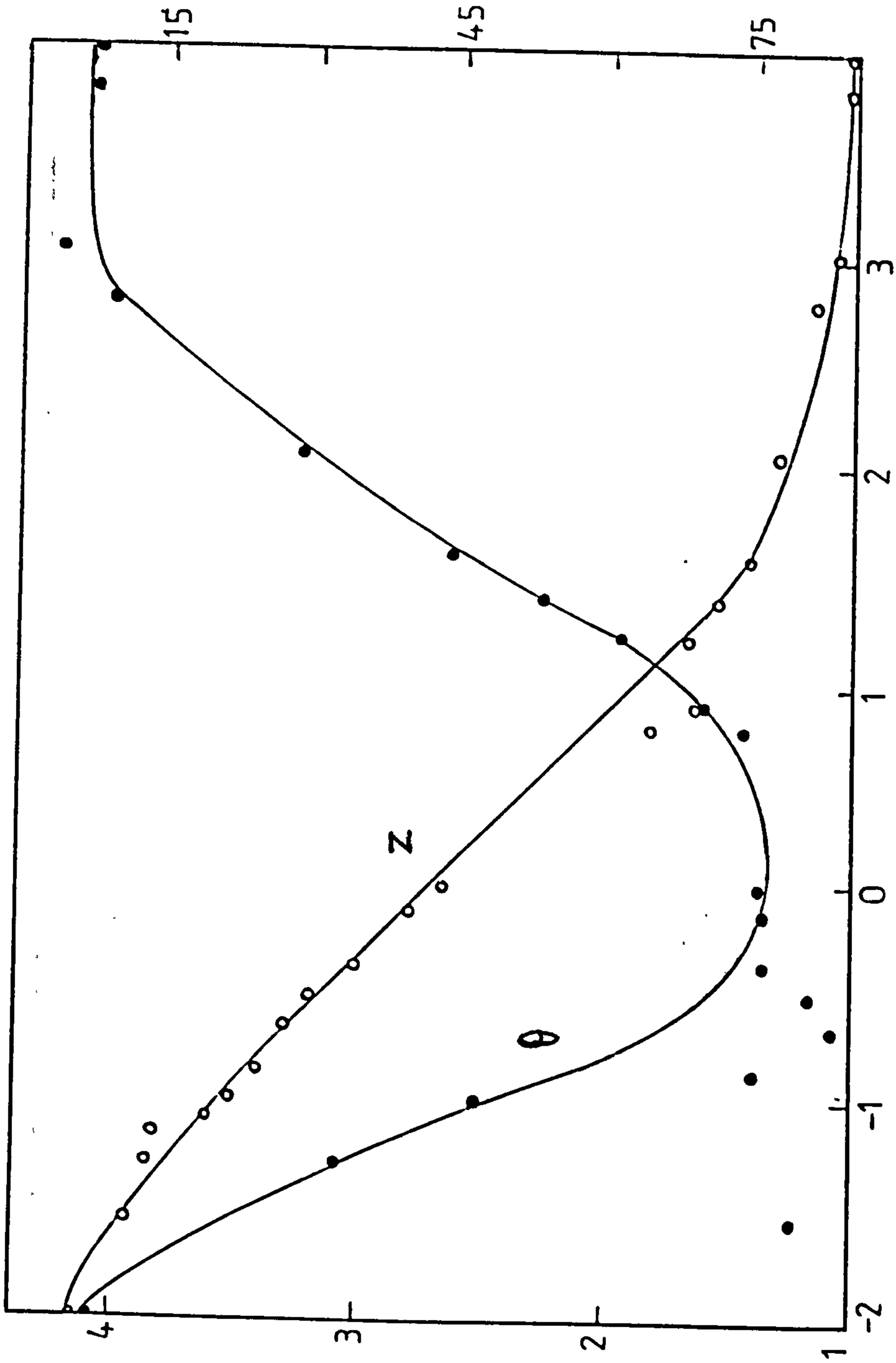

Fig.111 Logarithm of impedance and the phase angle plotted vs the logarithm of frequency for experiment at -0.447 V (SHE).

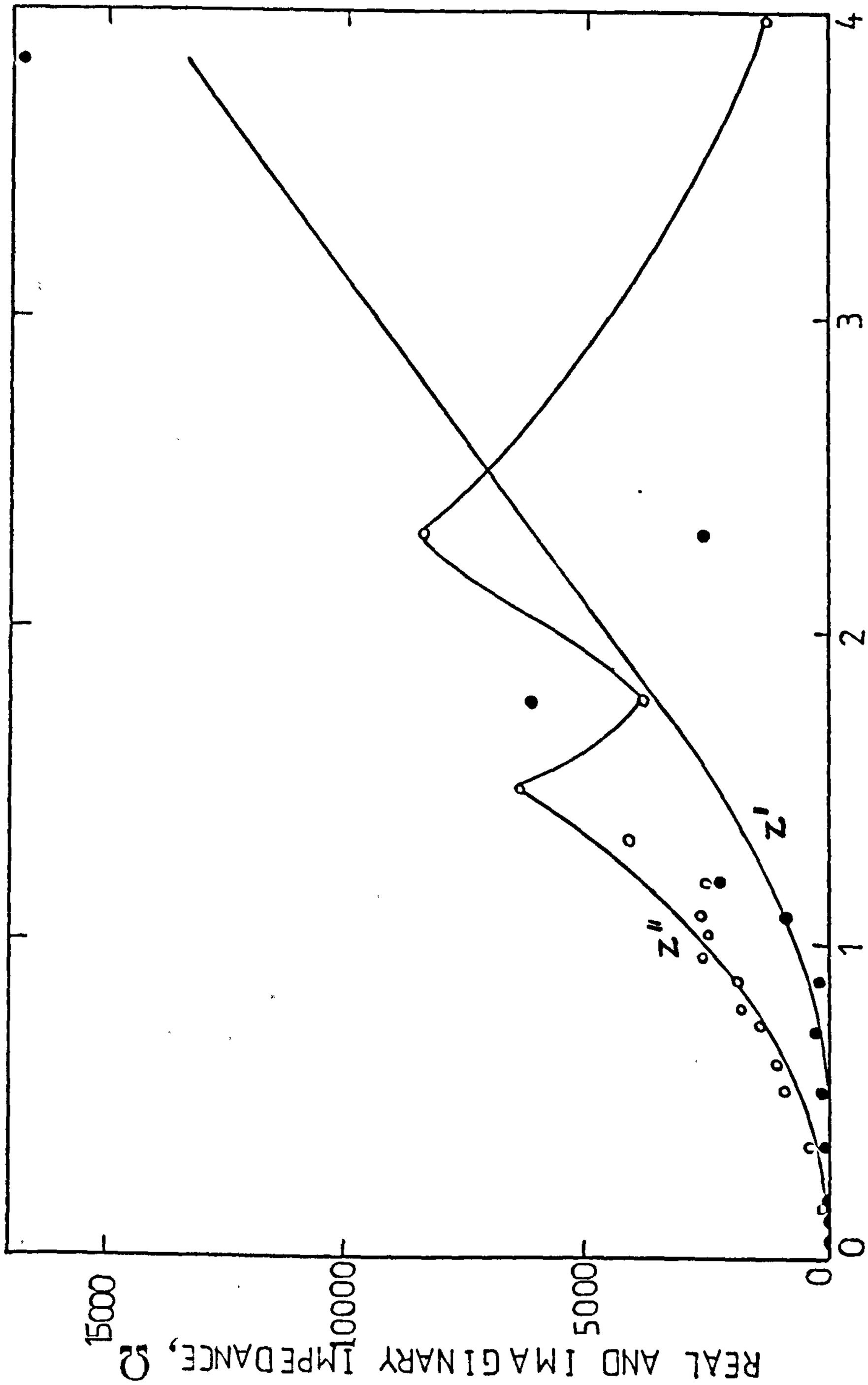

Fig.112 Real and imaginary impedance plotted vs $\omega^{1/2}$ for experiment at -0.447 V (SHE).

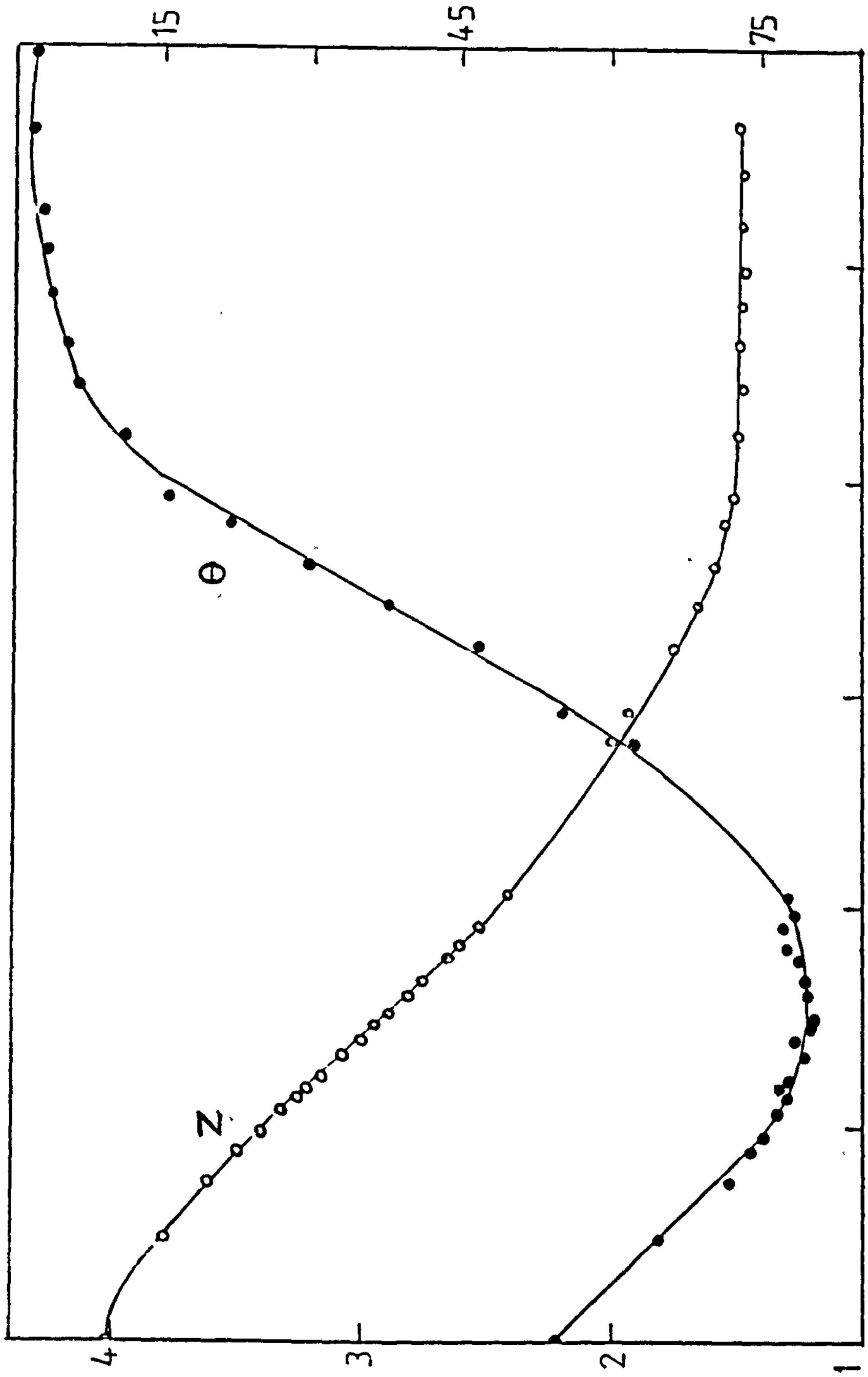

Fig 113 Logarithm of the impedance and the phase angle vs the logarithm of frequency for experiment at -0.136 v (SHE).

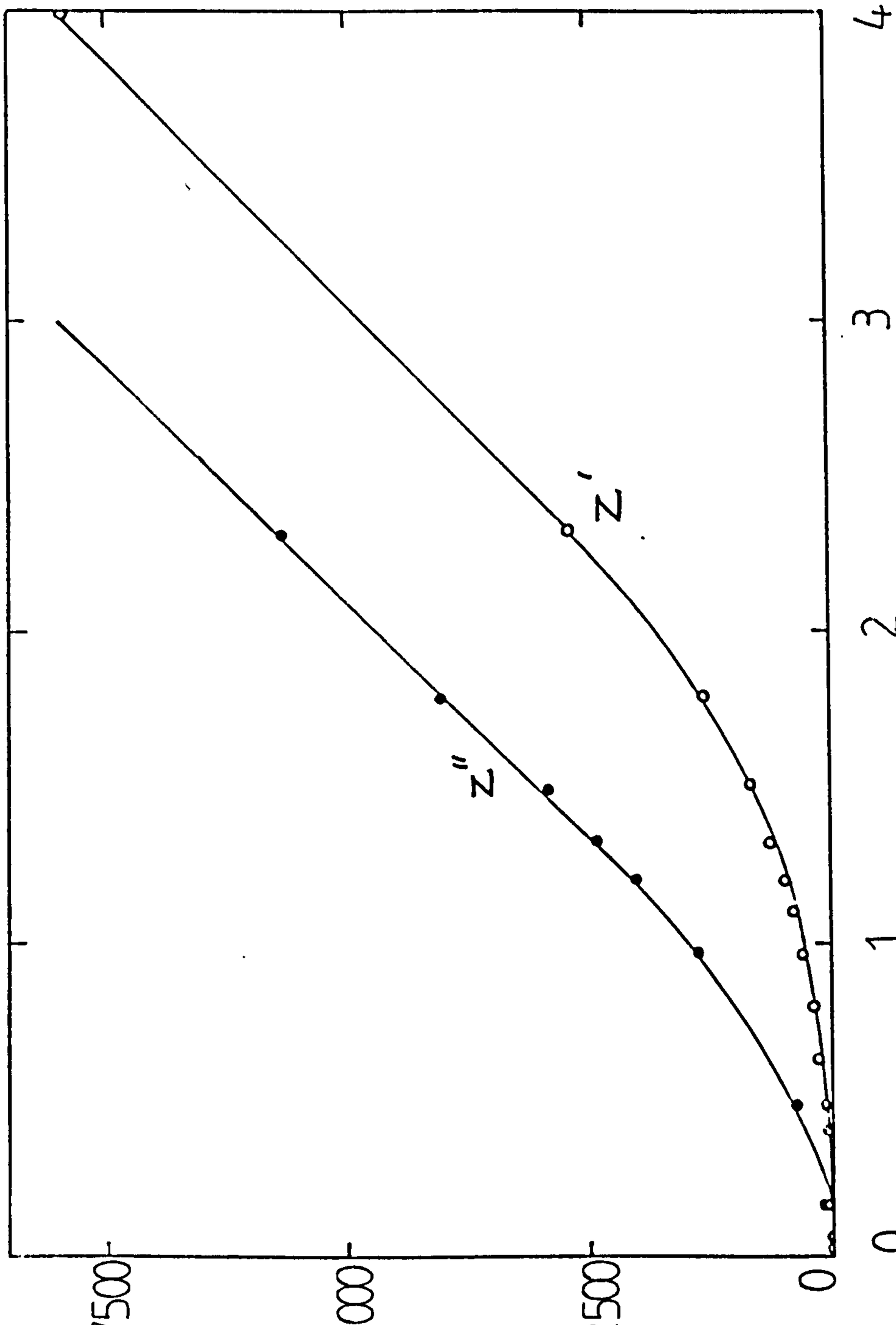

Fig.114 Real and imaginary impedances plotted vs $\omega^{-1/2}$ for experiment at -0.136 V (SHE).

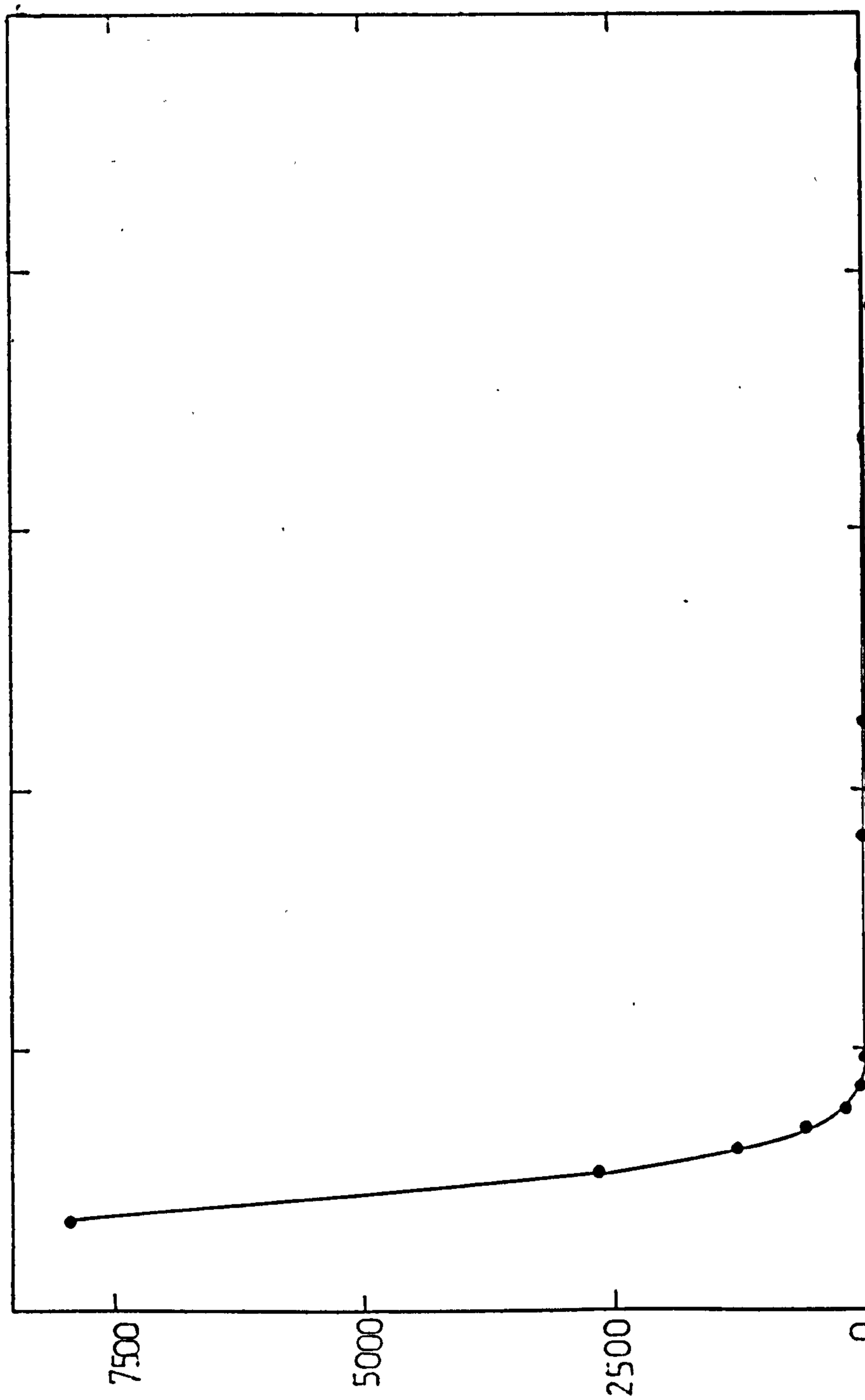

Fig.115 Real impedance vs $-\omega Z''$ plot for experiment at -0.136 V (SHE).

5.....DISCUSSION

The permeation results tabulated in Table 14 show the effect of systematic increase of charging current density (CCD) on the permeation current.This has been explored by several workers [304,305] and the consistency of the results indicates that the flux through the membrane is controlled by surface hydrogen concentration. The variable controlling the flux is the coverage of the electrode by hydrogen adatoms (θ). During the cathodic charging of iron and steel, a quasi-equilibrium exists between the hydrogen adsorbed on the surface, hydrogen dissolved in the interstices, atomic hydrogen adsorbed on the internal surfaces and molecular hydrogen formed in the micro-voids [314]. As the charging current is increased, this dynamic equilibrium is driven towards a higher surface coverage which in turn, makes more hydrogen atoms available for traversing the membrane. As the total concentration of hydrogen in a pure iron membrane is very low, reported to be 6 ppm [315],of which only a minute 0.6 ppm is lattice hydrogen[315], the steady state current density i_∞ increases to re-establish the equilibrium.Fig.69 and 70 show the increase observed in the steady state current density (i_∞) as a result of increase in CCD. The influence of increase in CCD is more pronounced at higher charging currents. This is in line with the proposed changes in HER as the surface coverage (θ) changes from the Langmurian coverage to Temkin isotherm at higher currents [189]. Fig.70 illustrates the

drastic decrease in the hydrogen permeation due to an increase in thickness from 0.07 mm to 1.07 mm. However, not all the hydrogen generated on the cathodic face is absorbed into the substrate.

Daft [190] has suggested that by using a CCD of 1600 μA cm^{-2}, the amount of hydrogen actually entering the membrane (in contrast to those forming gas bubbles) is around 70% of the total generated. In the present work the "current efficiency" defined as the ratio of the permeation current density to CCD (pictured in Fig.71) shows lower values. This indicate, not all of the hydrogen entering the substrate diffused out or, the recombination of hydrogen adatoms happens faster than proposed.

In order to establish that the flux is not controlled by the hydrogen-bulk trapping and/or hydrogen-surface trapping during the steady state permeation experiments, the $1/i_{\infty}$ vs L plots should cross through the origin [218,316]. Fig.74 shows such a graph for membranes of different thickness at different current densities.

The passing of the four lines through the origin indicates that diffusion of hydrogen was not dominated by the traps, although their existence has a bearing on the flux.This is clear from the rather large scatter of points for the line representing the lowest charging at $2.4\,\mu A c\bar{m}^2$ which is more prone to such

anomalies as not all the trapping sites are adequately saturated.

It is possible to show that the kinetics of hydrogen diffusion in the membranes were not trap controlled through the characteristics of the diffusion coefficient (D). The different ways of calculating the diffusivity coefficient by the use of various time constants [192,194]] are shown in Table 6. In the present work, the only time constant free from extraneous error was found to be (t_d) i.e. the decay relaxation time.In alkaline solutions, iron is quickly covered with a passive film whose reduction will incorporate additional time to the time constant used [193]. This will introduce error and sometimes much smaller diffusion values [193]. The effects of such fast film formation on iron in alkaline media has been noticed by other workers [317]. However, the interpretation of its implications has not always been straight forward.

As the room temperature diffusivity results calculated using the $D= L^2 / \pi^2 \cdot t$ formula tabulated in Table 14 show, there is a link between the calculated diffusion coefficient and the charging used.This is due to an increase in the occupation of the trapping sites in the membrane as the CCD increases, leading to diffusivity values more representative of lattice diffusion [106].

To avoid the effects of this concentration dependency on the diffusivity, a plot of Log L^2 vs Log t_d shown in Fig.73 could be used [23,203]. The relationship between the diffusivity and the thickness is well established[194]. Since :

$$L^2 = \pi^2 . D . t_d \qquad (237)$$

Taking logarithms,

$$\text{Log } L^2 = \text{Log } \pi^2 D + \text{Log } t_d \qquad (238)$$

A plot of Log L^2 vs Log t_d should be a straight line and give Log $\pi^2 D$ as the intercept on the Y-axis. Plot of Fig.73 has a slope of 44.2 as predicted from above (45) and gives the thickness and concentration independent value of 2.67×10^{-5} cm^2 s^{-1} for hydrogen diffusion in iron. This is in good agreement with other data published [117].

The activation energy for the diffusion of hydrogen in iron was also calculated. The relationship between the diffusion coefficient and the reciprocal of temperature is an Arrhenius type equation [13,16,117, 157,318]. Fig.72 shows the plots of calculated D values at different CCDs vs the reciprocal of temperature. The relationship between the CCD and diffusivity shows that the higher currents give higher diffusivity values since, permeation is influenced by trapping sites. As higher currents cause more of the traps to be saturated,the diffusion coefficient value tend towards those of lattice diffusion. The values of activation energy calculated from these plots as shown in Table 15 confirm this conclusion.

The calculated activation energies decreased from 28.08 kJ/mol for a sample charged at 2.4 μA cm^{-2}. to 10.26 kJ/mol for membranes charged at 482 μA cm^{-2}, the highest CCD used. This shows a decrease of more than 60%. However, it could also be shown that the number of abnormal sites in the membranes used were not unusually high to influence the results adversely. The reported trap binding energy in iron is 65 kJ/mol [319] and it could be expected that in a membrane with a high density of trapping sites i.e. $N_T/N_L \simeq 1$, the calculated activation energy to be equal to the sum of detrapping and lattice diffusion activation energies [319]. The fact that relatively small charging current of 120μA cm^{-2} led to the E_D and D values in very good agreement with those reported in the literature[117], indicating the very small effect of traps on diffusity in these experiments.

The small charging times needed to establish a stable flux also leads us to believe that the former conclusion as to the presence of only a few abnormal sites in the membrane has been correct. If the opposite were true, both the minimum CCD giving error free results and the charging periods would have been extremely large.

To avoid causing any internal or sub-surface damage to the membranes, the CCDs were kept well below the values published in the literature which are believed to cause such damage [203]. Xie et al[203] gives this threshold current as 13.5 mA cm^{-2} while Tetelman and Robertson report a value of 15.5 mA cm^{-2}

[320] both of which far exceed the highest CCD employed in this research.

The overall picture from the permeation and diffusion results was of positive effects of the preparation and procedural practices which were designed to minimize the damage to the membrane, before and during the experiments. Judging by the compatibility of the results with those published, the conclusions from these experiments could not be attributed to unsatisfactory surface preparation.

There have been some references to the effects of electrical fields on the mobility of diffusants in metals [321-323]. In the case of hydrogen, if this is proven to be the case, the protonic nature of it in iron could be safely assumed.

During permeation studies, an effective field is applied across the membrane with cathodic face the negative side and the potentiostatically-controlled side acting as the anode.No anomalous behaviour which could be attributed to the field effect during the charging was observed in experiments on thin membranes of 0.07 mm and 0.205 mm thick. As a result, it was concluded that such an effect (if any) should become apparent only in thicker membranes, as the relaxation time for membranes expressed by t_d is long enough to show minor changes in concentration due to field effects.

A series of permeation experiments were then carried out on membranes 1.07 mm thick.Fig.91 shows the decay fluxes observed on these membranes. As has been shown, at the cut off point of the charging current (start of the decay) the permeation current is enhanced by a small amount,before the hydrogen wave carrying the information on the new state of boundary conditions reaches the anodic face. This has been observed clearly for the CCD of 482 μA cm^{-2} and 120 μA cm^{-2} while the case of CCD of 2.4μA cm^{-2} is not so appreciable.The effect of a strong field would be felt by a reduction in the recorded permeation current (i_∞) during the charging phase, if the diffusant carries a positive charge. Upon interruption of the charging current,accepting the well argued hypotheses of the protonic hydrogen form in iron, it is expected that the flux should be actually enhanced.This has been effectively shown in the case of 120 and 482μA cm^{-2} CCDs on 1.07 mm thick iron membranes.

The logical step from here was to investigate the effect that even higher CCDs would have on the movement of hydrogen.This led to development of the 3-D experiments which has been described in detail previously. To observe the instantaneous movement of hydrogen in a thick specimen, the 3-D experiments could be more revealing. In our experiments, in common with low CCD experiments on 1.07 mm thick membranes, sudden collapse of the measured permeation current -especially during the early stages of charging or at later stages of decay- were observed. Clearly, this was due to low

hydrogen concentration and the interaction of hydrogen with the internal trapping sites. On increasing the charging current which led to high occlusion of hydrogen in these membranes,the steady state permeation flux was stable, while that of decay phase permeation transients still showed these sudden collapses.It is believed that at low hydrogen concentrations, the ratio between the number of occluded hydrogen atoms to the number of trapping sites proportionally is much less than in thinner membranes.This leads to the collapse of the flux as sufficient number of protons get immobilized by the existing traps. The fact that a substantial flux could be attained at very high current densities confirms this hypotheses.

The flux measurement results,in accordance with the 1.07 mm thick experiments, show a small increase in the permeation current after the termination of charging current. These experiments provided for the evaluation of the contributions of each of the potentiostatically controlled sides on the flux. No appreciable difference was measured on the other sides when taking various potentiostats out of the circuit. This could be explained by the fact that protons are only substantially attracted to the negative face and the positive fields are not strong enough to repel them. Alternatively, it could be argued that the field effect is only on the adatoms formed during the discharge step and once these enter the lattice, the field effect is no longer felt.

The lack of any effect when switching off different potentiostats supports this argument.Sukhotin et al [322] have shown the rate of proton transfer through iron membranes to be dependent on the potential used. They particularly stress the importance of this effect as they believe the kinetics of hydrogen to be basically migration controlled. On the basis of the results from the this work, such conclusions could not be supported while the role of migration as a component to the mobility of hydrogen is quite clear. The result of diffusion measurements in the 3-D experiments compare well with the thinner membranes.The value of 2.044×10^{-5} cm^2 s^{-1} calculated for these experiments using the mathematical model proposed in the Appendix 1, confirms the validity of the model. The very high CCD regime adopted seems to confirm that the lattice diffusion could only be achieved when the existing traps are saturated. The cube used was mild steel (having more impurities than the Armco iron used for the thin membrane experiments); its size necessitated extreme charging conditions.

As a result of a paper by Zakoczymski et.al [209] in which the possibility of a film free iron electrode, even at sufficiently cathodic potentials has been doubted, the following set of experiments were devised. Using the proposed procedure by the above authors,who argue for the use of EDTA (Ethylenediaminetetracetic Acid) as the substance capable of removing the film; solutions of 0.1 mol/l

NaOH were dosed with 0.1 mol/l of this reagent. A moderate charging current density of 1 mA cm^{-2} was used although in another paper the same authors claim that a special "sub-layer" is formed on iron upon its contact with NaOH and this sub-layer could only be removed using extremely high current densities during 40 - 50 hours of charging[299]. As was obvious to the author that the use of such currents could only lead to irreversible damage to the substrate, the film reducing properties of EDTA were investigated using the moderate CCD mentioned before. No appreciable difference in permeation fluxes were observed to indicate a film removal effect. Daft[190] working on the HER mechanism on iron in NaOH finds his electrodes film-free after relatively short times at very low CCDs.

It is the present author's opinion that the sublayer discussed in the above paper is the result of damage to the lattice due to the high currents used. The very high fluxes observed also could be explained by the mechanical degradation of the surface through HER. This results in an increased surface area , both due to the roughening effect and also through the deposition of highly active iron particles back on the cathode surface.

Vorkapic and Drazic[358] have shown that high cathodic currents lead to high rates of iron dissolution. They were able to reduce this rate significantly by connecting a strong magnet to the

electrode. This suggests that mechanical degradation of the surface under the influence of the HER is the main cause of the observed phenomenon.Evidence gathered from the literature and in the course of experiments in this research, exclude the possibility of a "reduction resistance" film as suggested by Zakrzymski et al.[303]

The relationship between overpotential during the charging experiments and surface coverage is of fundamental importance in understanding the mechanism of hydrogen entry into iron. In the present work,it was observed that the surface potential became more negative as the CCD increases.The value of η calculated from E vs Log t curves were used to elucidate the HER mechanism in this medium by plotting η against the reciprocal of the flux at different temperatures [189,218] Fig.89 shows the effect of change in the overpotential on the permeation current for experiments at different temperatures.

The theory of HER distinguishes between the two states of surface coverage i.e. low coverage where it is under Langmurian control and high coverage which follows the Temkin isotherm [217]. In all the curves plotted in Fig. 89 a distinctive break is observed towards high overpotentials which indicating a change of HER mechanism or coverage as the two are interlinked.The η vs Log i_c, Tafel plots shown in Fig.87 do not exhibit the same change of mechanism ; however, in some cases the experimental scatter could be interpreted as a break in the curves (see the 1.07 mm

curve and 65°C experiment). The overall values of $\partial\eta/\partial$Log ic as a diagnostic tool for evaluating HER has been used and found to be in good agreement with the proposed mechanism by Bockris et al who suggest a slope of 2RT/F =0.051 for a coupled discharge chemical desorption mechanism.In the present work, a slope of 0.060V/ decade was found which is in good agreement with their results.

The fact that hydrogen coverage has a bearing on the overpotential is well understood however, the changes in θ leading to wide variations in i_∞ and η are not usually discussed in terms of bulk properties of the substrate.For instance,the phenomenon of potential drift on a charging membrane has long been observed. Tafel[324] was first to observe the drift on iron cathodes in 1905, but Daft et al[190] see the changes in η with time only as a result of surface/electrolyte reaction.Kargol et al[197] observed changes in steady state potential (E_∞) with time during the galvanostatic charging of the membrane and attributed this to the change in charging medium or electrode surface condition [195,325]. However these authors neglect that part of their results which exhibits longer times required for attainment of steady overpotential for thicker membranes. This could indicate that the observed variation in η may be as a result of interactions between the bulk of the substrate and the surface hydrogen and not purely an electrolyte/substrate phenomenon.

It is this author's belief that the factor ignored in many discussions of this phenomenon is the role of diffusion in removing the adsorbed species away from the cathode surface. This will affect the rate constant for the adsorption step, K_{ads} since the removal of the products of that reaction accelerates the formation of more products, in this case adsorbed species. This means the surface coverage especially at the start of charging is not solely dependent on current density and pH as the following formula for θ. suggests:

$$\theta = \left(\frac{2K_{ads} C_{H^+}}{K_{ads}}\right)^{1/2} \exp(-\alpha \eta F/2RT) \qquad (239)$$

Since the rate of removal of the adsorbed species through diffusion process (in contrast to desorption via recombination route) plays a major part; The plots of η versus the reciprocal of membrane thickness in Fig.88 show increase in overpotential (more negative) with decrease in thickness. As the hydrogen movement through the iron membrane is fast, the adsorption rate constant K_{ads} is greater than K_{des} .

This implies that the rate constant for discharge reaction has to change in a way to maintain the supply of hydrogen atoms for a higher equilibrium between the adsorption-desorption step. Therefore, in physical terms, the surface concentration of hydrogen on a thin membrane is higher than that on a thicker one under identical conditions. This has been shown to be the case in the present results of over voltage

measurement on membranes of 0.07 mm, 0.205 mm and 1.07 mm thick. The flux shows a similar trend i.e. the hydrogen deposited in the thicker membranes establishes a much smaller flux as flux is inversely proportional to thickness ($J=DC_0/L$). Figs.69-70 show that under identical CCD the permeation of a membrane 1.07 mm thick, is much less than for a thinner 0.205 mm or 0.07 mm one.

Mathematical analysis of the thickness dependency of potential has been worked out here. According to Bockris and Subramanian [326], the hydrogen concentration in equilibrium with the surface hydrogen just inside the membrane (C_o) is:

$$C_o = 10^{3/4}.K_{des} \exp(-\eta F/4RT) \quad (240)$$

However, this equilibrium quantity could be expressed in terms of permeation current density (i_∞), egressing from a membrane as ;

$$C_o = L \cdot i_\infty /zFD \quad (241)$$

equating the two values of C_o, it is possible to work out the over potential as: (242)

$$\eta = \frac{2.303x4RT}{F} \text{Log} \frac{10^{3/4}.zFKdesD}{i_\infty} + \frac{2.303x4RT}{F} \text{Log} \frac{1}{L}$$

The above relationship could be simplified as;

$$\eta = A + 4RT/F \ln(1/L) \quad (243)$$

where A is a constant for any charging density and temperature equal to $4RT/F \ln(10^{3/4}.zFKdes\ D/i_\infty)$.

This model predicts a slope of 0.24 V/ decade for the plots of η vs Log1/L.In the present experiments however the slope was between 0.12-0.13 i.e. only half

the above value. Kargol et al[197] suggest a general formula based on the Bockris equation for the hydrogen fugacity as follows;

$$f_H = \exp(\eta F/Z^*RT) \qquad (244)$$

where Z^* could be -1/2, 1/2 or 2. In the light of the results investigated, this parameter represent the true condition of iron/hydrogen, when it adopts $Z^*=1/2$ value. Therefore the equation (241) using the value of $Z^*=1/2$ is modified to;

$$\eta = A + 2RT/F \ln(1/L) \qquad (245)$$

Fig.90 is obtained by plotting the overpotential of the membranes versus the reciprocal of temperature. Despite the scatter of points, the change to more negative potentials at lower temperatures and vice versa is clear. This could be explained in two ways. Firstly, the rate constant for adsorption-desorption mechanisms are temperature sensitive and as such less coverage occurs at higher temperature. The overpotenial variations on iron in terms of coverage as suggested by Kim and Wilde [219] shows this dependency

$$\theta = K \exp(- \eta F/RT) \qquad (246)$$

However, the change of coverage predicted on the basis of this mathematical modelling, is between 5-10% of the total coverage and as such could not account for the observed changes in this work. Furthermore, such explanation implies that the recombination reaction proceeds faster at higher temperatures to account for the lower (θ_H).However,the i_∞ vs ic curves (see Figs.69-70) show that at the same charging current, the amount

of hydrogen passing through a membrane is more in the case of a higher temperature experiment.It is therefore the diffusion process which provides the second interpretation ie the rapid inward diffusion of hydrogen away from the surface at higher temperatures leading to lower surface potentials.

The influence of hydrogen on the surface potential has been shown on other metal/hydrogen systems. Yayama et al [312] have demonstrated that the surface potential of $Ti\,Mn_{1.5}$ -H_x alloys becomes more negative as the concentration of hydrogen is increased. Further corroborative evidence exists to support the "diffusion dependent surface potential" hypotheses.

Hickling and Salt [327], followed HER experiments on different substrates and found Hg, W and electrodeposited metals need extremely short times to establish their steady state surface potential. In a series of experiments, they showed gold wires acting as cathodes have a drifting surface potential while the electrodeposited gold showed no drift at all. The same was true for platinized Pt wire which showed no drift while the drift on ordinary Pt wire never came to a rest.

Frankel and Latanision[328], were able to measure the associated potential changes in a Ni membrane under deformation while being continuously charged with hydrogen. They found an anodic shift of the surface

potential during the deformation which drifted back to more negative when the deformation stopped.The argument put forward by the above authors is based on the formation of new slip bands on the electrode surface during deformation.These slip bands, being more active will react with the aqueous environment and passivate leading to the observed increase in potential.

However, this explanation raises more questions than it answers. For example, if these fresh surfaces are filmed (even under cathodic conditions) to account for the observed increase in potential, why is the permeation flux on these membranes actually enhanced throughout the deformation period? It is well known that the permeability of hydrogen into a film clad Ni substrate is three orders of magnitude less than a film free electrode [83].

The postulation of a faster discharge on a fresh surface is not also proven as these surfaces are to be rapidly filmed to account for the change in potential.

Finally, if these changes were due to plastic deformation-as suggested- they should not be reversible which is contrary to EMF results (see Fig.116). These objections would not arise if the mechanism by which the potential variations occur is due to change in the surface coverage to a higher value than that during the deformation phase.

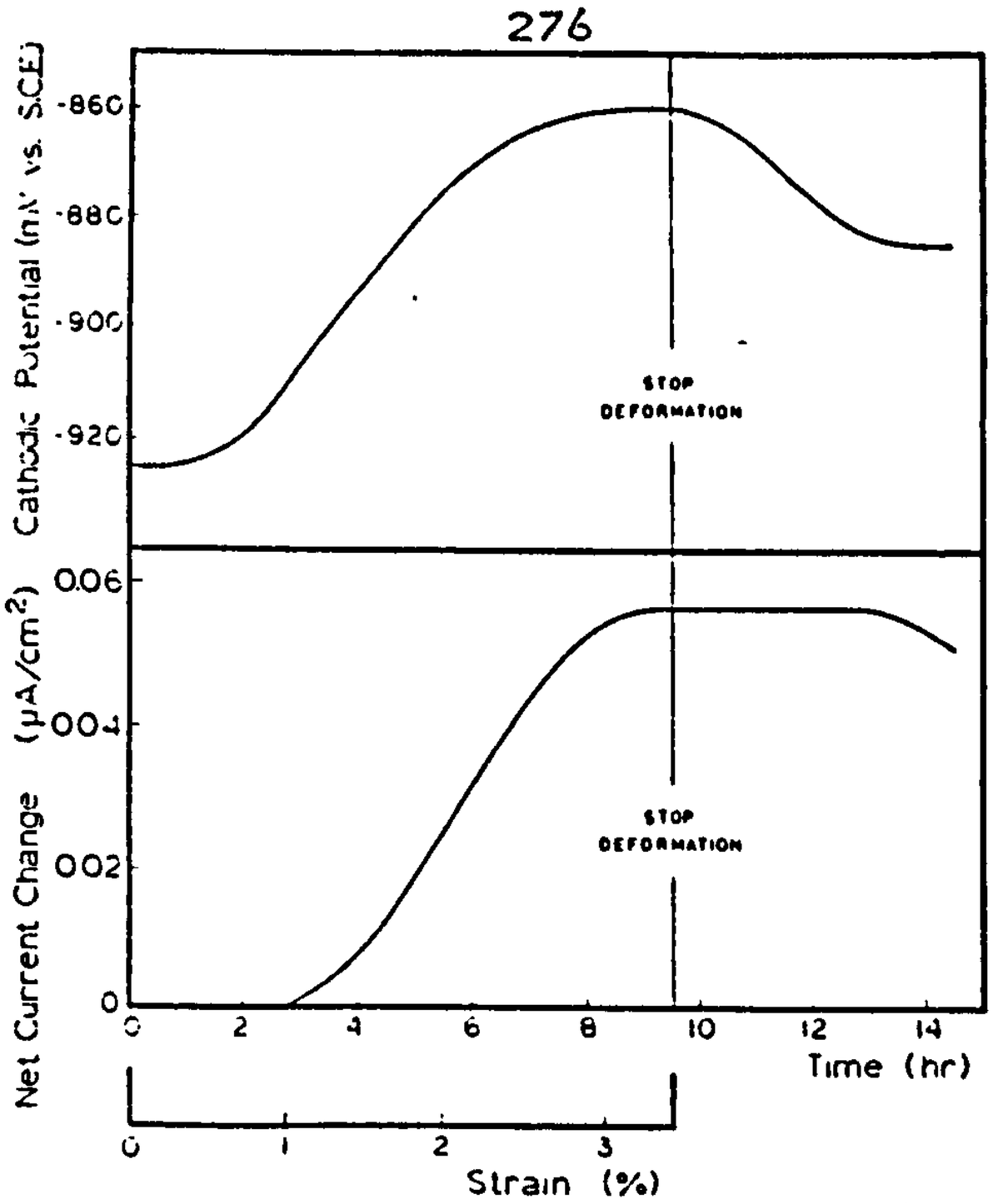

Fig.116 The potential-time, permeation flux-time curves for Ni membranes before, during and after deformation[329].

Such a hypothesis could be justified by the fact that hydrogen diffusion in Ni during deformation is 100-1000 times faster than when no deformation is occuring [330,356]. This obviously leads to a rapid flux which accounts for the increase in i_{∞}. Furthermore, as more hydrogen atoms move away from the internal sub-surface layer towards the bulk, the equilibrium between the hydrogen concentration just inside the membrane and the discharged hydrogen on the electrode is affected, resulting in a lower surface concentration during the deformation. This is believed to be sufficient to explain the observed changes as well as the reversibility of the results. It is noteworthy that since the potential shifts to more positive values during deformation,it indicates that hydrogen discharge occurs with less effort ie at more positive overpotentials. This phenomenon could also be explained using

the above hypothesis. As the rapid diffusion consumes the products of the Volmer reaction (discharge step) faster than they are produced;the disturbed equilibrium constant of the reaction needs to move to the right-as explained above- to generate more hydrogen which is then quickly removed since the inward diffusion is the rate determining step(rds). This could be justified using the already known kinetics and the thermodynamic characteristics of the HER [190] without any need for postulating changes in the mechanism of HER on Ni or assuming special properties for the filmed surfaces as discussed by Frankel[328].In a similar way, the changes observed by Salt and Hickling discussed earlier could be accounted for. For instance, the near instantaneous potential attainment of a mercury cathodic electrode could be explained by the extremely low diffusivity of hydrogen into Hg.As such, the change in the surface coverage due to hydrogen diffusion does not occur. On the other hand, the explanation for rapid attainment of potential by the electrodeposited materials,in contrast to bulk formed substrates, centres on the amorphous nature of electrodeposited films[28]. The structure of these amorphous films exclude grain bcundaries and many of the regions high in structural faults and defects. If a diffusion depends on grain boundary diffusion paths, an amorphous metal should drastically curtail or even stop it altogether. Kirchheim et al[311] have demonstrated a reduction of more than two orders of magnitude of the diffusion coefficient of hydrogen in amorphous Pd compared to its crystalline form. They

also showed the open circuit potential of the crystalline Pd to be much more noble than that of an amorphous Pd under identical cathodic CCDs. Nickel also has a grain boundary diffusivity value a hundred times more than its lattice diffusivity [329] and by removing these short circuits for hydrogen diffusion the surface coverage increases leading to more negative potentials compared to the crystalline structures.

In the course of the permeation experiments, the open circuit potential of the charging side was monitored long after the termination of the current. The result was a progressive climb to more noble values of potentials. The E-Log t curves show four distinctive breaks. The time duration for these breaks becomes progressively longer as the current density increases. The first break E_1, occurs at a potential of -1.05 ±0.02 V vs SCE, the second break E_2 happens at a potential of -0. 96 ±0.01 V vs SCE and the third and fourth breaks occur at - 0.75 +0.015 V vs SCE and -0.169+0.01 V vs SCE respectively.

These potentials correspond to the formation of a series of compounds on the surface.Using the proposed reactions for Fe/H_2O at different pH values summarised in Table 10,(passivity section),the following reactions have been chosen as a result of open circuit potential measurements. Electrode potential measurements are widely used as a diagnostic technique for the studies of passivation [330-332].

In the present work, the following three compounds were found to fit in a sequence of film nucleation and growth on iron in 0.1 mol/l NaOH. The first break corresponds to the following equations happening simultaneously,

$$2Fe+3H_2O \rightleftharpoons Fe_2O_3 + 6H^+ + 6e^- \quad (247)$$

$$E = -0.051 - 0.0591pH$$

$$@\ pH=12.7=-0.809\ V\ vs\ SHE$$

$$=-1.047\ V\ vs\ SCE$$

and

$$Fe+2\ H_2O \rightleftharpoons Fe(OH)_2 + 2H^+ + 2e^- \quad (275)$$

$$E = -0.047 - 0.0591pH$$

$$@\ pH=12.7=-0.800\ V\ vs\ SHE$$

$$=-1.042\ V\ vs\ SCE$$

This heterogeneous film formation process is very fast due to the thermodynamic propensity of iron to undergo this change.In the present experiments,the time between the start of nucleation and total surface coverage indicated by the attainment of the break point potential of -1.05 +0.02 V vs SCE was around 16 seconds. The potential thus measured is a mixed potential and as such shows a wide variation of $\pm$0.02 V. It is the opinion of the author that the film thus formed consists mainly of an inner layer of Fe_2O_3 containing a large number of water molecules with $Fe(OH)_2$ loosely settling on top.

The above reactions were not the only candidates for the film formation process as the observed potentials also correspond to those of FeO and

Fe_3O_4 formation. However, the fact that none of the above products could be followed in a logical chain of events based on the potential measurements, excludes them from the list. For instance FeO, an oxide with a potential close to the observed values, could not be followed beyond the first break. No mechanism based on this product could be proposed to account for the breaks happening at -0.96 V and -0.75 V vs SCE. In addition, the presence of Fe_2O_3 as a sublayer on iron electrodes is well documented [260,269,333,334].The film thus formed is established very quickly but it remains relatively thin. Kruger [335] has shown the total thickness of films formed on previously reduced iron electrodes in neutral solutions to be only 20Å after 1000 minutes of exposure. This implies that the film at this stage is no more than a few mono layers thick.

The second break occurs at a potential of -0.960+0.010 V vs SCE. This break in the potential-time curves is sensitive to the amount of hydrogen stored in the membrane and this is shown by its time dependency. The reaction taking place on the surface of the membrane occurs at the film/electrolyte interface. The fact that the $Fe_2O_3/Fe(OH)_2$ film formed at this stage is extremely thin, allows the migration of iron atoms through this layer to combine with water to form γ'-FeOOH on top. The assumption that iron diffuses out through oxide layers to engage OH^- or H_2O molecules or to combine with O is widely reported in the literature

[336-339] and as such does not require any deviation from the classical passivity models. The proposed reaction is as follows;

$$Fe+2H_2O \rightleftharpoons \gamma\text{-}FeOOH + 3H^+ + 3e^- \quad (248)$$

$E = 0.049 - 0.0591pH$

@ pH=12.7= -0.701 V vs SHE

= -0.941 V vs SCE

Here again a second reaction could be considered which will show the same potential at this pH. However the product which is $Fe(OH)_3$ as far as the present author is aware , has not been identified by any other worker on iron. Therefore in the absence of any corroborative evidence for $Fe(OH)_3$,the choice of γ-FeOOH seems justified. Furthermore, γ-FeOOH has long been suggested as a constituent of the multi-layer film on iron. During the time when γ-FeOOH is being formed effectively a mixed potential is being registered.One for the consolidation of Fe_2O_3 on the metal which continuously injects some of its water molecules back into the newly formed film on top.and the other which is the formation of the top layers.

As soon as the hydrogen activity and the thickness attained by the new film is such that energetically, the conversion of the $Fe(OH)_2$ to γ-FeOOH is favourable, a third reaction commences.

$$Fe(OH)_2 == \gamma\text{-}FeOOH + H^+ + e^- \quad (249)$$

$E = 0.240 - 0.0591pH$

@ pH=12.7 = -0.507 V vs SHE

= -0.750 V vs SCE

The film at the end of this stage will have only two layers, an Fe_2O_3 and a γ-FeOOH outer layer. The film formation process now concentrates on the thickening of these layers and also the redistribution of water molecules to the phase boundaries. The above reaction like the one preceding it, responds to the amount of hydrogen in the membrane and therefore could be prolonged or accelerated by the cathodic pretreatment prior to the onset of passivity.

The final break, however, has a very scattered distribution ie the minimum value observed here is -0.08 V vs SCE while the highest observed is around -0.25 V vs SCE.This wide degree of scatter, in contrast to the observations for other breaks, indicates that the cation deficient outer layer is continuously thickened and in doing so adopts varied potentials depending on the particular Fe/O ratio in the film. The role of hydrogen in such a case is more complex as it could be acting as a replacement cation.

This idea has been suggested by Kruger et al [270] and if applied in this case could explain the wide variations in potential because the hydrogen availability differs from experiment to experiment. Another relevant factor here is the incorporation of water molecules side by side with hydrogen as suggested by Okamoto[340]. The water molecules alter the Fe/O ratio and the scatter of the potentials could be

explained by the non-stoichiometric nature of the outer film.

The amount of water and hydroxyl molecules (OH) in this final structure may vary and that could be the cause of variations of slope in the E-Log t curves. However, the overall mechanism as proposed here remains the same. This model corresponds well with the one proposed by Sato et al [35,255] who found a similar double layer structure on iron in alkaline solution with the arrangement of layers in the same order as that proposed here.

The membranes on which these films were formed had all been precharged with hydrogen and therefore the passive films were affected by it in two possible ways. Firstly, all the passivation reactions proposed in this model generate hydrogen. This could be utilized to see if the chemical equilibria of these reactions are affected by the activity of stored hydrogen. If this were to happen, it could be expected that the duration of each reaction might be extended in direct proportion to the amount of hydrogen stored. Figs.82-86 show the effect of the CCD on the time taken for each of the above passivation potentials to be attained at different temperatures and thicknesses. There seems to be no question about the prolonging effect of charging current on the time to attain the break with the exception of the first break potential E1. This potential corresponding to the simultaneous formation

of Fe_2O_3 and $Fe(OH)_2$, seems to be unaffected by the charging current density used and by implication, the stored hydrogen concentration.

This could be explained by the fact the film formed at this stage, as Zakoczymski et al [341] put it is no more than a supersaturated hydroxide solution and not a solid oxide. This means that any hydrogen formed during this stage as well as the hydrogen effusing out of the membrane, will have little time to interact with the film.In thermodynamic terms, the products including hydrogen are removed from the reactants fast enough not to affect the forward rate of reaction. This situation lasts while no solid platform for interaction of hydrogen with film substance exists. At the end of the first stage, such a condition is established and the effect of hydrogen is shown.

All the plots for different temperatures and thicknesses show a striking increase in the time to attain potential with increase in CCD.Although the effects of temperature and thickness seem less pronounced it is obvious that hydrogen flowing out of the membrane interacts with the film formation process. The permeability of hydrogen in film free iron is around three orders of magnitude lower than that in a membrane covered with an oxide layer[83]. This drastic difference in permeability of film covered surfaces and the film-free ones raises the possibility that hydrogen concentration on the metal/film interface

is much higher than the film/electrolyte interface. This has been shown to be the case, and a large concentration gradient exists across the film [342]. As a result of this accumulation of hydrogen, the rate of escape through the film is the rds in the film growth during the second phase of passivity.

All the plots also show that the second stage of passivation i.e. γ-FeOOH formation to be sensitive to hydrogen concentration. The third plot in these figures shows a smaller slope, due to the fact that there is only one hydrogen atom generated in each act of film formation, compared to three such atoms in the γ-FeOOH formation during the second stage.

The final plots representing the E_4 break show little hydrogen effect.This could be as a result of two factors: first the amount of hydrogen in the membranes at these times is very small and the thickness of the film acts as a barrier to the hydrogen atoms effectively interfering with that process. Also hydrogen is incorporated in the film as a constituent which leads to a non-stoichiometric film with the potential determined by the degree of hydrogenation and water occlusion.However, even this final plot generally shows the progressive lengthening of the times, although the degree of scatter is much wider due to the above reasons.The role of hydrogen in passivation may be seen in works on other materials.However, the interpretation put forward is usually different from

that proposed here. Kim and Wilde [343] (Fig.117) show the effect of hydrogen formed in cathodic precharging on stainless steels. They found increased critical passivation current density due to this stored hydrogen, which they interpreted to be the result of hydrogen being oxidized upon egressing from the membrane. However, the fact that the maintenance CD was increased in direct proportion to the hydrogen concentration in the stainless steel electrodes could not be explained in this way. One basic problem with such explanation is that the permeability of oxide covered stainless steels is at least 1000 times less than that of the film free steels [83] An explanation based on the interaction of hydrogen with the film formation process could justify this increase in the electrical energy required to establish passivity.

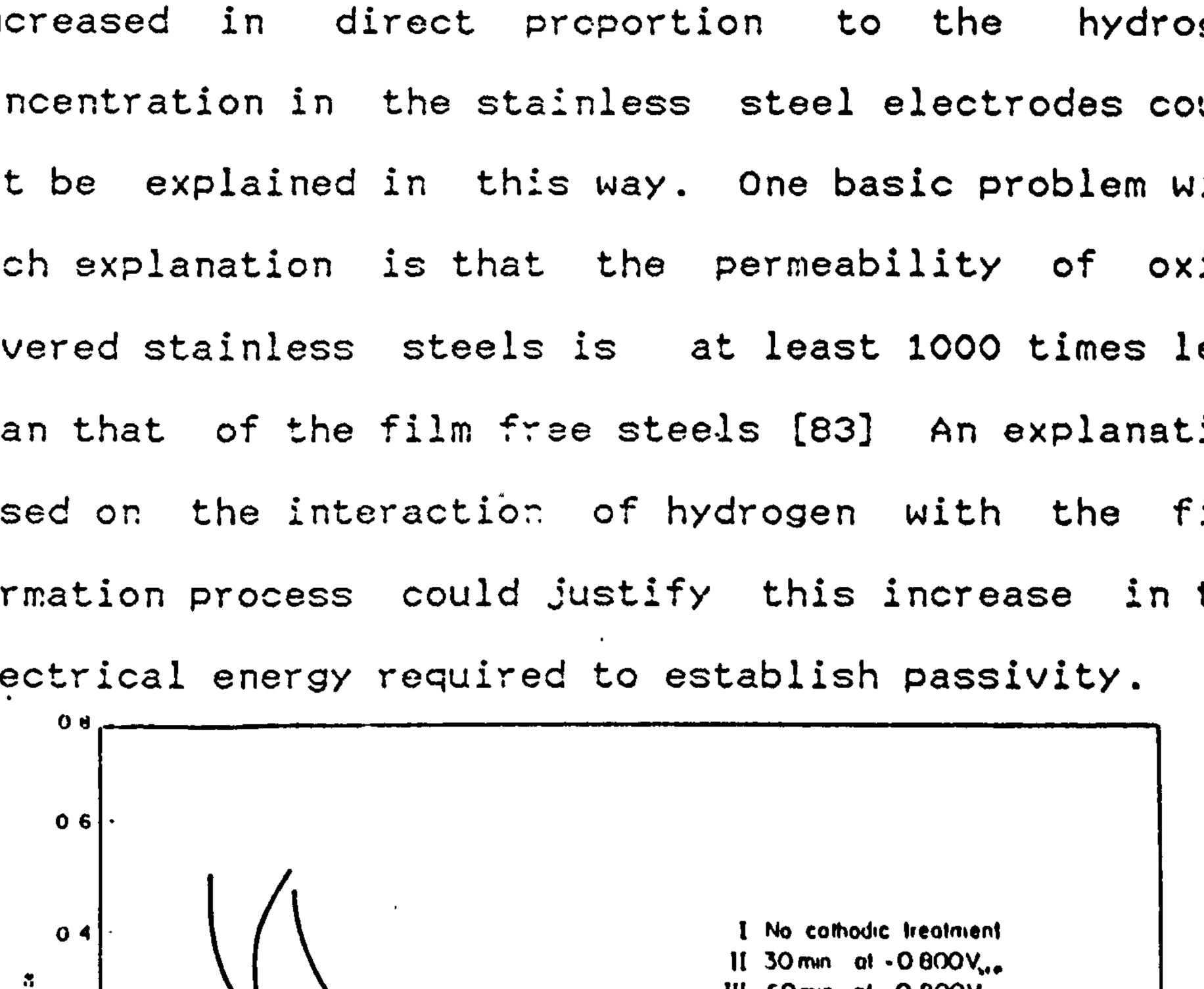

Fig.117 The effect of hydrogen concentration on the critical passivation current density in experiments on stainless steel. After Kim and Wilde[343].

In a recent publication,Oriani et al [344] have studied the effect of hydrogen on the pitting properties of Ni substrates charged with hydrogen. The anodic current,as a measure of passivity,showed drastic increase for those membranes charged with hydrogen when Cl^- ions were introduced into the solutions (see Fig.118)

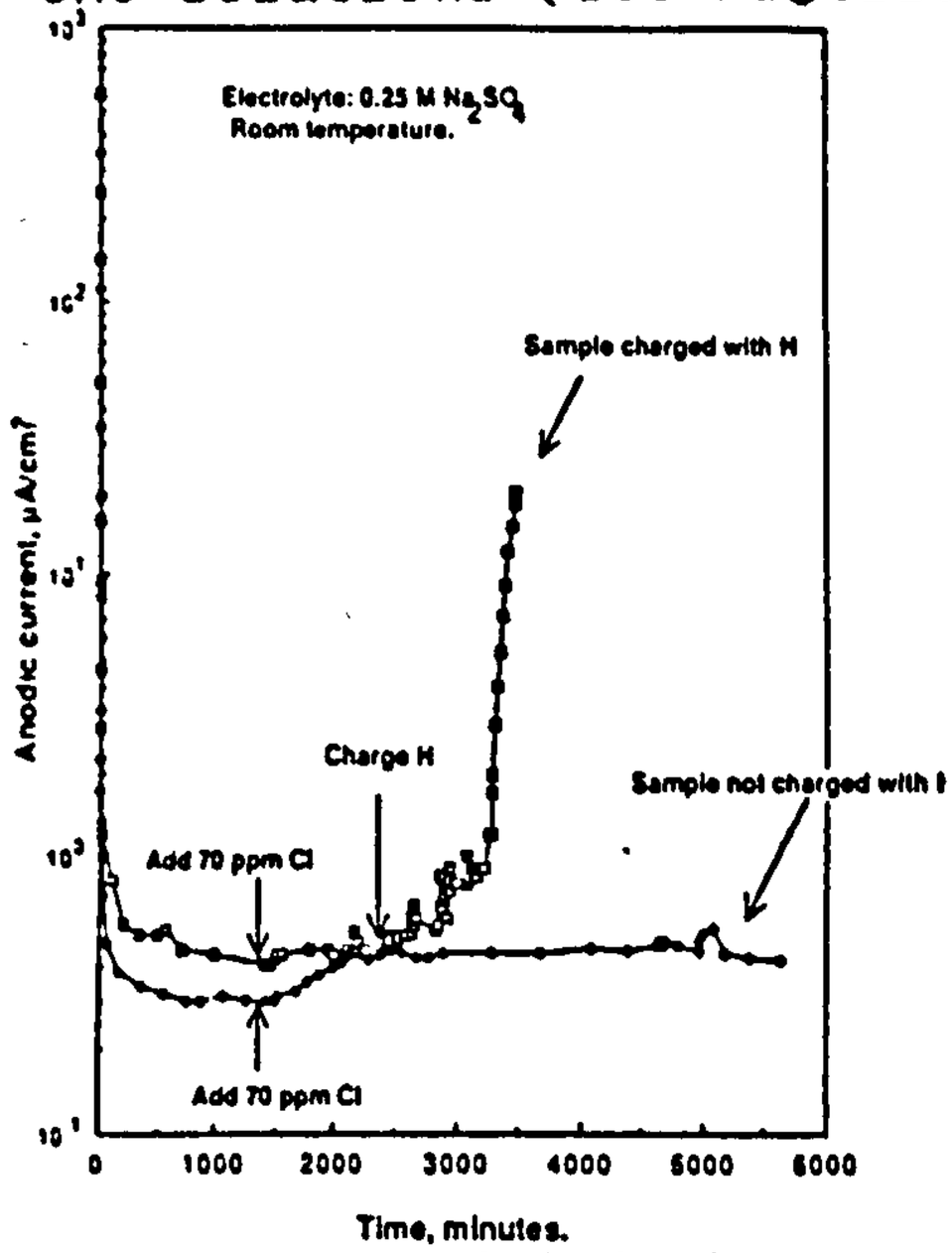

Fig.118 The membranes with hydrogen show a strong susceptibility for depassivation with introduction of aggressive (Cl^{-1}) anions After Oriani[344].

The membrane without hydrogen stayed totally unaffected by the Cl-bearing environment. This clearly shows the role hydrogen plays in weakening and perhaps reversing the film formation process.

In a similar experiment Zakvoczymski et al[341] report changes in the behaviour of iron during passivation in alkaline solution in the presence and absence of $Cl^-$and conclude this to be due to some variation in the composition and structure of the film. In this paper, they suggest a cathodic polarization pretreatment for their membranes which could well have

resulted in some hydrogen occlusion.It is this author's opinion that here again the depassivation properties of hydrogen could account for the acceleration in the pitting process without fundamental structure variation needed to explain it.

The proposed effect of dissolved hydrogen could be of fundamental importance, since in both "hydrogen embrittlement"and"stress corrosion cracking" phenomena, the passivation of the crack tips play a major role in propagation of the cracks [345,347]. In the case of stress corrosion cracking, the accepted theory is that the hydrogen liberated from the corrosive environment move preferentially ahead of the crack tip which itself is passivated under the influence of the medium.

Dmytrahk and Grabovski[254] claim that effective diffusivity of hydrogen is substantially affected by the pH of aggressive media on the passive layer. This assumption is inadequate to modify the extremely low diffusivity of hydrogen in the passive film to an extent sufficient to explain the processes involved.

For example, in the case of iron, the 100-1000 times reduction in the effective diffusivity could hardly be compensated by its enhancement as a result of Cl effect, proposed by the above authors.The figures given by these workers [254] for the change of diffusivity in film covered membrane shows an increase

by a factor of only two i.e. from $5x10^{-7}$ $cm^2 s^{-1}$ to $1x10^{-6}$ cm^2 s^{-1}.

However, applying the "hydrogen interaction model" proposed here, enough hydrogen could enter the stress field ahead of the crack tip before the hydrogen activity falls below a level which could influence the passivation appreciably. The proposed delay in film formation,could be of importance, not only in the cases of iron and steel for which the diffusivity values drop by up to three orders of magnitude, but it may also provide other routes for explaining cases such as Ta for which reductions of staggering 10^{10} times in hydrogen absorption is reported in the presence of oxide layers only 2-3 mono-layer thick[348]

A more elaborate mechanism by which hydrogen might have affected the passivation process would have been through a process of bonding between hydrogen/iron atoms. This would have resulted in preventing the iron atoms from migrating out towards the other reactants to form the passivation products. The binding energy between a pair of iron atoms is given as -0.25 eV at an average distance of 2.56 nm to 3.07 nm [349.350] while the strength of the Fe/H bond is reported to vary between -0.55 eV at an average distance of 1.9 nm by White and Kahn[351] to -0.62 eV at an average distance of 1.93 nm by Machlin[352].Therefore it could be argued that hydrogen stored in the membrane establishes a high coverage under the film [342] and in selected cases

forms a bond which being stronger than Fe/Fe bond could prevent iron from diffusing out and contributing to the film formation process.

The amount of hydrogen at the tail end of a permeation experiment drops to around 0.1 $\mu A cm^{-2}$ The number of moles represented by this current density would be $0.1x10^{-6}$ /96487 = $1.03x10^{-12}$ mol cm^2 s^{-1}. Since each mole of hydrogen has the equivalent of the Avagadro's No. atoms in it,the total number of hydrogen atoms per second reaching the surface of the charged electrode could be $1.03x10^{-12}$ * $6.02x10^{23}$ = $6.23x10^{11}$ atoms s^{-1}. The number of iron atoms on the unit area of such electrode is reported as $1.7x10^{15}$ atoms cm^{-2}, . [158],therefore the ratio of the hydrogen to iron atoms is $3.67x10^{-4}$ or nearly 4 atoms of hydrogen for every 10000 atoms of iron.

Although this represents the tail end of the permeation transient,the result obviously precludes the possibility of a major effect through"hydrogen binding" on the passivation process.Furthermore,if Fe/H binding were responsible for the decrease in the passivation rate, then it should have had the same effect on the last stage of passivation as on the first, second and third which is obviously not the case. The only logical conclusion is that hydrogen influences passivation by reversing the film formation reactions.

The role of hydrogen is preventing the passivity could have been demonstrated clearly if the same

membrane undergoing passivation could be shown to behave differently merely by changing the amount of hydrogen stored inside.

This was made possible by addition of As^{3+} to the charging solution after an experiment was completed on a membrane. As^{3+} is known to be a hydrogen promoter and therefore should drastically enhance the hydrogen concentration inside the membrane. However, the potential measurement result during the passivation phase on such membranes were totally unexpected.Fig.97 shows the potential-time plots for As doped membranes. It is evident that no E_3 or E_4 breaks are shown in the curves. This leads to the conclusion that somehow the whole film formation process has been affected.

Smialowski[353] has shown a reduction in the egress of hydrogen from iron membranes in the presence As, Sb, Se and Te - all known promoters - is due to the physical blockage of the metal sites for the entry of hydrogen.This has been born out in our experiments as it seems As^{3+} is incorporated in the film, altering its formation mechanism.

The same interference with the film formation process was observed when using EDTA (see Fig.96). Here, the cause could be the complex forming properties of EDTA which could prevent ferric ions bonding to hydroxyl ions.

In a series of different experiments, the reducing properties of stored hydrogen was tested by charging an already passive electrode face (monitored side) from the other side. Fig. 92-95 are the result of these experiments. The series of reduction plateaux observed reveal that the final phase of depassivation, attainable under such conditions is the E_2'=-0.960 V vs SCE.This is the potential for the second break in the E-Log t curves which has been shown to be the potential corresponding to the γ-FeOOH formation.

The effect of hydrogen activity in these experiments is evident by comparing time taken to reach this potential in experiments 92 and 93. Experiment 92 was carried out at 12 μA cm^{-2} while number 93 was conducted at 30 μA cm^{-2}.The eventual time to attain the E_2 break potential was in excess of 250 hours for an airborne film in experiment 92, decreasing to 70 hours on application of a higher CCD.Any increase in CCD was incapable of further reducing the surface potential from -0.980 V vs SCE as depicted in Fig.94. It seems that H has no effect on the film layer adjacent to the metal surface ie γ-Fe_2O_3 .

Fig.95 shows the results of an experiment designed to show whether hydrogen effect is different on an air-formed film to one formed in alkaline solution. This was achieved by reducing both sides of a membrane first and then allowing both sides to passivate up to a potential of -0.700 V vs SCE. At this

point the charging was re-established on one side. The change in potential on the other side is shown in Fig.95.

The time to attain a potential of-1.05 V vs SCE was short and between 2-3 hours.The final potential corresponding to E_1, never fell below this value but the fact that this potential was attained so quickly points to a difference between the air-formed film formed upon contact with air,and the γ- Fe_2O_3/ γ'-FeOOH formed exclusively in aqueous solution. It is obvious that the air-formed oxide, totally anhydrous in nature has a different morphology and probably is more coherent than the alkaline formed one. This explains the time variations between the two types of films.

AC impedance measurements were also used to establish the properties of the surface film.Fig.101-115 show the onset of film formation on a membrane previously charged with hydrogen at a CD of 100 μA cm^{-2} for 12 hours. The immediate charge transfer impedance reading at the potential of -1.02 V vs SCE is 159 $\Omega\, cm^2$ Considering that a freely corroding iron electrode in H_2SO_4 at pH=0 and potential of -1.0 V vs SCE shows an impedance of 120 Ωcm^2 , this result could be safely be extrapolated to confirm a film-free surface prior to the termination of CCD. This constitutes an extra proof for the existence of a film free cathodic surface prior to the passivation.

As has been stressed throughout this research no evidence of inadequate film reduction or impaired HER was found.This could have been seen as an unusually enhanced flux after long periods of charging or major discrepancies between the permeation current results obtained at the lower charging current densities where the possibility of "unreduced" passive film must be higher.

The AC impedance results were consistent in showing increases in the charge transfer impedance (R_{Ct}) This is the resistance to electron movement through the film and could be taken as evidence of film thickening. The equivalent circuit, based on the Bode plots shown in Fig.101-115 suggest the dielectric or semiconductor film model [354] as presented in Fig.119

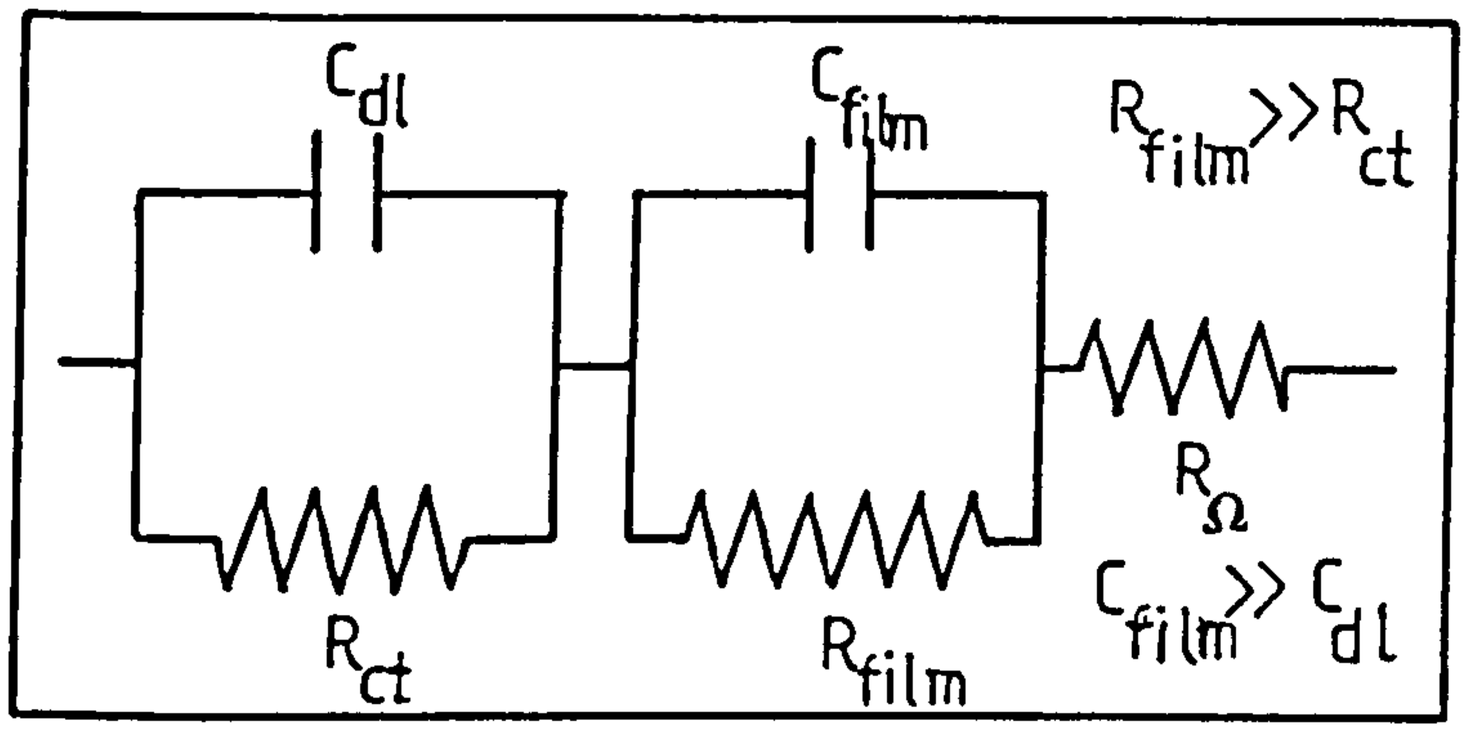

Fig.119 A semiconductor model for iron passivation. After Shiro Haruyama[354].

However using the Randles Z' and Z'' vs $\omega^{-1/2}$ plots, and the diagnostic criteria explained in the passivity section, the film growth seems to be only under charge transfer control i.e. $C_{film} < C_{dl}$ and a low film impedance. It is only at very high positive potentials

that the film shows the pseudo-capacitance expected from a semiconducting model. The R_Ω/σ ratio as diagnostic criteria for the model controlling the process, consistently shows a diffusion controlled mechanism.This contradicts the earlier findings showing a charge transfer controlled process.

Due to long periods of time needed for monitoring each AC impedance experiment, especially at high frequencies, the potential could not be fixed to correspond to the very important E_2 and E_3 breaks. All the experiments, up to the potential of -0.136 V vs SCE, show the film formation to be .under complete Warburg control also which confirms the effect of diffusing species. This implies that some diffusion process is involved in the film formation.

To determine whether the diffusion of ferrous or ferric ions is responsible for these results, ICAP spectroscopy experiments were carried out in which samples of the electrolyte next to the passivating face were analyzed for iron concentrations. The results shown in Table 17 indicate extremely low concentrations of iron. This could lead to the conclusion that it is not the deposition of Fe^{2+} or Fe^{3+} from the solution which is responsible for the diffusion controlled part of process. It is either, the movement of ferrous and ferric ions outwards through the film or the incorporation of OH ions or even the diffusion of H^+ and its effects on the film is registered as the Warburg

impedance. It is highly probable that all these three, occur simultaneously and contribute to the observed effect. The experiment conducted at -0.136 V vs SCE shown in Fig.113 exhibits a high impedance. This confirms the reports by Foley et al[270], Bloom and Goldenberg [355] that γ-Fe_2O_3 is a poor electronic conductor and as γ-FeOOH thickens,a progressive increase in impedance occurs.

Overall,the AC impedance experiments did not elucidate the mechanisms of passivity as much as the permeation and electrode potential measurements. This was mainly because the length of time required prevented the investigation of the very important E_2, E_3 and E_4 potentials.

6.....CONCLUSION

6.1 Using the known criteria reported for the surface preparation in the literature, it was shown that the permeation of hydrogen in the experiments carried out was only under diffusion control and also the diffusion process itself was not under trapping control.

6.2 A concentration independent diffusion value of 2.67×10^{-5} cm^2 s^{-1} was calculated in Armco iron which is in good agreement with the reported values in the literature.

6.3 The activation energies calculated showed a degree of concentration dependency. This was eliminated at charging current densities above 120 μA cm^{-2} which indicates that as the existing trapping sites are saturated, the activation energy tends to the lattice diffusion value. An activation energy of 10.26 kJ/mol was deduced from these experiments which is in close agreement with the lattice diffusion activation energy.

6.4 Experiments devised to show the effect of electro-migration of protons, have shown the contribution of this mode of transport to the permeation of hydrogen. This effect could only be shown where the lattice relaxation time (t_d) is long enough to show minor changes in concentration due to the field effect.

6.5 A cell, capable of monitoring the motion of hydrogen out of a thick cube has been constructed and tested.

6.6 Mathematical analysis of diffusion in a thick membrane in conjunction with the above experiments has been put forward. Based on this model, a diffusion coefficient of 2.04×10^{-5} $cm^2 . s^{-1}$ is determined for a 6.5 mm side cube of mild steel. This shows good agreement with the thin membrane diffusivity value.

6.7 Claims as to the impossibility of reducing an iron electrode without the use of EDTA reagent have been refuted and alternative arguments for results supporting such claims have been presented.

6.8 Tafel plots for hydrogen evolution reaction on iron electrodes confirm the coupled discharge, chemical desorption mechanism.

6.9 The effect of thickness of an electrode on its surface potential is investigated and a mechanism for the observed dependency is put forward. Mathematical analysis of the problem has led to the following relationship for the overpotential:

$$\eta = A + 2RT/F \ln 1/L$$

6.10 The effect of temperature on the overpotential has been investigated and qualitative analysis presented. Overpotential on an iron electrode during the hydrogen charging becomes more negative at lower temperatures and vice versa due to the rapid inward diffusion of hydrogen , away from the surface at

higher temperatures resulting in lower coverage and less negative potentials.

6.11 Potential drift observed on many metals upon application of cathodic polarization could be contrasted with metals such as Hg, W and electrodeposited metals with very low hydrogen diffusivity, to show the important role of hydrogen diffusion on this electrode characteristic .

6.12 Alternative analysis of the data in the literature, on the basis of the proposed role of hydrogen coverage/diffusion has been put forward. For example, nickel's change of potential under tensile stress could be explained much more straight forwardly through the role of hydrogen .

6.13 Hydrogen effusion from electrodes has been proposed as a technique for characterizing the passivation phenomenon on iron and steel and also nickel.

6.14 Iron membranes charged with hydrogen and left to passivate in 0.1 mol/l NaOH, have shown an open circuit potential which drifts to more positive values all the time. Every electrode will exhibit three distinctive breaks at -1.05 ±0.02 V vs SCE, - 0.96 ±0.01 V vs SCE and -0.75 ±0.015 V vs SCE with a fourth break showing a wider fluctuation around -0.167 V vs SCE.

6.15 A passivation mechanism based on the above potentials has been suggested as follows:

STEP1

$$2Fe+3H_2O \rightleftharpoons Fe_2O_3 + 6H^+ + 6e^-$$

$$Fe+2H_2O \rightleftharpoons Fe(OH)_2 + 2H^+ + 2e^-$$

STEP2 $Fe+2H_2O \rightleftharpoons \gamma\text{-}FeOOH+3H^+ + 3e^-$

STEP3 $Fe(OH)_2 \rightleftharpoons \gamma\text{-}FeOOH+ H^+ + e^-$

The final result is a two layer passive film made of $\gamma Fe_2O_3 / \gamma$-FeOOH.

6.16 The final potential break is the result of the growth and the decrease in the Fe/O ratio in the outer layer leading to more non-stoichiometry in the oxide.

6.17 The reason for the prolonged effect of hydrogen on the passivation , is the effect on the equilibrium constant of the reactions in stages 1, 2 and 3.

6.18 The low activity of hydrogen in the membrane, precludes the possibility of H/Fe bonding as an alternative mechanism for the observed increases in the time to attain the break point potentials.

6.19 The universal time to attain the first break E_1 at 16±1, is the proof of the loose binding of the first oxide formed and its saturation with water. This means hydrogen passes through the film without much effect on the equilibrium constant as there is no platform for interaction at this stage.

6.20 Hydrogen interaction mechanism proposed above, could be utilized to explain many sets of data in which the explansion put forward depends on the changes in the properties of the films or secondary effects,such as changes in the composition of the film Pitting phenomenon in hydrogen-charged, passivated Ni in the presence of Cl^-, was explained on the basis of

hydrogen interaction with the film rather than proposed variations in the film.

6.21 "Hydrogen interaction model", could also be used to explain certain aspects of crack propagation in hydrogen embrittlement and stress corrosion cracking. This serves to clarify how a small amount of hydrogen could enter stress fields ahead of the crack tips without the need to diffuse through the oxide films of extremely low permeability towards hydrogen.

6.22 Although no fundamental difference could be claimed to exist between the compounds forming the passive layers on an air-formed film and one formed in 0.1 mol/l NaOH, the morphology of them must be different, as no amount of hydrogen could depassivate an air formed film while a film formed exclusively in an electrolyte could be easily and rapidly reduced by diffusing hydrogen.

6.23 Using AC impedance, it was shown that a membrane entering passivity has an impedance of 159 $\Omega\ cm^2$. Since the impedance of a freely corroding iron electrode in H_2SO_4 at a similar potential is 120 Ωcm^2 it was possible to conclude that the surfaces used in these studies during the hydrogen charging were totally film free.

6.24 R_Ω/σ ratios and Randles plots resulted from the AC measurements both point to the fact that the reactions in the passivation process were under diffusion control. This could be the collective effect of H^+, Fe^{2+} or Fe^{3+} outward or OH^-, O^{2-} inward diffusion showing up as Warburg impedance.

6.25 No appreciable amount of Fe^{2+} or Fe^{3+} were found in analysing the electrolyte and therefore the deposition of these ions from the solution could not be responsible for the diffusion control of the process.

6.26 AC impedance measurements are not the best techniques for evaluating the effect of hydrogen on passivity.

7.....SUGGESTIONS FOR FURTHER WORK

The above conclusions have led to a considerations of the following items as being worthwhile for future researches:

7.1 Ellipsometric investigation of the film formation process on iron electrodes with stored hydrogen.

7.2 Investigation of the effect of hydrogen on passivity of mild steel and stainless steels.

7.3 Investigating the passivation mechanism of nickel using the hydrogen effusion technique.

7.4 Establishing the effect of cold work on the "hydrogen interaction model".

7.5 Investigation of the use of the internal traps and anti-traps to prevent HE and SCE, in the light of the "hydrogen interaction model".

7.6 3-D experiments on single crystals to elucidate the role of plane directions on the movement of hydrogen.

APPENDIX.1

The problem of three dimensional diffusion could be understood by solving the general Fick's second law:

$$1/D \cdot \partial C/\partial t = \nabla^2 C \qquad (1)$$

the boundary conditions in the case of 3-D experiments described in section 4 are:

$$C=0 \quad @ \quad -a<x<a \quad @ \quad t=0 \qquad (2)$$

$$C=0 \quad @ \quad -b<y<b \quad @ \quad t=0 \qquad (3)$$

$$C=0 \quad @ \quad -c<z<c \quad @ \quad t=0 \qquad (4)$$

$$C=0 \quad @ \quad x=-a \quad @ \quad t>0 \qquad (5)$$

$$C=C \quad @ \quad x=a \quad @ \quad t>0 \qquad (6)$$

$$C=0 \quad @ \quad y=-b \quad @ \quad t>0 \qquad (7)$$

$$C=0 \quad @ \quad y=b \quad @ \quad t>0 \qquad (8)$$

$$C=0 \quad @ \quad z=-c \quad t>0 \qquad (9)$$

$$C=0 \quad @ \quad z=c \quad t>0 \qquad (10)$$

The two boundary conditions (9) and (10) are not practically achievable and in the present experiments the very low concentrations present on these faces are approximated to zero in order to proceed to a meaningful solution to the diffusion problem.

The variables y and z may be eliminated by considering a Fourier series for a function of period 4b, which is an even function and f=1 if $0<y<b$ and f=-1 when $b<y<2b$. Then the function f(y) is represented by a cosine series of the form

$$f(y) = 1/2\ A_0 + \sum^{\infty} A \cos(n\pi y/2b) \qquad (11)$$

by the application of usual formula

$$b \cdot A_n = \int_0^b \cos(n\pi y/2b)dy - \int_b^{2b} \cos(n\pi y/2b)$$

$$= 4b/n\pi \sin(n\pi/2) \qquad (12)$$

In the particular case of $0 < y < b$

$$1 = 4/\pi \sum_{l=0}^{\infty} (-1)^l \cos\{(2l+b)\pi y/2l\}/(2l+1) \qquad (13)$$

where l is an integer (0,1,2,3,...). Then if we write a function C, dependent on x, y, z, and t as:

$$C(x,y,z,t) = \frac{16}{\pi} \sum\sum C_{l,m}(x,t) \frac{(-1)^{l+m}}{(2l+1)(2m+1)} \cos\left\{\frac{(2l+1)\pi y}{2b}\right\}$$

$$\cos\left\{\frac{(2m+1)\pi z}{2c}\right\} \qquad (14)$$

The boundary conditions on $y=\pm b$, $z=\pm c$ are automatically satisfied and we are left to solve

$$\frac{1}{D} \cdot \frac{\partial C}{\partial t} = \left\{ \frac{\partial^2}{\partial x^2} - \beta^2_{l,m} \right\} \cdot C_{l,m} \qquad (15)$$

where $$\beta^2_{l,m} = \pi^2/4\left\{ \frac{(2l+1)^2}{b^2} + \frac{(2m+1)^2}{c^2} \right\} \qquad (16)$$

Equation (15) is to be satisfied subject to the initial condition

$$C_{l,m} = 0 \quad @ \quad t=0 \quad @ \quad -a < x < a \qquad (17)$$

$$C_{l,m} = C \quad @ \quad x=-a \quad @ \quad t>0 \qquad (18)$$

$$C_{l,m} = 0 \quad @ \quad x=a \quad @ \quad t>0 \qquad (19)$$

By applying the Laplace transform

$$\mathcal{L}\{C_{l,m}\} = \bar{C}_{l,m} = \int_0^{\infty} \exp(-st) \cdot C_{l,m}(x,t)dt \qquad (20)$$

$$\mathcal{L}\{\frac{\partial C_{l,m}}{\partial t}\} = s\bar{C}_{l,m} \qquad (21)$$

Integrating by parts using the initial conditions and write for convenience β for $\beta_{l,m}$ and $p^2 = s/D + \beta^2$ we will have :

$$\frac{\partial^2 \bar{r}}{\partial x^2} - p^2 \bar{r} = 0 \qquad (22)$$

The boundary conditions are therefore expressed as:

$$\bar{r} = \bar{C}_{l,m}(-a,s) = C_o \cdot \int_o^\infty \exp(-st)\, dt$$

$$\bar{r} = -C_o/s \qquad @\ x=-a \qquad (23)$$

$$\bar{r} = \bar{C}_{l,m}(a,s) = 0 \qquad @\ \bar{r} = a \qquad (24)$$

Equation (22) and the second boundary condition is satisfied with:

$$\bar{r} = A\sinh\{p(a-x)\} \qquad (25)$$

and then using the first boundary condition

$$\bar{r} = C_0/s \, \frac{\sinh\{p(a-x)\}}{\sinh 2pa} \qquad (26)$$

This equation has now to be interpreted. The inversion integral gives:

$$\bar{r}(x,t) = 1/(2\pi i) \int_{C-i\infty}^{C+i\infty} \exp(st).\, \bar{r}(x,s)\, ds \qquad (27)$$

$$= C/(2\pi i) \int_{C-i\infty}^{C+i\infty} \frac{\exp(st)}{s} \, \frac{\sinh\{p(a-x)\}}{\sinh 2ap} ds \qquad (28)$$

Contributions will be made to the integral by singularities of the integra and in this case it just means

S=0 and/or Sin 2ap=0 Therefore the contribution from S=0 is:

$$\lim_{S \to 0} S \cdot \frac{C \exp(St)}{S} \cdot \frac{\sinh\{p(a-x)\}}{\sinh 2ap}$$

$$= C_o \frac{\sinh\{\beta(a-x)\}}{\sinh 2\beta a} \qquad (29)$$

The case of sinh 2ap =0 arises whenever $2ap = k\pi i$,(k= 0, ±1, ±2 ...). However k=0 does not give a singularity as :

$$\lim_{p \to 0} \frac{\sinh\{p(a-x)\}}{\sinh 2ap} = \frac{a-x}{2a} \qquad (30)$$

Thus the singularities to be considered are for k=+1,+2 etc., ie

$$s = -D\left\{\beta^2 + \frac{k^2 \pi^2}{4a^2}\right\} = -s_k \qquad (31)$$

Using the same approach as that used before, the contribution to the integral is:

$$\lim_{S_k+S \to 0} (S+S) \frac{C_o \exp(St)}{S} \cdot \frac{\sinh(p(a-x))}{\sinh 2ap}$$

$$= -\frac{C \exp(-st)}{s_k} i \sin\{\frac{k\pi}{2a}(x-a)\} \lim_{S_k+S \to 0} \frac{S_k+S}{\sinh 2ap} \qquad (32)$$

and by the L'Hopilal rule, the last limit is:

$$\frac{1}{[d/ds\ \sinh 2pa]} = \frac{1}{[2a\cosh 2pa\ dp/dS]_{S=-S_k}}$$

$$= \frac{(-1)^k}{2a}\,[2pD]_{S=-S_k}$$

$$= \{(-1)^k\, D\, k\pi i\}/\ 2a^2 \qquad (33)$$

To revert to equation (15) which again we rewrite using (γ) as:

$$\frac{1}{D}\cdot\frac{\partial\gamma}{\partial t} = \left\{\frac{\partial^2}{\partial x^2} - \beta^2\right\}\gamma \qquad (34)$$

subject to the initial conditions:

γ=0 @ -a<x< a @ t=0

$\gamma=C_0$ @ x=-a @ t>0

γ=0 @ x= a @ t>0

The steady distribution

$$\gamma_0 = C_0\,\frac{\sinh\{\beta\,(a-x)\}}{\sinh 2\beta a} \qquad (35)$$

satisfies the equation but not the initial boundary conditions . Now let $\gamma(x,t) = \gamma_0(x) + \gamma_1(x,t)$ so that $\gamma_1(x,t)$ satisfies the equation at the initial condition

$$\gamma_1(x,0) = -\gamma_0(x) \quad @ \quad t=0$$

while for t>0 , $\gamma_1(-a) = \gamma_1(a,t) = 0$

Put for convenience $\xi = a-x$

then, $$\gamma_1 = \sum_{k=1}^{\infty} F_k \sin\left(\frac{k\pi\xi}{2a}\right)\exp\left\{-D\left[\beta^2 + \frac{k^2\pi^2}{4a^2}\right]t\right\} \qquad (36)$$

so that

$$-C\,\frac{\sinh\beta\xi}{\sinh 2\beta a} = \sum_{k=1}^{\infty} F_K \sin\left(\frac{k\pi\xi}{2a}\right) \qquad (37)$$

where F_k according to the usual formula for a Fourier coefficient is:

$$F_k = \frac{-C_o}{a\,\sinh(2\beta a)} \int_0^{2a} \sinh\beta\xi \sin\left(\frac{k\pi\xi}{2a}\right) d\xi \qquad (38)$$

$$= \frac{-C_o}{a\,\sinh(2\beta a)}\, I_m \int_0^{2a} \cosh\left(\beta + \frac{ik\pi}{2a}\right) d\xi$$

$$= \frac{-C_o}{a\,\sinh(2\beta a)}\, I_m \left\{ \frac{\sinh[(\beta + ik\pi/2a)2a]}{\beta + ik\pi/2a} \right\}$$

$$= \frac{-C_o}{a\,\sinh(2\beta a)}\, I_m \left\{ \frac{(-1)^{k\{\beta - ik\pi/2a\}}}{\beta + [(k\pm\pi)/4a]} \sinh 2\beta a \right\}$$

$$= \frac{2\cdot\pi\cdot k\cdot C_o}{4a\beta + k\pi}$$

With the strong exponential time decay in the expression of $\gamma_1(x,t)$, this expression will clearly give a useful representation of the solution for moderate and long times. It will not in general be quite so convenient a representation for small values of time.

A standard property of the Laplace transform is however, that if an expansion could be found from the transform in a form valid for values of S that have large real parts, then if this expansion is inverted, term by term, a representation of the original function suitable for small values of time could be found. Now from equation (26)

$$\overline{r} = \frac{C_0\{\exp[p(a-x)]-\exp[-p(a-x)]\}}{s\{\exp(2pa) - \exp(-2pa)\}}$$

$$= \frac{C_0}{s}\exp[-p(a+x)]\{1-\exp[-2p(a-x)\{1-\exp(-4pa)\}^{-1}$$

$$= \frac{C_0}{s}\sum_{k=0}^{\infty}\{\exp[-p(a+2+4ka)]-\exp[-p(3a-x+4ka)]\} \quad (39)$$

Thus if f(t,d) has the Laplace transform ,[exp(-pd)]/s where $p=\sqrt{(s/D+\beta^2)}$, and this square root is interpreted in a way that when S has a large positive real part so 'p' has a simple pole at S=0 and a branch point at $s=-D\cdot\beta^2$. The contribution to f(t,d) from the pole is just, $\exp(-\beta\cdot d)$.

Note that this limit is independent of time.

$$\overline{r} = C_0\sum_{k=0}^{\infty}[f(t,a+ka)-f(t,3a-x+4Ka)]$$

To obtain the contribution from the branch point from a contour integral we write;

$$\frac{1}{2\pi i}\int_e \frac{\exp(st-Pd)}{} ds \quad (40)$$

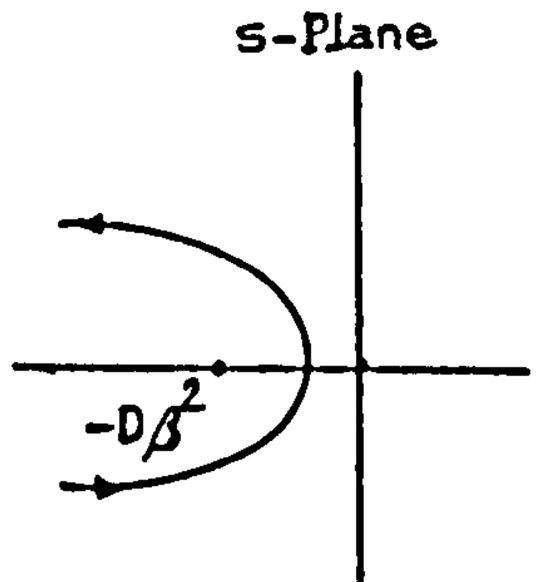

If we put $\zeta = s/D + \beta^2 = r\cdot\exp(i\cdot\theta)$ it is possible to write : (41)

$$\frac{\exp(-D\beta^2 t)}{2\pi i}\int_e \frac{\exp(\zeta Dt - d\sqrt{\zeta})\, d}{\zeta-\beta}.$$

Noting that $\sqrt{\zeta} = \sqrt{r}\ .\ \exp(i\,\theta/2)$ on AB, $\sqrt{\zeta}=-i\ \sqrt{r}$ etc., then the integral can be separated to give:

$$\frac{\exp(-D\pi^2 t)}{2\pi i}\left\{\int_{\infty}^{\delta}\frac{\exp(-rDt+id\sqrt{r}}{r+\beta^2}+\right. \tag{42}$$

$$\left.+i\delta\int_{-\pi}^{+\pi}\frac{\exp(\delta Dt\, e^{i\theta}-d\sqrt{\zeta}\, e^{i\theta/2}+i\theta)d}{\delta e^{i\theta}-\beta^2}+\int_{\delta}^{\infty}\frac{\exp(-rDt-id\sqrt{r})dr}{r+\beta^2}\right\}.$$

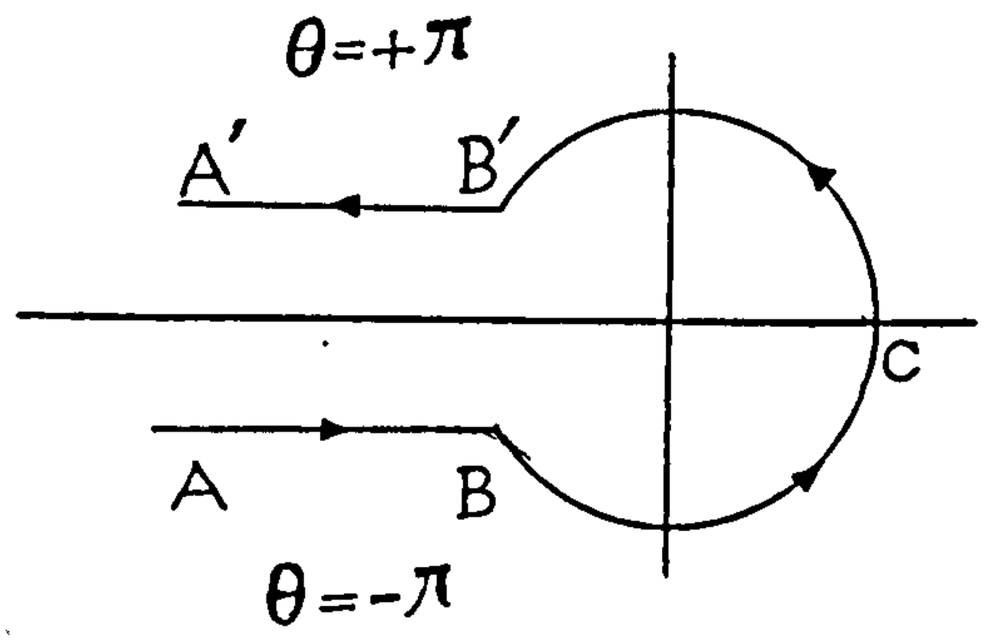

The second integral could be assumed to be a function of δ as $O(\delta)$ and the first and second integrals differ from integrals ∞ to 0 and 0 to ∞ also by term $O(\delta)$. If $\delta \longrightarrow 0$ the total contribution would be:

$$\frac{-\exp(-D\beta^2 t)}{\pi}\int_0^{\infty}\frac{\exp(-rDt)\sin(d\sqrt{r})dr}{r+\beta} \tag{43}$$

or if we put $r=\rho^2$,

$$\frac{-2\exp(-D\beta^2 t)}{\pi}\int_0^{\infty}\exp(-\rho^2 Dt)\sin(d\rho)\frac{\rho d\rho}{\rho^2+\beta^2} \tag{44}$$

Formal evaluation of this form is presented [ ] as:

$$\int_0^{\infty}\exp(-\beta x^2)\sin\alpha x\,\frac{x\,dx}{\gamma^2+x^2}= \tag{45}$$

$$=-\frac{\pi}{4}\exp(\beta\gamma^2)\left\{2\sinh\alpha\gamma+\operatorname{erf}\left[\gamma\beta-\frac{\alpha}{2\sqrt{\beta}}\right]\right.$$

$$\left.-\operatorname{erf}\left[\gamma\sqrt{\beta}+\frac{\alpha}{2\sqrt{\beta}}\right]\right\}.$$

where

$$\operatorname{erf} y=\frac{2}{\sqrt{\pi}}\int_0^{y}\exp(-z^2)\,dz$$

therefore

$$\int_0^{\infty} \exp(-\beta x^2)\, \sin\alpha x\, \frac{x\, dx}{r_+^2 x^2} \leqslant \int_0^{\infty} \exp(-\beta x^2\, \frac{\sin\alpha x}{x}\, dx$$

$$= \int_0^{\alpha} d\sigma \int_0 \exp(-\beta \cdot x^2 \cdot \cos\, \sigma \cdot x \cdot dx$$

$$= \int_0^{\alpha} d\sigma \int_{-\infty}^{+\infty} \exp(-\beta x^2 + i \cdot \sigma \cdot x)\, dx$$

$$= \int_0^{\alpha} d\sigma \int \exp(-\frac{-\sigma^2}{4\beta}) \int_{-\infty}^{+\infty} \exp[-\beta(x - \frac{i\sigma}{2\beta})^2]\, dx$$

$$= \pi/4 \int_0 \exp(-\sigma^2/4\beta)\, d\theta$$

$$= \operatorname{erf}(\frac{\alpha}{2\sqrt{\rho}}) \qquad (46)$$

The above expression renders positive exponentials in $\exp(\beta.r^2)$ and $\sinh \alpha r$ so that presumably theses large terms cancel each other out. However to use the above integral , numerical 1 of the expression is suggested. Finally, the overall effect on diffusion from the other dimensions is given as :

$$\int_0^{2a} dx \int_{-b}^{b} dy \int_{-c}^{c} \partial C/\partial t\, dz \qquad (47)$$

$$= \frac{16}{\pi^2} \sum_{l=0}^{\infty} \sum_{m=0}^{\infty} \frac{(-1)^{l+m}}{(2l+1)(2m+1)} \{ \int_0^{2a} \frac{\partial C_{l,m}(x,t)}{\partial t} dx \}$$

$$\int_{-b}^{+b} \int_{-c}^{+c} \cos\{\frac{(2l+1)\pi y}{2c}\} \cos\{\frac{(2m+1)\pi z}{2c}\}\, dy\, dz$$

$$= bc \sum_{l=0}^{\infty} \sum_{m=0}^{\infty} \frac{1}{(2l+1)^2 \cdot (2m+1)^2} \int_0^{2a} \frac{\partial C_{l,m}}{\partial t}\, dx$$

now the Laplace transform of $\int_0^{2a} \frac{\partial r}{\partial t}\, dx$ is given as:

$$\int_0^{2a} \{\text{Laplace Transform of } \frac{\partial r}{\partial t}\}\, dx$$

$$= \int_0^{2a} s\,\bar{r}\,(x,s)\, ds$$

$$= C_o \int_0^{2a} \frac{\sinh[p(a-x)]\, dx}{\sinh 2pa}$$

$$= C_o/p\ \frac{\cosh 2pa - 1}{\sinh 2pa} \qquad (48)$$

To interpret this, it is noted that the above expression depends only on p. "s" by itself does not appear and so we can use two further properties of Laplace transform.

(1)- If the L.T. of f(t) is f(s), the L.T. of a function f(at) is

$$\int_0^{\infty} \exp(-st)\, f(t)\, dt$$

$$1/a \int_0^{\infty} \exp[-\frac{s}{a}(at)]\, f(at)\, d(at) \qquad (49)$$

(2)- If the Laplace transform of f(r) is f(S), the L.T. of exp(-at) f(t) is :

$$\int_0^{\infty} \exp[-(s+a)r\ \ f(t)dt\ \ = f(s+a) \qquad (50)$$

Thus if F(t) is the function where L.T.is $\frac{C_o}{\sqrt{s}}$ Tanh$(a\sqrt{s})$ then $\sqrt{D}\, \exp(-D\beta^2 t)\ .\ F(t\sqrt{D})$ is the function where L.T. is C_o/p tanh pa. There could be found an expression for small values of t by using a similar form of expansion to that used above as:

$$= \frac{C_o}{\sqrt{s}} \tanh(a\sqrt{s}) = \frac{C_o}{\sqrt{s}} \frac{1-\exp(-2a\sqrt{s})}{1+\exp(-2a\sqrt{s})} \qquad (51)$$

$$= \frac{C_o}{\sqrt{s}} \sum_{k=0}^{k} (-1)^k \{\exp(-2ka\sqrt{s}) - \exp[-2(k+1)a\sqrt{s}\ ]\}$$

$$= \frac{C}{\sqrt{s}} - \frac{2C}{\sqrt{s}} \sum_{k=0}^{\infty} (-1)^k \exp[-2(k+1)\ a\sqrt{s}]$$

It could be shown that the inverse transform of $1/\sqrt{s}$ is $1/(\pi t)^{1/2}$ and of $\exp[-d\sqrt{s}]/\sqrt{s}$ is $\exp[-d^2/4t]/[\pi t]^{1/2}$

thus $$F(t)= \frac{C_o}{(\pi t)^{1/2}} \{1-2\sum_{k=0}^{\infty} (-1)^k \exp[-(k+1)^2 \frac{a^2}{t}]\} \qquad (52)$$

Note that this approximation of $\frac{C_o}{(\pi t)^{1/2}}$ for small t and tends to infinity as $t \longrightarrow 0$. This will give quite a good answer unless t is very large. Combining this result for long time experiments with equation (47) it is possible to derive an expression which could be used to interpret the results of 3-D experiments.

$$F(t)=bc\sum_{l=0}^{\infty} \sum_{m=0}^{\infty} \frac{1}{(2l+1)^2(2m+1)^2} \frac{C_o}{(\pi t)^{1/2}} \{1-\sum_{k=0}^{\infty} (-1)^k \exp[\frac{-(k+1)^2 a^2}{t}]\} \qquad (53)$$

Taking the two first terms of these summations, it is possible to write the following equation;

$$F(t)= \frac{bc \cdot C_o}{(\pi t)^{1/2}} [1-\exp(\frac{-a^2}{t})] + \frac{bc \cdot C_o}{81\ (\pi t)^2} [1+\exp(\frac{-4a^2}{t}) \qquad (54)$$

The C refers to the total concentrations of hydrogen on the charging side. This could be calculated by the use of the steady state flux values as:

$$C = L.i / zFD \qquad (55)$$

$$C_1 = \frac{b.i_1^{\infty}}{z.F.D} \qquad (56)$$

$$C_2 = \frac{b.i_2^{\infty}}{z.F.D} \qquad (57)$$

$$C_3 = \frac{2b.i_3^{\infty}}{z.F.D} \qquad (58)$$

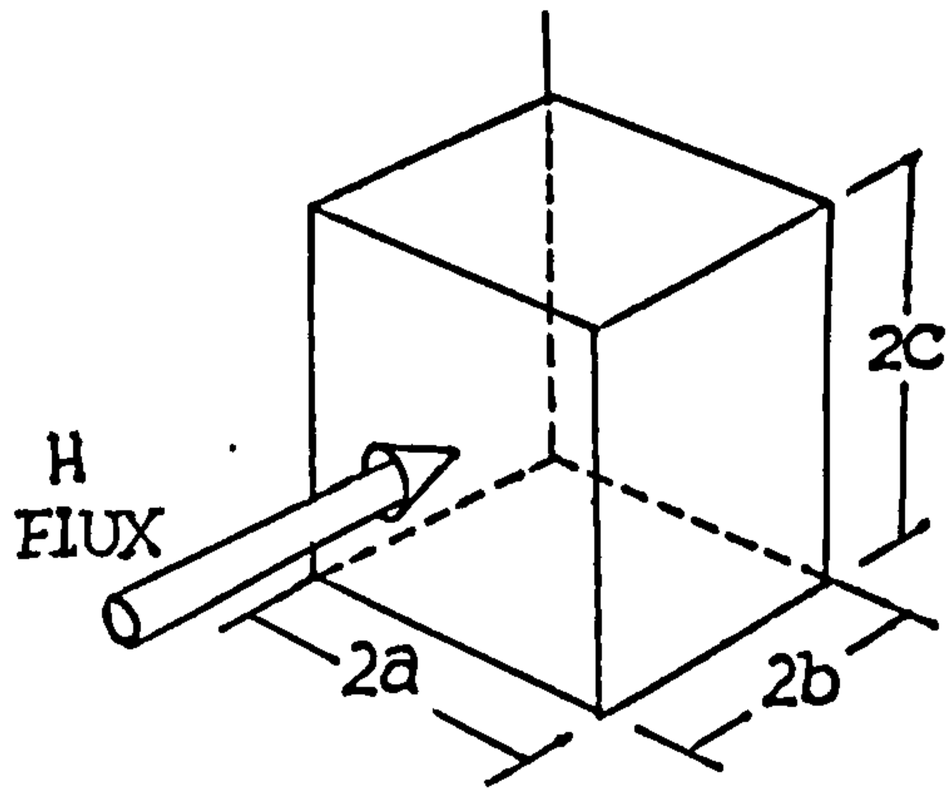

$$C_o = C_1 + C_2 + C_3 \qquad (59)$$

$$C = \frac{b(i_1^{\infty} + i_2^{\infty} + 2i_3^{\infty})}{z.F.D} \qquad (60)$$

Now if in part of F(t), the total flux out of the membrane we introduce

$$\frac{i_1^{\infty} + i_2^{\infty} + i_3^{\infty}}{zF} = bc \frac{b(i_1^{\infty} + i_2^{\infty} + 2i_3^{\infty})}{zFD(\pi t)^{1/2}} [1 - \exp(-a/t)]^2 + \frac{bc}{81} \frac{b(i_1^{\infty} + i_2^{\infty} + 2i_3^{\infty})}{zFD(\pi t)^{1/2}} [1 + \exp(-4a/t]^2 \qquad (61)$$

$$D = \frac{b^2 c(i_1^{\infty} + i_2^{\infty} + i_3^{\infty})}{(\pi t)^{1/2}(i_1^{\infty} + i_2^{\infty} + i_3^{\infty})} \left\{ 1 - \exp(-a/t)^2 + \frac{1 + \exp(-4a/t)^2}{81} \right\}$$

The application of this formula to the data available is described in section 4.

8.....REFERENCES

1 Ewe H., Justi E.W., Stephen K., Energy conversion, 13:, 109, (1973)

2 Alefeld G., Rationelle Energienutzung Durch Warmespeicherung, VDI, Bericht, 288, (1977)

3 Cleaves, H.E., Thompson J. G., "The Metal Iron" McGrawHill 441, (1935)

4 Sieverts A., Die Aufnhahme Von Gasen Durch Metalle(The absorption of gases by metals) ,Z. F. Metallkunde, 21:, 37-44, (1929)

5 Luckemeyer-Hasse L., Schenck H., Loslichkeit Von Wassertoff, Tech. Mitt. Kaipp, 1:, 121-126, (1933)

6 Pfeil L.B., The effect of Occluded Hydrogen on the Tensile Strength of Iron, Proc. Roy. Soc. (London), A 112: , 182, (1926)

7 Wach S. P., PhD Thesis , London University, (1966)

8 Engell H., Johnston J.E., L'Hydrogen Daus Les Metaux, Congres International, Paris , 60, (1972)

9 Eastman D.E., Cashion J.C., Switendick A.C., Phys. Rev. Lett., 30:, 35, (1971)

10 Quick N.R., Johnson H.H., Acta Metall., 26:, 903, (1978)

11 Domke E., PhD Thesis, Univ. Munster, FRG, (1971)

12 Miller R.F., Hudson J.B., Ansel G.S., Metall. Trans. A, 6A:, 117, (1975)

13 Yamakawa K. , Tsurutu T., Yoshizawa S., Boshoku Gijutsu , 30;, 501, (1981)

14 McLellan R.B., Acta Metall., 27:, 1655, (1979)

15 Katsuda H., McLellan R.B., Frankawa, K., J. Phys. Chem. Solids, 45:, 533, (1982)

16 Beck W., Bockris J'OM, McBreen J,Nanis L, Proc. R. Soc. A, 290:, 220, (1966)

17 McBreen J., PhD Thesis, Univ. Pennsylvania, PA, (1971)

18 Raczynoki W., Physica Status Solidi(a), 48:, K27, (1978)

19 Subramanyan P.K., PhD Thesis, Univ. Pennsylvania, PA, (1971)

20 Kumnick A.J., Johnson H.H., Metall. Trans.A, 5:, 1199, (1974)

21 Hagi H., Hayashi Y., Ohtani N., Trans. Jpn. Inst. Metals., 20:, 349:, (1979)

22 Mindyuk A.K., Svist E.I., Fiz-Khim Mekh. Mater, 9:, 36, (1972)

23 Devanathan M.A.V., Stachurski Z., Proc. Roy. Soc.,90:, A270:, (1962)

24 Devanathan M.A.V., Stachurski Z., J Electrochem. Soc., 110:, 886, (1963)

25 McBreen J., Nanis L., Beck W., J. Electrochem. Soc, 113:, 1218, (1964)

26 Alefeld G., Vokel J., (eds.), "Hydrogen in Metals II, Application Oriented Properties, Topics in Applied Physics, 29:, Springer, Berlin, Heibelberg, New York, (1978)

27 Bennett C.W., Burnham W.S., J. Phys. Chem., 21:, 107-149, (1917)

28 Frankenthal R.P., Kruger J. (eds.), "Passivity of Metals", Corrosion Monograph Series, The Electrochemical Society, Princeton, NJ, (1978)

29 Bech-Nielsen G, Electrochim. Acta, 21:,627, (1976)

30 Bockris J.O'M, Drazic D., Despic A.R/, Electrochim. Acta, 4:, 324, (1961)

31 Kue H. C., Landolt D., Electrochim. Acta, 18:, 421, (1973)

32 Cohen M., J. Electrochem. Soc., 121:, 1910, (1974)

33 Stern M., J. Electrochem. Soc., 105:, 638, (1958)

34 Uhlig H.H., J. Electrochem. Soc., 101:, 215,(1954)

35 Sato N., Kuto K., Noda T., Electrochim. Acta, 16:, 1909, (1971)

36 Sato N., Electrochim. Acta, 16:, 1683, (1971)

37 Haruyaman S., Ogura K., Nagasaki K., J. Electrochem. Soc. Jpn., 37:, 38, (1969)

38 Pourbaix M.,"Localized Corrosion", 20, NACE, Housteon, (1974)

39 Vetter K.J., Streblow H.H., Willgalis Ber. Bunserges Phys. Chem., 75:, 822, (1971)

40 Weast R.C.,"Handbook of Chemistry and Physics",56th addition, CRC Press, (1974)

41 Easterling K.,"Introduction to Physical Metallurgy of Welding", Butterworth, (1983)

42 Porter A.S., Tompkin F.C., Proc. Roy. Soc. London, A217:, 529-554, (1953)

43 Ransom C.M., Ficalora P.J., Metall. Trans., 11A:, 801, (1980)

44 Pecora L., Ficalora P.J., Metall. Trans. , 11A:, 801, (1980)

45 Bozso F., Ertl G., Grunze M., Weiss M., Appl. Surf. Sci., 1:, 103-119, (1977)

46 Pasco R.W., Ficalora P.J., Sci. Metall., 14:, 667-671, (1980)

47 Swets D.E., Frank R.C., Trans. Met. Soc. AIME, 221:, 1082, (1962)

48 Elkholy A., Galland J., Azou P., Bastien P., Acad. Sci. Ser., 284:, 363, (1977)

49 Bodenstein M., Z. Electrochem., 23:, 517,(1922)

50 Hill M.L., "Hydrogen Embrittlement in Metal Finishing", American Electroplaters Soc. Sym., Rheinhold Pub. Co. NY, (1961)

51 Hewitt, "Hydrogen in Steel", Iron and Steel Institue Special Report No. 73, 83, (1962)

52 Bastien P.G., "Physical Metallurgy of Stress Corrosion Fracture", AIME Sym., Pitsburgh, Interscience, NY, (1959)

53 de Kazinczy F., J. Iron Steel Ins., 177:, 85, (1954)

54 Garfalo F., Acta Metall., 8:, 504, (1960)

55 Farrel K., J. Iron Steel Inst., 188:, 457, (1965)

56 Petch N.J., Phil. Mag. 1:, 186, (1956)

57 Troiano A.R., Trans. Ame. Soc. Met. 47:, 892, (1955)

58 Tiller W.A., Schrieffer R.S., Scrip. Metall., 4:, 57, (1970)

59 Zappfe C.A., Siems S., Trans AIME, 145:, 225, (1941)

60 Sieradzki K., Ficalora P.J., Scrip. Metall,, 12:, 511, (1978)

61 Keirchheim R. "Overview 19", Acta metall., 130:, 1059-1068, (1982)

62 Kuk Y., Kruger T., Werkestoffe U. Korros, 34:, 179, (1983)

63 Christman K., Ertl G., Pignet T., Surf. Sci., 54:, 179, (1976)

64 Barker M., Rideal E., Nature, 174:, 1185, (1955)

65 Gibb T.R.P., "Nonstoichiometric Compounds" (Gould R.F. ed.), 39:, 99, in "Advances in Chemistry", (1963)

66 Switendick A.C.,"Topics in Applied Physics" Hydrogen in Metals I- Basic Properties, (Alefeld G., Volkel J. eds.), 101, Springe Verlag, Berlin, (1978)

67 Klyachko Yu. A., Kurin L.L., Federov S.N., Khim. Nauka Promyshl., 3:, 127, (1958)

68 Slabkovski I.S., Kripyakevich R.I., Vlyanie Robochichikh. Sredna. Svoiska Materialov, Akd. Nauk Ukr. USSR, Fiz-Mekhan. Inst., 3:, 19, (1964)

69 Fogel M., Zh. Experim. Teoret. Fiz., 28:, 711, (1955)

70 Boudart M., J. Chem. Phys., 23:, 753, (1955)

71 Suhrmann R., Z. Fizik. Chem., N.F., 12:, 128, (1975)

72 Kirst T.R., McQuistan R.B., Lichtmann D., Phys. Letters, 20:, 129, (1966)

73 Gradina Yu. V., Krepsheva L.B., Fiz Metall. Metalloved, 17:, 739, (1964)

74 Gradina Yu. V., Izv. VUZ, Chern. Metall., 41:, 126, (1961)

75 Weiner R.C., US 3, 181978(cl. 148-14), May 4 (1965), Appl. Apr.1, (1960), Mar. 25(1963)

76 Vitovec H.F., Proc. Amer. Petrol. Inst., 44:, 179, (1964)

77 Fletcher E.E., Elsea A.R., DMIC Rept., 202:, OTS G01389, 64, (1964)

78 Owe Berg T.G., Amer. Ceramic Soc. Symp., Paper 61, (1958)

79 Merlet J.G., Johnson H.H., Troiano A.R., JISI, 189:, 37, (1958)

80 Szummer A., Janko A., Pielaszek J., Bull. Acad. Polon. Sci. Seri. Sci. Chim., 19:, 33, (1971)

81 Janko A., Pielaszek J, Bull. Acad. Polon. Sci. Seri. Chim., 19:, 33, (1971)

82 Kuk Y., Sakurai T., Piekering H.W., International Field Emission Symposium, Tokyo, Japan, (1980)

83 Zamanzadeh F, PhD Thesis, Pennsylvania Univ., PA,(1980)

84 Dendramis A., VanZee H.J., Weltner Jr. W., Astrophysical J., 231:, 632, (1979)

85 Frey R., Kruger T., Werkestofte U. Korros., 34:, 179, (1983)

86 Lakomskii V.I., Automatic Welding, 7:, 50, (1962)

87 Bastien P.G., 8th Colloque Met., Centre Et Nucl. Seclay, 1-28, (1964)

88 Barrer R.M., Disc. Farad. Soc., 4:, 68, (1954)

89 Shved G.V., Karpenko V., Vliyanie Robochikh Sred na Svoistva Materialov, Akad. Nauk. Ukr. USSR Machinoved Automatiki, 2:, 159, (1963)

90 Guentherschulze A., Betz H., Kleinwaechter H., Z. Physik, 111:, 657, (1938/9)

91 Cheng C.H., Wei C.T., Beck P.A., Phys. Rev, 120:, 426, (1960)

92 Eguchi T., Marozumi S., J. Jpn. Inst. Met., 38:, 1019, (1974)

93 Engell N.N., Johnston J.E., L'Hydrogene Dans Les Matraux Conge's International, Paris, 60, (1972)

94 Bauer, G.S., Schmatz W., Just W., Proceedings of the 2nd International Congress on Hydrogen in Metals, Paris, (1977), Pergamon Press , Oxford, 2:, 2C15, (1978)

95 Verdan G., Rubin R, Kley W, Neutron Inelastic Scattering, pp. 223-31, Proc. IAEA Symp., Copenhagen, Vol.1, IAEA, Vienna, (1968)

96 Birchall J.H.L., Ross D.D., International Meeting on Hydrogen in Metals, Julich, March, 1972, Ber. Kernforschungs Anlage, Julich, 6:, 313-45, (1972)

97 Antonini M., Garstanjen H.D., Phys. Status Solidi, (a)34:, K153-157, (1976)

98 Wert Ch. A., "Trapping of Hydrogen in Metals", Topics II, Vol.29, (Alefeld G., Volkel J. eds.), 305, (1978)

99 Bastien P., Azou P., Plausquellec J., Compt. Rend., 224:, 1195, (1975)

100 Oriani R.A., Trans. Metall. Soc. AIME, 236:, 1368, (1966)

101 deKazinczy F., Jernkonterets Ann., 139:, 885-892, (1955)

102 Wagenblast H., Wriedt H.A., Metall. Trans., 2:, 1393-1397, (1971)

103 Peisl J., "Hydrogen in Metals I , Basic Properties", (Alefeld G., Volkel J. eds.), 75-100, Springer, Berlin, (1978)

104 Gonzalez O.D., Trans. Metall. Soc., 245:, 607, (1962)

105 Oriani R.A., Trans. Metall. Soc., 233:, 1878, (1965)

106 Oriani R.A., Acta Metall., 18:, 147-157, (1970)

107 Ferro A., J. Appl. Phys., 28:, 895, (1957)

108 Bryan W.L., Dodge B.F., Amer. Inst. Chem. Eng. J., 9:, 223, (1963)

109 Gibala R., Trans. Metal. Soc., 239:, 1575-1585, (1967)

110 Wallace J.P., Scripta Metall., 12:, 791, (1978)

111 Seeger A., Phys. Lett. A., 58A:, 137, (1976)

112 Springer T., "Hydrogen in Metals I, Basic Properties", (Alefeld G., Volkel J. eds.), 75-100, Springer, Berlin, (1978)

113 Stump N., Gissler W., Rubin R., Phys. Status Solidi, 54(b), 295-302, (1972)

114 Sugimoto H., Fukai Y., Phys. Rev. B., 22:, 670-680, (1980)

115 daSilva J. R. J., Stafford S.W., McLellan R. B., J. Less. Common Metals, 49:, 409-420, (1976)

116 Dunn W.W., McLellan R.B., Metall. Trans., 2:, 1079, (1971)

117 Kiuchi K., McLellan R.B., Overview 27, Acta Metall. , 31:, 7, 961-984, (1983)

118 da Silva J.R.G., McLellan R.B., J. Less Common Metals, 50:, 1, (1976)

119 Burraclough K.C., Murex Review, 1:, 305, (1954)

120 Bolton K., PhD Thesis, Univ. London, (1964)

121 Shanahan C.E.A., Cook F., J.I. Steel Ins., 190:, 381, (1958)

122 Matsuda F., Franklin T.C., J. Electrochem. Soc., 112:, 767, (1965)

123 Geller W., Sun T.H., Arch. Eisenhuttenw, 21:, 423, (1950)

124 Kubachewski O., "Iron Binary Phase Diagrams", Springer-Verlag, Berlin, 46, (1982)

125 Armbruster M.H., J. Amer. Chem. Soc., 65:, 1043, (1943)

126 Schrader H., Paranjpe V.G., Tisco, 1:, 13, (1954)

127 Fujita F.E., Trans. Jpn. Inst. Metals, 17:, 232, (1976)

128 Antonov V.E., Belash I.T., Ponayatovsky E.G., Scripta Metall., 16:, 203, (1982)

129 Smialowski M., "Hydrogen in Steel" , Pergamon Press, (1962)

130 Sieverts A., Z. Phys. Chem., 77:, 591, (1912)

131 Sieverts A., Zapf G., Moritz H., Z. Phys. Chem., Teil A, 183:, 19, (1938)

132 Sieverts A., Hagen H., J. Phys. Chem. , Teil A, 155, 314, (1931)

133 Martin E., Archs. Eisenhuult, 3:, 407, (1929)

134 Andrew J.H., Lee H., Quarrell A.G., J. I. Steel Ins., 16:, 140, (1942)

135 Stafford S.W., McLellan R.B., Acta Metall., 23:, 1463, (1974)

136 Asano S., Hara K., Nakai Y., Ohtani N., J. Jpn. Inst. Metals, 38:, 626, (1974)

137 Desante D.F., Tetelman A.S., Trans. Metall. Soc. AIME, 242:, 1473, (1968)

138 Harhai J.G., Lange K.W., Archs. Eisenhutt. , 46:, 237, (1975)

139 Choo W.Y., Lee J.Y., Metall. Trans. A, 13A:, 135, (1982)

140 Samuels L.E., Wallwork G.R., Inst. Metals, 85:, 177, (1956)

141 Kumnick A.J., Johnson H.H., Acta Metall., 28:, 33, (1980)

142 Bastien P., Azou P., Veysseyre H., Rev. Met. Mem. Soc., 61:, 203, (1964)

143 Johnson E.W., Hill M.L., Trans. Metall.Soc. AIME, 218:, 1104, (1960)

144 Harhai J.G., Visvanathan T.S., Davis H.M., A.S.M. Trans. Quart., 58:, 210, (1965)

145 Coe F.K., Moreton S., J. I. Steel Inst., 205:, 366, (1966)

146 Weinstein M., Elliot J.F., Trans. Metal. Soc. AIME, 227:, 382, (1963)

147 Schwarz a., Zitter H., Archs. Eisenhutt., 36:, 343, (1965)

148 McLellan R.B., Sutter , Acta Metall., 32:, (12), 2233-39, (1970)

149 Darken L.S., Smith K.P., Corrosion, 5:, 1, (1949)

150 Smith D.P., "Hydrogen in Metals", Chicago Univ., Press, Chicago, USA, (1978)

151 Beck W., Bockris J. O'M, Mcbreen J., Nanis L., Proc. Roy. Soc., 290A:, 220-235, (1966)

152 McNabb A., Foster P.K., Trans Metall. Soc. AIME, 227:, 618-27, (1963)

153 Pressoyre G.M., Metall. Trans., 10A:, 1571, (1979)

154 Manning J. K., Theory of Diffusion in "Diffusion", ASM Metals Park, Ohio, USA, (1973)

155 Pielaszek J.,Bull. Acad. Polon Sci. Ser. Sci. Chim. Geol. et Geog., 7:, 891, (1959)

156 Pielaszek J., Lunarska E., Bull. Acad. Polon. Sci. Ser. Sci. Chem. Geol. et Geog., 24:, 87, (1978)

157 Hirth J.P., Metall. Trans., 11A, 861, (1980)

158 Oriani R.A., Hirth J.P., Smialowski M. (eds.), "Hydrogen Degredation of Ferrous Alloys", Noyes Publications, USA, (1987)

159 Schumann G., Volkl J., Alefeld G., Phys. Stat. Sol. , 42:, 401, (1970)

160 Powers R.W., Doyle M.V., J. Appl. Phys., 30:, 514, (1959)

161 Kehr K.W., Theory of Diffusion ofHydrogen in Metals in "Hydrogen in Metals II, Topics in Applied Physics vol.28,", Alefeld G., Volkl J. (eds.), 197, Springer, Berlin, (1978)

162 Flynn C.P., Stoneham A.M., Phys. Rev.Lett., 21:, 891, (1968)

163 Springer T., Z. Phys. Chem., NF, 115:, 141, (1979)

164 Birnbaum H.I., Flynn C.P., Phys. Rev. Lett., 37:, 25, (1970)

165 Ritchie I.G., Dufrensue J.F., Moser P., Phys. Sta. Solidi (a), 52:, 331, (1979)

166 Handad R., Scripta Metall., 11:, 843, (1977)

167 Vineyard G.H., J. Phys, Chem. Solids, 3:, 121, (1957)

168 Flynn C.P., Stoneham A.M., Phys. Rev., 131:, 3966, (1970)

169 Kagan Yu. M., Klinger M. I., J. Phys., C7:, 2791, (1974)

170 Stoneham A.M., J. Nucl. Mater., 69/70:, 109, (1979)

171 Kedzierzawski P., Diffusion of Hydrogen and its Isotopes in Iron Alloys, in "Hydrogen Degredation of Ferrous Alloys", pp. 261, (Oriani A.R., Hirth J.P., Smialowski M. eds.), Noyes Pub. NJ, USA, (1987)

172 Wagner H., Horner H., Advans. Phys., 23:, 587, (1974)

173 Bausch R., Horner H., Wagner H., J. Phys. Chem. Solid State Phys., 8:, 2559, (1975)

174 Horner H., Wagner H., J. Phys. Chem. Solid State Phys., 7:, 3305, (1974)

175 Bauer H.C., Volkl J., Trtkowski J., Alefeld G., Z. Physik, B29, 17, (1978)

176 Wagner H, Elastic Interactions and Phase Transformations in Coherent Metal-Hydrogen alloys,in "Topics in Applied Physics", vol.28,Hydrogen in Metals I, (Alefeld G., Volkl J. eds.) pp 5-51, Springer, Berlin, (1987)

177 Crank J, "The Mathematics of Diffusion", second ed., Oxford Uni. Press, (1979)

178 Wu E., J. Electrochem. Soc., 20:, 2126, (1987)

179 IIno M., Acta Metall.,30:, 377-383,(1982)

180 IIno M., Metall. Trans. A, 18A:, 1559, (1987)

181 IIno M., Metall. Trans. A, 16A:, 401 , (1985)

182 Leblond J.B., Dubois D., Acta Metall., 31:, 10, 1471, (1983)

183 IIno M., Acta Metall., 30:, 367-375, (1982)

184 Kirchheim R., Acta Metall., 18:, 147, (1970)

185 Hohler B., Kronmuller H., Z. Phys. Chem. NF., 114:, 93, (1979)

186 Caskey G.R., Pilinger W.L., Metall. Trans. A, 6A:, 1571, (1978)

187 Lin R.W., Johnson H.H., Acta Metall., 30, 1819, (1982)

188 Robertson W.M., Scripta Metall., 15:, 137-139, (1981)

189 Bockris J. O'M, McBreen J., Nanis L., J. Electrochem. Soc., 112:, 1025, (1965)

190 Daft E.G., Bohnenkamp K., Engell H.J., Corrosion Sci., 19:, 591, (1979)

191 Parly J.G., Acta Metall. 26:, 1215-1223, (1978)

192 Chaudhari B.S., Radhakrishnan T.P., Surf. Techn., 22:, 1367-1376, (1984)

193 Nanis L., Namboudhiri T.K.G., J. Electrochem. Soc.,119:, 691, (1972)

194 Boes N., Zuchner H., J. Less Common Met., 49:, 223, (1976)

195 Early J.G., Acta Metall., 26:, 1215, (1978)

196 Fullenwider M.A., J. Electrochem. Soc., 122:, 648, (1975)

197 Kargol J.A., Fiore N.F., Coyle R.G., Metall. Trans. A, 12A:, 663, (1973)

198 Daynes H., Proc. Roy. Soc.A, 97:, 286, (1920)

199 Barrer R.M., "Diffusion in and Through Solids", Cambridge Univ. Press, (1951)

200 Huffine C.L., Williams J.M., Corrosion, 16:, 430, (1960)

201 Wach S.P., Miodvnick A.P., Corros. Sci., 8:, 271-279, (1968)

202 Bockris J. O'M, Subramanyan P.K., J. Electrochem. Soc., 118:, 7, 1114, (1971)

203 Xie S.X., Hirth J.P., Corrosion, 38:, 2, 486-493, (1982)

204 IIno M., Scripta Metall., 20, 823-828, (1986)

205 Park Y., Waber J.T., Scripta Mettal., 19:, 1095-1100, (1985)

206 Lee J., Waber J.T., Park. Y., Scripta Metall., 20, 823-828, (1986)

207 Bockris J. O'M, Drazic D.M., "Electrochemical Science", Ch 2, Taylor and Francis Ltd., London, (1972)

208 Pentland N., Bockris J. O'M, Sheldon E., J. Electrochem. Soc., 104:, 3, 182-194, (1957)

209 Shreir L.L.(ed.), "Corrosion Vol.1", pp 9.50, Newnes-Butterworth, London, second Ed., (1976)

210 McBreen J., Genshaw M.A., "Fundamental Aspects of Stress Corrosion Cracking", (Staehle R.W., Forty A.J., Van Rooyen D. eds.), NACE, Houston, 51, (1968)

211 Bockris J.O'M, McBreen J., Nanis L., J. Electrochem. Soc., 113:, 11, (1966)

212 Kelly E.J., J. Electrochem. Soc., 112:, 124, (1965)

213 Bagotskaya I.A., Z. Fiz. Khim., 36:, 2667, (1962)

214 Frumkin A.N., "Advances in Electrochemistry and Electrochemical Engineering", (Delahey P., ed.), vol.3, Interscience Publishers Inc., NY,USA, 375, (1963)

215 Bockris J.O'M, Thacker R., Technical Report No.3, Office of Naval Research, Contract No. NR 551(22)NR 036-028, (1959)

216 Horiuti J., Toya T., "Chemisorbed Hydrogen", Report from the Institute for Metal Catalysis, Hokaido Uni., Sapporo, Jpn., (1968)

217 Zakroczymski T., Entry of Hydrogen into Iron alloys from the Liquid Phase,in "Hydrogen Degredation of Ferrous Alloys",(Oriani R.,Hirth P.,Smialowski M. eds.), pp 215-250, Noyes Pub. NY , (1987)

218 Devanathan M.A.V., Stachurski Z., J. Electrochem. Soc., 111:, 619-623, (1964)

219 Kim C.D., Wilde B.E., J. Electrochem. Soc.,118:, 202, (1971)

220 Kita H., J. Electrochem. Soc., 113:, 11, 1095-1111, (1966)

221 Marcus P., Oudar J., Gas-Iron Surface Equilibria in "Hydrogen Degredation of Ferrous Alloys", (Oriani R., Hirth P., Smialowski M. eds.), Noyes Pub. NY, (1987)

222 Muscat J.P., Newns D.M., Prog. Surf. Sci., 9:, 1, (1978)

223 Nordlander P., Holloway S., Noskov J.K., Surf. Sci., 136:, 59, (1984)

224 Toyoshima T, Somorjai G.A., Catal. Rev. Sci. Eng., 19, 105, (1979)

225 Leygraf C., Hultquist G., Surf. Sci., 61:, 69, (1976)

226 McIntyre N.S., Zetarwk D.G., Owen D., Appl. Surf. Sci., 2:, 55, (1978)

227 Van Santen R.A., Surf. Sci., 53:, 35, (1975)

228 Cavalier J.C., and Chornet E., Surf. Sci., 60:, 125, (1976)

229 Kato H., Sakisaka Y., Nishijima M., Onchi M., Surf. Sci., 107:, 20, (1981)

230 Lagos M., Surf. Sci. 122:, 1601, (1982)

231 Bond G.C., "Catalysis by metals", Academic Press, NY,(1962)

232 Messer R.P., Briant C.L., Acta Metall., 30:, 457, (1982)

233 Tomoshov N., "Theory of Corrosion and Protection of Metals" pp 7-325, Translated by Tytell B. et al, McMillan Co., NY, (1966)

234 Gmelin, "Handbush der Anorganischen Chemie", Teil, 59A:, 313, Berlin, 1929-1932

235 Faraday M., Letter to M. Faraday quoted in "Experimental Researchs in Electricity", 238, Dover Pub. NY, (1965)

236 Bewell P.B., Cohen M., J. Electrochm. Soc., 111:, 5, 508, (1964)

237 Chihum J.F., J.Phys. Chem., 89:, 566-573, (1930)

238 Uhlig H.H., Z. Electrochem. 62:, 700, (1958)

239 Uhlig H.H., Passivity and its Breakdown on Iron and Iron based alloys, 21, USA-Japan Seminar, NACE, Houston, (1976)

240 Fromhold Jr A.T., Kruger J., J. Electrochem. Soc., 120:, 722, (1973)

241 Ali S.I., Wood G.C., Br. Corrosion J., 4:, 133, (1969)

242 Pourbaix M., "Atlas of Electrochemical Equilibria in Aquous Solution", Pergamon Press and Celecor, (1966)

243 Mauralidharan V.S., Veerashamugamani M., J. Appl. Electrochem., 15:, 675-683, (1985)

244 Keddam M., Mattos O.R., Takeouti H., J. Electrochem. Soc., 128:, 2, 266, (1981)

245 Ogura K., Wada H., Electrochem. Acta, 25, 913-917, (1980)

246 Sato N., Cohen M., J.Electrochem. Soc., 111:, 5,(1964)

247 Wilcox G.D., Gabe D.R., Br. Corrosion J.,19:, 4, (1984)

248 Sato N., "Surface Electrochemistary",Takamura T., Kozawa A., (eds.)

249 Epelboin I., Gabrielli C., Keddam M., Takenouti H., Electrochem. Acta, 20:, 913-916, (1975)

250 Nishimra R., Kudo K., Proc. 8th Int. Cong. on Metallic Corrosion, (8th ICMC), 1:, 6-11, Pub. DECHEMA, W.G., (1981)

251 Lukac C., Lumsden B., Smialowski S, Staehele R.W., J. Electrochem. Soc., 122:, 1571-1579, (1975)

252 Asami k., Hashimoto K., Shimodaira S., Misawa T., Corrosion Sci., 14:, 279-289, (1974)

253 Vetter K.J., "Passive Films and Protective Coating", (Fischer H, Hauffe K., Wiederholt W.eds.),Springer, Berlin, Gottingen-Heidelberg, 72-89, (1956)

254 Dmytrakh I.N., Grabovskii R.S., Sov., Mat. Sci., 21:, 4, 314-317, (1985)

255 Vetter K.J., "Electrochemical Kinetics", Academic Press, NY, (1967)

256 Heusler K.K., Weil K.G., Bonhoeffer K.F., Z. Physik. Chem., 15:, 149, (1958)

257 Arvia A. J., Proc. 8th Inter. Cong. on Metallic Corrosion, Mainz, FRG, 6-11 sept. 1981, DECHEMA, (1981)

258 Uhlig H.H., Corrosion Sci., 7:,325, (1967)

259 Muller W.J., Z. Electrochem., 33:, 401, (1927)

260 Sato N., Kudo K., Nishimura R., J. Electrochem. Soc., 123:, 1419, (1976)

261 Sato N., Passivity and its Breakdown on Iron and Iron based Alloys, USA-Jpn Seminar, 1, Nace Houston, (1976)

262 Ohtsuka T., Kudo K., Sato N., J. Jpn. Inst., Met., 40:, 124, (1976)

263 Sakashiki M., Sato N., J. Electrochem. Soc., 62:, 127, (1975)

264 Noda T., Kudo K., Sato N., J. Jpn. Inst. Met., 37:, 951, 1088, (1973)

265 Revie R.W., Barker B.G., Bockris J. O'M, J. Electrochem. Soc., 122:, 1460, (1975)

266 Revie R.W., Bockris J. O'M., Barker B.G., Surf. Sci., 52:, 664, (1975)

267 Nagayama M., Cohen M., J. Electrochem. Soc., 110:, 670, (1963)

268 Leibengath J.L., Cohen M., J. Electrochem. Soc., 119:, 987, (1972)

269 Vetter K.J., Z. EleKtrochem. 62, 642, (1958)

270 Foley C.L., Kruger J., Bechtold C.J., J. Electrochem. Soc., 114:, 994, (1967)

271 Bockris J. O'M., Genshaw M., Brusic V., Symp. Faraday Soc., 4, 177, (1970)

272 Bech-Nielsen G., Electrochim. Acta, 18:, 671, (1973)

273 Bech-Neilsen G., Electrochim. Acta, 19:, 821, (1974)

274 Bech-Neilsen G., Electrochim. Acta, 20:, 619, (1975)

275 Bech-Neilsen G., Electrochim. Acta, 23:, 425, (1978)

276 Geena D., El-Miligy A.A., Lorenz W.J., Corrosion Sci., 13:, 505, (1973)

277 Geena D., El-Miligy A.A., Lorenz W. J., Corrosion Sci., 14:, 657, (1974)

278 El-Miligy A.A., Geena D., Lorenz W.J.,Electrochim. Acta, 20:, 273, (1975)

279 Morsi M.A., Elewady Y.A., Lorbcer P., Lorenz W.J., Werkst. U. Korros., 31:, 108, (1980)

280 Ebersbach U., Schwabe K.,Pitter K., Electrochim. Acta, 12:, 927, (1967)

281 Ebersbach U., Konig P., Electrochim. Acta, 14:, 773, (1969)

282 Ebersbach U., Kreysa G., Schwabe K., Electrochim. Acta, 17:, 445, (1972)

283 Frank U.F., Fitzhungh R., Z. Electrochem. Acta, 65:, 156, (1961)

284 Epelboin I., Gabrielli C., Keddam M., Takenouti H., Z. Physik. Chem. NF98, 225, (1975)

285 Vilche J.R., Arvia A.J., J.Electrochem. Soc., 123:, 1061, (1976)

286 Real S.G., Vilche J.R., Arvia, A.J, Corrosion Sci., 20:, 563, (1980)

287 Bard A.J., Faulkner L.R., "Electrochemical Method ,Fundamentals and Applications", John Wiley and Sons USA, (1980)

288 Armstrong R,D., Edmondson M., Electrochem. Acta, 18:, 937, (1973)

289 Epelboin I., Keddam M., J. Electrochem. Soc., 117:, 1052, (1970)

290 Sluyters J.H., Rec. Trav. Chim., 79:, 1092, (1960)

291 Armstrong R.D., et al, J.Electrochem. Soc., 48:, 150, (1973)

292 Armstrong R.D., et al, Electrochemistry, 6:, 90, (1976)

293 Haryama S., Proc. 5th Int. Cong. Met. Corrosion, Tokyo, Japan, (1972)

294 Randles J.E.B., Disc. Faraday Soc., 1:, 11, (1947)

295 Rebach M., Sluyters J.H., "Electrochem. Chem." , 14:, Ch.1, Pub. Dekker, NY, (1969)

296 Cole R.H., Cole K.S., J. Chem. Phys., 9:, 34, (1941)

297 Cole R.H., Cole K.S., J. Chem. Phys. 10:, 98, (1942)

298 Delevie R., Electrochim. Acta, 10, 395, (1965)

299 Szklarska-Smialowska Z., Zakroczymski T., Fan C.J., J.Electrochem. Soc., 132:, 2543, (1985)

300 Graham T., Proc. Roy. Soc.m 16:, 422, (1968)

301 Lewis F.A., "The Palladium and Hydrogen System", Academic Press, London, (1967)

302 Lewis F.A., Surf. Techn., 11, 1-16, (1980)

303 Zakroczymski T., Szklarska-Smialowska Z, J. Electrochem. Soc., 132:, 11, 2548, (1985)

304 Bockris J. O'M, Genshaw M., Fullenwider M.A., Electrochim. Acta, 15:, 47-60, (1970)

305 Kumnick A.J., Johnson H.H., Metall. Trans. A, 6A:, 1087, (1975)

306 Gileadi E., Fullenwider M.A., Bockris J. O'M, J. Electrochem. Soc., 113:, 9, 926, (1966)

307 Kirchheim R., Albert E., Froumn E., Scripta Metall., 11:, 651, (1977)

308 Ishikawa T., McLellan R.B., Acta Metall., 33:, 11, 1979-1985, (1985)

309 Kirchheim R., McLellan R.B., J.Electrochem. Soc., 127:, 11, 2419, (1980)

310 Sohina I.A., Aleksanderova G.S., Rotinyan A.L., Nefyodov A.N., Sov. Electrochem., 11:, 1466-1468, (1985)

311 Kirchheim R.,Szokefalvi-Nagy A., Stolz U., Speilling A., Scripta Metall.,19:, 843-846, (1985)

312 Yayama H., Hirakawa K., Tomokiyo A., Mem. Fac. Eng. Kyushu Uni., 45:, 1, (1985)

313 Newman J.F., Shreir L.L., Corrosion Sci., 9:, 631, (1969)

314 Interrante C.G., Proceedings First International Conference on Current Solutions to Hydrogen Problems in Steels, (Interante C.G., Pressouyre G.M. eds.), 3, ASM Metals Park, Ohio, USA, (1982)

315 Kim C.D., Loginow A.W., Corrosion, 24:, 10, 313-318, (1968)

316 Shanabarger M.R., Taslami A., Nelson H.G., Acta Met. 15:, 929-933, (1981)

317 Wach S.P., Miodownik A.P., Mackowiak J., Corrosion Sci., 271-285, (1966)

318 Reicke E., Proc. 8th Int. Cong. on Metallic Corrosion, (8th ICMC), 1, 605-610, Pub. DECHEMA, (1981)

319 Hashimoto K., Meshii M., Scripta Metall., 19:, 9, 1075-1079, (1985)

320 Tetleman A.S., Robertson W.D., Acta Metall., 11:, 415, (1963)

321 Sukhotin A.M., Supelova E.v., Reingeverts M.D., Sov. Electr., 20:, 12, 1532-36, (1984)

322 Namboodhiri T.K.C., Nanis L., Acta Metall., 21:, 663-672, (1973)

323 Stark P., Acta Met., 26:, 1139-1142, (1978)

324 Tafel J., Z. Phyzikal Chem., 50A:, 641, (1905)

325 Dull D.L., Raymond L., ASTM-STP, 543:, 20-23, (1974)

326 Bockris J.O'M., Subramanyan P.K., Electrochim. Acta, 16:, 2169, (1971)

327 Hickling A., Salt F.W., Trans. Faraday Soc., 36:, (1940)

328 Frankel G.S., Latanision R.M., Metall. Trans. A, 17A:, 861-867, (1986)

329 Tsuru T., Latanision R.M., Scripta Metall., 16:, 575-578, (1982)

330 Wright H.J.L., Hunter R.J., Aust. J. Chem., 26:, 1183, (1973)

331 Wright H.J.L., Hunter R.J., Aust. J. Chem., 26:, 1191, (1973)

332 Gaudin A.M., Fuerstenan D.W., Min. Eng., 7:, 66, (1955)

333 Seo M., Lumsden J.B., Staehle R.W., Surf. Sci., 42:, 337, (1974)

334 Stockbridge C.D., Sewel P.B., Cohen M., J. Electrochem. Soc., 108:, 928, (1961)

335 Kruger J., J. Electrochem. Soc., 110:, 654, (1963)

336 Wroblowa H., Brusic V., Bockris J. O'M., J. Phys. Chem., 75:, 2823,(1971)

337 Ord J., De Smet, J. Electrochem. Soc.,113:, 1288,(1966)

338 Moshtev R.V., Electrochim. Acta, 15:, 657, (1976)

339 Cabrera N., Mott N.E., Rep. Prog. Phys. 12:, 163, (1948)

340 Okamoto G., Proceedings of the Fifth International Congress on Metallic Corrosion , 8, NACE, Houston (1974)

341 Zakroczymski T., Fan C.J., Szklarska-Smialwska Z., J. Electrochem. Soc., 132:, 12, 2868-2871, (1985)

342 Pyun S.I., Oriani P.A., Corrosion Sci., 44:, 12, (1988)

343 Kim C.D., Wilde B.E., Corrosion Sci., 10:, 735-744, (1970)

344 Armaconqui M.E., Oriani R.A., Corrosion, NACE, 44:, 696-698, (1988)

345 Oriani R.A., "Hydrogen Embrittlement of Steels", Ann. Rev. Mater. Sci., 8:, (2), 32&-357, (1978)

346 Marichev V.A., Zashch. Met. , 16:, 5, 531-543, (1980)

347 Marichev V.A., Sov. Mat. Sci., 21:, 1,pp 5-11, (1985)

348 Fromm E., Coll. Abs. of the 2nd JIM on Int. Symp. on Hydrogen Metals, Minikami, Jpn., pp 147-157, (1979)

349 Johnson R.A., Phys. Rev., 134:, A1329-A1334, (1964)

350 Johnson R.A., Phys. Rev., 145:, 423-433, (1966)

351 White P., Kahn L.R., "Hydrogen Effects in Metals", Op. Cit., pp 723-730

352 Machlin E.S., J. Less Common Metals, 63:, 1-30, (1979)

353 Smialowski M., "Proc. of Conf. on Stress Corrosion Cracking and Hydrogen Embrittlement of Iron Based alloys", (Staehle R.W., Hochmann J., McCright R.D., Slater J.E., eds.), NACE, Houston, 405, (1977)

354 Horuyan S., Tsuru T., Impedance Chara. of Passive Iron, in "Passivity of Metals", (Frankental R.P., Kruger J. eds.), 564-584, (1978)

355 Bloom M.C., Goldenberg L., Corrosion Sci., 5:, 623, (1965)

356 Grodshteyn and Ryzlik," Tables of Integrals , series and Products", p.494

357 Wang C.H.,Bernstein I.M., Acta Metall. 34:, 6, 1001-1010, (1986)

358 Vorkapić L.Z., Drazic D.M., Corros. Sci. 19, 643-651, 1979.